



UNIVERSITAT DE
BARCELONA

Targeting mitochondrial metabolism in cancer: development and validation of PEPCK-M and PYCR1 inhibitors

Marc Aragó Belenguer,

ADVERTIMENT. La consulta d'aquesta tesi queda condicionada a l'acceptació de les següents condicions d'ús: La difusió d'aquesta tesi per mitjà del servei TDX (www.tdx.cat) i a través del Dipòsit Digital de la UB (diposit.ub.edu) ha estat autoritzada pels titulars dels drets de propietat intel·lectual únicament per a usos privats emmarcats en activitats d'investigació i docència. No s'autoritza la seva reproducció amb finalitats de lucre ni la seva difusió i posada a disposició des d'un lloc aliè al servei TDX ni al Dipòsit Digital de la UB. No s'autoritza la presentació del seu contingut en una finestra o marc aliè a TDX o al Dipòsit Digital de la UB (framing). Aquesta reserva de drets afecta tant al resum de presentació de la tesi com als seus continguts. En la utilització o cita de parts de la tesi és obligat indicar el nom de la persona autora.

ADVERTENCIA. La consulta de esta tesis queda condicionada a la aceptación de las siguientes condiciones de uso: La difusión de esta tesis por medio del servicio TDR (www.tdx.cat) y a través del Repositorio Digital de la UB (diposit.ub.edu) ha sido autorizada por los titulares de los derechos de propiedad intelectual únicamente para usos privados enmarcados en actividades de investigación y docencia. No se autoriza su reproducción con finalidades de lucro ni su difusión y puesta a disposición desde un sitio ajeno al servicio TDR o al Repositorio Digital de la UB. No se autoriza la presentación de su contenido en una ventana o marco ajeno a TDR o al Repositorio Digital de la UB (framing). Esta reserva de derechos afecta tanto al resumen de presentación de la tesis como a sus contenidos. En la utilización o cita de partes de la tesis es obligado indicar el nombre de la persona autora.

WARNING. On having consulted this thesis you're accepting the following use conditions: Spreading this thesis by the TDX (www.tdx.cat) service and by the UB Digital Repository (diposit.ub.edu) has been authorized by the titular of the intellectual property rights only for private uses placed in investigation and teaching activities. Reproduction with lucrative aims is not authorized nor its spreading and availability from a site foreign to the TDX service or to the UB Digital Repository. Introducing its content in a window or frame foreign to the TDX service or to the UB Digital Repository is not authorized (framing). Those rights affect to the presentation summary of the thesis as well as to its contents. In the using or citation of parts of the thesis it's obliged to indicate the name of the author.



UNIVERSITAT DE
BARCELONA

Thesis for doctoral degree (PhD)

**Targeting mitochondrial metabolism in
cancer: development and validation of
PEPCK-M and PYCR1 inhibitors.**

Marc Aragó i Belenguer

L'Hospitalet de Llobregat, 2022

Thesis for doctoral degree (PhD)

**Targeting mitochondrial metabolism in cancer: development
and validation of PEPCK-M and PYCR1 inhibitors.**

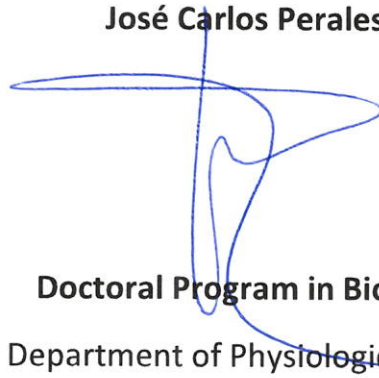
By

Marc Aragó i Belenguer



Under supervision of

José Carlos Perales Losa



Doctoral Program in Biomedicine

Department of Physiological Sciences.

Faculty of Medicine and Health Sciences.

L'Hospitalet de Llobregat, May 2022



**UNIVERSITAT DE
BARCELONA**

INDEX

INDEX

INDEX	5
LIST OF FIGURES AND TABLES	9
ABBREVIATIONS.....	15
INTRODUCTION	19
Cancer.....	21
Introduction.....	21
Hallmarks of cancer	22
Sustained proliferative signaling	22
Enabled replicative immortality	24
Resistance to cell death.....	24
Induced angiogenesis	25
Invasion and metastasis	25
Immune evasion	26
Genome instability	26
Tumor inflammation.....	27
Deregulated cellular energetics.....	27
Metabolism.....	28
Enzymes.....	28
Bioenergetics	29
Glycolysis	30
Gluconeogenesis.....	31
Tricarboxylic acid cycle and oxidative phosphorylation.....	32
Fatty acid metabolism	35
Pentose phosphate pathway.....	36
Regulation of metabolism by signaling pathways and transcription factors	37
PI3K-AKT-mTOR pathway	37
Nuclear factor erythroid 2-related factor 2 (Nrf2)	38
Myc	38
Hypoxia-inducible factors (HIF)	39
TP53	39
AMP activated protein kinase (AMPK)	40
Cancer metabolism.....	41
Warburg effect	41
TCA cycle & OXPHOS	43

Glutamine metabolism	44
Serine synthesis pathway	45
One-carbon metabolism.....	46
Lipid metabolism	47
Metabolic diversity and plasticity.....	49
Phosphoenolpyruvate carboxykinase (PEPCK).....	51
PEPCK-C	51
PEPCK-M	53
PEPCK inhibitors	56
Proline metabolism.....	58
Proline catabolism	59
Proline biosynthesis.....	59
PYCR inhibitors	63
Drug discovery	65
Structure-based drug discovery	66
Molecular docking	67
Molecular dynamics	68
AIMS	69
RESULTS AND DISCUSSION	73
CHAPTER 1: PEPCK-M INHIBITORS	75
Target engagement	75
Kinetic evaluation	77
Cellular target engagement.....	79
Preclinical validation of iPEPCK-2 and its target (PEPCK-M) for cancer treatment.....	81
Antineoplastic activity in cancer cell lines.....	81
In vivo PEPCK-M inhibition in mouse xenograft models	85
PEPCK-M role in glucose physiological conditions	92
Metabolite quantification by GC-MS.....	92
Transcriptomic analysis	94
Development of PEPCK-M selective inhibitors.....	99
iPEPOs ADME profile	100
Evaluation of inhibitory potency in recombinant protein.....	101
Target engagement	102
Antineoplastic activity	103
CHAPTER 2: PYCR INHIBITORS	105

In silico-guided discovery of PYCR1 inhibitors for cancer therapy	105
PYCR1 structural insights	105
Virtual screening protocol	107
2 nd Virtual screening campaign.....	112
Inhibition mechanism	115
Analog search	117
Study of hit conformations by molecular dynamics simulations	118
PY13 optimization.....	120
Compounds without the tricycle moiety	125
Preliminary evaluation in cancer cell lines	130
CONCLUSIONS	135
MATERIALS AND METHODS.....	139
Computational procedures.....	141
Virtual screening.....	141
Molecular dynamic simulations.....	141
Cell culture.....	143
Cell lines.....	143
Stable PCK2-overexpressing MCF7	143
Pancreatic islets culture.....	143
Gene and protein expression quantification	144
RT-qPCR	144
RNA extraction and reverse transcription PCR.....	144
Real-time PCR (qPCR)	144
Western Blot.....	145
RNA-seq	147
Target engagement	148
Expression of recombinant proteins <i>E. coli</i>	148
Transformation.....	148
Procurement of competent <i>E. coli</i>	149
Protein expression & purification.....	149
PEPCK activity	151
PYCR1 ACTIVITY ASSAY	153
Cellular thermal shift assay (CETSA).....	154
Metabolites quantification	156
Perchloric acid extraction.....	156

INDEX

PEP determination.....	156
G6P determination	157
Glucose stimulated insulin secretion.....	157
Metabolite quantification by GC-MS.....	158
Cell biology evaluation	160
Viability evaluation	160
MTT assay	160
Crystal violet	160
Annexin V.....	161
Anchorage independent growth: soft agar	162
Wound healing assay.....	162
Cell cycle	162
<i>In-vivo</i> studies in animal models	164
Pharmacokinetics of iPEPCK-2 by HPLC.....	164
Xenograft models	164
Statistical analysis.....	166
BIBLIOGRAPHY	167

LIST OF FIGURES AND TABLES

INTRODUCTION

Figure I-1: Estimated age-standardized incidence and mortality of the 15 most common cancers in 2020 worldwide.....	21
Figure I-2: The hallmarks of cancer.	22
Figure I-3: Free energy diagram of an enzymatic reaction.....	29
Figure I-4: Glycolysis & gluconeogenesis.....	31
Figure I-5: TCA cycle.	33
Figure I-6: Oxidative phosphorylation.....	34
Figure I-7: Pentose Phosphate Pathway.....	36
Figure I-8: Serine and one-carbon metabolism.....	47
Figure I-9: PEPCK-M is the PEPCK isoform preferentially expressed in tumors of diverse origin.	55
Figure I-10: Gluconeogenesis/glycolysis and branching biosynthetic pathways.	56
Figure I-11: P5C-proline cycle in cancer.	62
Figure I-12: PYCR1 inhibitors	63
Figure I-13: Drug development process.	65

RESULTS AND DISCUSSION

Figure R-1: Pairwise sequence alignment for human PEPCK-C (PCK1; UniProtKB: P35558) and PEPCK-M (PCK2; UniProtKB: Q16822).....	76
Figure R-2: PEPCK inhibitors	76
Figure R-3: Docking analysis.	77
Figure R-4: Inhibition of purified human recombinant PEPCK-C and PEPCK-M by iPEPCK-2 and 3-MPA.....	78
Figure R-5: Cellular target engagement by CETSA.....	79
Figure R-6: Glucose stimulated insulin secretion (GSIS) inhibition.	80
Figure R-7: Western blot analysis of PEPCK-M and PEPCK-C levels in HEK-293 and SW-480 wild type and PCK2del/del clones.....	81
Figure R-8: iPEPCK-2 treatment inhibits cell growth.....	82
Figure R-9: Apoptosis by annexin V assay.	82
Figure R-10: PEPCK-M inhibition reduces cell viability under glucose deprivation.....	83
Figure R-11: PEPCK-M inhibition reduce anchorage independent growth.....	83
Figure R-12: PCK2 expression affects anchorage independent growth.	84
Figure R-13: PEPCK-M inhibition non-significantly reduces migration in a wound healing assay.	85
Figure R-14: Plasmatic concentration of iPEPCK-2	86
Figure R-15: In vivo evaluation of iPEPCK-2 antitumoral activity in two murine subcutaneous xenograft models.	87
Figure R-16: Analysis of tumor histopathology from HEK-293 and SW-480 explants.....	88

Figure R-17: Toxicity evaluation of iPEPCK-2 treatment.	89
Figure R-18: Metabolite quantification by GC-MS after iPEPCK-2 treatment.	93
Figure R-19: OXPHOS evaluation by high resolution respirometry with Oxygraph.	94
Figure R-20: Heatmap of the differentially expressed genes.	94
Figure R-21: Selected gene sets enriched in iPEPCK-2 treated cells.	95
Figure R-22: Selected signaling gene sets enriched in DMSO treated cells.	95
Figure R-23: Selected metabolic gene sets enriched in the DMSO treated group.	96
Figure R-24: Selected cell division related enriched gene sets in DMSO treated cells.	96
Figure R-25: Enrichment gene map of significant results from GSEA	97
Figure R-26: Strategy followed to develop PEPCK-M selective inhibitors.	99
Figure R-27: Structure of the synthesized inhibitors with the tryphenylphosphonium group (iPEPO family).	100
Figure R-28: Glucose stimulated insulin secretion (GSIS) inhibition.	102
Figure R-29: Evaluation of in vitro target engagement by Cellular thermal shift assay.	103
Figure R-30: iPEPO-2 activity on cancer cells.	104
Figure R-31: PYCR1 structural insights.	106
Figure R-32: Schema of the followed screening protocol.	107
Figure R-33: PYCR1 binding site.	108
Figure R-34: Purchased compounds resulting from the virtual screening.	109
Figure R-35: Enzymatic assay set up.	109
Figure R-36: PY04 inhibition mechanism.	111
Figure R-37: PY04's analogs.	111
Figure R-38: PY04_2 MD simulation.	112
Figure R-39: Workflow diagram of the second HTVS strategy.	113
Figure R-40: Structure of the compounds selected in the second virtual screening	114
Figure R-41: Lineweaver-Burk plots of hit compounds.	115
Figure R-42: Most probable binding modes of PY13, PY16, PY17.	116
Figure R-43: PY13 and PY17 analogs.	118
Figure R-44: Study of binding mode stability of hit compounds by MD simulation.	119
Figure R-45: Conformation of the carboxylate moiety of PY13 in both binding modes.	120
Figure R-46: Schema followed during the optimization of PY13.	120
Figure R-47: Analysis of PY13 binding mode by 300 ns of molecular dynamic simulation.	121
Figure R-48: First proposed PY13 modifications based on PYCR1 cavities.	122
Figure R-49: Analysis of PY27 binding mode by 300 ns of molecular dynamic simulation.	123
Figure R-50: Analysis of PY28 binding mode by 300 ns of molecular dynamic simulation.	124
Figure R-51: Proposed PY13 modifications substituting the tricyclic moiety.	125

Figure R-52: Evaluation of PY38 by 250 ns of molecular dynamic simulation.	126
Figure R-53: Evaluation of PY39 by 250 ns of molecular dynamic simulation.	127
Figure R-54: Evaluation of PY41 by 250 ns of molecular dynamic simulation.	128
Figure R-55: Evaluation of PY42 by 250 ns of molecular dynamic simulation.	129
Figure R-56: Evaluation of the linker length.....	129
Figure R-57: Treatment with PYCR1 inhibitors reduce viability in cancer cell lines.....	130
Figure R-58: Metabolites quantification by GC-MS after PY27 treatment.....	131
Table R-1: Microsomal stability of iPEPCK-2 in human and mice microsomes.	85
Table R-2: Pharmacokinetic parameters.	86
Table R-3: Results of % of inhibition of cytochromes by iPEPO-1 at 10 μ M.	101
Table R-4: Microsomal stability of iPEPO-1 in in human/mouse/rat microsomes.....	101
Table R-5: Evaluation of inhibitory potency in purified human recombinant PEPCK-C and PEPCK-M	102
Table R-6: Evaluation of purchased compounds in the enzymatic assay.....	110
Table R-7: Evaluation of the VS selected compounds through the enzymatic assay.....	113
Table R-8: Predicted physicochemical descriptors and ADME parameters by SwissADME.....	115
Table R-9: Evaluation of PY13 & PY17 analogs by the enzymatic assay.....	117
Table R-10: Inhibition potency of PY13 analogs with substituents in R ₁ and R ₂	123
MATERIALS AND METHODS	
Figure MM-1: Reaction evaluated in the PEPCK assay.....	151
Figure MM-2: Reaction evaluated in the PYCR1 assay.....	153
Table MM-1: Master mix for reverses transcription using High-Capacity cDNA Reverse Transcription Kit.	144
Table MM-2: RT-PCR protocol.....	144
Table MM-3: Mixtures for qPCR.....	145
Table MM-4: Composition of RIPA buffer for protein extraction.	145
Table MM-5: Composition of loading buffer for western blot sample preparation.	146
Table MM-6: Antibodies used in western blot.....	147
Table MM-7: Reagents for restriction analysis.....	149
Table MM-8: Composition of Lysis, Wash, and Elution buffers.	151
Table MM-9: PEPCK reaction buffer composition.....	151
Table MM-10: PEPCK reaction buffer composition.....	152
Table MM-11: Reagents to add to PEPCK reaction buffer after CO ₂ charge.....	152
Table MM-12: PYCR1 reaction buffer.....	153

LIST OF FIGURES AND TABLES

Table MM-13: PYCR1 reaction buffer.....	154
Table MM-14: Reaction buffer for PEP determination	156
Table MM-15: Reaction buffer for G6P determination.....	157

ABBREVIATIONS

3MPA	3-mercaptopycolinic acid
2PG	2-phosphoglycerate
3PG	3-phosphoglycerate
ACC	Acetyl-CoA carboxylase
ADP	Adenosine diphosphate
AMPK	AMP-activated kinase
ATP	Adenosine triphosphate
CETSA	Cellular thermal shift assay
CoA	Coenzyme A
CV	Cristal violet
DEPC	Diethyl pyrocarbonate
DHP	3,4-dihydroproline
ECM	Extracellular matrix
EMT	Epithelial to mesenchymal transition
ER	Endoplasmic reticulum
F6P	Fructose-6-phosphate
FBPase	Fructose-1,6-bisphosphatase
FBS	Fetal bovine serum
G3P	Glyceraldehyde-3-phosphate
G6PDH	Glucose-6-phosphate dehydrogenase
GFP	Green fluorescent protein
Gln	Glutamine
GSAL	Glutamate- γ -semialdehyde
GSIS	Glucose-stimulated insulin secretion
H	Enthalpy
H-bonds	Hydrogen bonds
KD	Knock-down
KO	Knock-out
LDH	Lactate dehydrogenase
MD	Molecular dynamics
MTT	3-(4,5-dimethylthiazol-2-yl)-2,5-diphenyl-2H-tetrazolium bromide
NAD ⁺ /NADH	Nicotinamide adenine dinucleotide oxidated/reduced state
NADP ⁺ /NADPH	Nicotinamide adenine dinucleotide phosphate oxidated/reduced state
NFLP	N-formyl-L-proline

ABBREVIATIONS

NSCLC	Non-small cell lung carcinoma
OAA	Oxalacetate
OXPHOS	Oxidative phosphorylation
P/S	Penicillin/Streptomycin
P5C	Δ -1-pyrroline-5-carboxylate
P5CS	Δ -1-pyrroline-5-carboxylate synthase
PC	Pyruvate carboxylase
PDH	Pyruvate dehydrogenase
PDK	Pyruvate dehydrogenase kinase
PEP	Phosphoenolpyruvate
PEPCK	Phosphoenolpyruvate carboxykinase
PFK	Phosphofructokinase
PPP	Pentose Phosphate Pathway
Pro	Proline
PRODH/POX	Proline dehydrogenase/oxidase
PYCR	Pyrroline-5-carboxylate reductase
R5P	Ribose-5-phosphate
ROS	Reactive oxygen species
rT	Room temperature
S	Entropy
SDS	Sodium dodecyl sulfate
shRNA	Short-hairpin RNA
siRNA	Small interfering RNA
TCA cycle	Tricarboxylic acid cycle
THFA	Tetrahydrofuroic acid
TPP	Triphenylphosphonium
VS	Virtual screening
α -KG	Alpha ketoglutarate
Δ G	Binding free energy

INTRODUCTION

Cancer

Introduction

Cancer is a large group of diseases characterized by the uncontrolled growth of a population of transformed cells that can affect almost any organ or tissue of the body. Among these population of transformed cells, some of them have the potential to invade contiguous tissues and spread to other organs. The last process is called metastasis, and it is the principal cause of death related to cancer (Ferlay et al., 2020).

Cancer is the second leading cause of death worldwide and in Europe, behind ischemic heart disease. In 2018, it is estimated that it caused 9.6 million deaths. The number of newly diagnosed cancers in Europe had increased around 50% in the last 20 years (from 2.1 million in 1995 to 3.1 million in 2018). However, cancer related deaths showed a blunted increase (20%), thanks to the advances in cancer research and prevention programs. However, it is predicted that cancer incidence will continue to rise during the coming decades (Ferlay et al., 2018, 2020; Hofmarcher et al., 2020; Hulvat, 2020; Keum & Giovannucci, 2019).

Breast, colorectal, lung, cervical and thyroid cancer are the most common types of cancer in women, while Lung, prostate, colorectal, stomach and liver cancer are the most common among men (Ferlay et al., 2020). The incidence and mortality of the most common cancers worldwide are represented in Figure I-1.

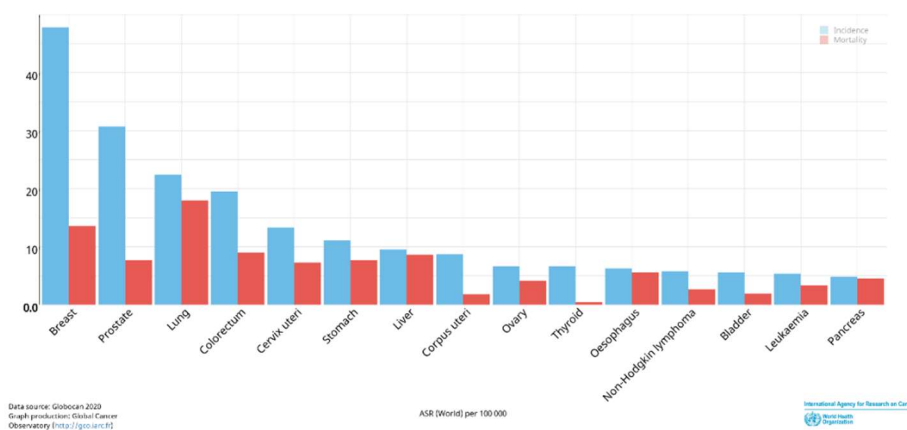


Figure I-1: Estimated age-standardized incidence and mortality of the 15 most common cancers in 2020 worldwide. The age-standardized rate per 100,000 inhabitants of incidence (blue) and mortality (red) are showed in the graph (Ferlay et al., 2020).

Evolution of multicellular organisms dictated a strict control on cell proliferation. Cell growth regulation is essential to maintain cellular and tissue organization, and therefore ensure a proper function. There are indeed cells in proliferation in adult multicellular organisms (e.g. blood cells progenitors, intestinal stem cells, epidermal stem cells), but the process is highly regulated to avoid aberrant proliferation (Cooper, 2000).

After accumulating genetic mutations in key genes (oncogenes and tumor suppressors), some cells gain the capacity to avoid the control mechanisms that bind them to multicellular state, and they start dividing without control. Interestingly, cancer cells seem to have evolved back to unicellular organisms which its unique purpose is divide as much as possible (Alberts B et al., 2002; Nedelcu, 2020). The origin of the mutations is diverse, mutations can be inherited from the progenitors or caused by external factors: physical (radiation), chemical (electrophiles) or biological (human papillomaviruses) carcinogens (Parsa, 2012).

Hallmarks of cancer

There are more than 100 different types of cancer; it is an heterogenous group of diseases. Hanahan and Weinberg suggested that all the different cancer genotypes are the manifestation of ten defined alterations in cell physiology: the hallmarks of cancer (Figure I-2). In the year 2000 Hanahan and Weinberg firstly proposed six characteristics (sustained proliferative signaling, evasion of growth suppressors, enabled replicative immortality, induced angiogenesis, resistance to cell death, and capacity of invasion and metastasis). A decade later, they revised their work taking into account the new scientific discoveries on the field, and they included two new hallmarks (immune evasion and deregulated cellular energetics) and to enabling characteristics (genome instability and tumor inflammation) into the original hallmarks (Hanahan & Weinberg, 2000, 2011).

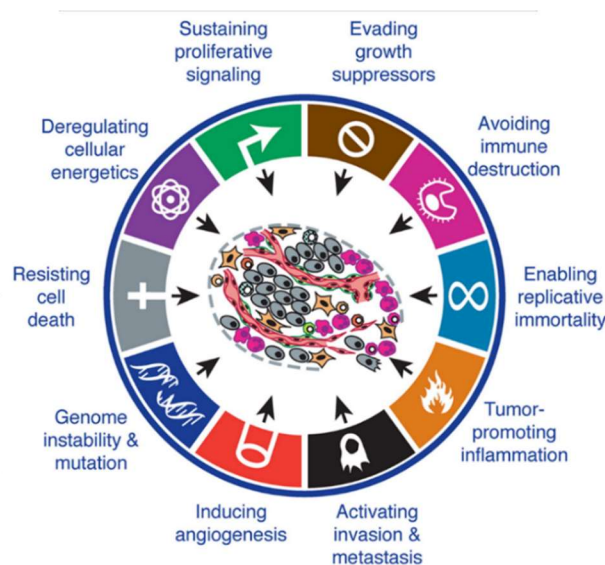


Figure I-2: The hallmarks of cancer. Adapted from Hanahan & Weinberg 2011.

Sustained proliferative signaling

The production and release of growth signals (mainly growth factors) is carefully controlled in healthy tissues (Alberts B et al., 2002). Growth factors bind plasma membrane receptors, most of them containing a tyrosine kinase domain in the intracellular domain that initiate the signaling cascade that will end up promoting cell division. Cancer cells gain the ability to over-activate growth-signaling pathways by different mechanisms: by

autocrine stimulation (producing growth factors themselves), by achieving an hyperresponsive phenotype (augmenting the amount of growth factor receptors in the cell surface or with structural alterations on the receptor that increase the response to ligand) , by stimulating the tumor microenvironment cells that will end up secreting growth factors , or by structural alterations in proteins downstream in the signaling pathway that will lead to a constitutive activity of that (Bhowmick et al., 2004; Kattan & Hancock, 2020; Lemmon & Schlessinger, 2010; Witsch et al., 2010).

For example, the PI3K-AKT-mTOR pathway is highly active in many cancers. The origin of its overactivation could be caused by many alterations along the pathway. The overexpression of insulin-like growth factor (Bol et al., 1997), overexpression of the receptors (Weber et al., 2002), gain of function of the PI3K subunit (Ligresti et al., 2009), loss of function of PTEN (Álvarez-Garcia et al., 2019), gain of function in AKT (Yi & Lauring, 2016), loss of function of TSC1 and TSC2, and activating mutations of mTOR (Grabiner et al., 2014).

Evasion growth suppressors

Besides increasing proliferative signaling, cancer cells should bypass the control mechanisms that negatively regulate cell growth. Many of these mechanisms are orchestrated by tumor suppressor genes, which ensure that there is no abnormal proliferation. Two of the most well-known tumor suppressors are pRb and p53 proteins.

RB protein prevents excessive growth by inhibiting the cell cycle progression (from G1 to S phase) until the cell is ready to divide. RB is regulated by phosphorylation, in the active form (hypophosphorylated) it binds to the transcription factors of the E2F family, and thereby inhibit the transcription of genes that stimulate DNA replication and cell cycle progression. Interestingly Rb function is disrupted in most human cancers (Dick & Rubin, 2013).

TP53, also known as “the guardian of the genome” is the most famous tumor suppressor. Among its functions, p53 could sense many intracellular inputs (e.g. DNA damage, metabolite levels, oxygen concentration) and if the conditions are not optimal it can arrest cell cycle (at G1) until the conditions have been normalized (J. Chen, 2016).

In addition, normal cells stop proliferating when they form cell to cell adhesions. Merlin, the product of NF2 gene, mediates the contact inhibition of proliferation by coupling cell surface adhesion molecules (e.g., E-cadherin) to transmembrane receptor tyrosine kinases (growth factor receptors). Merlin sequestration of the growth factor receptors hinders its ability of emitting mitogenic signals. Interestingly, contact cell inhibition is lost in most cancer cells (Curto et al., 2007; Mendonsa et al., 2018).

Enabled replicative immortality

Telomeres are repetitive and conserved sequences at the ends of the chromosomes, and its function is to protect the genomic DNA. Since the DNA polymerase is not able to replicate the 5' ends of the chromosomes, after every division, somatic cells shorten the end of the chromosomes about 50-200 bp. Due to the continuous shortening, after certain divisions, the telomeres are lost and the cells suffer DNA damage entering in replicative crisis, and therefore apoptosis or senescence. For this reason, somatic cells can divide only a limited number of times.

Telomerase is a specialized DNA polymerase that adds the telomeric repeats at the end of the chromosomes extending the telomeres. This enzyme is expressed in stem cells, germ cells, and some immune cells but it is not expressed in somatic cells. About 85% of cancer cells reactivate the expression of telomerase achieving unlimited proliferative potential (Akincilar et al., 2016; Shay & Wright, 2005).

Resistance to cell death

The cancer cell expansion depends on the cell proliferation as well as the cell death rate. Apoptosis is a form of programmed cell death that occurs without inflammation and it is involved in the regulation of many physiological and pathological processes. Among other functions, apoptosis is responsible to eliminate "damaged" cells (DNA damage, viral infections) to avoid cancer and other pathologies. It is triggered in response to diverse physiologic stresses that cancer cells suffer during tumorigenesis or as a result of anticancer therapy.

Apoptosis can be activated by two main pathways: the intrinsic or the extrinsic pathway. The intrinsic pathway is triggered by diverse intracellular signals (e.g., DNA or mitochondrial damage) and occurs with the release of cytochrome C to the cytosol. The extrinsic pathway is activated through extracellular death inducing signals that bind membrane receptors. Both pathways end up activating a family of latent proteases (caspases), that start the proteolytic cascade.

Once apoptosis is activated there is no way back, for this reason the trigger of these process is very regulated. There are families of pro-apoptotic and anti-apoptotic proteins, and the relation between both groups is what decides cell fate. Bax and Bak are pro-apoptotic proteins that trigger apoptosis creating pores in the mitochondria to release cytochrome C and other apoptotic signaling proteins. The anti-apoptotic proteins of the Bcl-2 family (e.g., Bcl-XL, Bcl-2) carry out its purpose by binding to (and therefore, inhibiting) Bax and Bak (X. Xu et al., 2019).

In addition to determine if the cell is going to enter cell cycle arrest, p53 can induce apoptosis if the sensed signal (mainly DNA damage) is severe enough. P53 activates apoptosis by upregulating the expression of PUMA and NOXA, two pro-apoptotic proteins that bind to Bcl-2 anti-apoptotic proteins that will release Bax and Bak enabling them to initiate apoptosis (Junttila & Evan, 2009).

Cancer cells success evading apoptosis by various mechanisms. The most common is the lost p53 tumor suppressor function. Alternatively, cancer cells reach this end by upregulating the anti-apoptotic proteins (Bcl-2, Bcl-XL, ...), downregulating the pro-apoptotic ones (Bax, Bak, PUMA, ...), and by breaking the ligand induced cell death pathway (e.g., decreasing the expression of death receptors) among others (Fulda, 2009).

Induced angiogenesis

Tumors require a continuous supply of nutrients and oxygen as well as a way to evacuate the carbon dioxide and other metabolic residues. Tumors are able to generate new blood vessels that irrigate them by a process named angiogenesis. We can find angiogenesis in the adulthood in some physiological processes such as wound healing or adaptation to muscle exercise. However, the activation of angiogenesis in such processes is just transitory. In contrast, angiogenesis is always activated during tumor progression (Lugano et al., 2020).

Vascular endothelial growth factor (VEGF) is the main angiogenesis activator, it signals via tyrosine kinase receptors (VEGFR 1-3). The expression of VEGF can be activated by hypoxia and oncogene signaling. In contrast, thrombo-spondin 1 (TSP-1) inhibits angiogenesis also binding to membrane receptors of the endothelial cells (Ferrara, 2009; Kazerounian et al., 2008).

Since the activation of angiogenesis in tumors is always activated with a mix of unbalanced proangiogenic signals, the newly formed blood vessels are typically aberrant. Unlike vasculature from a normal tissue, tumor blood vessels are disorganized, with excessive and irregular branching, larger than the normal, fenestrated. This leads to an erratic blood flow and an impairment in nutrient and waste products exchange. Therefore, the distribution of nutrients and oxygen is heterogenous in the tumor leaving areas with low nutrient availability, ischemia, and necrosis (Nagy et al., 2010).

Invasion and metastasis

While primary tumors could be successfully treated by surgery and adjuvant chemo/ radiotherapy, metastasis is largely incurable. In addition, metastatic tumors are usually resistant to current therapies. This is why more than 90% of cancer related deaths are due to metastasis.

The formation of metastasis is a succession of complex mechanisms named the metastatic cascade. Firstly, cells from the primary tumor invade the neighbor tissue (local invasion). Then some cells could intravasate into the blood vessels, most of the cells would die during the transport through the vasculature, but some of them will survive and extravasate into the parenchyma of a distant organ. Few of these cells would adapt to the new microenvironment forming micrometastases. The micrometastases can remain latent during years, until the cells restart the proliferation at metastatic sites generating macroscopic and clinically detectable metastatic tumors (Ganesh & Massagué, 2021; Massagué & Obenauf, 2016).

Among the myriad of processes involved in the metastatic cascade, the epithelial to mesenchymal transition (EMT) features prominently. During the EMT, epithelial cells develop the ability to invade, resist stress, and disseminate. It is a reversible process, during the formation of micrometastases, cells that have undergone to EMT and migrated to a distant tissue, had to switch back to an epithelial morphology. Another important ability for invasion is the capacity to disassembly of the extracellular matrix and its constituents. This is performed by a family of enzymes named metalloproteinases, the expression of which plays an essential role during invasion but also proliferation, survival, immune evasion, and angiogenesis (Fares et al., 2020; Valastyan & Weinberg, 2011).

Immune evasion

Genetic mutations leading to potential tumor initiation cells are quite abundant during lifetime, however the immune system is responsible to identify these cells and eliminate them. This concept agrees with the higher incidence of cancer in immunodeficient human and mice. However, cancer is also found in immunocompetent individuals, showing that sometimes cancer cells find the way to evade the immune system surveillance.

The last theory on the fight of the immune system against cancer is called immunoediting. It has three different phases: elimination, equilibrium, and evasion. The elimination phase occurs when the incipient tumors are successfully eliminated by the immune system. If the cancer cells are not completely eliminated, then is when the equilibrium phase take place. The immune system restraints cancer progression avoiding the formation of tumors, but it fails at eliminating them. Cancer cells can then enter to dormant states that could last for years at this point. Some cancer cells may escape from immune control and start growing freely, entering to the evasion phase. This evasion could take place through different mechanisms such as reducing immune recognition, increasing resistance to immune cells attacks, or by setting up an immunosuppressive tumor microenvironment (Muenst et al., 2016).

Genome instability

Tumorigenesis is a microevolutionary process where mutations take place in single cells, and if they lead to acquisition of favorable features, they persist. Tumor progression though, is a multistep process of successive subclonal expansions. The acquisition of most of the hallmarks described takes place by this process. However, the genome maintaining systems (such as p53) watch over DNA integrity and would activate cell cycle arrest or apoptosis if mutations are detected. Therefore, the genome maintaining machinery should be “switched off” in cancer cells to enable the increased mutation rate, and therefore facilitate the apparition of mutations favorable for the tumorigenic process. The defects in these systems could be found in the DNA damage sensors, in the repair machinery, or in the molecules that inactivate the mutagenic molecules (Negrini et al., 2010; C. I. Wu et al., 2016).

Furthermore, some of the tumorigenic phenotypes could be achieved by epigenetic modifications such as DNA methylation and histone modification (Esteller, 2009; Hanahan, 2022).

Tumor inflammation

Cancer appearance is linked to chronic infection, diet, obesity, inhalation of pollutants or tobacco, alcoholism. All these factors had in common that they curse with chronic inflammation. Inflammation is a protective response to a loss of tissue homeostasis, however, when inflammation becomes chronic it becomes harmful and may lead to disease.

The chronic inflammation can contribute to the acquisition of some of the hallmark capabilities described by supplying bioactive molecules to the tumor microenvironment. Macrophages (the predominant immune cells in chronic inflammation) together with leukocytes can release these bioactive molecules such as growth factors, survival factors, proangiogenic factors, cytokines, chemokines, extracellular enzymes, and high levels of reactive oxygen species that can act as mutagenic agents. Furthermore, this signaling can also lead to the suppression of the immune cells that cancer progression (Elinav et al., 2013; N. Singh et al., 2019).

Deregulated cellular energetics

Finally, cells in continuous proliferation have different metabolic requirements than differentiated cells. Thus, cancer cells modify their metabolism in order to fulfil their needs, in a process known as metabolic reprogramming. Alterations of many pathways have been described in cancer cells, the most reported being the increase of glycolysis known as the Warburg effect. Furthermore, the availability of some nutrients could be compromised in some areas of the tumor and the ability of cancer cells to adapt to these environments could determine its fate (vander Heiden & DeBerardinis, 2017). This hallmark will be further discussed below as it is the main focus of this thesis.

Metabolism

Metabolism is the sum of all the chemical transformations that take place in a cell or organism to sustain life. It includes a myriad of biochemical reactions and transport processes that occur in a coordinated manner to fulfil four main functions: i) obtain energy available to run cellular processes from degrading nutrients from the environment, ii) convert nutrients into building blocks (e.g., amino acid, fatty acids) and their polymerization into macromolecules (e.g., proteins, polysaccharides), iii) synthesize and degrade biomolecules in specialized cellular functions, and iv) the elimination of metabolic waste and xenobiotics. Metabolic reactions are often grouped into metabolic pathways, which are a group of interconnected reactions that accomplish a given role.

Metabolism can be generally divided into catabolism and anabolism. Catabolism consists in the degradation of complex macromolecules to simpler ones. Catabolic pathways release energy, some of which can be conserved as ATP and reductive power (NAD(P)H and FADH₂). In contrast, anabolism consists in the biosynthesis of complex macromolecules from simpler ones. Anabolic reactions often require an input of energy (in the form of ATP or reductive power) (Judge & Dodd, 2020; Nelson & Cox, 2000).

In order to maintain cellular and organism homeostasis, adapt to the external environment, and perform its tissular function, metabolic fluxes (and therefore, metabolite pools) must be tightly regulated. Regulation is performed by key metabolic sensors (such as AMPK, which sense ATP/AMP ratio), hormones and growth factors (B. Xiao et al., 2011).

Enzymes

Most of the biochemical reactions that take place in cells are catalyzed by enzymes. Enzymes enable reactions that otherwise would not take place, or would take place much slowly, by reducing their activation energy (Figure I-3). They accomplish this by providing a specific environment where the reaction is energetically more favorable. Specifically, the reaction takes place inside a pocket of the enzyme called the active site, where there are specific amino acids that bind the substrates and catalyze the reaction (by modulating the conformation of the substrates, stabilizing highly reactive intermediates, etc). Interestingly, enzymatic catalysis does not modify the reaction equilibrium, it just increases the rate of the reaction.

Furthermore, enzymes are the primary regulation point for modulating metabolism, and therefore maintaining metabolic homeostasis. Enzymatic activity can be regulated at different levels: it can be regulated by substrate and product concentrations; by allosteric binding of a metabolic intermediate or coenzyme that senses the metabolic state of the cell; by covalent modifications (such as phosphorylation) of allosteric sites; or by modifying the intracellular concentration of the enzyme. The later mechanism could be achieved by increasing the enzyme synthesis or degradation rates. Interestingly, extracellular signals such as

hormones and growth factors can end up modulating the enzymatic activity through various of the described mechanisms (Nelson & Cox, 2000).

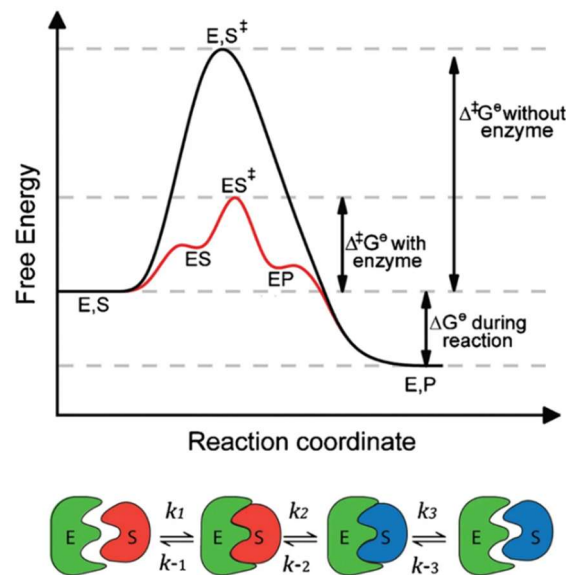


Figure I-3: Free energy diagram of an enzymatic reaction. The catalyzed reaction (red) exhibit a lower Gibbs activation energy ($\Delta^\ddagger G$) compared with the uncatalyzed reaction (black). However, the thermodynamic equilibrium stays unchanged (ΔG). (E, enzyme; S, substrate; P, product; ES, enzyme–substrate complex; EP, enzyme–product complex; ‡, transition state). Figure adapted from Hess et al., 2019.

Bioenergetics

Metabolism is a dynamic process where there is a continuous and coordinated synthesis and degradation of biomolecules in order to fulfil cell requirements. Many of the synthetic pathways are energetically unfavorable, therefore, they need an external contribution of energy to take place. Cells can use the energy stored on the phosphate bond of ATP to enable the endergonic reactions by coupling them to the ATP hydrolysis. Moreover, energy can also be stored in electron-exchange carriers or redox “couples”, such as electron NADH, NADPH, FADH₂, and FMNH₂. These carriers can accept or donate electrons allowing both oxidation and reduction reactions, for example those required for the biosynthesis of compounds such as fatty acids, require various oxidation-reduction reactions that need an electron donor to take place. In redox reactions, one molecule gives electrons (therefore, gets oxidized) to a second one that accept them (and therefore, gets reduced).

As previously described, catabolic pathways break nutrients and complex molecules to obtain simpler and smaller ones. During this process, energy stored in the broken bonds of the molecules degraded, is released. And cells, can benefit from this release if coupling these catabolic reactions to ATP synthesis (from ADP + Pi) directly or indirectly through the generation of an energy containing redox couple such as NADH or FADH that can be later oxidized in the oxidative phosphorylation (OXPHOS) pathway to generate ATP. Other catabolic pathways might result in the generation of a reduced NAD(P)H equivalents that can be then utilized

for biosynthetic processes and to obtain energy through OXPHOS. In conclusion, catabolic pathways aim to obtain energy, reductive power, and smaller molecules needed for the biosynthesis of building blocks.

Glycolysis

Glucose is the most abundant monosaccharide, and it constitutes the major source of energy and carbons (for anabolic processes) in most living organisms. Glucose can be oxidized to pyruvate by glycolysis, a pathway present in almost all living cells. It is also known as Emden-Meyerhof-Parnas (EMP glycolysis) in honor of the biochemists that made the major contributions to completely elucidate this pathway in 1940. Only a few prokaryotic organisms metabolize glucose through other pathways, such as the Entner-Doudoroff or hexose monophosphate pathways (Akram, 2013a; Lunt & vander Heiden, 2011; Nathan Entner & Doudoroff, 1952; Nelson & Cox, 2000).

Glycolysis is a pathway formed by 10 consecutive cytosolic reactions that oxidize glucose to two pyruvate molecules. Glycolysis can be divided in two phases: the preparatory phase and the payoff phase (Figure I-4). The preparatory phase requires energy (2 ATP molecules) and ends up splitting the fructose 1,6-bisphosphate into two three-carbon phosphorylated sugars: glyceraldehyde 3-phosphate (G3P) and dihydroxyacetone phosphate (DHAP). During the second payoff energy phase, the G3P is oxidated to pyruvate generating 2 ATP and 1 NADH molecules. Since DHAP can be reversibly converted to G3P by phosphotriose isomerase, the amount of total amount of energy formed in this phase is 4 ATP and 2 NADH per glucose molecule. Therefore, the net energy yield is 2 ATP and 2 NADH. Pyruvate formed in this process can be metabolized to acetyl-CoA and enter the tricarboxylic acid (TCA) cycle to get completely oxidated to CO₂ and H₂O (Akram, 2013a; Nelson & Cox, 2000).

In the presence of oxygen, NADH formed during glycolysis can be recycled to NAD⁺ by donating the electrons to the electron transport chain (ETC) to generate more energy. However, glycolysis does not need oxygen to work. Under hypoxic and anoxic conditions cells should find a way to regenerate NAD⁺, in most cases fermentation is the solution. During fermentation NADH can be re-oxidated by donating its electrons to a terminal acceptor that will be finally excreted by the cell (primary as an alcohol or an acid). For example, animal cells under hypoxic conditions can reduce pyruvate to lactate recycling the NADH formed during glycolysis (Akram, 2013a; M. Müller et al., 2012; Nelson & Cox, 2000).

Besides generating reductive power and energy, glycolysis is a major supply of carbons for other catabolic and anabolic pathways (Figure I-4). For example, glucose-6-phosphate can be oxidized through the pentose phosphate pathways to obtain NADPH -for fatty acid synthesis- and pentoses needed for nucleotide synthesis (Patra & Hay, 2014). Other intermediates are precursors of amino acid synthetic pathways, such as 3-phosphoglycerate (3PG) that is used in the serine synthesis pathway (Mattaini et al., 2016). Fructose-6-phosphate (F6P) can be used for the synthesis of hexosamines, basic for protein glycosylation (X. Liu,

Blaženović, et al., 2021); or together with G3P, can enter the non-oxidative branch of the pentose phosphate pathway. In addition, DHAP is needed for glycerol 3-phosphate synthesis, important for lipogenesis (Rotondo et al., 2017).

All the reactions that constitute glycolysis are reversible with three exceptions. The reactions catalyzed by the hexokinase (from glucose to glucose-6-phosphate), phosphofruktokinase (from fructose 6-phosphate to fructose 1,6-bisphosphate), and pyruvate kinase (from phosphoenolpyruvate to pyruvate), are irreversible and are highly regulated (Akram, 2013a; Nelson & Cox, 2000).

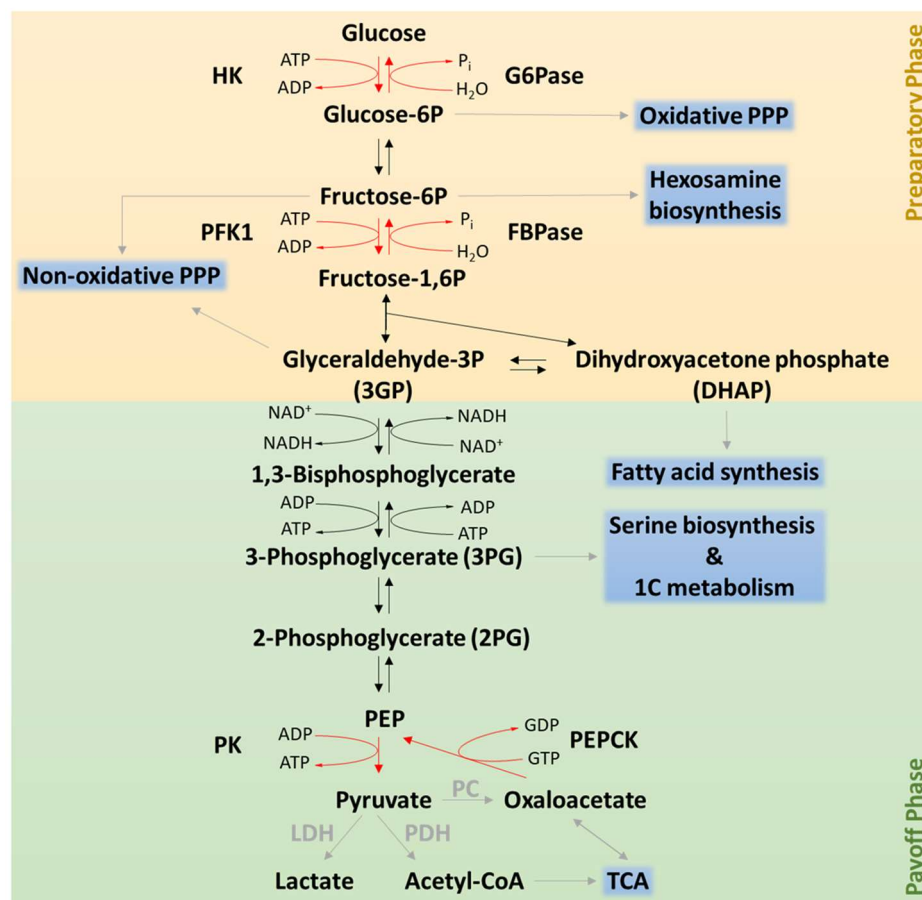


Figure I-4: Glycolysis & gluconeogenesis. Glycolysis can be divided into two phases: the preparatory phase, which requires energy and ends up splitting the fructose 1,6-bisphosphate into two three-carbon phosphorylated sugars: glyceraldehyde 3-phosphate (G3P) and dihydroxyacetone phosphate (DHAP). And the payoff energy phase, where the G3P is oxidated to pyruvate generating 2 ATP and 1 NADH molecules. Glycolysis and gluconeogenesis share the same reactions (which are reversible) except three steps catalyzed by: hexokinase (HK) or glucose-6-phosphatase (G6Pase); phosphofruktokinase 1 (PFK1) or fructose-1,6-bisphosphatase (FBPase); pyruvate kinase (PK) or phosphoenolpyruvate carboxykinase (PEPCK).

Gluconeogenesis

Gluconeogenesis is the pathway that generates glucose from non-carbohydrate substrates, mainly lactate, glutamine, alanine, and glycerol. In humans, gluconeogenesis is restricted to a few tissues and its function is to control glucose homeostasis. It mainly takes place in the liver, but it also occurs in kidney and intestine.

It shares most of the enzymes of glycolysis, although the reactions work in the opposite direction (Figure I-4). However, there are three irreversible reactions that are exclusive to the gluconeogenic pathway. These reactions are catalyzed by phosphoenolpyruvate carboxykinase (PEPCK), fructose 1,6-bisphosphatase (FBPase), and glucose 6-phosphatase (G6Pase) (Figure I-4). Gluconeogenic flux is regulated through these three enzymes, by transcriptional factors and activators/inhibitors. Importantly, glycolysis and gluconeogenesis regulation must be coordinated to avoid energy futile cycling since gluconeogenesis is a highly endergonic process (Grasman et al., 2019; Judge & Dodd, 2020; Nelson & Cox, 2000; Z. Wang & Dong, 2019).

Tricarboxylic acid cycle and oxidative phosphorylation

The Tricarboxylic acid (TCA) cycle, also known as citric acid cycle or Krebs cycle, is the final common oxidative pathway of carbohydrates, proteins, and lipids. Described by Hans Adolf Krebs in 1937, TCA cycle is a mitochondrial cyclic pathway that fully oxidize acetyl-CoA to CO₂ and H₂O. Coupled with oxidative phosphorylation (OXPHOS), TCA cycle is the major source of ATP in aerobic organisms, accounting for 2/3 of the total ATP generation. Furthermore, TCA cycle and OXPHOS are responsible for 2/3 of the oxygen consumption of the whole body (Akram, 2013b; Baldwin & Krebs, 1981).

The TCA cycle is constituted by eight consecutive reactions that form a closed loop (Figure I-5). Each cycle fully oxidizes a molecule of acetyl-CoA, mainly coming from glycolysis and fatty acid oxidation, to CO₂ and H₂O and generates energy in form of GTP (one molecule) and redox power (three NADH and one FADH₂). Reduced cofactors (NADH and FADH₂) generated during TCA cycle are fed into the oxidative phosphorylation electron transport chain (ETC) to generate more energy (Figure I-6) (Akram, 2013b; Nelson & Cox, 2000).

NADH and FADH₂ initially donate electrons to ETC, to complex I and II respectively. Electrons are transferred across the different components of the ETC releasing small amounts of energy in each step. Finally, during the last step of electron transfer, electrons end up reducing O₂ to H₂O molecules. The energy released during the electron transfer is used to pump protons across the inner mitochondrial membrane forming an electrochemical proton gradient. The energy stored in this proton gradient can be used by the ATP synthase to generate ATP by allowing protons to return to the mitochondrial matrix (dissipating the gradient), which couples the proton flux to ATP synthesis. Up to 3 ATP molecules can be obtained from each NADH molecule, and up to 2 ATP molecules from each FADH₂. These values can be diminished depending on the uncoupled respiration (due the proton leak). In conclusion, up to 12 ATP molecules can be generated through the TCA cycle and OXPHOS per each acetyl-CoA molecule (Gnaiger & MitoEAGLE Task Group, 2020; Nelson & Cox, 2000; Nolfi-Donagan et al., 2020).

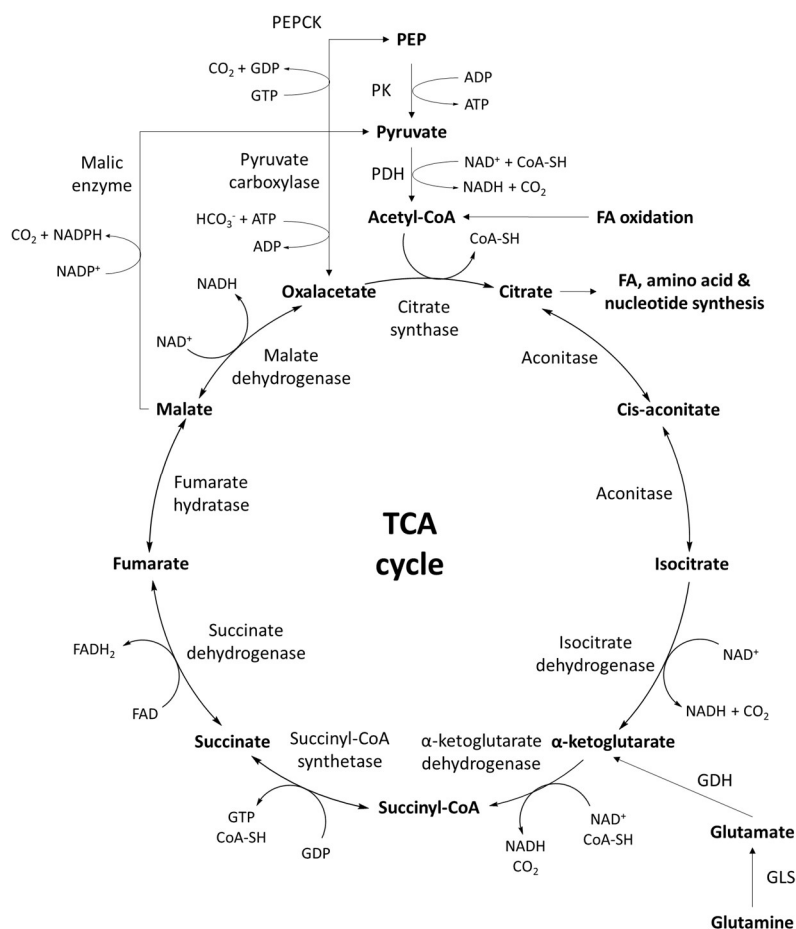


Figure I-5: TCA cycle. Oxalacetate condenses with acetyl-CoA to form citrate. Citrate is isomerized to isocitrate, which can undergo oxidative decarboxylation forming α -ketoglutarate and reducing a NAD⁺ cofactor. α -ketoglutarate dehydrogenase catalyzes the oxidative decarboxylation of α -ketoglutarate to succinyl-CoA producing NADH. The thioester bond of succinyl-CoA is cleaved forming succinate, and the energy released is coupled to GTP formation. Succinate is converted to fumarate reducing a FAD molecule, which donates electrons to ubiquinone. Fumarate is then hydrated to malate, which is finally converted back to oxalacetate generating another NADH molecule. Some anaplerotic (pyruvate carboxylase reaction and glutaminolysis) and cataplerotic (PEPCK and malic enzyme reactions) reactions are also represented in the figure.

TCA cycle flux needs to be coordinated with OXPHOS to maintain energetic balance in cells. Interestingly, high energetic levels (high ATP and NADH concentrations) slow down the TCA cycle flux while ADP and NAD⁺ would stimulate it. The cycle is mainly regulated by three enzymes: citrate synthase, isocitrate dehydrogenase, and α -ketoglutarate dehydrogenase. Citrate synthase is inhibited by high levels of ATP, NADH, and succinyl-CoA. Isocitrate dehydrogenase is inhibited by high NADH concentration. And high concentrations of succinyl-CoA and NADH inhibit α -ketoglutarate dehydrogenase. Similarly, high OAA levels slow down the TCA flux inhibiting succinyl dehydrogenase. Furthermore, the TCA cycle can also be regulated by calcium and some transcriptional factors – such as HIF1 α which promotes the expression of pyruvate dehydrogenase kinase 1 (PDK1), that inhibits pyruvate dehydrogenase lessening acetyl-CoA production and therefore, the TCA cycle flux- (Akram, 2013b; J. W. Kim et al., 2006; Nelson & Cox, 2000; Wan et al., 1989).

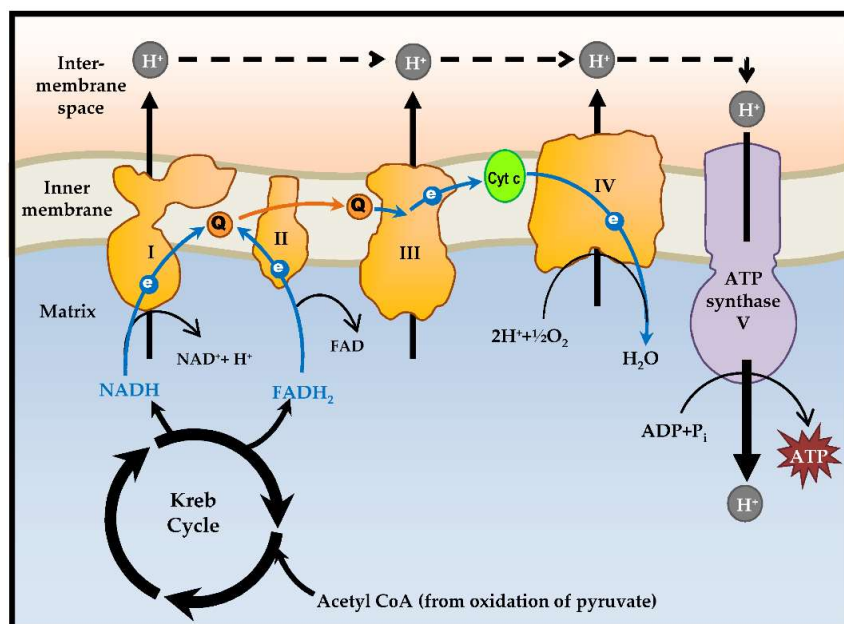


Figure I-6: Oxidative phosphorylation. Reduced cofactors (NADH and FADH₂) generated during TCA cycle are fed into the oxidative phosphorylation electron transport chain to generate energy. Electrons are transferred across the different components of the ETC releasing small amounts of energy which is used to pump protons across the inner mitochondrial membrane to the intermembrane space, forming an electrochemical proton gradient. Oxygen is the last electron acceptor, and its reduction forms a water molecule. Finally, ATP is formed by the dissipation of the proton gradient through ATP synthase. Figure from Mohamed Yusoff 2015.

Besides the catabolic role of the TCA cycle, it provides metabolites from the cycle that act as building blocks for biosynthetic pathways, such as the synthesis of carbohydrates, non-essential amino acids, and fatty acids. For example, citrate can be exported to the cytosol, where it will be converted to oxalacetate (OAA) and acetyl-CoA for nucleotide and lipid synthesis. The export of TCA cycle intermediates for other purposes is called cataplerosis (“emptying”). Interestingly, TCA intermediates used in cataplerotic pathways need to be replenished by anaplerotic (“filling-up”) pathways to keep the TCA cycle running. Two important anaplerotic pathways are glutaminolysis -which apportions α -ketoglutarate from glutamine-, and the pyruvate carboxylase (PC) reaction -which converts pyruvate to OAA-. Therefore, the TCA cycle is considered an amphibolic pathway since it has both catabolic and anabolic functions (Akram, 2013a; Nelson & Cox, 2000).

Furthermore, it has been demonstrated that TCA cycle metabolites can play an active role in cell signaling through controlling transcription factors and modifying chromatin structure. For example, succinate and fumarate inhibit 2-oxoglutarate-dependent dioxygenases, a group of enzymes that include histone demethylases, modifying histone methylation and therefore gene expression (Martínez-Reyes & Chandel, 2020).

In conclusion, the high energetic production potential, the convergence between lipid, amino acid, and carbohydrates metabolism, and the bioactive activities of its intermediates make the TCA cycle one of the most important pathways of cell metabolism.

Fatty acid metabolism

Fatty acids are a diverse group of biomolecules with three main biological functions: source of energy, building blocks for cell structure components (i.e., cell membranes), and precursors of second messengers (such as eicosanoids).

The oxidation of fatty acids takes place in the mitochondria, and it consists in the repetition of a four-step process termed β -oxidation. During β -oxidation, two carbon units are removed from the fatty acid in form of acetyl-CoA. This process generates one NADH and one FADH₂ molecules that can feed the ETC for energy obtention. Before starting the β -oxidation fatty acids need to be activated, this activation is performed by a family of enzymes called acyl-CoA synthetases which catalyze the addition of a coenzyme A molecule to the fatty acid. During the activation, an ATP molecule is converted to AMP. Therefore, the total ATP yield of fatty acid oxidation is up to 17 ATP for each 2 carbon units minus 2 ATP spent in the fatty acid activation.

In addition to a potent energy source, fatty acids are key components of cellular structures such the cytoplasmatic membrane. The synthesis of fatty acids takes place in the cytosol, and it is a highly endergonic process that requires several NADPH molecules. Interestingly, it mainly occurs in the liver and the adipose tissue. Since acetyl-CoA cannot cross the mitochondrial membrane, it has to be transported to the cytosol as citrate and then, converted back to acetyl-CoA and oxalacetate. The first reaction for fatty acid biosynthesis is the carboxylation of acetyl-CoA to malonyl-CoA by acetyl-CoA carboxylase (ACC), it consumes one ATP molecule, and it is the rate-limiting step. Then, malonyl-CoA undergoes polymerization to obtain fatty acids. This is catalyzed by fatty acid synthase (FAS) and consumes 2 NADPH molecules for each elongation step.

Regulation of fatty acid synthesis and oxidation is essential to avoid energy waste. ACC is the rate-limiting step in fatty acid biosynthesis, and it is regulated by various mechanisms. It is regulated allosterically by citrate (activation) and long chain fatty acids (inhibition). Furthermore, it is regulated by phosphorylation. AMP-activated protein kinase (AMPK) can phosphorylate ACC, and therefore inhibit it, when there are low energy levels. It can also be phosphorylated/de-phosphorylated in response to different hormones such as glucagon or insulin. Additionally, hormones and growth factors can further regulate fatty acid metabolism by regulating the expression of enzymes such as FAS. The oxidation of fatty acids is regulated by the NADH/NAD⁺ ratio (high levels of NADH would inhibit the β -oxidation). Malonyl-CoA also inhibits fatty acid oxidation by inhibiting CPT1, therefore blocking the entry of fatty acids to the mitochondria (Judge & Dodd, 2020; Kalish et al., 2012; Nelson & Cox, 2000).

Pentose phosphate pathway

The pentose phosphate pathway (PPP) is the major source of NADPH and it is necessary for the synthesis of ribonucleotides. The PPP has two distinct paths (Figure I-7): the oxidative and nonoxidative branches. The oxidative branch oxidizes glucose-6-phosphate to ribose-5-phosphate (R5P) in three irreversible reactions to yield 2 NADPH molecules. The nonoxidative branch consists of a series of reversible reactions that allows the interconversion of fructose-6-phosphate and glyceraldehyde-3-phosphate to ribose-5-phosphate without generating NADPH. Both branches take place in the cytosol.

Glucose 6-phosphate dehydrogenase (G6PDH) is the rate-limiting enzyme of the oxidative branch. The enzymes of the pathway are allosterically regulated by its own products. Furthermore, the expression of PPP enzymes is regulated by different signaling pathways such as mTOR or PI3K. Interestingly, G6PDH is the most regulated enzyme of the pathway, since it determines the G6P flux that enters into the oxidative branch of the PPP.

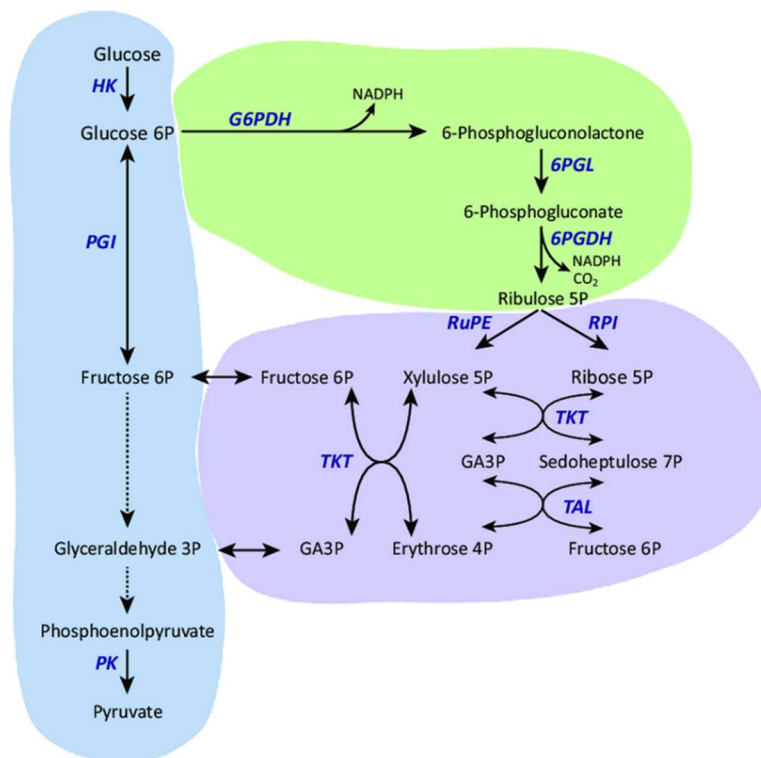


Figure I-7: Pentose Phosphate Pathway. Glucose can be metabolised via glycolysis or through the pentose phosphate pathway, branching at glucose 6-phosphate. The glycolytic pathway is shaded in blue and enzymes hexokinase (HK), phosphoglucose isomerase (PGI), and pyruvate kinase (PK) are marked. Other reactions between fructose 6-phosphate and glyceraldehyde 3-phosphate (GA3P) are summarised through the presence of dotted lines. The oxidative branch of the pentose phosphate pathway, shaded in green, comprises the enzymes glucose-6-phosphate dehydrogenase (G6PDH), 6-phosphogluconolactonase (6-PGL), and 6-phosphogluconate dehydrogenase (6PGDH). The nonoxidative branch, shaded in purple, comprises the enzymes ribulose-5-phosphate epimerase (RuPE), ribose-5-phosphate isomerase (RPI), transketolase (TKT), and transaldolase (TAL). Figure from Kovářová & Barrett, 2016.

The reversibility of the nonoxidative branch in addition to its regulation by product, allows the PPP flux adaptation to the metabolic requirements of the cell. For instance, cells that have high NADPH demand rather than R5P, recycle R5P into the glycolytic pathway as F6P and G3P. Furthermore, F6P can be converted back to G6P to replenish the oxidative branch generating more NADPH (Eggleston & Krebs, 1974; Judge & Dodd, 2020; Nelson & Cox, 2000; Patra & Hay, 2014).

In addition to biosynthetic pathways such as fatty acid synthesis, NADPH is required for glutathione (GSH) synthesis to deal with oxidative stress -in part generated by reactive oxygen species (ROS)-. The oxidative branch of the pentose phosphate pathway is the largest contributor to cytosolic NADPH generation. However, there are additional pathways that can produce NADPH. Among these, we can find the reactions catalyzed by malic enzyme (ME), isocitrate dehydrogenase (IDH), and one carbon metabolism enzymes (Hosios & vander Heiden, 2018).

Regulation of metabolism by signaling pathways and transcription factors

To achieve high efficiency and avoid energy and carbon waste, metabolism is modulated in a coordinated manner. Multiple enzymes and metabolic pathways are regulated simultaneously by signaling pathways and transcription factors to accomplish different cell functions, often activated by the same signaling pathways and transcription factors. In this section, some of these pathways/transcription factors most relevant to the focus of thesis would be briefly introduced.

PI3K-AKT-mTOR pathway

The PI3K-AKT-mTOR signaling pathway regulates a large array of cellular functions, including cell survival, cellular proliferation, differentiation and stem cell properties, migration, angiogenesis and metabolism. It is activated by binding of signaling peptides (mainly growth factors) to tyrosine kinase receptors. Binding triggers and activates PI3K by recruitment to the plasmatic membrane, PI3K catalyze the phosphorylation of phosphatidylinositol 4,5-bisphosphate (PIP₂) to phosphatidylinositol 3,4,5-trisphosphate (PI3P). Contrariwise, PTEN is a phosphatase that catalyze the dephosphorylation of PI3P to PIP₂, preventing the over-activation of the pathway. PI3P recruits and activates different effectors such as AKT, a serine/threonine kinase. Activated AKT (pAKT), modulates a wide array of proteins by phosphorylation such as TSC2, AS160, FOXO, and GSK3 β among others. The phosphorylation of these proteins promotes cell survival and proliferation, glycolysis, fatty acid and glycogen synthesis (Pons-Tostivint et al., 2017; Revathidevi & Munirajan, 2019; Vanhaesebroeck et al., 2010).

The proteins TSC1 and TSC2 are constitutively a dimer that inhibits the mTORC1 complex, when AKT phosphorylates the TSC1/2 complex, it releases mTORC1 inhibition. The mammalian target of rapamycin complex (mTORC1) is a master regulator of cell metabolism, it activates protein, lipid and nucleotide biosynthesis, inhibits autophagy and modulates energy metabolism. Furthermore, it promotes cellular

processes such as cell proliferation, cell survival, invasion, and angiogenesis. Through phosphorylation of proteins that regulate the translation of RNA such as S6 kinases and 4EBFPs, mTORC1 increases ribosome biogenesis and the expression of a heterogeneous group of proteins that will promote many of the functions described before. For example: anti-apoptotic proteins (Bcl2), cell cycle activators (cyclin D1, cMyc, CDK2), proteins involved in metastasis (MM9), the transcription factor HIF1 α (that activates glycolysis and angiogenesis), and pro-angiogenic proteins (VEGF). It also modulates lipid and nucleotide biosynthesis through SREBP, and inhibits autophagy through ULK, ATG13 and FIP200 inhibition. Additionally, TSC1/2 complex and therefore mTORC1 activity, can be also regulated by the Ras-MAPK pathway (that ends up activating mTORC1), and AMPK, Wnt pathway (GSK3 β) and p53 that lead to mTORC1 inhibition. Furthermore, mTORC1 activity can be activated by nutrient availability (especially the amino acids leucine and arginine, but also glutamine) independently to TSC1/2 (Hara et al., 1998; Huang & Manning, 2009; Laplante & Sabatini, 2012; Pons-Tostivint et al., 2017).

Moreover, there is a second mTOR complex: mTORC2. Active mTORC2 activates AKT (creating a positive feedback loop of PI3K-AKT-mTOR pathway), SGK1 and different isoforms of PKC (G. Yang et al., 2015).

Nuclear factor erythroid 2-related factor 2 (Nrf2)

Nrf2 pathway is one of the main pathways in the fight against oxidative stress. In low oxidative stress conditions, Nrf2 binds to Keap1 which mediates its ubiquitination and subsequent degradation in the proteasome. However, during oxidative stress, reactive oxygen species (ROS) and other electrophiles oxidize Keap1 sensor cysteines inducing a conformational change that release Nrf2 (inhibiting its degradation). Free Nrf2 can then translocate to the nucleus and perform its transcriptional factor function. Nrf2 induces the expression of enzymes that participate in the obtention of NADPH (G6PDH, ME1, IDH1), the glutathione metabolism, xenobiotics metabolism, and other antioxidant genes to fight the oxidative stress. Furthermore, Nrf2 upregulates the expression of other genes coding for glycolytic enzymes (and glucose transporter GLUT1), PPP enzymes, enzymes of the serine synthesis pathway and one carbon metabolism (nucleotide synthesis). Interestingly, Nrf2 activates the expression of key genes related to lipid metabolism, however, this response varies depending on the cell type. Moreover, Nrf2 plays a role in endoplasmic reticulum stress (ER stress), caused by protein synthesis defects under oxidative stress conditions or nutrient scarcity, activating the unfolded protein response. Accordingly, it activates the expression of autophagy related genes, proteasome subunits, and ATF4 among others (He, Antonucci, & Karin, 2020; He, Antonucci, Yamachika, et al., 2020; Mitsuishi et al., 2012; Pi et al., 2010; Tonelli et al., 2018).

Myc

Myc is a family of three transcription factors (i.e., c-Myc or MYC, n-Myc, and l-Myc) that controls the transcription of a large number of genes. The set of genes regulated by MYC may be context specific, however

it generally promotes the expression of genes that promote and support cell proliferation, mitochondria biogenesis and cell cycle progression. Furthermore, MYC also reprograms cell metabolism to match the enhanced demand of anabolic metabolites upregulating pathways such as glycolysis or glutaminolysis, and the synthesis of nucleotides, amino acids, and folate among others (Dejure & Eilers, 2017; Goetzman & Prochownik, 2018; Soucek et al., 2008).

Interestingly, MYC expression is activated by growth factors and proliferating signals (such as PI3K-AKT-mTOR, Wnt, Notch JAK, and STAT3 pathways). Moreover, MYC can be regulated posttranslationally by phosphorylation at different sites. For example, phosphorylation by cyclin dependent kinases (CDK), MAPK, and Ca²⁺/calmodulin-dependent protein kinase II- γ (CaMKII γ) enhance its stability while phosphorylation by GSK3 β induces MYC degradation (Farrell & Sears, 2014; Gu et al., 2017; P. Liu et al., 2017).

Hypoxia-inducible factors (HIF)

Hypoxia-inducible factors is a family of heterodimeric transcription factors in charge of modulating the adaptation to hypoxia. HIF mediate this adaptation to hypoxia by upregulating genes that activate angiogenesis and genes that promote glycolysis coupled to lactate production. HIF is mainly regulated by the HIF α subunit: in normoxic conditions HIF α is hydroxylated by prolyl hydroxylase enzymes (PHDs) leading to its ubiquitination and degradation in the proteasome. Oxygen and α -ketoglutarate are necessary for PHDs function, while succinate and fumarate inhibit them. Therefore, in low oxygen conditions (hypoxia) PHDs are inhibited, and consequently, HIF α stabilized. Stabilized HIF α forms the active HIF heterodimer and translocate to the nucleus to perform its function. Furthermore, there are more mechanisms that regulate HIF function. For example, mTORC1 promotes HIF1 α expression; it can be phosphorylated in different sites destabilizing the HIF α subunit (by GSK3 β) or enhancing its nuclear translocation (MAPK) (Benita et al., 2009; Laplante & Sabatini, 2012; Nagao et al., 2019; Sodhi et al., 2001).

TP53

P53 induces cell cycle arrest and DNA repair or apoptosis if cellular stress (DNA damage) is sensed. It is a transcription factor, but it also performs its function through protein interactions. P53 modulates the metabolism at different levels. It inhibits the PI3K-AKT-mTOR pathway by inducing PTEN and Parkin expression, it also promotes the expression and activation of different proteins that inhibit mTORC1 (AMPK, TSC1/2). Activation of p53 induces the degradation of HIF α through Parkin expression. Additionally, p53 represses (directly or indirectly) the expression of many enzymes and transporters of the glycolytic pathway such as hexokinase 2, PGAM1, GLUT (1, 3 and 4), and MTC1 among others. All these p53 activities lead to a decrease on the glycolytic flux. Additionally, p53 inhibits the PPP (by inhibiting G6PDH), the serine biosynthesis pathway (PHGDH inhibition), and lipid biosynthesis (through SREBP-1 downregulation and reduced NAPH synthesis). P53 participate in the maintenance of the oxidative phosphorylation machinery.

Additionally, p53 increases the TCA flux by inhibiting PDK2 (activation of PDH) and upregulating fatty acid oxidation and glutaminolysis. Interestingly, nucleotide biosynthesis can be activated or inhibited by p53 depending if the aim is to repair the DNA or induce cell cycle arrest (Franklin et al., 2016; P. Jiang et al., 2011; J. Liu et al., 2019; Matoba et al., 2006).

AMP activated protein kinase (AMPK)

AMP activated protein kinase senses low cellular ATP levels and by phosphorylating diverse proteins regulates the metabolism to increase ATP (increasing its production and inhibiting its consumption). When activated, AMPK inhibits multiple biosynthetic pathways. Active AMPK inhibits lipid synthesis at different levels: it inhibits ACC and HMG-CoA and at the transcriptional level it phosphorylates SREBP-1. It inhibits mTORC1 pathway by stabilizing TSC1/2 and by inhibiting the mTORC1 RAPTOR subunit. AMPK also inhibits gluconeogenesis. Additionally, AMPK activates a series of catabolic pathways to increase ATP production. It increases glycolytic flux by increasing GLUT1 and GLUT4 presence in the membrane and by phosphorylating PFKFB3 that regulates PFK1. AMPK activation also stimulates fatty acid oxidation. Furthermore, its activity phosphorylates transcription factors that regulate genes involved in the mitochondrial biogenesis, autophagy and lysosomal degradation (Bergeron et al., 2001; Carling et al., 1987; Herzig & Shaw, 2017; Y. Li et al., 2011; B. Xiao et al., 2011).

Cancer metabolism

Cells direct nutrients into metabolic pathways to maintain homeostasis and perform specific cell-type functions. Many of the basic cellular processes involved in the maintenance of homeostasis or needed for basic cellular functions (maintenance of ion gradients, transport processes, protein turnover, etc) are endergonic, and therefore coupled to ATP hydrolysis. To provide the energy necessary for these processes, cells rely on degradation of available nutrients. For instance, full oxidation of glucose to CO₂ and H₂O through the TCA cycle coupled to OXPHOS is a highly efficient way to generate the required ATP. Furthermore, it is one of the preferred sources of ATP production in non-proliferating cells. In addition to metabolically support the same housekeeping functions, proliferating cells (including cancer cells) need to generate all the building blocks necessary to duplicate the cell components and start the cellular division. Interestingly, many mitogenic signaling pathways overactivated in cancer -such as PI3K-AKT-mTOR and cMyc- lead to changes in metabolism to support cell proliferation (DeBerardinis, Lum, et al., 2008; Fritz & Fajas, 2010; Heiden et al., 2009; Heiden Vander et al., 2011; Mayers & vander Heiden, 2015; Tarrado-Castellarnau et al., 2016).

Furthermore, metabolic reprogramming can play an essential role in the acquisition of other cancer hallmarks and selective advantages such as immune evasion, metastatic potential, genetic instability, and drug resistance (C. H. Chang et al., 2015; Cruz-Bermúdez et al., 2019; Havas et al., 2017; Ho et al., 2015; Lahiguera et al., 2020; J. Lu, 2019).

Warburg effect

Alterations on several metabolic pathways in cancer cells have been described, but no one has received more attention than the differential metabolism of glucose. In the 1920s Otto Warburg observed that cancer cells consume higher amounts of glucose than nonproliferating cells. Moreover, Warburg noticed that cancer cells tend to “ferment” glucose to lactate even in the presence of oxygen instead of metabolizing it through the TCA cycle and OXPHOS (Warburg et al., 1927). This phenomenon is described as aerobic glycolysis or Warburg effect. Warburg firstly hypothesized that this phenomenon was due to mitochondrial defects (and therefore, impaired aerobic respiration) (Warburg, 1956). However, further research demonstrated that mitochondrial respiration is intact in most cancer cells and it is used for ATP production (L. B. Sullivan et al., 2015; Weinhouse, 1976; Zu & Guppy, 2004). Furthermore, inhibition of mitochondrial respiration suppresses tumor growth (Gui et al., 2016; Wheaton et al., 2014).

Accordingly, cancer cells metabolize most of the glucose through aerobic glycolysis secreting lactate instead of a most efficient oxidation through TCA and oxidative phosphorylation in terms of ATP production (2 ATP from aerobic glycolysis vs 36 ATP from OXPHOS) (Nelson & Cox, 2000). Inefficient ATP production seems to be a problem only when nutrients are scarce, and it is not the case of the irrigated areas of the tumor. Furthermore, the metabolic requirements of proliferating cancer cells go well beyond ATP, and these are also

justification for cancer cells to switch to a primarily glycolytic phenotype. Proliferating cells need to duplicate all the cellular contents prior to division, therefore, they have high requirements for building blocks (amino acids, lipids, and nucleotides). Biosynthesis of these building blocks has more requirements besides ATP (such as NADPH or carbons). For instance, the synthesis of palmitate requires 7 molecules of ATP, 14 molecules of NADPH and the carbons of 8 acetyl-CoA molecules. A glucose molecule can provide up to 36 ATP molecules if oxidized through the TCA cycle, more than 5 times the ATP required for the biosynthesis of a palmitate molecule. However, 7 molecules of glucose are needed to obtain the necessary NADPH through the PPP, and the necessary carbons, in form of acetyl-CoA, can be obtained from 3 glucose molecules. Similarly, the carbon and NADPH requirements for nucleotides and amino acid synthesis are higher than the requirements for ATP. Furthermore, glycolytic intermediates are precursors for anabolic pathways that contribute to nucleotide, amino acid, and lipid synthesis (Chaneton & Gottlieb, 2012; Heiden et al., 2009; Lunt & vander Heiden, 2011; Pavlova & Thompson, 2016).

Regeneration of NAD^+ is necessary to maintain the glycolytic flux, and to synthesize oxidized molecules such as nucleotides and amino acids. High ATP slows the mitochondrial regeneration of NAD^+ through OXPHOS. Interestingly, reduction of pyruvate to lactate through lactate dehydrogenase (LDH) regenerates NAD^+ allowing a continuous glycolytic flux (Luengo et al., 2021). The glycolytic flux may contribute to NADPH synthesis through the PPP and to feed biosynthetic pathways that use glycolytic intermediates as precursors (glycerol synthesis, glycosylation moieties synthesis, serine synthesis pathway, etc) (Hosios & vander Heiden, 2018).

The rapid uptake and consumption of glucose from the tumor microenvironment has also been shown to participate in the evasion of the immune system (Cassim & Pouyssegur, 2020). Low glucose availability, caused by its massive consumption by cancer cells, impairs the immunogenic activity of T cells (Ho et al., 2015). Furthermore, lactate secretion by tumor cells is capable to reduce the pH of the tumor microenvironment. This reduction of the pH undermines tumor immune response of T and NK cells (A. Brand et al., 2016; Husain et al., 2013). Similarly, lactate induces M2-like polarization of tumor resident macrophages which are associated to more aggressive tumor characteristics (they support angiogenesis, treatment resistance, and secretion of immunosuppressive molecules) (Colegio et al., 2014; Jayasingam et al., 2019).

Far from being just a waste product, lactate secreted by cancer cells undergoing aerobic glycolysis fuels the TCA cycle and other anabolic pathways in cancer cells with low glucose availability (Faubert et al., 2017; Leithner et al., 2014; Sonveaux et al., 2008). Lactate also promotes HIF1 α and VEGF secretion by tumor-associated endothelial cells (Sonveaux et al., 2012). Finally, lactate may also promote invasion through stimulating hyaluronic acid production by fibroblasts (Stern et al., 2002) and increasing the metalloproteinases activity by reducing pH (Rothberg et al., 2013).

During metastasis, cancer cells detach from the extracellular matrix (ECM) to migrate. The detachment from the ECM induces the production of ROS, which can lead to a type of cell death called anoikis, a barrier to metastasis. Switch to an aerobic glycolytic metabolism prevents the entry of carbons into mitochondrial respiration, which is the main source of ROS. In addition, glycolytic metabolism may promote the usage of PPP to produce NADPH to fight oxidative stress. Overall, the reduction of ROS levels prevents the induction of anoikis, supporting metastasis (K. A. Brand & Hermfisse, 1997; Kamarajugadda et al., 2012; J. Lu et al., 2015).

Increased glucose consumption in tumors led to the development of diagnosis tools such as ^{18}F -deoxyglucose positron emission tomography, which is used in the clinic for tumor diagnosis, staging, and monitoring the response to treatment (Almuhaideb et al., 2011).

Different transcription factors and signaling pathways have been described to promote the Warburg effect. HIF1 promotes the expression of glucose transporters (GLUT1 and GLUT3) and glycolytic enzymes such as PKM2, HK2, ALDA, ENOL, PGK1 and LDHA (Ebert et al., 1995; W. Luo et al., 2011; Masoud & Li, 2015; Semenza et al., 1994). Furthermore, HIF1 mediates the expression of PDK1 which inactivates PDH, blocking the entry of glycolytic carbons to the TCA cycle (J. W. Kim et al., 2006). The PI3K-AKT-mTOR pathway increases the expression of HK2 and the membrane expression of GLUT1 (Elstrom et al., 2004; Zhou et al., 2020; Zhuo et al., 2015). Furthermore, mTORC1 promotes the expression of transcription factors such as HIF1 α and cMyc that have an active role in the regulation of the glycolytic pathway (Laplante & Sabatini, 2012). Likewise, the oncogene cMyc promotes the expression of GLUT1, LDHA, ENO1, GAPDH, PFKM, HK2 and PKM2 (Goetzman & Prochownik, 2018; J. Kim et al., 2004; Osthus et al., 2000; Shim et al., 1997). Additionally, many cancers have mutations in p53, one of these mutations lead to TIGAR (TP53-induced glycolysis and apoptotic regulator) regulation and subsequent glycolysis activation (Bensaad et al., 2006).

TCA cycle & OXPHOS

Unlike Warburg initially postulated, mitochondrial metabolism is not impaired in cancer cells. While some tumors have a prominent oxidative phenotype (using high levels of oxidative phosphorylation), others show a high glycolytic phenotype. Nevertheless, the majority of ATP is still produced by oxidative phosphorylation (Fan et al., 2013; Zong et al., 2016; Zu & Guppy, 2004). In addition to provide ATP, OXPHOS regenerates NAD^+ (consuming NADH to pump protons across the membrane). NAD^+ is needed to catabolize reduced nutrients as well as for the synthesis of oxidized biomolecules. Furthermore, OXPHOS inhibition by metformin has showed to limit the NAD^+ regeneration impacting cell growth and tumorigenesis (Birsoy et al., 2015; Gui et al., 2016; Luengo et al., 2021; Wheaton et al., 2014).

The TCA cycle plays an important role in anabolism generating building blocks to feed biosynthetic pathways. Pyruvate from glycolysis (via pyruvate carboxylase) and glutamine (via glutaminase) are the two major

anaplerotic metabolites that replenish the TCA cycle when its intermediates are used for biosynthetic purposes (Sellers et al., 2015; Yuneva et al., 2007; Zong et al., 2016).

Many cancers have mutations in various TCA cycle enzymes. It is common in acute myeloid leukemia and gliomas to have mutations in isocitrate dehydrogenase 2 (IDH2) or the cytosolic isoform IDH1. Mutant IDH1 and 2 generate high amounts of the oncometabolite 2-hydroxyglutarate (2-HG). 2-HG is a reduced form of α -ketoglutarate and it is formed at low amounts in normal conditions. Normally, 2-HG is rapidly eliminated by specific dehydrogenases. However, in cells with mutated forms of IDH1/2 2-HG accumulates in the cell overwhelming the normal clearing mechanism. High levels of 2-HG alter gene expression by inhibiting α -ketoglutarate-dependent dioxygenases (including histone and DNA demethylases) (Chowdhury et al., 2011; Dang et al., 2016; D. Ye et al., 2018). Similarly, accumulation of succinate and fumarate - by loss of function mutations of succinate dehydrogenase (SDH) and fumarate hydratase (FH) - can also lead to altered gene expression by a similar mechanism than 2-HG (Dalla Pozza et al., 2020; Isaacs et al., 2005; Martínez-Reyes & Chandel, 2020; M. Xiao et al., 2012).

Moreover, mitochondrial metabolism generates reactive oxygen species (ROS), which might play an essential role during tumorigenesis (Aggarwal et al., 2019; Weinberg et al., 2010).

Glutamine metabolism

Glutamine is the most abundant amino acid in plasma, reaching concentrations up to 0.9 mM in this fluid (Bergstrom et al., 1974; Cynober, 2002). Although it is a non-essential amino acid, glutamine may turn essential in cancer cells where it is the second most consumed nutrient, only after glucose (Lacey & Wilmore, 1990).

Glutamine plays an important role in anaplerosis, replenishing the TCA cycle when its intermediates are used for biosynthetic purposes. Furthermore, it serves (together with glutamate) as the major nitrogen source for amino acid and nucleotide biosynthesis. In addition to these anabolic functions (providing both carbons and nitrogen for biosynthesis), glutamine participates in the production of ATP and NADPH (through malic enzyme) and contributes to glutathione metabolism (de Vitto et al., 2015; DeBerardinis, Sayed, et al., 2008; Deberardinis & Cheng, 2009; Hosios & vander Heiden, 2018; Kurmi & Haigis, 2020).

In fact, glutamine “addiction” in cancer cells is one of the main features of metabolic reprogramming. The main genes involved in glutamine metabolism are upregulated in cancer cells: there is increased expression of glutamine transporters (SCL1A5), glutaminase (GLS), glutamate dehydrogenase (GLUD) and transaminases (Scalise et al., 2017; Still & Yuneva, 2017). The oncogene c-Myc actively participates in the transcriptional program that stimulates glutaminolysis regulating GLS1, SLC1A5 among others (Bernfeld & Foster, 2019; W. Liu, Le, et al., 2012; Still & Yuneva, 2017; Wise et al., 2008). Furthermore, glutamine deprivation leads to apoptosis in cancer cells with activated c-Myc (Yuneva et al., 2007).

The inhibition of glutaminase by genetic and pharmacologic models blocks proliferation, migration and tumorigenicity in cancer cell lines and hinders tumor growth in xenograft models (Lampa et al., 2017; H. Y. Liu et al., 2021; Lobo et al., 2000; J. Zhang et al., 2019). Consistently, the potent glutaminase inhibitor telaglenastat (CB-839), which has shown antitumoral activity both *in vitro* and *in vivo* (Gross et al., 2014; Y. Zhao et al., 2020), is currently under clinical trial for different solid (colorectal, renal, NSCLC, etc) and hematologic (acute myeloid and lymphocytic leukemia, multiple myeloma, non-Hodgkin's lymphoma, etc) malignancies (Meric-Bernstam et al., 2019; US National Library of Medicine, 2022). Hence, the search for potent and specific glutaminase inhibitors for therapeutic purposes is an active field (E. Costa et al., 2021; C. R. Wu et al., 2018).

Serine synthesis pathway

Serine is a non-essential amino acid that is critical for the biosynthesis of many biomolecules. Serine is the precursor of the non-essential amino acids glycine and cysteine. Glycine is used for the synthesis of porphyrins, and together with cysteine are needed for glutathione biosynthesis essential for dealing with ROS. Serine is necessary for the synthesis of sphingolipids and phospholipids. Furthermore, the conversion of serine to glycine provides carbons to the one-carbon metabolism pathway (Labuschagne et al., 2014; Locasale, 2013; Mattaini et al., 2016; Nelson & Cox, 2000).

Although serine can be obtained from the environment, phosphoglycerate dehydrogenase (PHGDH) and the other enzymes of the serine synthesis pathway (SSP) - phosphoserine aminotransferase (PSAT) and phosphoserine phosphatase (PSPH) – are highly expressed in many cancers (Liao et al., 2019; Mattaini et al., 2016; Ravez, Spillier, et al., 2017). In fact, the expression of PHGDH, the first enzyme of this biosynthetic pathway, turns to be important for cancer progression (DeNicola et al., 2015; Possemato et al., 2011; Ravez, Corbet, et al., 2017; M. R. Sullivan, Mattaini, Dennstedt, Bosenberg, et al., 2019; M. R. Sullivan, Mattaini, Dennstedt, Nguyen, et al., 2019). Furthermore, PHGDH inhibition (or genetic depletion) significantly hinders tumor growth and cell survival, even when exogenous serine is available (Mullarky et al., 2016; Pacold et al., 2016). However, cancer cells dependence on SSP and the increased expression of its enzymes is not extended to all cancer types (Tajan et al., 2021). In addition, there is one study which showed that PHGDH knockdown did not affect tumor maintenance in different breast cancer models (J. Chen et al., 2013).

Different studies showed that dietary serine restriction can slow tumor growth and sensitize cancer cells to chemotherapy (Gravel et al., 2014; Maddocks et al., 2012, 2017; Muthusamy et al., 2020; Y. Shi et al., 2012). However, cancer cells can adapt to serine starvation by activating the flux towards the SSP. Serine is an allosteric activator of the M2 isoform of pyruvate kinase (PKM2), an isoform expressed in proliferating and cancer cells (Dayton et al., 2016). Therefore, when serine levels are low there is a decrease in PKM2 activity, which redirects part of the glycolytic flux towards the SSP (Chaneton et al., 2012; J. Ye et al., 2012). Additionally, serine starvation activates ATF4, which activates the transcription of the SSP enzymes (DeNicola

et al., 2015). In a similar manner, the activation of KRAS, c-Myc, MDM2, mTORC1, HIF1 α , or NRF2 leads to an increased expression of SSP enzymes (Ben-Sahra et al., 2016; DeNicola et al., 2015; Nilsson et al., 2012; Samanta et al., 2016). In contrast, p53 represses PHGDH expression (Y. Ou et al., 2015). Interestingly, cells with increased expression of SSP enzymes become resistant to exogenous serine starvation (Méndez-Lucas et al., 2020; M. R. Sullivan, Mattaini, Dennstedt, Nguyen, et al., 2019). Nevertheless, it has been shown that pharmacologic PHGDH inhibition increases the therapeutic effectivity of serine limited diet (Tajan et al., 2021).

One-carbon metabolism

One-carbon metabolism includes both the folate and the methionine cycles. It allows cells to generate and use one-carbon units (methyl groups) for biosynthetic purposes and methylation reactions (Newman & Maddocks, 2017). Many of the enzymes involved in these pathways have both mitochondrial and cytosolic isoforms. The function of some of these isoforms can be redundant (D. D. Anderson & Stover, 2009; Tibbetts & Appling, 2010).

Serine, together with other amino acids, are the major donors of one-carbon units into the one carbon metabolism pathways. During the conversion of serine to glycine, one carbon unit is transferred to tetrahydrofolate (THF) -which is synthesized from dietary folic acid and acts as a universal one-carbon acceptor- to generate methylene-THF. Then, this one-carbon unit can be used for the synthesis of purine and pyrimidine nucleotides through the folate cycle enzymes. Although the synthesis of THF from dietary folic acid consumes NADPH, methylene-THF can be oxidized to formyl-THF to generate NADPH (Hosios & vander Heiden, 2018; Labuschagne et al., 2014; Locasale, 2013; Newman & Maddocks, 2017; Tibbetts & Appling, 2010).

The methionine cycle allows to generate S-adenosylmethionine (SAM), which can be used as a universal methyl donor in methylation reaction. Once the methyl group is transferred from SAM to an acceptor molecule (for example DNA) during a methylation reaction, S-adenosylhomocysteine (SAH) is obtained. SAH can be recycled into the methionine cycle to homocysteine, which can be converted back to methionine and SAM with the donation of a methyl group from methyl-THF (obtained from methylene-THF by methylenetetrahydrofolate reductase). The methionine cycle can also provide cysteine, necessary for glutathione synthesis (Locasale, 2013; Newman & Maddocks, 2017; Tibbetts & Appling, 2010). Methylation of DNA and histones is of great importance to epigenetic regulation. For instance, hypermethylation of certain tumor suppressors genes can cause its loss of function (Greger et al., 1989; Kottakis et al., 2016; Kulis & Esteller, 2010; Roberti et al., 2021; Teperino et al., 2010).

Since its importance for nucleotide biosynthesis, REDOX maintenance (through glutathione and NADPH synthesis), and regulation of the methylation donor pool; one-carbon metabolism is vital for cancer cells. It

is not surprising then, that many antineoplastic drugs are targeting this pathway (Luengo et al., 2017; Newman & Maddocks, 2017). The antimetabolites methotrexate and pemetrexed both inhibit dihydrofolate reductase (DHFR), the enzyme that allows the reduction of folate (from the diet) and dihydrofolate to THF (Walling, 2006). Moreover, pemetrexed is also described to inhibit thymidylate synthase (TYMS) and SHMT (Daidone et al., 2011). Both antifolate molecules are still extensively used in anticancer therapy for a wide range of cancer types, including breast cancer, bladder cancer, lymphomas, and acute lymphoblastic leukemia among others (Chabner & Roberts, 2005; Luengo et al., 2017). The uracil analog 5-fluorouracil (5-FU) and its prodrug capecitabine inhibit TYMS blocking the formation of thymidine nucleotides for DNA synthesis. These compounds remain widely used in breast and diverse gastrointestinal cancers therapy (Heidelberger et al., 1957; Rudy & Senkowski, 2022; Wagner et al., 2006). Finally, the purine analogs 6-mercaptopurine and 6-thioguanine inhibit phosphoribosyl-1-pyro-phosphatase (PRPP) amidotransferase, the first enzyme in de novo purine biosynthesis (downstream this pathway accepts one carbons unit from 10-formyl THF). Both purine analogs have been successfully used in the clinic to treat different types of leukemia (Crowel et al., 2022; Elion, 1989).

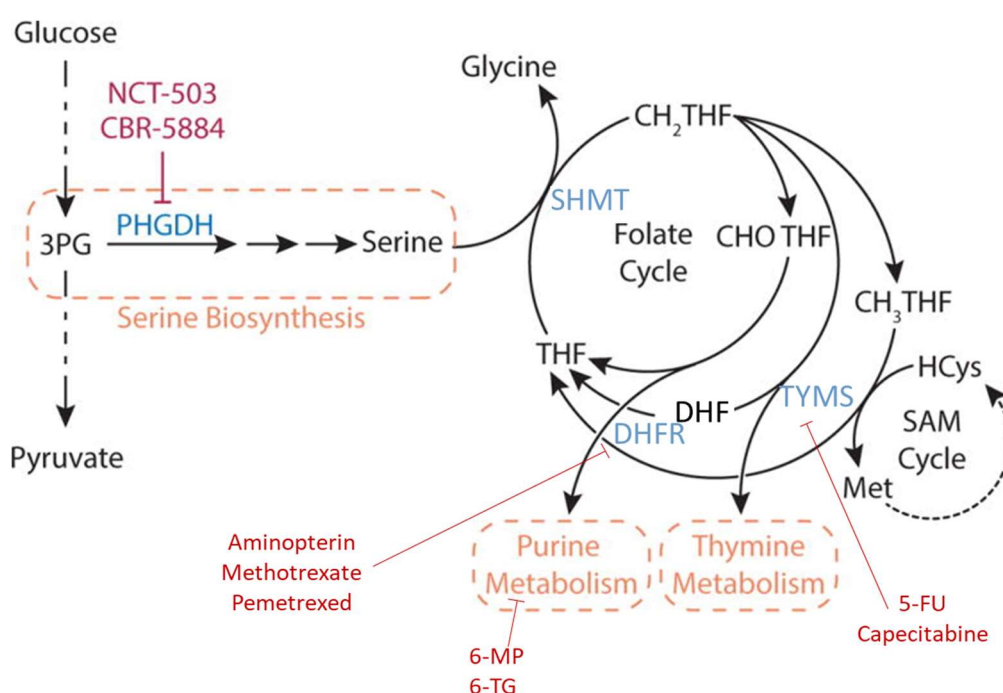


Figure I-8: Serine and one-carbon metabolism. During the conversion of serine to glycine, one carbon unit is transferred to tetrahydrofolate (THF) to generate methylene-THF. Then, this one-carbon unit can be used for purine and pyrimidine nucleotides synthesis, methylation reactions (through SAM regeneration), and NADPH generation through the folate cycle enzymes. Different antineoplastic drugs used in cancer therapy target this pathway as showed in red. Figure adapted from Luengo et al., 2017.

Lipid metabolism

Proliferating cancer cells have an increased need for lipids for cytoplasmic membrane formation during cell division. Cancer cells can obtain lipids through both biosynthesis and exogenous uptake. It has been observed

that different cancer types overexpress enzymes from the fatty acid synthesis pathway (such as ATP citrate lyase, ACLY, and fatty acid synthase, FASN), which are normally only expressed in the liver or proliferating tissues (Baenke et al., 2013; Khwairakpam et al., 2015; Koundouros & Poulogiannis, 2019; C. F. Li et al., 2017). On the other hand, lipids can be taken from the environment by different transporters. The best known are CD36 - also known as fatty acid translocase -, the fatty acid transport protein family (FATPs or SLC27) and plasma membrane fatty acid binding proteins (FABPpm). High expression of CD36 correlates with poor prognosis in several tumor types, including melanoma, ovarian, breast, gastric, and prostate cancer. Moreover, CD36⁺ cells have been shown to be potential metastatic initiating cells, and CD36 inhibition successfully impaired metastasis formation in different cancer models (Calvo et al., 1998; Koundouros & Poulogiannis, 2019; Ladanyi et al., 2018; Pascual et al., 2016; Watt et al., 2019). Additionally, the accumulation of fatty acids in lipid droplets can be used to maintain lipid homeostasis, avoid lipotoxicity, and as a source of ATP and NADPH (for ROS detoxification) during metabolic stress conditions. Interestingly, the uptake and accumulation of FA in lipid droplets is particularly relevant in hypoxic conditions, where the expression of FABP3 and FABP7 is induced by HIF1 α (Bensaad et al., 2014; Koundouros & Poulogiannis, 2019; Munir et al., 2019).

The composition of the plasmatic membrane determines its stability and physical properties, which can play an important role during cancer progression (Koundouros & Poulogiannis, 2019). De novo lipogenesis mainly generates saturated and monounsaturated fatty acids. Which are more stable than polyunsaturated because they have fewer double bonds susceptible to peroxidation. Therefore, an increase of fatty acid biosynthesis would lead to a higher proportion of saturated (and monounsaturated) fatty acids in the plasmatic membrane. Furthermore, cancer cells with higher saturated fatty acids in the membrane are more resistant to oxidative stress induced by chemotherapeutic drugs such as doxorubicin (Rysman et al., 2010). On the other hand, membranes with unsaturated fatty acids are more fluid. Similarly, membranes with low cholesterol content tend to be more fluid. Fluidity of the plasmatic membrane allows cells to modulate its shape, which is essential to EMT and intravasation and extravasation from blood vessels during the metastasis formation (Sok et al., 2002; W. Zhao et al., 2016). Nevertheless, rigid membranes due to high cholesterol (and saturated fatty acids) content are more impermeable to chemotherapeutic agents promoting drug resistance (Heilos et al., 2018). Increased cholesterol membrane concentrations support the formation of lipid rafts. Lipid rafts are microdomains of the plasmatic membrane with high cholesterol and saturated phospholipids which facilitate the accumulation tyrosine kinase receptors that would induce oncogenic signaling (George & Wu, 2012; Y. C. Li et al., 2006).

Lipids can further support cellular survival and proliferation playing an active role in signaling. Phosphatidylinositols can be phosphorylated and act as a secondary messenger in the PI3K-AKT-mTOR pathway (Cantley, 2002; Koundouros & Poulogiannis, 2019). Other important class of bioactive lipids are

eicosanoids. Eicosanoids are a large family of bioactive molecules generated through the metabolism of arachidonic acid by cyclooxygenase (COX), lipoxygenase (LOX) and P450 epoxygenase pathways. Many of them are implicated in inflammation and can contribute to cancer progression. Furthermore, inhibition of cyclooxygenase by non-steroidal anti-inflammatory drugs (NSAIDs) may be beneficial for cancer therapy (Mostafa et al., 2022; O'Malley et al., 2022; D. Wang & Dubois, 2010; Z. Zhang et al., 2018).

Metabolic diversity and plasticity

Metabolic reprogramming in cancer cells is tightly coordinated by different signaling pathways such as PI3K-AKT-mTOR, c-Myc, HIF1 α . Furthermore, lineage of the origin cell type, nutrient availability, and tumor microenvironment also play an important role defining the metabolism of cancer cells. Depending on the aforementioned variables, cancer cells can display a wide variety of metabolic phenotypes. The metabolic phenotype can define the aggressivity of the tumor, resistance to chemotherapy, and prognostic values. It can also uncover specific vulnerabilities that can be pharmacologically targeted (Iurlaro et al., 2014; Luengo et al., 2017; Mayers & vander Heiden, 2017; Pavlova & Thompson, 2016; vander Heiden & DeBerardinis, 2017).

For example, 40% of diffuse large B cell lymphoma (DLBCL) patients do not respond to the first line therapy: a combination of rituximab, cyclophosphamide, doxorubicin, vincristine, and prednisone (R-CHOP). Interestingly, the metabolic phenotype of DLBCL cells showed to have a prognosis value: the patients with DLBCL cells that had an "oxidative" phenotype (GAPDH-low) had worst prognosis and R-CHOP response than the patients with DLBCL cells with a "glycolytic" phenotype (GAPDH-high). The treatment with OXPPOS (metformin), glutaminolysis (L-asparaginase), and mTORC1 inhibitors (KTM) to R-CHOP refractory GAPDH-low DLBCL patients successfully improved the therapeutic outcome. 75% of these patients showed complete response after one cycle of KTM (Caro et al., 2012; Chiche et al., 2019; Sehn & Gascoyne, 2015).

Interestingly, metabolic heterogeneity is found inside the tumor (Patel et al., 2014). In solid tumors, it is common to have different oxygen and nutrients concentration among the different areas of the tumor. This is caused mainly by a deficient vasculature due erratic angiogenesis and high nutrient consumption. In consequence, it is common to find areas of the tumor with lower oxygen and nutrient concentrations. Cancer cells are able to survive in nutrient limitation conditions thanks to their great metabolic plasticity (DeBerardinis & Chandel, 2016; Mayers & vander Heiden, 2015; Pavlova & Thompson, 2016).

Cancer cells can use opportunistic modes of nutrient acquisition to survive during nutrient limitation: they can obtain amino acids from the digestion of extracellular proteins internalized by micropinocytosis (Commisso et al., 2013; Kamphorst et al., 2015). In a similar manner, nutrients can be obtained from the digestion of phagocytosed apoptotic bodies (Stolzinger & Grune, 2004). Furthermore, cells can engulf and digest neighbor cells to obtain nutrients in a process named entosis (Durgan & Florey, 2018; Overholtzer et al.,

2007). All these processes are stimulated by KRAS activation and mTORC1 repression (Overholtzer et al., 2007; Palm et al., 2015). Cells can also obtain the metabolic intermediates that they need to survive by recycling macromolecules through autophagy (DeBerardinis & Chandel, 2016; Kimmelman & White, 2017).

Different cell populations in the tumor microenvironment cooperate to take advantage of the metabolic heterogeneity and overcome nutrient limitation (Mayers & vander Heiden, 2015; M. R. Sullivan & vander Heiden, 2019). For example, lactate released by the most glycolytic cells (Warburg phenotype) can be used as a fuel for OXPHOS and cataplerosis by the cells with a “more oxidative” phenotype (Feron, 2009; Guillaumond et al., 2013; Montal et al., 2019a; Sonveaux et al., 2008). Similarly, it has been described that cancer associated fibroblasts can acquire a Warburg phenotype and secrete lactate that can be used by cancer cells (Pavlidis et al., 2009). In ovarian cancer, cancer cells can use fatty acids provided by visceral adipocytes (Ladanyi et al., 2018).

Phosphoenolpyruvate carboxykinase (PEPCK)

Phosphoenolpyruvate carboxykinase (PEPCK) is the enzyme that catalyzes the GTP-dependent reversible decarboxylation of oxalacetate (OAA) to phosphoenolpyruvate. To take place, the reaction requires bivalent metal ions (magnesium or manganese). The PEPCK reaction allows the cell to bypass the last irreversible step from glycolysis, allowing gluconeogenesis to take place. Furthermore, it is the only reaction that connects the TCA cycle with glycolytic intermediates above pyruvate (H. C. Chang & Lane, 1966; Z. H. Chen et al., 2002; Escós et al., 2016a; Lee et al., 1981; Nordlie & Lardy, 1963; Yu et al., 2021).

In eukaryotes, PEPCK activity is distributed between two very similar isoenzymes: a cytosolic (PEPCK-C) and a mitochondrial one (PEPCK-M). Both, PEPCK-C and PEPCK-M are encoded by nuclear genes, PCK1 and PCK2 respectively. Although both isoenzymes are almost identical and catalyze the same reaction with similar kinetic properties, they are differentially regulated and expressed (Hanson & Patel, 1994; Méndez-Lucas et al., 2014a; Yu et al., 2021).

Interestingly, the distribution of PEPCK isoforms varies in different animal species. While most of the studied species (human, cows, dogs, cats, sheep) present similar activity of both isoforms in the liver; the cytosolic isoform accounts for almost all the PEPCK activity – between 90 and 99% - in rats, hamsters, and mice. On the other hand, PEPCK-C activity in rabbits represents only the 10% of the total hepatic PEPCK activity. Furthermore, some bird species (i.e. chicken and pigeon) only express the PEPCK-M isoform in their livers after hatching (Nordlie & Lardy, 1963; Söling et al., 1973; J. Yang et al., 2009).

PEPCK-C

PEPCK-C is highly expressed in gluconeogenic and glyceroneogenic tissues such as the liver, kidneys, adipose tissue, and small intestine. PEPCK-C expression is regulated by diet and hormones (insulin, glucagon, and glucocorticoids) and its main function is glucose homeostasis. Fasting induces PEPCK-C expression via transactivation of its promoter in response to cAMP, glucocorticoids, and thyroid hormone. In the other hand insulin represses PCK1 transcription (Hanson & Reshef, 1997; Yu et al., 2021). In addition, PPAR- γ , c-Jun/c-Fos-binding element, SREBP-1, nuclear factor 1, and retinoic acid response element have been described to regulate PCK1 expression (Chakravarty et al., 2004; Devine et al., 1999; Fos et al., 1992; Hall et al., 1992; Leahy et al., 1999). Half-life of PEPCK-C in the liver is about 6-8 h while its mRNA half-life is 30-60 min (Hopgood et al., 1973; Tilghman et al., 1974). In addition to this short half-life, the absence of allosteric regulators, suggests that the enzyme is regulated by transcription/degradation rate and substrate concentrations. Furthermore, it has been described that PEPCK-C degradation can be regulated by acetylation in three lysine residues (Beale et al., 2007; W. Jiang et al., 2011; Y. yi Lin et al., 2009; Y. Xiong et al., 2011).

PEPCK-C plays a major role in glucose homeostasis. As mentioned above, PEPCK-C mediates the first rate-limiting gluconeogenic reaction. PCK1 whole body knockout caused hypoglycemia in a murine model, furthermore, the animals died 2-3 days after birth (Hakimi et al., 2005; She et al., 2000). Early postnatal expression of PCK1 in the liver by adenovirus administration in PCK1-KO pups partially rescued the hypoglycemia allowing its survival (Semakova et al., 2017). Oddly, PCK1 liver-specific knockout mice were euglycemic. However, these animals developed liver steatosis as a result of impaired cataplerosis and subsequent TCA cycle flux reduction (Beale et al., 2007; Burgess et al., 2004; She et al., 2000, 2003). Coherently, PCK1 overexpression led to hyperglycemia, hyperinsulinemia, and insulin resistance in mice (Valera et al., 1994). The kidneys and small intestine have also been described as gluconeogenic tissues, with a smaller contribution to glucose homeostasis than the liver (Mithieux et al., 2004; Schoolwerth et al., 1988).

Triglycerides (TG) constitute a major lipid storage and important energy source. TG are formed by three fatty acids and a glycerol molecule. Glyceroneogenesis is the synthesis of the glycerol moiety of TG from pyruvate, glutamine, or any TCA intermediate. Glyceroneogenesis mainly takes place in the liver and adipose tissue, and it importantly contributes to the plasmatic TG concentration (Kalhan et al., 2001). Adipose-specific PCK1 knockout coursed with reduced TG storage in adipose tissue in a murine model. Moreover, some of the mice showed lipodystrophy and slight hyperglycemia (Olswang et al., 2002). In contrast, PCK1 overexpression in adipose tissue leads to obesity in mice. Interestingly, these animals were euglycemic and did not show symptoms of metabolic syndrome (Franckhauser et al., 2002). However, they develop severe insulin resistance (and type 2 diabetes) if fed with high-fat diet (Franckhauser et al., 2006). In a similar manner, cytosolic PEPCK plays a role in the mammary gland during lactation, it contributes to lipid synthesis (the major component of milk besides water) through glyceroneogenesis (Bobrovnikova-Marjon et al., 2008; Hsieh et al., 2009).

In addition, PEPCK-C activity is also important for glyceroneogenesis in the skeletal muscle. Glyceroneogenesis is the principal contributor of TG production in skeletal muscle (Nye et al., 2008). Skeletal muscle-specific overexpression of PCK1 increased the intramuscular fat content and reduced the subcutaneous and visceral adipose tissue depots. Interestingly, the overexpression of PCK1 had a significative impact in physical activity: mice overexpressing PCK1 in the skeletal muscle could run 5 km at 20 m/min without stopping while control mice could run 0.2 km at this speed. The muscle of these mice showed an increased oxidative metabolism and mitochondrial biogenesis. Furthermore, plasmatic insulin and leptin concentrations were lower than control mice and the lifespan and reproductive capacity were extended (Hanson & Hakimi, 2008). Interestingly, the phenotype observed in these mice caught the attention of the alimentary sector where high intramuscular fat is recognized as a quality trait in pork (Ren et al., 2017).

Surprisingly, Xu et al. recently reported that PCK1 might have a kinase activity. Phosphorylated PCK1 (by AKT) would translocate to the endoplasmic reticulum where it would phosphorylate INSIG1 and INSIG2. This

phosphorylation would disrupt the interaction with sterols and SCAP, leading to the activation of SREBP and posterior transcription of lipogenesis-related genes (increasing tumorigenesis) (D. Xu et al., 2020).

PEPCK-M

Despite PEPCK-M was firstly discovered and it was used to elucidate the gluconeogenic pathway by Utter and Kurahashi, the metabolic role of PEPCK-M in mammals has been less studied (Stark & Kibbey, 2014; Utter & Kurahashi, 1953). In contrast with the cytosolic isoform, PEPCK-M is expressed in gluconeogenic (liver, kidney, small intestine) and non-gluconeogenic tissues such as pancreatic β -cells, heart, skeletal muscle, neurons, immune cells (T and B-cells), fibroblasts, and undifferentiated cells like embryonic stem cells, different progenitors, and cancer cells (Alvarez et al., 2016; Brearley et al., 2020; Brown et al., 2016; Z. Li et al., 2019; H. Ma et al., 2019; Méndez-Lucas et al., 2013; Stark et al., 2009; Yu et al., 2021). Unlike PCK1, PCK2 expression is not regulated by diet and hormones (Modaressi et al., 1998). Our laboratory showed that PCK2 is transcriptional regulated by ATF4, the master regulator of ER and amino acid stress response pathways. PEPCK-M was upregulated by effectors of this pathway by recruiting ATF4 to a consensus AARE site located at the PEPCK-M proximal promoter (Méndez-Lucas et al., 2014a). Additionally, PEPCK-M protein is more stable than the cytosolic isoform, with a half-life beyond 50 h (Hanson & Patel, 1994).

In human liver, mitochondrial PEPCK is expressed in a similar proportion than the cytosolic isoform. However, its role in gluconeogenesis has not been completely elucidated. It is hypothesized that PEPCK-M would participate in gluconeogenesis as observed in birds. Additionally, it could present metabolic advantages with respect to PEPCK-C pathway because it does not need to shuttle OAA and reducing equivalents (malate shuttling) from the mitochondria to the cytosol (Arinze et al., 1973; Gamble & Mazur, 1967; Hanson & Reshef, 1997; Stark & Kibbey, 2014). The expression of PCK2 in the liver of mice where PCK1 has been depleted – unlike human, mouse liver expresses almost exclusively the cytosolic isoform - partially rescued the defects in gluconeogenesis, TCA cycle, and lipid metabolism. In addition, when PEPCK-M was expressed in the presence of PEPCK-C, the gluconeogenic capacity was amplified (Méndez-Lucas et al., 2013). Consequently, this evidence suggest that PEPCK-M might have an important role in gluconeogenesis in humans.

In addition to the possible gluconeogenic role, PEPCK-M contributes to glucose homeostasis by modulating insulin secretion in pancreatic β -cells. PEPCK-M together with pyruvate kinase (PK) and PC, constitute the PEP cycle. In this cycle, PEP from glycolysis is converted to pyruvate by PK which can enter to the TCA cycle in form of OAA by the PC reaction. This OAA can be converted back to PEP by PEPCK-M, note that during this last reaction mitochondrial GTP (mt-GTP) is consumed. Unlike ATP, GTP transport between mitochondria and cytosol is very slow. Therefore, it might be used as a rheostat of mitochondrial metabolism (it is formed by the TCA cycle enzyme succinyl CoA synthetase). Hypothetically, the PEP cycle allows the recycling of mt-GTP and the coupling of the TCA cycle activity with glucose stimulated insulin secretion (GSIS) in β -cells (Kibbey et al., 2007). Silencing of PEPCK-M blunted GSIS in rat insulinoma INS1 cells (Stark et al., 2009). In a similar

manner, impaired insulin secretion and elevated plasmatic glucose during fasting was observed in PCK2 knockout mice (Abulizi et al., 2020a). The PEP cycle would accelerate the TCA cycle by regenerating mt-GDP, necessary for the succinyl CoA synthetase reaction. Furthermore, it would allow to export the mt-GTP energy to the cytosol as ATP in brown adipose tissue (Drahota et al., 1983; Stark & Kibbey, 2014).

PEPCK-M is expressed in undifferentiated cells, and it might be important for embryogenesis and development. Mice liver expresses almost exclusively the cytosolic isoform, however the mitochondrial isoform is preferentially expressed during fetal development (Hanson & Patel, 1994). Interestingly, neural progenitors, which are dependent on lactate metabolism, depend on PEPCK-M activity to support anabolic functions and maintain their progenitor phenotype (Alvarez et al., 2016).

Furthermore, it has been observed that PEPCK-M is overexpressed in several human tumors (including breast, prostate, thyroid, lung, colorectal, gastric, cervix, bladder, and pancreatic cancers among others) and cancer cell lines (Figure I-9) (Chu et al., 2017; Fernández-Coto et al., 2018a; Y. Hu et al., 2020; Leithner et al., 2015; N. Li et al., 2018; S. Luo et al., 2017; Smolle, Leko, Stacher-Priehse, et al., 2020; Vincent et al., 2015; J. Zhao et al., 2017a). Expression of PEPCK-M in cancer cells has been proposed to provide a selective growth advantage through cataplerosis and biosynthetic processes, especially in glucose scarcity. As mentioned before, nutrient limitation and ER stress inducers activate the unfolded protein response (UPR) and amino acid response (AAR) which increase ATF4 expression. ATF4 directly up-regulates PCK2 transcription by binding to its promoter. Consistently, knocking-down PEPCK-M in human breast carcinoma cells (MCF7) under stress tips the balance of the cell towards apoptosis whereas overexpressing PEPCK-M enhanced cell survival (Méndez-Lucas et al., 2014b). The importance of chronic ER-stress to induce adaptive responses in cancer cells *in vivo* suggested that the pathway is crucial to cancer cell metabolism and progression. In the same line, different investigators observed that PEPCK-M was crucial for survival and proliferation of lung cancer cells under glucose deprivation. PEPCK-M enabled the utilization of carbons from glutamine and lactate to synthesize glycolytic intermediates necessary for biosynthetic processes such as serine and glycine biosynthesis, and one carbon metabolism. In this context, PEPCK-M not only increased cell survival under glucose-limited conditions but also enabled glucose-independent proliferation. PEPCK-M inhibition or silencing with siRNA or shRNA significantly impair cell survival and proliferation in these conditions (Leithner et al., 2015; Vincent et al., 2015). Similarly, Montal et al. showed that PEPCK was overexpressed in colorectal cancer. They demonstrate that PEPCK promoted tumor growth by increasing anabolism (via cataplerosis), and glutamine and glucose metabolism. Although their observations implicated the cytosolic isoform, they might contribute to clarify the role of PEPCK activity in cancer (Montal et al., 2015). PCK2 silencing in pancreatic neuroendocrine tumors inhibited its proliferation and sensitized it to treatment with mTOR inhibitors such as everolimus and sunitinib (Chu et al., 2017). Overall, PEPCK-M plays an important role during cancer progression which place it as a potential emerging target for cancer treatment.

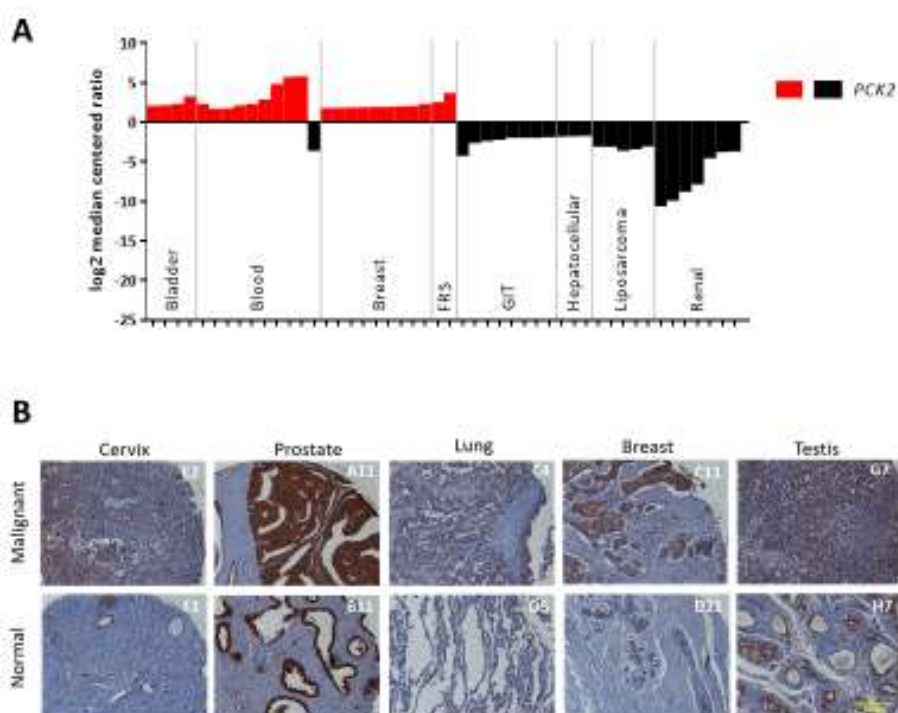


Figure I-9: PEPCK-M is the PEPCK isoform preferentially expressed in tumors of diverse origin. (A) PCK1 and PCK2 expression in tumors from various tissues (FRS stands for female reproductive system, and GIT stands for gastro-intestinal). Graphical representation of log₂ median-centered ratio of PCK1 (empty bars) and PCK2 (solid bars) present in each dataset analyzed using Oncomine at oncomine.org (analysis type: cancer versus normal, threshold at $P = 1E-5$ and top gene rank 10%). Red or black colored boxes represent overexpressed or under-expressed for each dataset, respectively. Missing values for PCK1 expression were not significant or were not present in dataset. **(B)** Immunohistochemical analysis of PEPCK-M expression in selected types of tumors and their matched non-neoplastic tissue microarray BCN962 (US Biomax). Tissue was briefly counterstained with hematoxylin. Scale bar = 200 μ m. Figure from Hyroššová et al., 2021.

It is important to note that PEPCK activity might not only participate gluconeogenesis, but especially in countless pathways that branch out of the glycolytic pathway (serine/glycine synthesis and 1-carbon metabolism pathways, glyceroneogenesis, PPP from F6P, PEP cycling, protein glycosyl moiety formation from F6P, etc.) as discussed above, and therefore the concept of “incomplete” gluconeogenesis might provide a better framework for the current understanding of the pathway in the metabolic adaptations required for cancer progression, and the need for developing novel pharmaceuticals to target this crossroads activity (Figure I-10).

Interestingly, well differentiated tumors originated in gluconeogenic tissues - such as liver and kidney – where PEPCK-C enzyme activity is not lost, PEPCK isozymes could act as tumor suppressors. In these instances, PEPCK might induce cataplerosis to generate glucose, inhibiting both glycolysis and TCA cycle, and causing an energetic crisis (Grasmann et al., 2019; M. X. Liu et al., 2018; H. Shi et al., 2016; Tang et al., 2018).

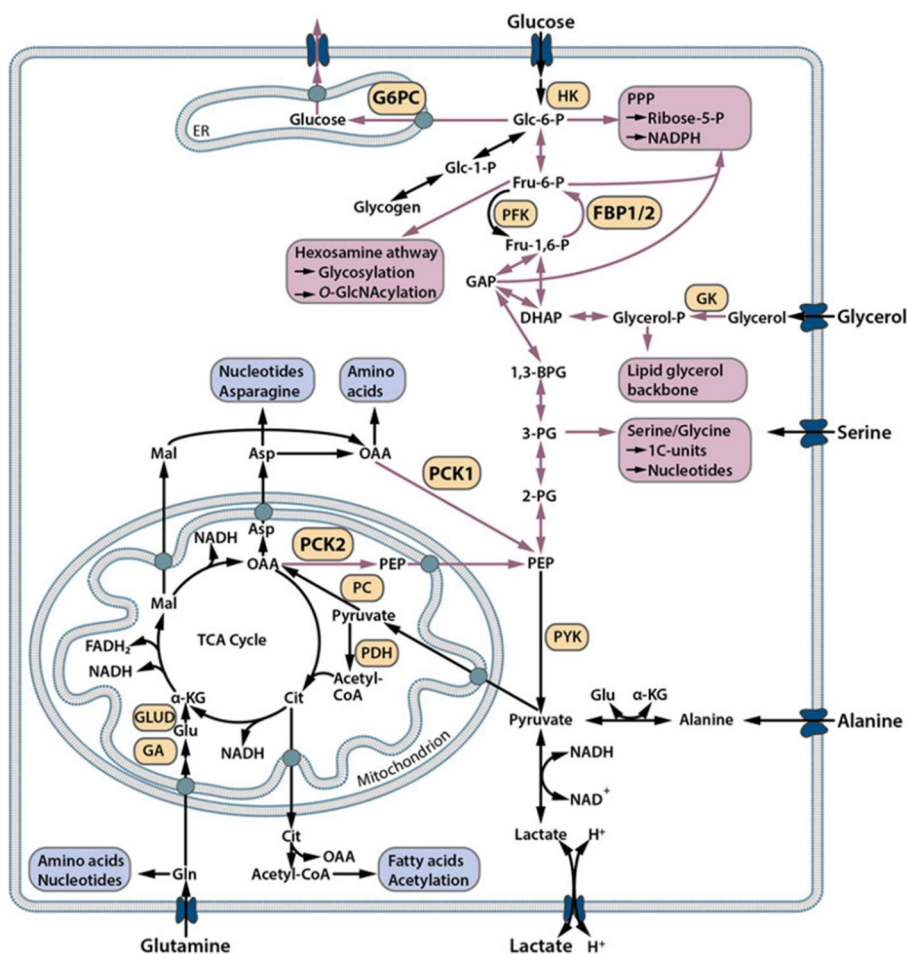


Figure I-10: Gluconeogenesis/glycolysis and branching biosynthetic pathways. Phosphoenolpyruvate carboxykinase isoforms (PCK1 & PCK2), mediate the initial step of gluconeogenesis and link the TCA cycle with the glycolytic pool. Further steps in gluconeogenesis (red arrows) are mediated by bi-directional enzymes and fructose-1,6-bisphosphatase (FBPase) and glucose-6-phosphatase (G6PC). “Incomplete” gluconeogenesis allows the synthesis of cellular building blocks from non-carbohydrate precursors (red boxes) and requires the action of PCK1/2 and to some extent also FBP1/2. Biosynthetic pathways independent of gluconeogenesis are depicted in blue. Figure from Grasmann et al., 2019.

PEPCK inhibitors

3-Mercaptopicolinic acid (3-MPA) was described to inhibit gluconeogenesis in rat liver and kidneys in 1973 (DiTullio et al., 1974). A couple years later, it was found that the gluconeogenesis inhibition by 3-MPA was through PEPCK inhibition (Jomain-Baum et al., 1976). It was able to inhibit both cytosolic and mitochondrial isoforms. However, at low concentrations it showed to be more selective for the cytosolic isoform, probably due to low mitochondrial permeability (Robinson & Oei, 1975). The mechanism of action of 3-MPA has been recently elucidated. Balan et al propose that 3-MPA would inhibit PEPCK by its binding in two different binding sites: an allosteric one that would reduce the affinity for GTP; and a binding site in the catalytic center where it would compete with PEP/OAA (Balan et al., 2015). In 2015, Leithner et al. successfully inhibited PEPCK-M with 3-MPA in lung cancer cells and spheroids, achieving a reduction in cell growth and viability (Leithner et al., 2015). However, its low inhibition potency ($K_i \approx 150\mu\text{M}$), modest mitochondrial membrane

permeability, and poor selectivity – it was also reported to inhibit glucose 6-phosphatase – render unfeasible to consider 3-MPA for a therapeutic approach (Foster et al., 1994).

At the beginning of the century, PEPCK was a promising target for type 2 diabetes. Its essential role in the gluconeogenesis in addition to diverse overexpression PEPCK models (which display hyperglycemia), had placed PEPCK as a promising target for lowering glycemia (Gómez-Valadés et al., 2008; Rosella et al., 1995; Valera et al., 1994). In this context, multiple inhibitors were developed. Among them, a family of 3-alkyl-1,8-dibenzylxanthines developed by Hoffmann-La Roche stood out for its potency in the nanomolar range. These compounds were reported as the first non-substrate like GTP-competitive inhibitors for PEPCK-C (Foley et al., 2003a, 2003b; Pietranico et al., 2007). This family of compounds was patented but it was abandoned after a few years. Other inhibitors have been described, including substrate analog inhibitors (Hidalgo et al., 2016; Stiffin et al., 2008). However, the inhibitory capacity of the newly developed PEPCK-C inhibitors was not tested in PEPCK-M.

Proline metabolism

Proline is a non-essential amino acid with a unique structural feature: it is the only proteogenic amino acid that has a secondary amine instead of a primary amine. The pyrrolidine ring gives proline a conformational rigidity which turns to have a unique role in the formation of secondary structures. Proline is essential for collagen production, the principal component of the extracellular matrix (ECM). Besides protein synthesis, proline plays important roles in different biological processes such as redox and energetic homeostasis, stress protection and apoptosis. Furthermore, proline metabolism has been described to support cancer progression (D'Aniello et al., 2020; Geng et al., 2021; Krishnan et al., 2008; W. Liu, Le, et al., 2012; Y. Liu et al., 2005; Natarajan et al., 2012; Nelson & Cox, 2000; Phang, 1985; Tanner et al., 2018; Vettore et al., 2021).

Proline can be synthesized from glutamate or ornithine. The first step consists in the formation of glutamate- γ -semialdehyde (GSAL) which can be catalyzed by Δ -1-pyrroline-5-carboxylate synthase (P5CS, encoded by ALDH18A1 gene) from glutamate, or by ornithine aminotransferase (OAT) from ornithine. GSAL spontaneously cycles forming Δ -1-pyrroline-5-carboxylate (P5C) losing one water molecule. Finally, the last step is the reduction of P5C to L-proline, which is catalyzed by pyrroline-5-carboxylate reductase (PYCR). In proline catabolism, proline can be converted back to P5C by proline dehydrogenase/oxidase (PRODH/POX). Then P5C can be metabolized by P5C dehydrogenase (P5CDH) to glutamate or by OAT to ornithine (D'Aniello et al., 2020; Geng et al., 2021; Tanner, 2019).

A ribosome profiling approach used to identify metabolic vulnerabilities in tumors revealed that kidney cancer cells had higher proline requirements than non-tumoral cells. Breast cancer cells also showed an increased requirement for proline, raising the possibility that it may be a common feature of different tumor types (Loayza-Puch et al., 2016). This hypothesis was supported by the fact that many cancer types overexpress proline biosynthetic enzymes (D'Aniello et al., 2020; W. Liu et al., 2015). Interestingly, significant increases in proline concentration in embryonic stem cells activate a phenotype transition similar to the EMT that occurs in cancer cells during the metastatic formation (D'Aniello et al., 2015). Moreover, several studies correlate extracellular proline uptake (from collagen during ECM remodeling) and increased proline biosynthesis with metastasis formation and tumor aggressivity (D'Aniello et al., 2020; Geng et al., 2021).

Collagen is the principal component of the extracellular matrix, and about 25% of collagen amino acids are proline. Half of the collagen proline is hydroxylated by prolyl-4-hydroxylases (P4Hs) in the endoplasmic reticulum. Proline hydroxylation is essential for the stabilization of the triple helix of collagens (D'Aniello et al., 2020). Accumulation of collagen near tumors has been associated with metastasis formation (S. Xu et al., 2019). Interestingly, overexpression of P4Hs promotes cancer progression (proliferation, invasion and metastasis) and correlates with poor prognosis in different cancer types, including melanoma, glioma, B-cell lymphoma, cervix, and breast cancer (Gilkes et al., 2013; W. Jiang et al., 2018; Q. Li et al., 2019; J. Lin et al.,

2020; G. Xiong et al., 2014). Consistently, PH4 silencing or inhibition reduced tumor aggressiveness (G. Xiong et al., 2014). Different pathways control collagen synthesis and deposition, for example TGF β increases proline biosynthesis to support collagen production and deposition. Collagen can modify ECM properties, for example it increases ECM stiffness which promotes EMT and metastatic dissemination (Pankova et al., 2019; Schwörer et al., 2020). Collagen can also modulate signaling pathways by binding to specific receptors (S. Xu et al., 2019). Moreover, collagen can act as a proline storage which can be released during ECM remodeling by metalloproteinases in the tumor microenvironment (Olivares et al., 2017; Phang et al., 2010).

Proline catabolism

The oxidation of proline to P5C by PRODH is coupled to the electron transport chain via reduction of membrane-bound ubiquinone or coenzyme Q. Therefore, the first step of proline metabolism contributes to ATP production. However, it also contributes to ROS production (Donald et al., 2001; Tanner, 2019). Further oxidation by P5CDH provides glutamate which can enter to the TCA cycle as α -KG (anaplerosis).

Proline oxidation by PRODH contributes to ATP synthesis as well as anaplerosis but generates ROS which can decrease cell survival. Therefore, PRODH has been described to have anti- and pro- tumoral effects (D'Aniello et al., 2020; Geng et al., 2021; Huynh et al., 2020). For example, in colorectal cancer, PRODH-dependent ROS generation induced apoptosis and autophagy. Moreover, proline has antioxidant properties and protect cells from ROS. PRODH activity decrease proline levels reducing its antioxidant protection and amplifying ROS effects (Krishnan et al., 2008; Wondrak et al., 2005). Overexpression of PRODH reduced DNA synthesis blocking the cell cycle and reduced HIF signaling by increasing α -KG concentrations (Donald et al., 2001; Krishnan et al., 2008; Y. Liu et al., 2006, 2008, 2009). On the other hand, proline catabolism by PRODH increased survival and proliferation of different cancer cells under nutritional and oxidative stress (Natarajan et al., 2012; Olivares et al., 2017; Pandhare et al., 2009). It also improved survival of cancer cells under hypoxic conditions (W. Liu, Glunde, et al., 2012). Furthermore, in breast and lung cancer, PRODH has been described to promote migration, invasion and metastasis formation by inducing EMT (Elia et al., 2017; Y. Liu et al., 2020). Interestingly, PRODH expression is induced by p53, PPAR γ and AMPK and repressed by Myc (Geng et al., 2021). Summarizing, the role of PRODH in cancer may be dependent on tumor environment and cancer type.

Proline biosynthesis

The expression of proline biosynthetic genes (ALDH18A1 and PYCR) is promoted by c-Myc, TGF β and PI3K-AKT signaling (Craze et al., 2017; W. Liu, Le, et al., 2012; Schwörer et al., 2020). In a similar manner, it has been described that myeloid zinc finger 1 (MZF1) promotes the transcription of ALDH18A1 and PYCR1 by interacting with PARP1 and E2F1 in neuroblastoma. Interestingly the inhibition of this pathway with small peptides suppressed proline synthesis and tumorigenesis (Fang et al., 2019). In 2015 D'Aniello et al.

described a regulation loop of proline biosynthetic enzymes by the amino acid starvation response (AAR). They described that a decrease in the intracellular proline levels courses with unloaded tRNA. Then, unloaded tRNA bind Gcn2 which activates by phosphorylation the transcription factor Eif2 α increasing ATF4 transcription. ATF4 promotes the transcription of proline biosynthesis genes (ALDH18A1 and PYCR1) and amino acid transporters. Consequently, an increase of intracellular proline inhibited this pathway (D'aniello et al., 2015). In contrast with proline catabolism, proline biosynthesis has been described to protect the cells against oxidative stress (Kuo et al., 2016).

Expression of proline biosynthesis pathway enzymes correlates with poor prognosis in cancer. It has been described that P5CS and PYCR are upregulated in different tumor types compared with the surrounding non-pathological tissue. Furthermore, its high expression correlates with advanced tumor grade, aggressive phenotype (more metastasis), resistance to chemotherapy, and poor overall survival in hepatocellular (Z. Ding et al., 2020) and renal carcinoma (Weijin et al., 2019), lung (Cai et al., 2018; D. Wang et al., 2019), breast (J. Ding et al., 2017; Shenoy et al., 2020), bladder (Du et al., 2021), colorectal (Yan et al., 2019), and gastric cancer (S. Xiao et al., 2020).

In melanoma, where proline synthesis is upregulated, P5CS silencing reduced proliferation, viability, and tumor growth in xenograft models by inhibiting protein synthesis via GCN2 activation (Kardos et al., 2015). In addition, P5CS knock-out increases cancer cells sensitivity to lipogenesis inhibition impairing tumor growth *in vivo* (M. Liu et al., 2020).

Interestingly, there is strong evidence that the enzyme catalyzing the last step of proline biosynthesis has an active role in cancer progression and is emerging as a novel target for cancer therapy.

Pyrroline-5-carboxylate reductase (PYCR) (EC 1.5.1.2) catalyzes the NAD(P)H-dependent reduction of P5C to L-proline. In humans PYCR activity is distributed into three isoenzymes: PYCR1, PYCR2, and PYCRL (also known as PYCR3), encoded by different genes located in different chromosomes. Sequence alignment showed that PYCR1 and PYCR2 had 84.9 % identity, while PYCR1 and PYCRL (which is 40 amino acids shorter) had 45.1 % identity. Both, PYCR1 and PYCR2 are localized in the mitochondria preferentially catalyzing the formation of proline through glutamate using NADH as a cofactor. On the other hand, PYCRL is mainly localized in the cytoplasm and principally participates in the proline synthesis from ornithine using NADPH as a cofactor. Interestingly, PYCR1 and PYCR2 are inhibited by high proline concentrations in contrast with PYCRL (de Ingeniis et al., 2012; C. A. A. Hu, 2021; Y. Li et al., 2021; Merrill et al., 1989). Several isoforms of each isozyme can be formed by alternative splicing, however most of them are unlikely to be active enzymes (Bogner et al., 2021). The crystal structure of human PYCR has been resolved showing a decameric structure that consist of a pentamer of homodimers. Interestingly, the homodimer is the basic catalytic unit and have two catalytic sites (Christensen et al., 2017; Meng et al., 2006).

In addition to the aforementioned transcriptional regulation (together with P5CS), the androgen receptor has been found to promote PYCR1 expression in prostate cancer (Jariwala et al., 2007). The expression of PYCR1 is negatively regulated by miR-448 and miR-328-3p in lung cancers (J. Lu et al., 2021; D. Wang et al., 2019). PYCR1 activity can also be regulated by post-translational modifications: PYCR1 can be acetylated in the lysine 228 by acetyltransferase CREB-binding protein (CBP), this acetylation can be removed by SIRT3. Hyperacetylation on K228 – which is on the dimerization domain - reduced PYCR1 activity by destabilizing the homodimers (S. Chen et al., 2019). Finally, kindlin2 inhibits PYCR1 degradation. This process can be stimulated by ECM stiffness via PINCH1 (Guo et al., 2019, 2020; Y. Li et al., 2021).

Different groups had studied the relevance of PYCR1 in breast cancer models. They have demonstrated that PYCR1 silencing or knock-out reduced proliferation, migration, invasion, metastasis formation, and sensitize cancer cells to chemotherapy in cellular and xenograft models (J. Ding et al., 2017; W. Liu et al., 2015; Loayza-Puch et al., 2016; Shenoy et al., 2020). In lung adenocarcinoma and NSCLC, PYCR1 was shown to increase cell proliferation, repress apoptosis and promote migration and invasion through EMT induction. PYCR1 knockdown successfully impaired proliferation, migration and invasion by affect JAK/STAT signaling (Cai et al., 2018; Gao et al., 2020; W. Liu et al., 2015; Sang et al., 2019; D. Wang et al., 2019). Du et al. reported that PYCR1 knockdown reduced proliferation and invasion in bladder cancer cellular and animal models while its overexpression increased them. They proposed that PYCR1 knockdown downregulates the AKT/Wnt/ β -catenin signaling pathway resulting in tumorigenesis inhibition (S. Du et al., 2021). In colorectal cancer, PYCR1 knockdown inhibited proliferation, migration, EMT, drug resistance, and increased apoptosis (Sattar Alaqbi et al., 2022; S. Xiao et al., 2020; Yan et al., 2019). Other authors described similar behavior after PYCR1 silencing in prostate cancer, gastric cancer, melanoma, and hepatocellular carcinoma (Z. Ding et al., 2020; S. Xiao et al., 2020; Zeng et al., 2017; Zhuang et al., 2019). Interestingly, PYCR1 knockdown showed no effect in non-cancerous cells (Z. Ding et al., 2020). Although PYCR1 is the most studied isoenzyme, the other isoforms could also play a role in cancer progression (W. Liu et al., 2015; R. Ou et al., 2016; Sattar Alaqbi et al., 2022).

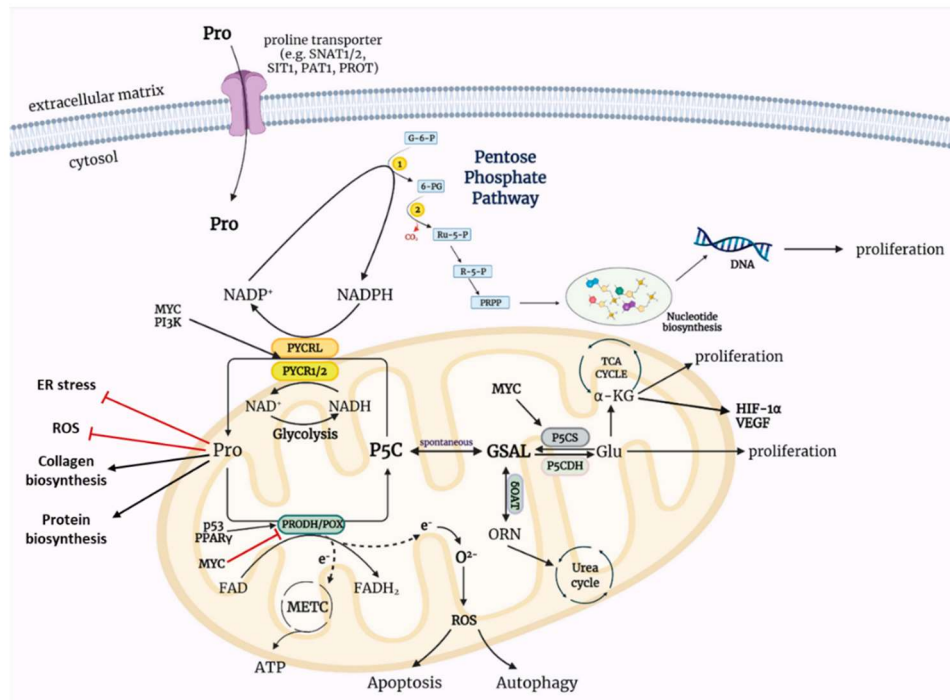


Figure I-11: P5C-proline cycle in cancer. The activity of P5C-proline cycle enzymes is accompanied by transport of redox equivalents between the mitochondria and the cytosol that modulate cellular processes (such as proliferation, survival, autophagy, metastasis formation) with an impact on cancer progression. This cycle modulates NAD(P)⁺/NAD(P)H ratios in the cell leading to regulation of glycolysis and the oxidative branch of the pentose phosphate pathway and increasing building blocks production. It also regulates ROS levels supporting/inhibiting cell survival and activating signaling pathways. Figure adapted from Chalecka et al., 2021.

Proline biosynthesis has been recently described to parametabolically promote glycolysis and the oxidative branch of the pentose phosphate pathway by regenerating NAD(P)⁺. Consequently, PYCR inhibition modified NAD⁺/NADH and NADP⁺/NADPH ratios and reduced glycolytic flux and the activity of the oxidative branch of PPP. Furthermore, this inhibition affected cancer cell proliferation (W. Liu et al., 2015). In the same line, Ding et al. performed a non-targeted metabolomics study in hepatocellular carcinoma cells with PYCR1 knockdown reporting a decrease in glycolysis, PPP, and nucleotide metabolism related metabolites. They also report a reduction in the glycolytic flux. Interestingly, NADP⁺ supplementation partially rescued the reduction of proliferation of PYCR1 knockdown cells (Z. Ding et al., 2020). These findings suggest that proline biosynthesis reprogramming would support anabolism in a similar manner than the Warburg effect in cancer cells.

Once proline has been synthesized by the different PYCR isoenzymes, it can be converted back to P5C by PRODH forming the P5C-proline cycle (Figure I-11). The P5C-proline cycle plays an important role in tumor metabolism through enhancing glycolysis, PPP, maintaining the cytosolic levels of pyrimidine nucleotides, and generates ROS to activate signaling pathways (Chalecka et al., 2021; Phang, 2019; Phang et al., 1981; Tanner et al., 2018).

PYCR inhibitors

The aforementioned evidence suggests that PYCR1 could be an emerging cancer therapy target. However, few PYCR inhibitors have been described so far. L-tetrahydro-2-furoic acid (THFA) is a proline analog that inhibits PYCR in the millimolar range (Zhu et al., 2002). THFA also inhibits PRODH and has been previously used to target cancer metabolism (Elia et al., 2017; Sahu et al., 2016). Recently, Christensen et al. performed an *in crystallo* screening with around 30 proline analogs identifying five PYCR inhibitors. N-formyl-L-proline (NFLP) was the most potent inhibitor with a K_i of 100 μM and a competitive (with P5C) mechanism. The treatment of breast cancer cells with NFLP inhibited proline biosynthesis and impaired spheroid growth in a similar manner than PYCR knockdown (Christensen et al., 2020).

Another family of inhibitors has been recently reported by Milne et al. They performed a small-scale screening that identified pargyline as a PYCR1 inhibitor with an IC_{50} of 198 μM . Then, they modified pargyline structure to assess the structure activity relationship. Finally, they obtain a compound that inhibits PYCR with an IC_{50} of 8.8 μM by an unknown mechanism. The treatment of breast cancer cells with compound this pargyline analog lowered intracellular proline levels and inhibited proliferation (Milne et al., 2019).

A few years ago, Bayern patented a group of PYCR inhibitors for neoplastic diseases treatment. They report that the inhibitors had an IC_{50} around 1-10 μM and they did not show any data in cancer cells. The current status of the patent is withdrawn/abandoned (Sylvia Gr newald et al., 2019).

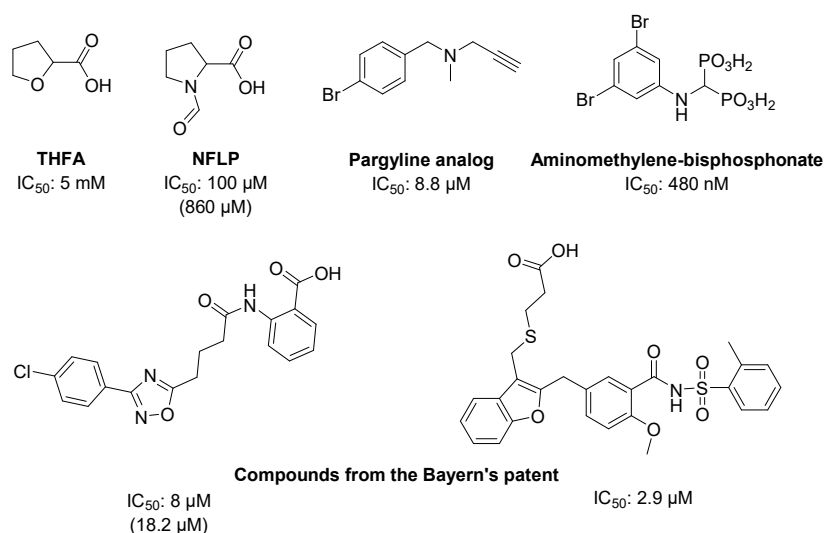


Figure I-12: PYCR1 inhibitors. Selection of up to date described PYCR1 inhibitors structures with their described IC_{50} . Some of the compounds have been tested in our laboratory (IC_{50} in brackets).

Lastly, a family of phenyl-substituted aminomethylene-bisphosphonates was reported to inhibit human PYCR1 with an IC_{50} below 1 μM (Forlani et al., 2021). This family was previously described to inhibit P5C reductase in plants, and the compounds were used as herbicides (Forlani et al., 2007, 2008, 2013). Interestingly, these compounds inhibited human PYCR1 by competitive inhibition with NADPH but not P5C.

These compounds successfully inhibit proliferation in breast cancer and chronic myelogenous leukemia cell lines. However, the antiproliferative activity of the compounds was dramatically reduced in the presence of FBS. As the authors argue this is most likely consequence of the compounds binding to BSA or other serum components which may prevent the compound from entering the cell. This represents a severe pharmacokinetic limitation which could be an important obstacle for in vivo treatments (Forlani et al., 2021).

Drug discovery

Developing a new drug for a disease is highly challenging. It is a complex process that can take between 10 to 17 years, its costs can exceed a billion USD, and its success rates are pretty low (Hughes et al., 2011).

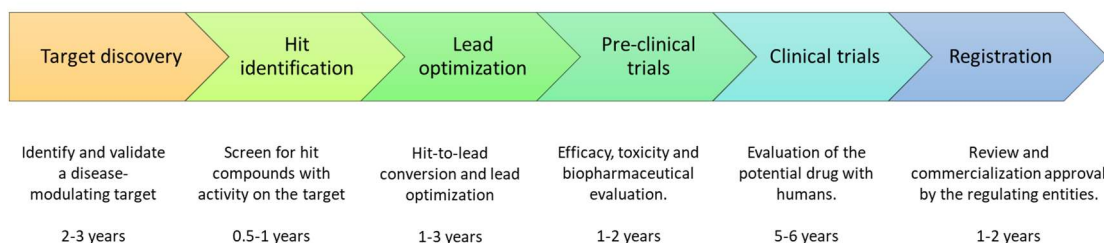


Figure I-13: Drug development process. The different stages of the drug development process from target discovery to registration for commercialization. This process takes from 10 to 17 years and the probability of success is lower than 10%.

The first step consists in the target identification and validation. Basic research – which often takes place in academia – lead to the identification of a target: a protein, gene or RNA that causes or plays an important role in the disease of interest. This target has to be validated in order to justify a drug discovery effort, mostly using *in vitro* and *in vivo* genetic models.

The second step is the hit discovery and consists in the identification of *hit* molecules. A hit is a molecule which has experimentally demonstrated a desired activity against a target. Hits can be identified in screening processes, which can follow multiple strategies. For example, large libraries of chemical libraries can be entirely tested in high throughput screenings (HTS) (Fox et al., 2006); focused screenings test smaller subsets of molecules that are likely to have an activity based on previous knowledge of the target (Boppana et al., 2009); in fragment screenings small molecules are assayed and crystallized with the target to obtain building blocks to generate larger molecules (Knight et al., 2022); virtual screenings use computational methods to select a small subset of molecules with high probabilities of being active from large libraries (Gimeno et al., 2019).

Then it starts the hit-to-lead or lead optimization phase where hits are optimized to more potent compounds: leads. In this phase hits undergo several modifications to increase its potency and improve its pharmacokinetic properties (for example taking into account Lipinski's Rule of Five) (Hoffer et al., 2018; Lipinski et al., 2001). This process ends up with multiple leads that are tested *in vitro* and *in vivo* in preclinical trials. The best(s) candidate is selected to start clinical trials where it will be evaluated in humans before its approval by the regulatory agencies. It is estimated that less than 10 % of clinical candidates entering clinical trials will be approved as a drug (C. H. Wong et al., 2019).

Structure-based drug discovery

Structure-based drug discovery are computational methods that use information of the protein three-dimensional structure to rationally design and optimize compounds to obtain a lead or a drug candidate. These approaches try to predict how the ligand binds the receptor and estimate the binding free energy (ΔG). Afterwards, this information is used to design new compounds or modify existing ones to increase its potency (A. C. Anderson, 2003; Batool et al., 2019; Śledź & Caflisch, 2018). When the protein structure is not available there are ligand-based methods that use information of known active ligands to obtain more potent compounds (Favia, 2011).

The binding of a molecule to a protein has associated a change of binding free energy (ΔG), which is the difference of energy between the bound and unbound states. The changes of binding free energy determine the binding between a ligand and the protein. The ligand-protein binding can only occur spontaneously when the ΔG is negative. Furthermore, the stability of the ligand-protein complex is determined by the magnitude of the difference between the bound and unbound free energies. The two ΔG main contributors are the binding enthalpy (ΔH) and entropy (ΔS) as described in Equation I-1 (X. Du et al., 2016; S.-Q. Liu et al., 2012).

$$\Delta G = \Delta H - T\Delta S \quad \text{(Equation I-1)}$$

Enthalpy integrates the total energy of a thermodynamic system, the sign of it determines if a process is exothermic (energetically favorable) or endothermic (energetically unfavorable). The binding enthalpy is defined by the energetic changes consequence of the formation and disruption of noncovalent interactions (eg. hydrogen bonds, ion pairs, dipolar interactions, Van der Waals interactions, etc). Importantly, binding enthalpy integrates not only ligand-protein interactions but also solvent interactions.

Entropy measures the distribution of heat energy over the thermodynamic system, it can also be viewed as a measure of the disorder and randomness in atoms and molecules of the system. It can be divided into three terms (Equation I-2). The ΔS_{solv} is the entropic change of the solvent associated to the release of solvent molecules previously buried in the binding pocket. It usually contributes favorably to the binding. The ΔS_{conf} is the entropic change resulting of changes in the conformational freedom of the ligand and protein due the binding. It can contribute favorably or unfavorably to the binding. Finally, the $\Delta S_{r/t}$ is the entropic change due the loss of translational and rotational degrees of freedom of the ligand and protein due the complex formation. It always contributes unfavorably to the binding.

$$\Delta S = \Delta S_{\text{solv}} + \Delta S_{\text{conf}} + \Delta S_{r/t} \quad \text{(Equation I-2)}$$

In general, large favorable changes in enthalpy due the formation of a new non-covalent interaction are associated with an entropic penalty due to mobility restrictions, and the other way around. This phenomenon is known as enthalpy-entropy compensation and led to moderate changes ΔG . Therefore, the effect of

enthalpy and entropy are both important for rational drug design. The optimization campaigns aim to accomplish the larger decrease in binding free energy, maximizing the favorable contributions while minimizing the penalties (X. Du et al., 2016; S.-Q. Liu et al., 2012; Perozzo et al., 2004).

Molecular docking

Molecular docking is a computational method that aims to accurately predict the ligand conformation and orientation in the binding pocket (binding mode). In addition, a scoring function aims to approximately predict the affinity of the ligand to the protein by evaluating the molecular interactions. It is a well-known and widely used method because of its high speed and efficiency (Kitchen et al., 2004; Pinzi & Rastelli, 2019). There are many programs to perform molecular docking between ligand and proteins, such as Auto-Dock (Goodsell & Olson, 1990), rDock (Ruiz-Carmona et al., 2014), Glide (Friesner et al., 2006), and GOLD (Jones et al., 1997) among others. Most of the programs work in a similar manner using a two-step process.

In the first step, the programs generate docking poses (defined conformation and orientation for a ligand in the binding pocket). Since even small molecules can have several degrees of freedom that lead to an enormous number of possible conformations, two types of search algorithms are used to sample this myriad of conformations. The systematic approaches aim to sample all the degrees of freedom in a molecule by slight modifications in structural parameters gradually changing the conformation of the ligand. On the other hand, the stochastic approaches make random changes in the structural parameters of the molecule that are later evaluated (Ferreira et al., 2015).

The second step consist in the evaluation of the generated poses by a scoring function. The different programs aim to approximate the binding free energy with simplified calculations that can be divided in three categories: force field-based, empirical or knowledge-based. The force field-based calculations estimate the binding energy by considering the contribution of bounded and unbounded terms in a general master function. The major limitation of force field-based functions is their inaccuracy estimating entropic contributors and that they neglect the solvent. Empirical approaches use several functions that aim to reproduce experimental data to estimate the binding free energy. The principal advantages are they speed and the incorporation of non-enthalpic contributions (entropy and solvation). However, they accuracy depends on the data used for defining the parameters. Finally, knowledge-based calculations use functions to reproduce experimental structures (not binding energies as the empirical methods). Similarly to empirical approaches, their advantages are their speed and simplicity, while they may fail evaluating interactions underrepresented in the training sets (Englebienne & Moitessier, 2009; Ferreira et al., 2015; Gohlke et al., 2000; Murray et al., 1998).

Most docking programs are able to successfully predict the correct binding mode of the ligand in a protein binding site. However, the scoring functions remain inaccurate leading to wrong free energy binding predictions.

Another limitation of molecular docking is that most of the programs consider the protein a rigid structure, while actually, both the ligand and receptor, undergo conformational changes during molecular recognition to (J.-H. Lin, 2012). Different methods have been created to solve this issue, and some of them use molecular dynamics simulations (Salmaso & Moro, 2018; Wong, 2015).

Molecular dynamics

Molecular dynamics (MD) simulations apply Newton's equations of motion to determine the position and speed of every atom of a system. In contrast with docking that provides a "picture" of the ligand-protein complex, MD simulations put the docking "picture" in motion providing a "movie" where the interactions between the protein, the ligand and solvent molecules can be observed in a more realistic way.

Since the first MD simulations of proteins in 1977, many programs have been developed including AMBER (Case et al., 2005), CHARMM (Brooks et al., 2009), and GROMACS (Berendsen et al., 1995) among others.

The "movement" is generated by iteratively solving Newton's second law for each atom of the system over small time steps (Equation I-3). The potential energy (V) is calculated using force fields, which are parametrizations of the energy that are formed by multiple bounded (e.g. bonds, angles, and dihedrals) and non-bounded (e.g. Van der Waals and electrostatic interactions) terms. Actual force fields are well parametrized for proteins but often fail to describe small molecules accurately (because they are more diverse). For this reason, there are specific tools to parametrize each ligand individually (e.g. Antechamber) (Nam, 2021; Salsbury & Jr., 2010; Śledź & Caflisch, 2018).

$$f_i(t) = m_i a_i(t) = - \frac{\partial V(x(t))}{\partial x(t)} \quad \text{(Equation I-3)}$$

It has to be noted that a typical system with a protein, a ligand and the solvent might have thousands of atoms. And therefore, the resolution of the equation for all of them is a computationally expensive process.

Furthermore, many modifications of the classical molecular dynamics simulations have been developed to address specific issues or improve its performance. For example replica-exchange molecular dynamics is used to enhance the sampling (Itoh & Okumura, 2022), and relative binding free energy simulations can be used to accurately estimate binding free energies (Cournia et al., 2017). On the whole, molecular dynamics simulations are an essential tool for drug design projects since can be used to confirm binding modes, study molecular interactions, and predict binding free energies of new compounds among others.

AIMS

As mentioned in the introduction, metabolic reprogramming supports cancer progression, but it also induces specific metabolic dependencies and vulnerabilities that can be targeted for therapeutic purposes. As we and others have previously observed, PEPCK-M and PYCR1 provide growth advantages to cancer cells and promote cancer progression.

Therefore, the main aim of this thesis is to develop and validate selective inhibitors targeting PEPCK-M and PYCR1 as cancer therapeutics. The specific aims towards this objective will be:

- Explore the cross-inhibitory potential of a previously described PEPCK-C inhibitor (iPEPCK-2) to modulate PEPCK-M activity in recombinant protein assays, and in cellular models.
- Validate PEPCK-M inhibition with iPEPCK-2 for cancer therapy in cellular and animal models.
- Explore the mechanisms by which PEPCK-M inhibition hinders cancer progression
- Develop isoform-selective PEPCK-M inhibitors by modulating its mitochondrial delivery.
- Discovery, development and initial validation of PYCR1 inhibitors using computational and experimental tools.

RESULTS AND DISCUSSION

CHAPTER 1: PEPCK-M INHIBITORS

Target engagement

Because of recent findings on PEPCK mitochondrial isoform and its impact in cancer biology (Grasmann et al., 2019), the development of compounds targeting this pathway for cancer indications has gained new interest. The family of 3-alkyl-2,8-dibenzylxanthines developed by Hoffman-La-Roche is the most potent group of PEPCK inhibitors reported so far. This family inhibited PEPCK-C by a GTP-competitive mechanism (Pietranico et al., 2007). However, their inhibitory capacity has not been tested against PEPCK-M. A pairwise sequence alignment for PEPCK-C and PEPCK-M amino acid sequences showed high sequence identity (69 %) and similarity (82 %) between both isoforms (Figure R-1). A computational approach including homology-modeling and molecular docking studies was performed by Dr. F. Javier Luque's laboratory to assess the cross-inhibitory potential of these family of inhibitors. Furthermore, a group of these inhibitors was synthesized by Dr. M^a Carmen Escolano's laboratory to further evaluate their activity as PEPCK-M inhibitors (Figure R-2).

Taking advantage of the high identity and similarity, and since the structure of PEPCK-M has not been resolved yet, the PDB structure of human PEPCK-C co-crystallized with a GTP-competitive inhibitor of the selected family (PDB ID: 2GMV) (Pietranico et al., 2007) was used as a template to generate a structural model of PEPCK-M with Swissmodel. Superposition of the reference PDB structure for PEPCK-C, and the homology model built for PEPCK-M is shown in Figure R-3A. This comparison highlighted the preservation of residues in the binding pocket, and a few differences in residues around the edges of the pocket filled by the crystallographic ligand. Among them, K342T, K524H, K529R, and G570R are located at less than 8 Å from the ligand in the GDP-binding site.

Autodock4 was used to dock a selected compound of the family (here named iPEPCK-2) in the GDP-binding site of PEPCK-M. The two most interesting docking poses found for iPEPCK-2 are reported in Figure R-3B and C. The xanthine moiety is stably placed in a sub-cavity surrounded by N292, W516, F525, W527, and F530. The two oxygen atoms participate in hydrogen-bonding interactions with N292 and N533. Water-mediated polar interactions are also observed between the protonated nitrogen of the xanthine scaffold and the backbone oxygens of W527 and W516. The 2 fluoro-benzene is inserted in a subpocket and stabilized by hydrophobic interactions with L293 and M296 (not shown). Two different orientations were, however, found for the pyrazole-4-sulfonamide moiety. In one case (Figure R-3B), this fragment matches the arrangement found in the crystallographic ligand in 2GMV, which involves the stacking of the pyrazole ring with F530. In the second case (Figure R-3C), a key difference in the vicinity of the binding pocket is the sulfonamide group interaction exclusive for the guanidine moiety of R588 in PEPCK-M (G570 in PEPCK-C).

RESULTS AND DISCUSSION

PEPCK-M_HUMAN	1	MAALYRPGRLRNWHGLSPLGWPSCRSIQTLRVLSGDLGQLPTGIRDFVEH	50
		...:.. .. : ..:..	
PEPCK-C_HUMAN	1	MPPQLQNGLNLS-----AKVVQGSLSLDPQAVREFLEN	33
PEPCK-M_HUMAN	51	SARLCQPEGIHICDGTEAENTATLTLLQQGLIRKLPKYNNCWLARTDPK	100
		:	
PEPCK-C_HUMAN	34	NAELCQPDHIHICDGSEENGRLLGQMEEEGILRRLKKYDNCWLALTDPR	83
PEPCK-M_HUMAN	101	DVARVESKTVIVTSPQRDTVQLPPGGARGQLGNWMPADFPQRAVDERFPG	150
		: 	
PEPCK-C_HUMAN	84	DVARIESKTVIVTQEQRDTVPIPKTGL-SQLGRWMSEEDFEKAFNARFPG	132
PEPCK-M_HUMAN	151	CMQGRMTMYVLPFSMGPVGSPLSRIGVQLTDSAYVVASMRIMTRLGTPVLQ	200
		:	
PEPCK-C_HUMAN	133	CMKGRMTMYVIPFSMGLPSPLSKIGIELTDSPIYVVASMRIMTRMGTPVLE	182
PEPCK-M_HUMAN	201	ALGDGDFVKCLHSVQPLTGQGEVPSQWPCNPEKTLIGHVPDQREIISFG	250
		:	
PEPCK-C_HUMAN	183	AVGDGEFVKCLHSVGCPLPLQKPLVNNWPCNPELTLIAHLPDRREIISFG	232
PEPCK-M_HUMAN	251	SGYGGNSLLGKKCFALRIASRLARDEGWLAEHMLILGITSPAGKKRYVAA	300
		
PEPCK-C_HUMAN	233	SGYGGNSLLGKKCFALRMASRLAKEEGWLAEHMLILGITNPEGEKKYLAA	282
PEPCK-M_HUMAN	301	AFPS SACGKTNLAM MRPALPGWKEVCVGGDDIAWMRFDSEGRRLRAINPENGF	350
		
PEPCK-C_HUMAN	283	AFPS SACGKTNLAM MNPSLPGWKEVCVGGDDIAWMKFDAQGHRLRAINPENGF	332
PEPCK-M_HUMAN	351	FGVAPGTSAT T TNPAMATIQSNTIFTNVAETSDGGVYWEGIDQPLPPGVT	400
		
PEPCK-C_HUMAN	333	FGVAPGTSV K TNPNAIKTIQKNTIFTNVAETSDGGVYWEGIDEPLASGVT	382
PEPCK-M_HUMAN	401	VTSWLGKPKPGDKPCAHPNSRFCAPARQCPIMDPAWEAPEGVPIDAII	450
		:	
PEPCK-C_HUMAN	383	ITSWKNKEWSSEDGEPCAHPNSRFACTPASQCPIIDAAWESPEGVPIEGII	432
PEPCK-M_HUMAN	451	FGG RR PKGVPLVYEAFNWRHGVPVGSAMRSESTAAAHEHGKIIMHDPFAM	500
		
PEPCK-C_HUMAN	433	FGG RR PAGVPLVYEALSWQHGVFGAAMRSEATAAAHEHGKIIMHDPFAM	482
PEPCK-M_HUMAN	501	RPFYGYNFGHYLHWSMEGRKGAQLPRI FHV NWFRDEAGHFLW PGFGE	550
		
PEPCK-C_HUMAN	483	RPFYGYNFGKYLHWSMAQHHPAAKLPKIFHV NWFRKDKGKFLW PGFGE	532
PEPCK-M_HUMAN	551	N ARVLDWICRRLEGEDSARETPIGLVPKEGALDLSGL RA IDTTQLFSLPK	600
		:	
PEPCK-C_HUMAN	533	N SRVLEWMEFNRIDGKASTKLTPIGIYPKEDALNLKGL GH INMMELEFSISK	582
PEPCK-M_HUMAN	601	DFWEQEVDIRSYLTEQVNQDLPKEVLAELEALERRVHKM	640
		:	
PEPCK-C_HUMAN	583	EFWEKEVEDIEKYLEDQVNADLPCEIEREILALKQRISQM	622

Figure R-1: Pairwise sequence alignment for human PEPCK-C (PCK1; UniProtKB: P35558) and PEPCK-M (PCK2; UniProtKB: Q16822). Aminoacidic changes located at/near the inhibitor binding site are highlighted in red. The sequence alignment showed that both PEPCK isoforms had a sequence identity of 69 % and a similarity of 82 %.

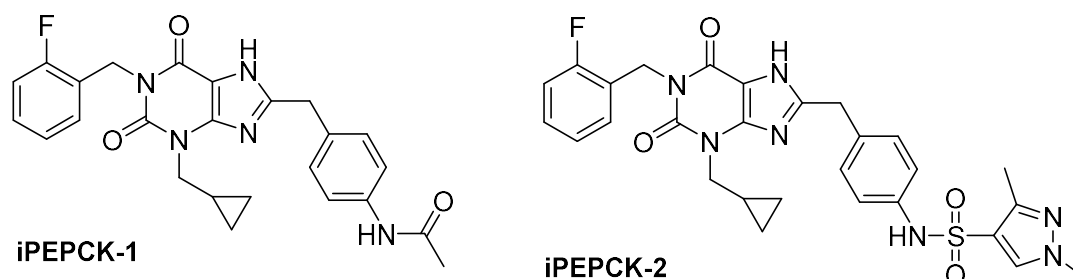


Figure R-2: PEPCK inhibitors synthesized by M^a Carmen Escolano's lab as described by Aragón et al. in the Supporting Information (Aragón et al., 2020).

Based on the high sequence similarity between PEPCK-C and PEPCK-M (see above), we hypothesized that PEPCK-C inhibitory compounds described by Pietranico et al. (synthesized here as iPEPCK-2) would properly

dock onto PEPCK-M, especially since the residues that shape the binding pocket are mostly preserved. Consistently, the two orientations predicted from docking calculations for the benzyl-4-sulfonamide-5-chloro-1,3-dimethyl-1H-pyrazole moiety matched the arrangement found in the crystallographic ligand in 2GMV (on PEPCK-C), which is characterized by the stacking of the pyrazole ring with the benzene moiety of F530, with a minor deviation on the second case due to the interaction of the sulfonamide group with the guanidine moiety of R570. Notably, this interaction is enabled by the replacement of G570 in PEPCK-C by R in PEPCK-M, which is one of the few differences found close to the binding pocket. These data suggest that the inhibitor might inhibit PEPCK-M in a similar manner and unveil the possibility to explore selectivity toward PEPCK-M in the future by exploiting the differences in residues located at the edge of the binding site in the two isoforms.

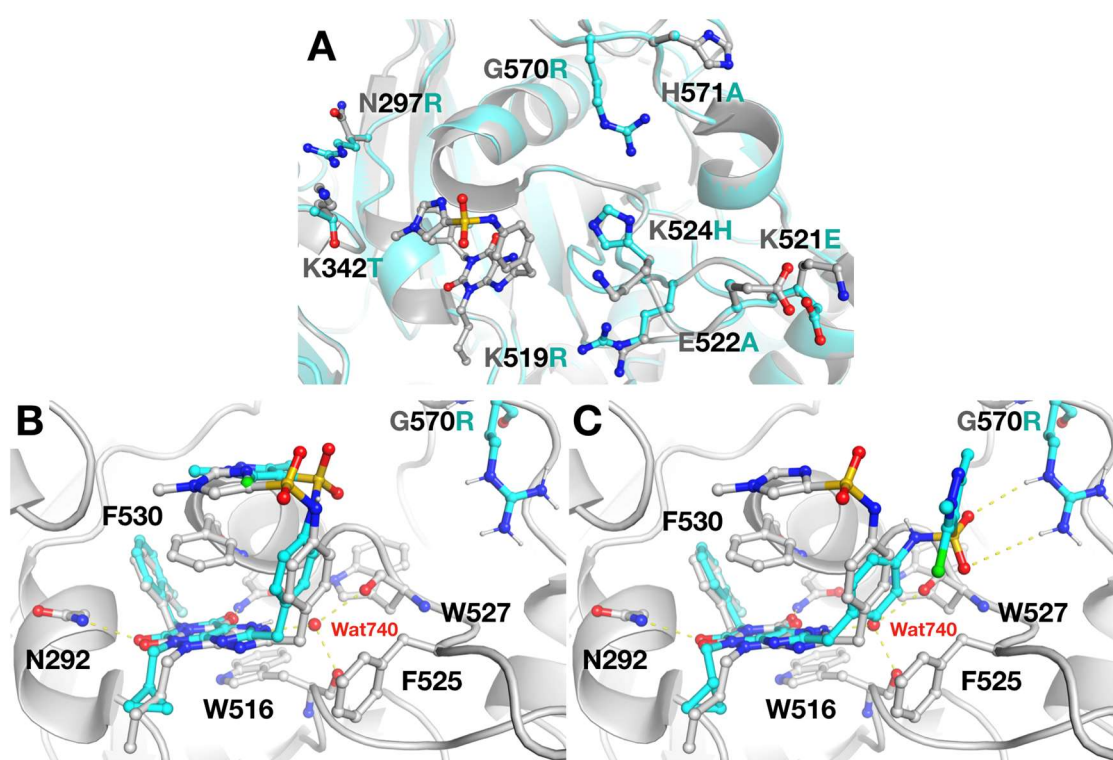


Figure R-3: Docking analysis. (A) Superposition of human PEPCK-C (PDB ID: 2GMV; grey) and human PEPCK-M (in cyan). Changes in residue content at/around the binding pocket are highlighted, and the crystallographic pose of the inhibitor (N-(4-[[3-butyl-1-(2-fluorobenzyl)-2,6-dioxo-2,3,6,7-tetrahydro-1H-purin-8-yl]methyl]phenyl)-1-methyl-1H-imidazole-4-sulfonamide) is shown as sticks. (B, C) Representative docking poses for iPEPCK-2 (in cyan) in the GDP-binding site. The reference crystallographic protein-ligand complex (PDB ID: 2GMV) is shown in grey. The G570R mutation is highlighted in cyan/blue. Numbering of residues based on the sequence of PEPCK-C.

Kinetic evaluation

To experimentally confirm the in-silico predictions and evaluate the potency of the inhibitors, a kinetic assay with recombinant PEPCK-C and PEPCK-M was set up. To determine PEPCK activity, the PEPCK reaction was coupled to malate dehydrogenase (MDH) which reversibly converts oxalacetate to malate consuming a NADH

molecule. NADH consumption (and formation) can be determined by spectrophotometry, thus reflecting PEPCK activity. The reaction can be assayed in both directions as described in Materials and Methods.

Human recombinant PEPCK-C and PEPCK-M were produced in our laboratory by expression on a prokaryote system and subsequent purification. Interestingly, PEPCK-C expressed by BL21 *E. coli* cells was active while PEPCK-M was not. We firstly hypothesized that the mitochondrial targeting sequence - which is found in the first exon and removed once the protein has entered the mitochondrial matrix (Kibbey, 2016)– was hindering the correct folding of PEPCK-M. Therefore, we cloned PCK2 gene without the mitochondrial leading peptide (removed by site-directed mutagenesis) into an expression vector and expressed it in BL21 *E. coli*. Nonetheless, PEPCK-M protein without leading peptide remained inactive (data not shown). Finally, the activity issue was solved expressing PCK2 (wild-type gene) in ArcticExpress *E. coli*, which highly express chaperonins from *Oleispira antarctica* to overcome protein misfolding (Escós et al., 2016b; Ferrer et al., 2003).

The inhibitory capacity of iPEPCK-2 was assayed in both PEPCK isoforms. Furthermore, 3-mercaptopicolinic acid (3-MPA), a commercial low-potency PEPCK inhibitor, was used as a positive control. The assayed compounds successfully inhibited both PEPCK isoforms with a similar potency. iPEPCK-2 was the most potent inhibitor for both isoforms with an IC_{50} of 117.4 nM for PEPCK-M and 60.7 nM for the cytosolic isoform (Figure R-4).

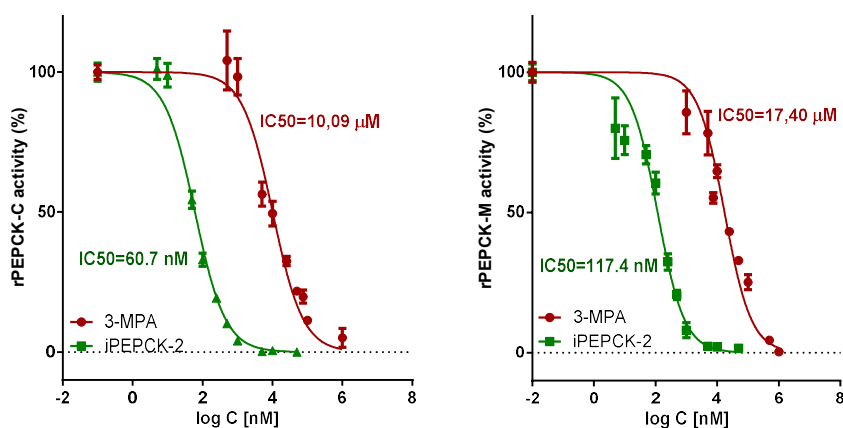


Figure R-4: Inhibition of purified human recombinant PEPCK-C and PEPCK-M by iPEPCK-2 and 3-MPA. IC_{50} for both isoforms are noted for every plot. Data are means \pm SEM. The inhibition curve was adjusted by the nonlinear regression fit tool from GraphPad Prism.

Activity assays on human recombinant PEPCK-M and PEPCK-C confirmed cross-inhibition by this family of inhibitors. IC_{50} values obtained in PEPCK-C activity assays were in the expected range (Pietranico et al., 2007), and 2-orders of magnitude lower than 3-MPA (Jomain-Baum et al., 1976). Similar potencies were found for PEPCK-C and PEPCK-M, as can be realized from the resemblance of the binding pockets in the two isoforms as predicted computationally.

Cellular target engagement

Once demonstrated that iPEPCK-2 can inhibit PEPCK-M *in vitro* in a kinetic assay, the arising question was whether it could enter into the cell and reach the mitochondria to successfully inhibit PEPCK-M. It is not a banal question since many drugs had trouble reaching the mitochondria (A. Singh et al., 2021). For example, it has been described that the PEPCK inhibitor 3-MPA inhibits preferentially the cytosolic isoform due to poor mitochondrial membrane permeability (Robinson & Oei, 1975).

The capacity to reach the mitochondria and inhibit PEPCK-M in a cellular context was confirmed using a cellular thermal shift assay (CETSA) (Figure R-5). This assay is based on ligand-induced stabilization of proteins (Jafari et al., 2014). All inhibitors tested thermally stabilized PEPCK-M in live MEF cells, which express exclusively the PEPCK-M isoform (Méndez-Lucas et al., 2014b), confirming the accessibility to, and the binding and interaction with PEPCK-M in the mitochondrial matrix by both inhibitors. The capacity of the inhibitors to stabilize PEPCK-M against thermal denaturation was dose-dependent. A quantitative evaluation of target engagement at various doses of inhibitor demonstrated that iPEPCK-2 had the highest affinity for PEPCK-M, as compared to 3-MPA (ITDRFcetsa, dose of inhibitor achieving a 50% stabilization at 60 °C, was 5.08 vs 303.9 μ M for iPEPCK-2 and 3-MPA, respectively) (Figure R-5B). PEPCK thermal stabilization was further assayed in rat hepatoma FAO cell line, which express both cytosolic and mitochondrial PEPCK isoforms (Figure R-29). In this context, thermal stabilization of both PEPCK isoforms presented similar kinetics, ruling out that compartmentalization of the mitochondrial isoform presents a relevant hinder to target engagement.

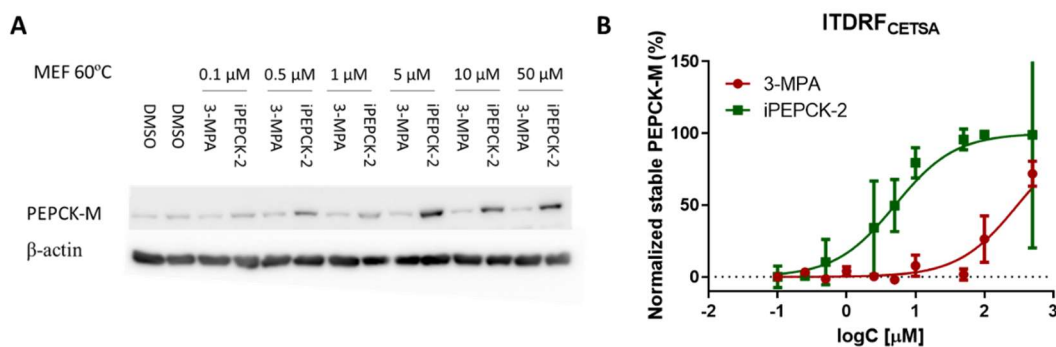


Figure R-5: Cellular target engagement by CETSA. (A) Representative Cellular Thermal Shift Assay (CETSA) at varying concentrations of inhibitors. PEPCK-M specific signal is detected by western blot in MEF cell extracts after 30 min incubation with different concentrations of 3-MPA and iPEPCK-2, prior to thermal treatment at 60 °C. (B) Calculated isothermal dose response fingerprint (ITDRFcetsa) for both inhibitors. Data are means \pm SEM. The curve was adjusted by the nonlinear regression fit tool from GraphPad Prism.

To evaluate the capacity of iPEPCK-2 to inhibit PEPCK-M driven pathways in an in-cell assay where PEPCK-C is not present, we took advantage of the role of this isoenzyme relaying glucose metabolism and insulin secretion (GSIS) in pancreatic β -cells, previously demonstrated using genetic models and inhibitory oligonucleotides (Stark et al., 2009). We therefore analyzed GSIS inhibition by treating mouse isolated

pancreatic islets (Figure R-6A) and rat insulinoma INS-1 cells (Figure R-6B) with increasing concentrations of iPEPCK-2. These studies confirmed that iPEPCK-2 treatment inhibited GSIS in a dose-dependent manner, functionally demonstrating the mitochondrial targeting in cellular models. The studies with INS1 cell line were performed by Dr. Juan Moreno-Felici and Dr. Anna Vidal-Alabró.

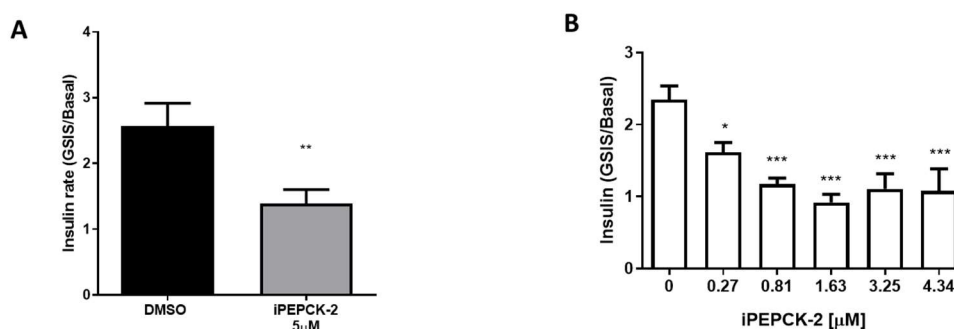


Figure R-6: Glucose stimulated insulin secretion (GSIS) inhibition. Effects of iPEPCK-2 and 3-MPA on mice isolated pancreatic islets (**A**) and INS1 (**B**) glucose-stimulated insulin production shown as a ratio of insulin concentration measured in the presence of 20mM over 3mM glucose. Data are means \pm SEM. A t-test, one-way Anova and a Sidak multiple comparison test were used. Statistical significance at * $p < 0.05$, ** $p < 0.01$, *** $p < 0.001$ vs vehicle control.

Furthermore, Dr. Juan Moreno-Felici in our laboratory evaluated the capacity of iPEPCK-2 to inhibit PEPCK isoforms *in vivo* by assessing hepatic gluconeogenesis and insulin secretion (Aragó et al., 2020). Hepatic gluconeogenesis in rodents is mainly driven by PEPCK-C (Méndez-Lucas et al., 2013; Semakova et al., 2017). In fasted mice, systemic *in vivo* glucose production is assayed as the glycemic response to a bolus administration of pyruvate. In this setting, glycemia reflects the net contribution of glucose synthesis to glucose homeostasis. iPEPCK-2 (10 and 25 mg/kg) and 3-MPA (50 mg/kg) had a significant negative impact on basal glycemia 5-hours after administration, and over the glycemia excursion observed after the pyruvate bolus, as compared to DMSO treated mice. These data suggest that 3-MPA and iPEPCK-2 inhibit hepatic gluconeogenesis *in vivo*. To assess PEPCK-M specific inhibition *in vivo*, we evaluated pancreatic β -cell secretion of insulin in response to an intraperitoneal glucose bolus (IGTT). In this assay, glucose-stimulated insulin secretion generates a peak of plasma insulin after a 2 g/kg glucose bolus is administered intraperitoneally in fasted mice. The animals in this test were submitted to inhibitor treatment just 2-hours before the glucose bolus to avoid significant effects on basal glycemia. Treatment with iPEPCK-2 (10 mg/kg) showed a blunted insulin secretion response to glucose as compared to vehicle and 3-MPA (50 mg/kg) treated mice. 3-MPA reduction of insulin secretion was not statistically significant, suggesting inefficient target engagement as compared to the successful targeting of liver PEPCK-C demonstrated in the previous experiment, or a problem to successfully reach pancreatic β -cells. Therefore, iPEPCK-2 inhibits PEPCK-M *in vivo* in pancreatic β -cells, although it is non-selective for the mitochondrial isoform as it also inhibits hepatic gluconeogenesis. These data provided the first evidence that targeting PEPCK-M could be useful to inhibit

insulin secretion in a physiological context since previous experiments using oligonucleotides to silence PEPCK-M in rats had not provided evidence of action on a healthy pancreas (Stark et al., 2014).

Overall, the experiments shown successfully demonstrated the molecular and functional PEPCK-M target engagement by iPEPCK-2 *in vitro*, *in-cell* and *in vivo*.

Preclinical validation of iPEPCK-2 and its target (PEPCK-M) for cancer treatment

As previously mentioned in the introduction, PEPCK-M is present in pancreatic β -cells (Stark et al., 2009), tumor cells (Méndez-Lucas et al., 2014b; Smolle, Leko, Stacher-Priehse, et al., 2020) and neuronal progenitors (Alvarez et al., 2016), hinting at a possible role for the enzyme in proliferative cell metabolic adaptations. Indeed, our laboratory and others have validated this enzyme as a cancer target in several genetic models, both *in vitro* and *in vivo* (Chu et al., 2017; Leithner et al., 2014; Méndez-Lucas et al., 2014b; Park et al., 2014). Therefore, we aimed to validate iPEPCK-2 in a preclinical cancer indication by assaying viability, invasion, and *in vivo* tumor growth using epithelial HEK-293, epithelial breast carcinoma MCF7, cervix cancer HeLa, and human colon carcinoma cells from epithelial HCT-116 and mesenchymal SW-480 origins. These cell lines express high levels of PEPCK-M and the cytosolic isoform is undetectable (Figure R-7). To evaluate target selectivity and test for off-target events, the impact of iPEPCK-2 in tumor cell viability was also assessed in cells lacking PEPCK-M using knock-out clones of HEK-293 (HEK-293-PCK2^{del/del}) and SW480 (SW480-PCK2^{del/del}) previously generated in our laboratory using CRISPRCas9 by Dr. Petra Hyroššová (Figure R-7).

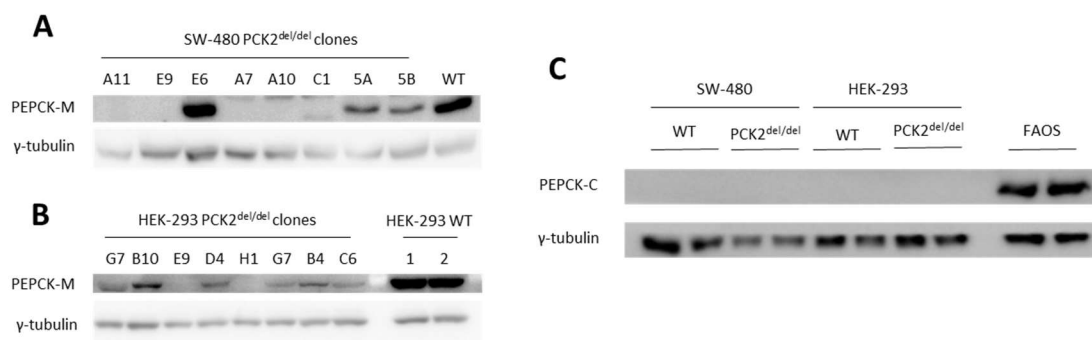


Figure R-7: Western blot analysis of PEPCK-M and PEPCK-C levels in HEK-293 and SW-480 wild type and PCK2^{del/del} clones. PEPCK-M levels of different SW-480 (A) and HEK-293 (B) PCK2^{del/del} CRISPRCas9 clones. SW-480 A7 and HEK-203 H1 clones were the clones used in further experiments. PEPCK-C levels of WT and PCK2^{del/del} clones (C). FAOS cell line lysate, which express high levels of PCK1 and PCK2, was added as a positive control.

Antineoplastic activity in cancer cell lines

Treatment with iPEPCK-2 significantly reduced DMSO-normalized proliferation in wild type MCF7, MDA-MB-231, and SW480 cells grown in optimal culture conditions (Figure R-8) without affecting cell viability (Figure R-9: A-C). Changes in cell growth induced by iPEPCK-2 were dependent on the presence of PEPCK-M, since

when tested in MDA-MB-231-PCK2^{del/del} and SW480-PCK2^{del/del} cells the compound did not show additional effects beyond those consequence of knocking-out the gene (Figure R-8: D-F), at least within the range of iPEPCK-2 (0.1-10 μ M) utilized in the validation assays. All in all, these data suggest target selectivity and no significant off-target effects.

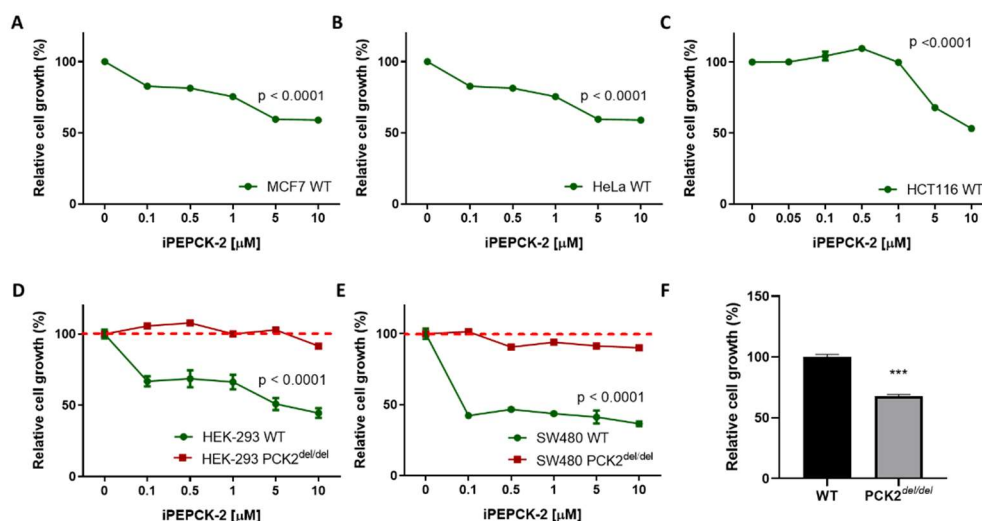


Figure R-8: iPEPCK-2 treatment inhibits cell growth. Cell growth of MCF7 (A), HeLa (B), HCT116 (C), HEK-293 wild-type and PCK2^{del/del} (D) and SW480 wild-type and PCK2^{del/del} (E) after a 72-hours treatment with increasing concentrations of iPEPCK-2 in high glucose media. Cell growth inhibition due PCK knock out in HEK-293 cells at 72h (F). Viable cells were stained by MTT and quantified by spectrophotometry. Data are means \pm SEM (3 independent experiments were performed with n=5 in each experiment shown in panels). A one-way Anova and a Sidak multiple comparison test was used. Statistical significance at *p < 0.05, **p < 0.01, ***p < 0.001 vs vehicle control.

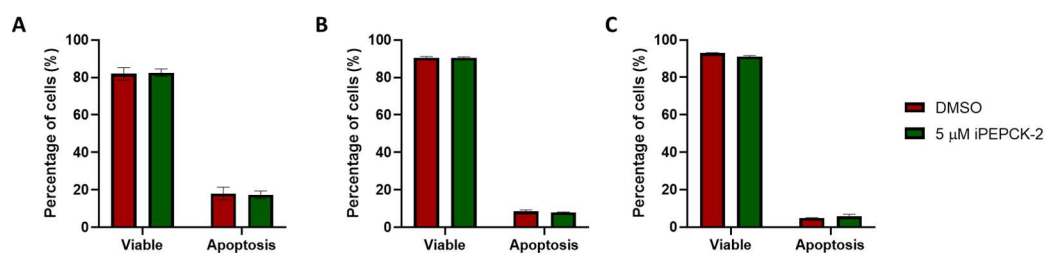


Figure R-9: Apoptosis by annexin V assay. Percentage of viable and apoptotic cells observed after 72 hours of iPEPCK-2 (5 μ M) treatment in high glucose media on MCF7 (A), HeLa (B), and HCT116 cells (C). Cells were stained with Annexin V-APC and Sytox Green and analyzed by flow cytometry. Data are means \pm SEM. A one-way Anova and a Sidak multiple comparison test was used. Statistical significance at *p < 0.05, **p < 0.01, ***p < 0.001 vs vehicle control.

PEPCK-M participates in pro-survival mechanisms engaged by nutrient limitation through the ER-stress pathway, and silencing the gene exacerbates ER-stress-mediated apoptosis (Méndez-Lucas et al., 2014b). Consistently, PEPCK-M inhibition decreased the DMSO-normalized viability of cancer cells coping with nutrient stress after 48 hours of glucose deprivation (Figure R10). These effects mimicked the consequences

of PEPCK-M loss in HEK-293-PCK2^{del/del} and SW480-PCK2^{del/del} when compared to their wild-type counterparts (Hyroššová et al., 2021).

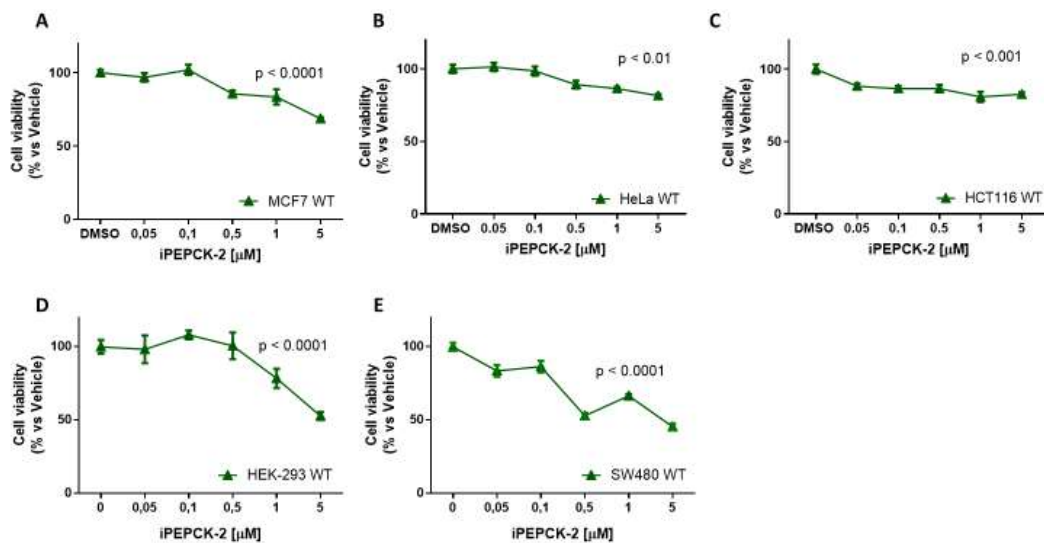


Figure R-10: PEPCK-M inhibition reduces cell viability under glucose deprivation. Cell survival of wild-type MCF7 (A), HeLa (B), HCT116 (C), MDA-MB-231 (D), and SW480 (E) in glucose-free media after 48-hours of treatment with iPEPCK-2. Viable cells were stained by MTT and quantified by spectrophotometry. Data are means \pm SEM (3 independent experiments were performed with $n=5$ in each experiment shown in panels). A one-way Anova and a Sidak multiple comparison test was used.

A physiologically relevant model to evaluate the response of cancer cells to diffusion constraints in nutrient supply is colony formation and growth in an anchorage-independent manner. Anchorage-independent growth during invasion and metastatic processes is also an important hallmark in cancer progression (Mori et al., 2009). iPEPCK-2 and 3-MPA treatment significantly reduced MCF7 colony formation when seeded in soft agar (Figure R-11), although 3-MPA was less effective. Cells under iPEPCK-2 treatment formed 87 % less colonies than the control group.

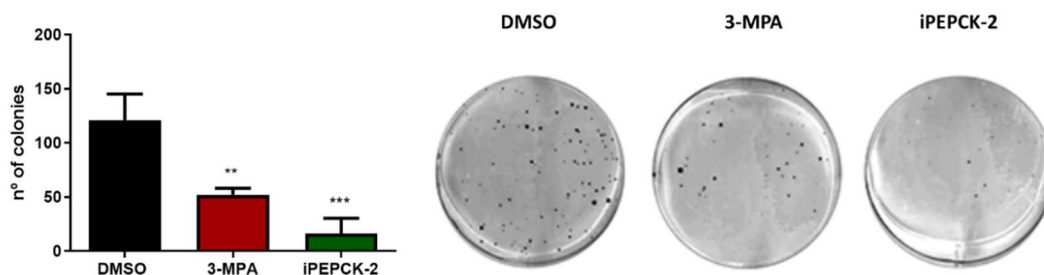


Figure R-11: PEPCK-M inhibition reduce anchorage independent growth. Colonies formed when MCF7 cells were seeded in soft agar and treated with PEPCK-M inhibitors (5 μ M) for 2 weeks. Representative photographs of 2-week colonies formed in each treatment group are noted. Data are means \pm SEM. A one-way Anova and a Sidak multiple comparison test was used. Statistical significance at * $p < 0.05$, ** $p < 0.01$, *** $p < 0.001$ vs vehicle control.

The same phenotype was observed in different PCK2 silencing models. For instance, HCT116 and HeLa (Figure R-12 A-B & Hyroššová et al., 2021) cells with silenced PCK2 using shRNA formed less colonies than the ones

treated with a non-targeting shRNA (sh-Ctrl). Although there were no differences in the number of colonies formed by cells overexpressing PCK2 (oe-PCK2) compared with sh-Ctrl, the size of the colonies formed by oe-PCK2 seem to be larger (Figure R-12 A-B). Interestingly, when cells were seeded in soft agar under glucose exhaustion conditions (1mM glucose), PCK2 overexpression provided an advantage compared with sh-Ctrl whereas cells with reduced PCK2 expression could not form hardly any colony (Figure R-12 C). These results showed the importance of PEPCCK-M expression in anchorage independent growth, especially in low glucose conditions when PEPCCK-M became crucial for cell growth and survival.

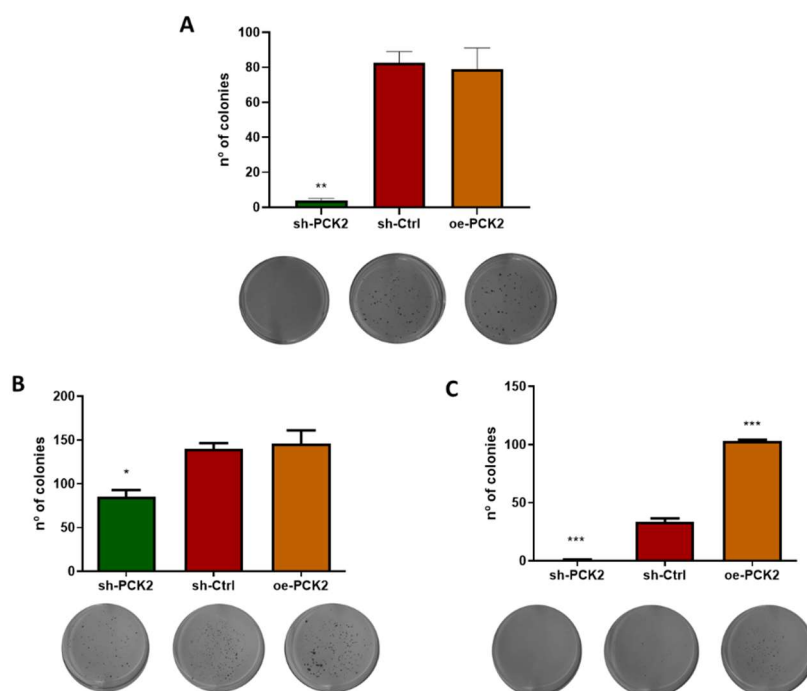


Figure R-12: PCK2 expression affects anchorage independent growth. (A) Colonies formed when HCT116 wild-type, PCK2 silenced (sh-PCK2), and PCK2 overexpressed (oe-PCK2) cells were seeded in soft agar in high glucose medium for 2 weeks. (B-C) Colonies formed when HeLa wild type, PCK2 silenced (sh-PCK2), and PCK2 overexpressed (oe-PCK2) cells were seeded in soft agar in media with 5 mM (B) or 1 mM (C) glucose for 2 weeks. Representative photographs of 2-week colonies formed in each treatment group are noted. Data are means \pm SEM. A one-way Anova and a Sidak multiple comparison test was used. Statistical significance at * $p < 0.05$, ** $p < 0.01$, *** $p < 0.001$ vs vehicle control.

Cell migration is essential for many physiological and pathological processes, for example embryonic development, wound repair, invasion and metastasis, and angiogenesis. Wound healing assays are used to evaluate cell migration in cultured cells. After forming an artificial wound in a cell monolayer, cells start to migrate to close the wound until cellular contacts are re-established (Freitas et al., 2021; X. Wang et al., 2019). PEPCCK-M inhibition by iPEPCCK-2 did not significantly hindered migration and wound healing in mouse embryonic fibroblast (MEF) cells (Figure R-13). Nevertheless, a non-significantly reduced migration tendency can be observed in iPEPCCK-2 treated cells. Therefore, more experiments should be performed to clarify the PEPCCK-M role in cell migration.

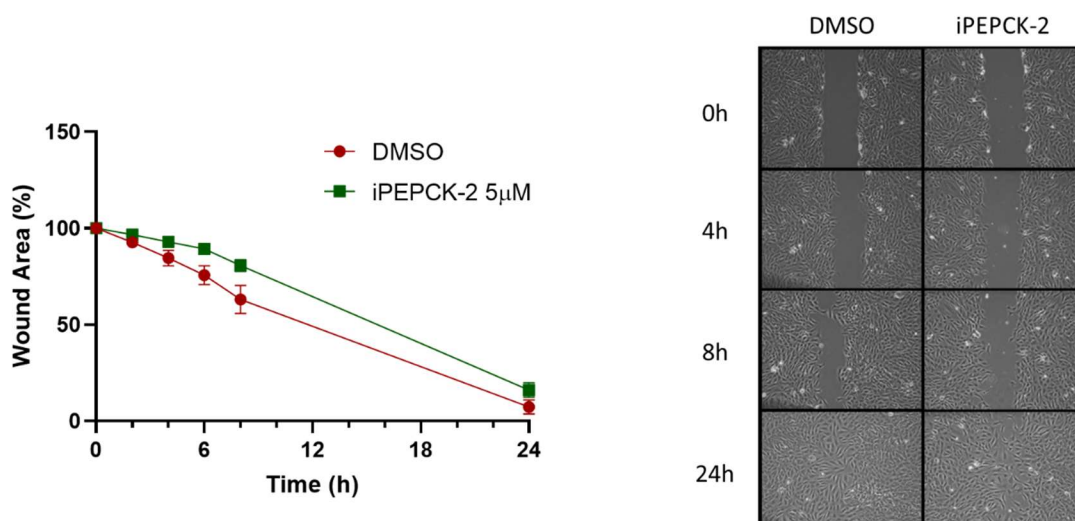


Figure R-13: PEPCCK-M inhibition non-significantly reduces migration in a wound healing assay. Migration of MEF cells treated with DMSO or iPEPCK-2 (5 μM) after a wound was made in a monolayer of confluent cells. The area of the wound was calculated using ImageJ at different time points. Representative photographs of different time points are noted. Data are means \pm SEM (one experiment was performed with $n=3$). A two-way Anova test with paired data was used. The treatment factor was not significant with a $p = 0.0749$.

In vivo PEPCCK-M inhibition in mouse xenograft models

Before evaluating iPEPCK-2 as *in vivo*, we performed basic ADMET and pharmacokinetic studies in collaboration with Dr. Belén Pérez from the Universitat Autònoma de Barcelona and Dr. Maria I. Loza and Dr. José Brea from Innopharma Screening Platform of the Universidad de Santiago de Compostela. *In vitro* ADMET assays showed good human and murine microsomal stability with a half-life of 119 min and 75% of compound remaining after 60 min in mice microsomes, predicting good *in vivo* pharmacokinetics (Table R1).

Species	Remanent at 60min (%)	$t_{1/2}$ (min)	Clint ($\mu\text{L}/\text{min mg protein}$)
Human	68.71	123.36	5.62
Mouse	74.95	119.66	5.79

Table R-1: Microsomal stability of iPEPCK-2 in human and mice microsomes.

This was confirmed in murine *in vivo* pharmacokinetic studies with plasma concentrations of iPEPCK-2 measurable after 15 min of administration and maintained for 8 hours, with a C_{max} (0.86 $\mu\text{g}/\text{mL}$ or 1405 nM) at 30 min and $t_{1/2\beta}$ at around 2 hours (Figure R-14 and Table R2). The narrow differences in AUC_0^t and AUC_0^∞ showed complete exposure and good bioavailability of iPEPCK-2 after intraperitoneal administration in the described conditions. iPEPCK-2 was not found in the brain at the working concentrations, suggesting that the compound did not cross the blood brain barrier. We had classified iPEPCK-2 as to have uncertain BBB permeation based on data from *in vitro* PAMPA assays (P_e value of 2.6 ± 0.2) (J. Müller et al., 2015). No

additional warning on toxicity were measured on cell viability assays in human MRC-5 fibroblast at 100 μ M or on hERG inhibition (5 ± 1 at 10 μ M). Finally, we found that iPEPCK-2 has acceptable solubility (61 μ M at 37 $^{\circ}$ C in 1% DMSO, 99% PBS).

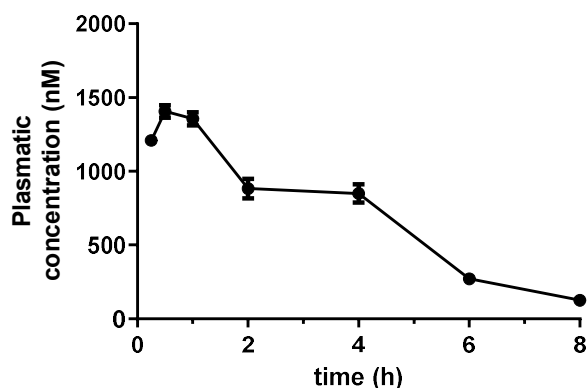


Figure R-14: Plasmatic concentration of iPEPCK-2 at various times (15 min to 8 h) after an intraperitoneal administration of 8 mg/kg, as determined by HPLC/UV-VIS at 290 nm. Data are means \pm SEM (n=4 in each time point).

AUC_{0[∞]}	238.2 μ g min/ml
AUC_{0[†]}	218.7 μ g min/ml
Tmax	0.5 h
Cmax	0.86 μ g/ml
t_{1/2β}	1.8 h

Table R-2: Pharmacokinetic parameters.

We next examined the capacity of inhibitor iPEPCK-2 to blunt tumor growth in two xenograft murine models. Colon carcinoma (SW480) or transformed kidney embryonal (HEK-293) cells were subcutaneously injected in both flanks of athymic mice and allowed to grow until measurable at the surface of the skin. Mice were randomly split into two different groups treated with a daily intraperitoneal injection of 8 mg/kg of iPEPCK-2 or vehicle for a variable period depending on the biological features of each model. The dose and dosage interval were decided according to the pharmacokinetic study.

Whereas vehicle treatment did not impede tumor growth, iPEPCK-2 treatment halted tumor growth in either xenograft models, as measured both by continuous evaluation of volume under-the-skin and final weight (Figure R-15). Histopathology of tumor samples from treated or untreated breast carcinoma or colon carcinoma tumors showed marked differences in both groups, with prominent necrosis observed in iPEPCK-2 treated tumors and reduced tumor cell burden overall (Figure R-16).

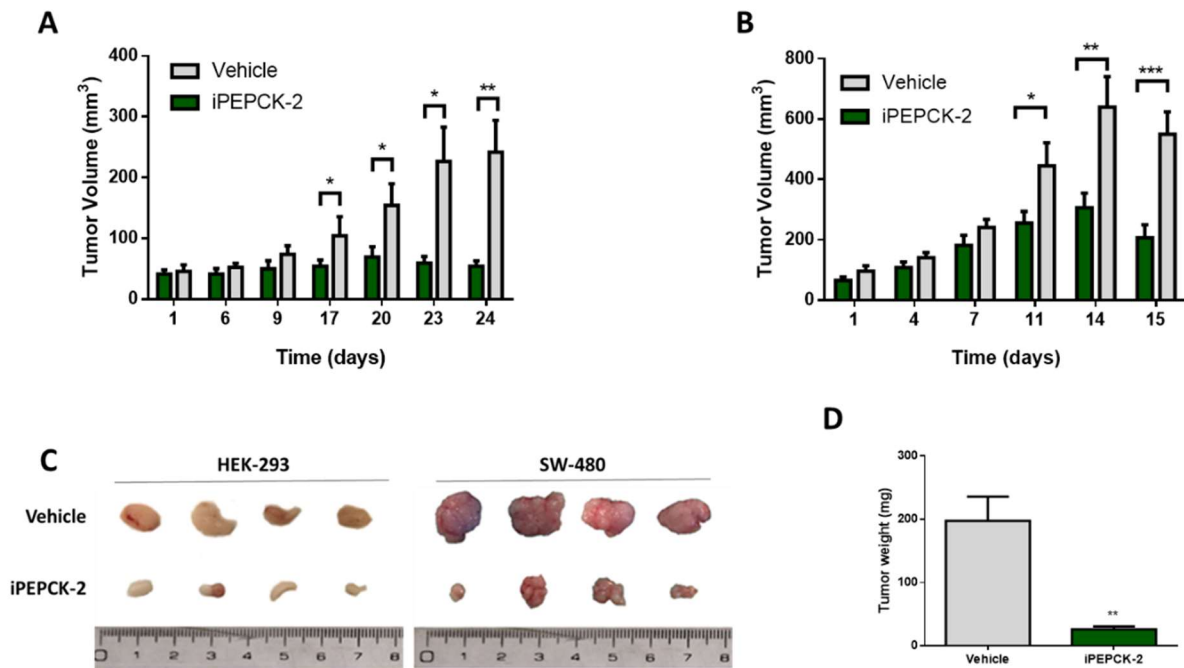


Figure R-15: In vivo evaluation of iPEPCK-2 antitumoral activity in two murine subcutaneous xenograft models. (A–B) Over-the-skin tumor volume ($[\text{short length}^2 \times \text{long length}]/2$) from HEK-293 (A) and SW-480 (B) cells implanted into both flanks of BALB/C nude mice. Once the tumors grew sufficiently large to be measurable, animals were randomly grouped and daily treated with 8 mg/kg of iPEPCK-2 or vehicle intraperitoneally. (C) Representative tumor explants are shown. (D) HEK-293 tumors were weighted at the time of sacrifice. Data are means \pm SEM ($n=5$ in each experiment shown in panels, except for HEK-293 control group containing $n=3$ due to animal issues upon tumor over growth). A one-way Anova and a Sidak multiple comparison test was used. Statistical significance at $*p < 0.05$, $**p < 0.01$, $***p < 0.001$ vs vehicle control.

Furthermore, no signs of apparent toxicity were observed upon close inspection; specifically, there was no macroscopic affectation of the liver or the spleen, weight loss (Figure R-17 A-B), lethargy or major health-related disturbance apparent on mucosae or skin quality. There were no differences in the glycemia and insulinemia between the experimental groups at the end-point (data not shown). The histopathological analysis of eosin and hematoxylin-stained tissue sections from different organs did not show any sign of apparent toxicity (Figure R-17 C).

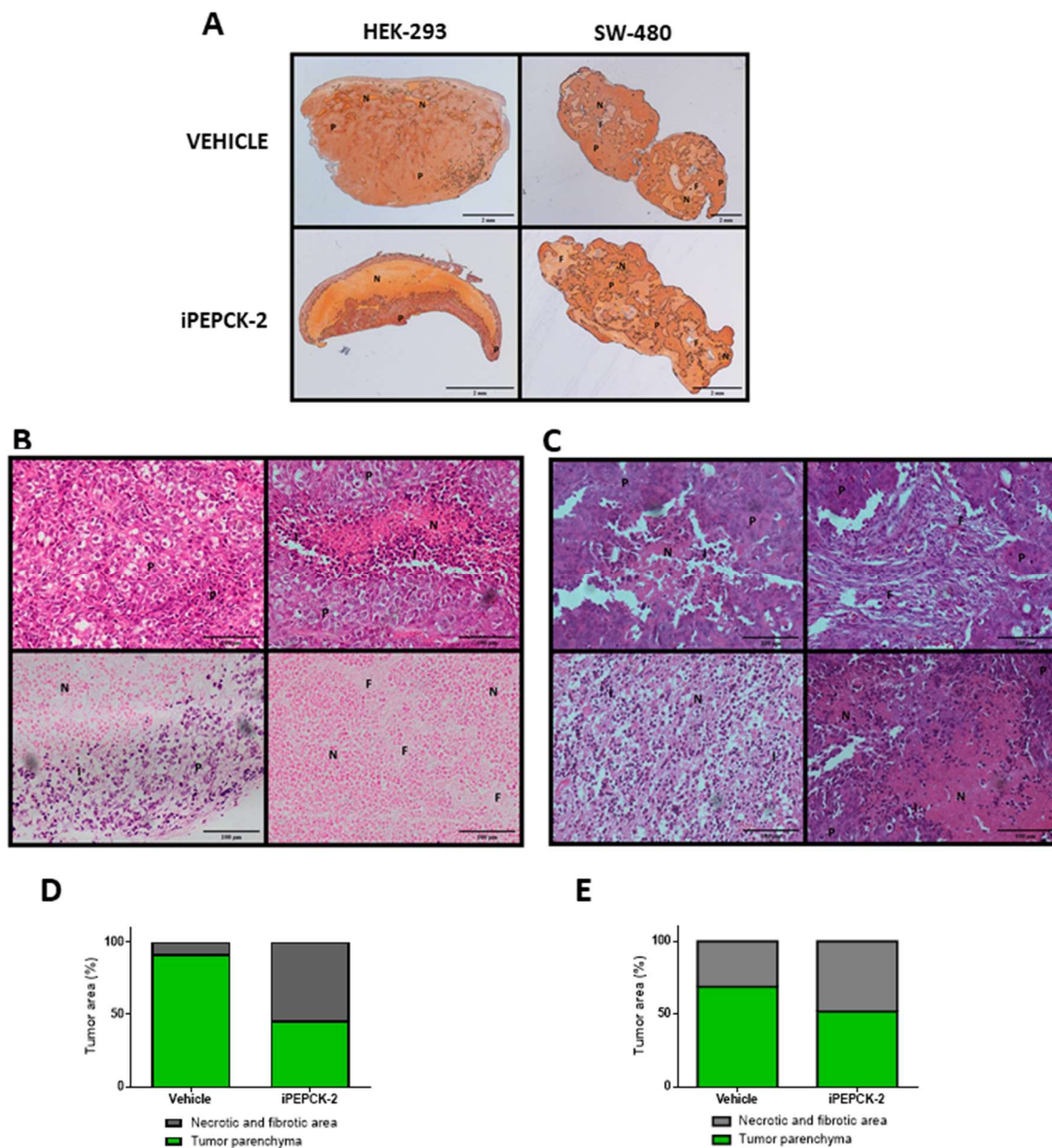


Figure R-16: Analysis of tumor histopathology from HEK-293 and SW-480 explants. Full size H&E-stained tumor sections (A). Reference H&E-stained tumor sections (200x) from HEK-293 (B) and SW480 (C) explants indicating various histology features: P: tumor parenchyma; F: fibroblasts; N: necrotic areas; I: immune system infiltration. (D-E) Quantification of tumor parenchyma versus necrotic plus fibrotic areas of HEK-293 (D) and SW480 (E) tumors. The area means were quantified using Image J “Trainable Weka segmentation” Plug-in in full size tumor sections. 100x and 200x sections were used as a template to detect the different areas and the results were confirmed by microscopy.

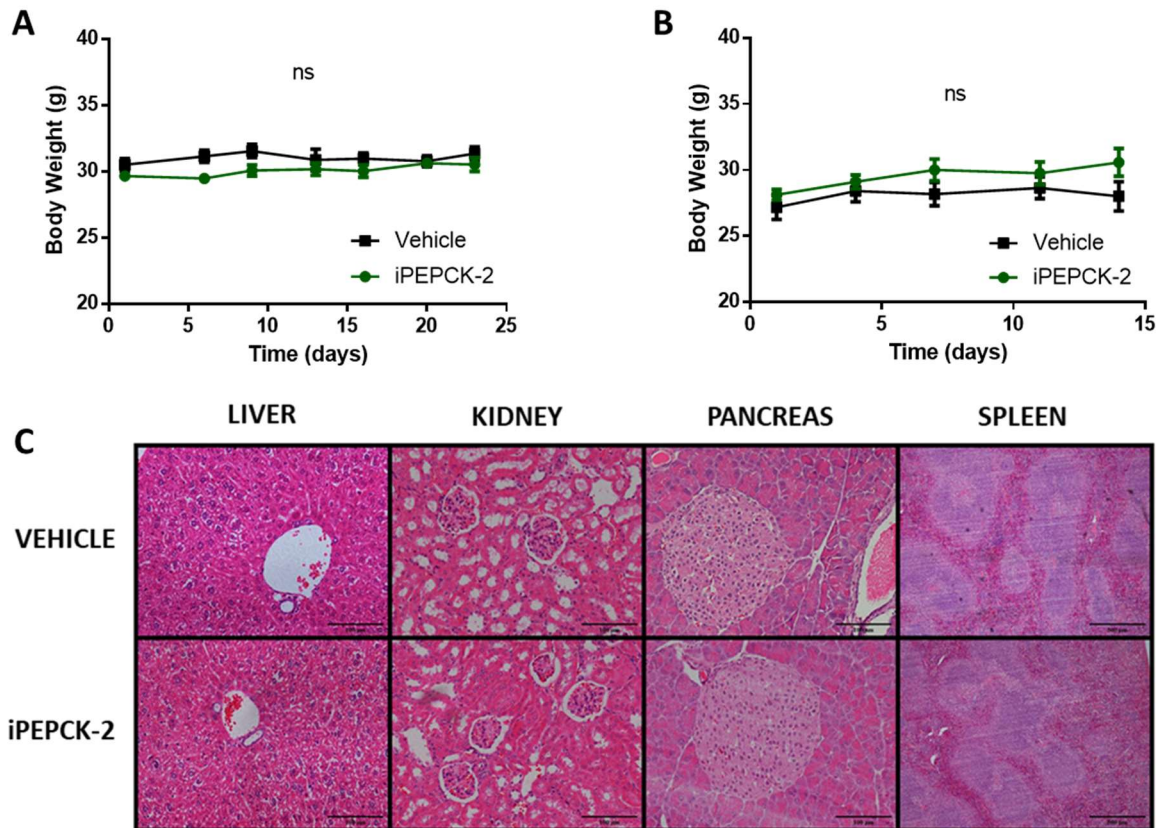


Figure R-17: Toxicity evaluation of iPEPCK-2 treatment. (A-B) Animals growing HEK-293 (A) and SW-480 (B) tumors were weighted periodically over the course of the experiment to detect health-related issues. (C) Representative H&E stained sections from various organs (liver, kidney, pancreas and spleen) to show no sign of apparent toxicity. Data are means \pm SEM (n=5 in each experiment except for HEK-293 control group containing n=3 due to animal issues upon tumor over growth; at least n=3 sections per tumor were produced and examined to produced panel C and representative photographs).

As the high similarity and identity between both PEPCK isoforms and the *in-silico* calculations suggested, iPEPCK-2 could successfully inhibit PEPCK-M. Furthermore, it could reach the mitochondria and inhibit PEPCK-M in cellular and animal models as demonstrated by CETSA and GSIS inhibition. This is differential to the classical PEPCK inhibitor 3-MPA, probably because limited mitochondrial bioavailability as determined in our CETSA assays, thus exhibiting lower inhibition potency for the mitochondrial isoform in pancreas in our GSIS assays and in the literature (Robinson & Oei, 1975).

Interestingly, the insulin secretion inhibition by iPEPCK-2 in mice insinuated a potential therapeutic opportunity in type 2 diabetes besides hepatic gluconeogenesis inhibition. The initial steps of type 2 diabetes courses with continuous high levels of glucose in blood - and incipient insulin resistance - that lead to chronic load of β -cells due the elevated insulin synthesis and secretion rates. The chronic stress then drives high levels of ROS and ER-stress which end up in a situation termed " β -cell exhaustion" in which β -cells fail to secrete insulin properly. This pre-diabetic stage progresses to overt hyperinsulinemia (to compensate the insulin resistance). However, persistence of this pathological state leads to the irreversible death of β -cells by apoptosis causing overt type 2 diabetes (Poitout & Robertson, 2008; Swisa et al., 2017). In this context

insulin secretion inhibition with PEPCK-M inhibitors -together with a dietary intervention and insulin administration - could potentially contribute to reduce β -cell stress, and therefore β -cell death (Abulizi et al., 2020b; Ryan et al., 2004; Teague et al., 2011).

In the last decade, several authors reported that PEPCK-M is overexpressed in a wide variety of tumors - including colorectal carcinoma, melanoma, gastric, breast, prostate, lung, and pancreatic cancer –, and its expression was related with more aggressive phenotypes and worst prognosis (Chaika et al., 2012; E. I. Chen et al., 2007; Chu et al., 2017; Chun et al., 2010; Fernández-Coto et al., 2018b; J. Zhao et al., 2017b). In a similar manner, some tumors express high levels of PEPCK-C (Chaika et al., 2012; Y. Li et al., 2015, 2018; Montal et al., 2015) which would play a similar role than the mitochondrial isoform.

In this context, we used iPEPCK-2 to demonstrate a role of PEPCK-M in cancer cell proliferation and viability under glucose deprivation in various cell lines. Furthermore, in the soft agar anchorage independent model PEPCK-M inhibition (or silencing) drastically reduced the total number of colonies formed. Interestingly, PEPCK-M overexpression increased the number of colonies only under glucose exhaustion conditions, pointing to a role of PEPCK-M to shuttle carbons from glutamine and other substrates through the TCA cycle to the glycolytic pool and its branched pathways (serine synthesis, glycerol synthesis, one-carbon metabolism, etc.)-(Hyroššová et al., 2021; Leithner et al., 2014; Montal et al., 2019b).

Our data is consistent with previous observations on the role of this pathway in cancer cell viability. A significant proportion of the tumoral cells are found in nutrient-poor environments. The elevated proliferation rate of tumoral cells combined with the aberrant angiogenesis are the cause of the nutritional heterogeneous tumoral microenvironment. The tumoral microenvironment is characterized by steep oxygen and nutrients gradient from the blood vessels to the tumor parenchyma (Ackerman & Simon, 2014; Martin et al., 2016). The elevated metabolic flexibility of cancer cells allows them to adapt to these poor-nutrient environments. In this context, a cancer supportive role for PEPCK-M has been most extensively described. In 2014, our laboratory reported that PEPCK-M expression was stimulated in nutrient limited conditions via ATF4. Moreover, PEPCK-M activity sustained cell proliferation and survival (Méndez-Lucas et al., 2014b). In 2015, Vincent et al. demonstrated that PEPCK-M could enable growth in glucose deprivation conditions in lung cancer cells by providing carbons from the TCA cycle to synthesize biosynthetic intermediates (i.e. serine, glycine, ATP) (Vincent et al., 2015). Similarly, Leithner et al. in 2018 reported that PEPCK-M mediated the synthesis of glycerol phosphate from noncarbohydrate precursors such as glutamine or lactate in lung cancer cells (Leithner et al., 2018). Furthermore, PEPCK-M activity was necessary to maintain the level of glycerophospholipids (the major constituents of cellular membranes). In addition, in 2019 Montal et al. described that PEPCK allowed colon cancer cells to use lactate for biosynthetic purposes in poor-nutrient conditions (Montal et al., 2019b). Interestingly, lactate secreted by the most “glycolytic” cells (which exhibit a classical Warburg phenotype) of the tumor could be used as a nutrient for other tumor cells. In this scenario

PEPCK would play an enabling role in nutrient selection for the synthesis of biosynthetic intermediates derived from the glycolytic pool (through cataplerosis).

Reduced tumor growth *in vivo* in the two xenograft models confirmed that PEPCK-M expression offers a growth advantage to cancer cells and its inhibition could be a useful anticancer strategy. As previously described, the rapid proliferation and aberrant angiogenesis cause a nutrient-poor microenvironment in tumors and PEPCK-M expression increases metabolic flexibility allowing the use of glucose alternative nutrients such as lactate (relatively abundant in the tumor microenvironment, and usually recycled by tumoral cells) for biosynthetic purposes (Ackerman & Simon, 2014; Montal et al., 2019b). In addition to the reduced tumor growth, the tumors of the treated animals presented large necrotic areas that could be explained by the reduction of the PEPCK-M-dependent metabolic flexibility. Moreover, the treatment with iPEPCK-2 was consistent with other xenograft models with PEPCK knock-down/out (Hyroššová et al., 2021; Montal et al., 2015; Vincent et al., 2015). In MEF cells PEPCK-M inhibition slightly reduced cell migration in the wound healing assay. Similarly, Hu et al. observed that PCK2 downregulation inhibited invasion and metastasis formation in laryngeal carcinoma cells (Y. Hu et al., 2020). PEPCK-M might contribute to migration, invasion, and metastasis formation by preventing anoikis through balancing oxidative stress (Bluemel et al., 2021; Hyroššová et al., 2021; Kamarajugadda et al., 2012; J. Lu et al., 2015). However, our current data is very limited with regards to the characterization of PEPCK-M role in migration and invasion and its possible mechanisms.

Importantly, adverse effects secondary to liver PEPCK-C or pancreatic PEPCK-M inhibition were not substantiated in mice by our limited evaluation. Any other sign of apparent toxicity was observed in the animals. Furthermore, pharmacokinetics profile and the good bioavailability, with no crossing of the brain blood barrier, are good starting grounds for the prospective use of this compound in further clinical testing.

Our data *in vivo*, together with a myriad of other observations in our laboratory, points to the possibility that PEPCK-M has a role in tumor metabolism beyond glucose or nutrient deprivation. In this sense, Montal et al. also reported that PEPCK activity increased glucose and glutamine utilization in colorectal cancer cells under high glucose conditions. Similarly, PEPCK promoted cancer progression by enhancing anabolic metabolism and activating mTORC1 (Montal et al., 2015). Consistently, Hu et al. reported that PCK2 silencing reduced glucose uptake in laryngeal cancer cells. Its silencing also reduced cell proliferation, migration, and invasion (Y. Hu et al., 2020). In our laboratory, we recently described that PEPCK-M allowed the synthesis of biosynthetic intermediates derived from the glycolytic pool (i.e., serine, glycine) from glutamine carbons under glucose limitation. Furthermore, PEPCK-M silencing reduced TCA cycle flux and proline levels even in high glucose conditions while PEPCK-M overexpression increased intracellular proline concentration. Consistent with reduced proline levels, PEPCK-M silencing increased ROS in both glucose conditions. Furthermore, PEPCK-M silencing reduced cell viability, anchorage independent growth and tumor growth in

subcutaneous xenograft models (Hyroššová et al., 2021). Bluemel et al. also reported an increase of oxidative stress (higher ROS and lower reduced glutathione levels) when silencing PEPCK-M in starved lung cancer cells (Bluemel et al., 2021). However, they propose that PEPCK-M silencing increases mitochondrial respiration increasing ROS production. Notably, Bluemel et al., described that PEPCK-M reduces TCA cycle flux in contrast with Montal et al. and our observations, where PEPCK-M increased glutamine utilization and the TCA cycle flux. In 2017, Chu et al. also reported that PEPCK-M silencing reduced respiration in pancreatic neuroendocrine tumors (Chu et al., 2017).

We also described that PEPCK-M could modulate intracellular PEP levels even in the presence of glucose (Moreno-Felici et al., 2019). Importantly, PEP could inhibit SERCA – a Ca^{2+} channel which regulate the return of cytosolic Ca^{2+} to the ER – activity. SERCA inhibition leads to increased calcium levels which activate different signaling pathways and transcription factors such as NFAT as c-Myc which support cancer progression. Interestingly, oncogenic KRAS signaling has been described to upregulate the expression of metabolic enzymes such as PCK2, PCK1, and aspartate metabolizing enzymes in colorectal cancer cells promoting tumor formation (Doubleday et al., 2021). PEPCK has also been reported to activate mTORC1 pathway by increasing glutamine intracellular levels (Montal et al., 2015). Furthermore, PCK2 silencing sensitize pancreatic neuroendocrine cancer cells to the mTORC inhibitors (Chu et al., 2017).

PEPCK-M role in glucose physiological conditions

Although the mechanism by which PEPCK-M provides a growth advantage in low-nutrient conditions is well described, how PEPCK-M supports cancer progression when glucose availability is not an issue remains unclear. As described above, some authors have also observed that PEPCK-M plays a role in these conditions by promoting glucose and glutamine uptake, and anabolic metabolism (Grasmann et al., 2019; Montal et al., 2015; Yu et al., 2021). In our laboratory, we observed that PEPCK-M promotes the TCA cycle, proline metabolism, oncogenic signaling, and reduces the oxidative stress (Hyroššová et al., 2021; Moreno-Felici et al., 2019).

We decided to perform transcriptomic analysis in HCT116 colorectal cancer cells treated with 5 μ M iPEPCK-2 or DMSO for 24 h in physiological glucose conditions (5 mM) to elucidate the mechanisms by which PEPCK-M inhibition (by iPEPCK-2) might hinder cancer progression. We also quantified different metabolite concentration by GC-MS in the same conditions.

Metabolite quantification by GC-MS

PEPCK-M inhibition led to a reduction of PEP concentration even in the presence of glucose (Figure R-18) as previously demonstrated by biochemical methods in Moreno-Felici et al. Furthermore, the concentration of other glycolytic metabolites such as 3-PG was also reduced by iPEPCK-2 treatment, and a tendency was observed in pyruvate. In contrast with the observations made by Hyroššová et al. (2021) and Montal et al.

(2015), the intracellular concentration of the TCA metabolites remained unchanged suggesting that the TCA cycle flux was not affected by PEPCK-M inhibition in the presence of 5 mM of glucose. However, more studies with C^{13} -labeled metabolites such as glutamine or glucose are necessary to clarify the effects of PEPCK-M inhibition on TCA flux, and glucose and glutamine utilization.

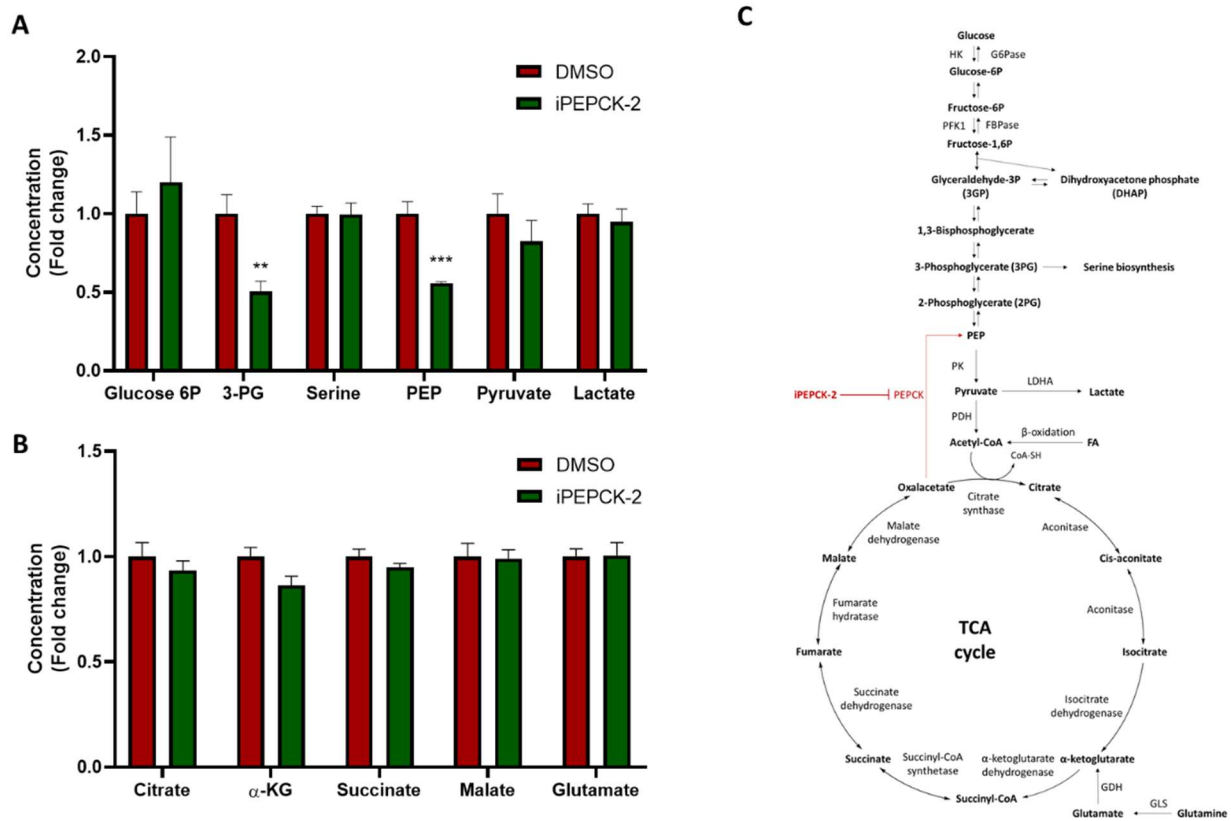


Figure R-18: Metabolite quantification by GC-MS after iPEPCK-2 treatment. Metabolites were extracted and analyzed by GC-MS from HCT116 cells after a 24-hours treatment with 5 μ M of iPEPCK-2 in 5 mM glucose media. (A-B) Concentration of the metabolites from glycolysis/gluconeogenesis (A) and the TCA cycle (B). (C) Schematic view of glycolysis/gluconeogenesis and the TCA cycle pathways. Data are means \pm SEM (2 independent experiments were performed with $n=3$ in each experiment). Multiple t-test comparison was used. Statistical significance at * $p < 0.05$, ** $p < 0.01$, *** $p < 0.001$ vs vehicle control.

The oxygen consumption was measured in HCT116 and MCF7 wild type cells after the treatment with iPEPCK-2 by high resolution respirometry (Oxygraph 2k) to evaluate OXPHOS (Figure R-19). Additionally, the respiration was also evaluated in MCF7 cells overexpressing PCK2 (oe-PCK2). In contrast with the observations of Bluemel et al., 2021, which described that PCK2 silencing increased OXPHOS in lung cancer cells, the inhibition/overexpression of PEPCK-M did not affect respiration. These results are consistent with the quantified metabolites by GC-MS, where it can be observed that the TCA metabolites did not vary.

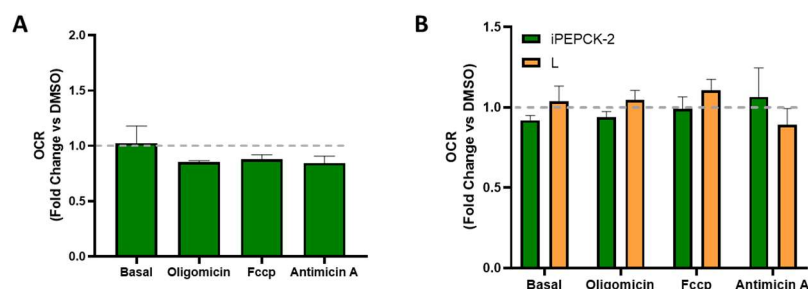


Figure R-19: OXPPOS evaluation by high resolution respirometry with Oxygraph. Oxygen consumption in HCT116 WT (A) and MCF7 WT and oe-PCK2 (B) cells. Data are means \pm SEM. A one-way Anova and a Sidak multiple comparison test was used. Statistical significance at * $p < 0.05$, ** $p < 0.01$, *** $p < 0.001$ vs vehicle control.

Transcriptomic analysis

Differential expression analysis between both groups (iPEPCK-2 or DMSO treated cells) yielded 175 significantly differently expressed genes (Figure R-20). Among them, we can find reduced expression of specific subsets of genes codifying for enzymes of the serine synthesis pathway (PSAT1, SHMT2) and glycolysis (LDHA, LDHB, PGAM1). Genes involved in autophagia, negative regulation of c-Myc (NDGR1) and the MAPK pathway (DUSP4) are expressed at higher levels in iPEPCK-2 treated group.

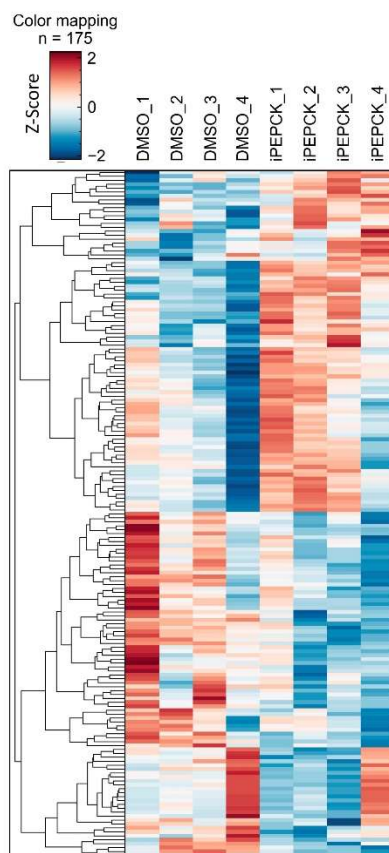


Figure R-20: Heatmap of the differentially expressed genes. The Z-score of the significant differentially expressed genes (p adjusted value < 0.05) was calculated, the results were hierarchical clustered and plotted in a heatmap using InstantClue software.

A gene set enrichment analysis (GSEA) for both groups using the Canonical Pathways databases resulted in 56 gene sets significantly enriched in the iPEPCK-2 treated group and 316 gene sets significantly enriched in the DMSO treated group.

The MYC repression pathway gene set was enriched in the iPEPCK-2 treated group (Figure R-21) consistent with results recently reported by our lab where PEPCK-M inhibition reduced PEP intracellular concentration which led to an increase of SERCA activity and reduced Ca^{2+} -dependent signaling including calcineurin, NFAT (and downstream c-Myc) (Moreno-Felici et al., 2019). Consistently, NFAT signaling, calcineurin signaling pathway, and MYC activation pathway gene sets were enriched in the control group (Figure R-22).



Figure R-21: Selected gene sets enriched in iPEPCK-2 treated cells.

Gene sets related to the oxidative stress response such as the Nrf2 pathway, and oxidative stress induced senescence, are enriched in iPEPCK-2 treated group (Figure R-21). The expression of Nrf2 related genes suggests that there is a higher level of oxidative stress (ROS) when PEPCK-M is inhibited as described by us and others (Bluemel et al., 2021; Hyroššová et al., 2021). The gene set related to senescence and autophagy in cancer is also enriched in iPEPCK-2 treated cells (Figure R-21). On the other hand, PEPCK-M has been reported to activate mTORC1 by increasing intracellular amino acid levels (through increasing glutamine uptake, TCA cycle flux, and anabolic metabolism) (Montal et al., 2015). Interestingly, mTORC1 mediating signaling gene set is enriched in the control group (Figure R-22). Furthermore, mTORC1 activation inhibits autophagy through ULK, ATG13, and FIP200 inhibition (Laplante & Sabatini, 2012). One might speculate that these changes reflect a reduction of metabolic flexibility limiting the bioavailability of nutrients and building blocks would imbalance proteostasis.

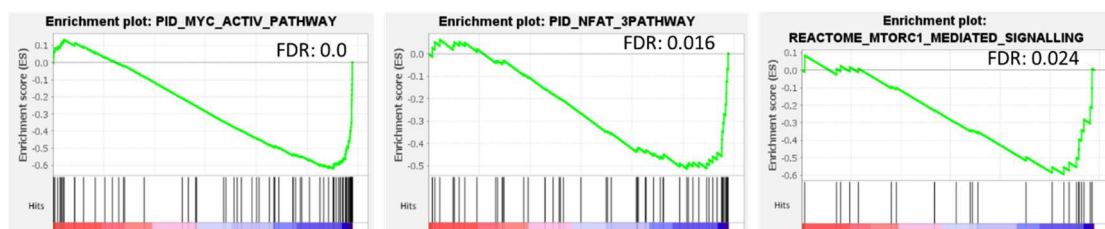


Figure R-22: Selected signaling gene sets enriched in DMSO treated cells.

A group of metabolism related gene sets were enriched in the control group (Figure R-23), including gene sets related with glycolysis and gluconeogenesis pathways (and branching pathways such as serine biosynthesis and pentose phosphate pathways), TCA cycle and OXPHOS, amino acids metabolism, and nucleotide metabolism (one carbon metabolism). In general, pathways related with cancer metabolic

reprogramming that could support anabolic metabolism (directly or indirectly) and may be upregulated by oncogenic signals (such as c-Myc, HIF1- α , or mTORC1). Interestingly, PEPC-M enables the direct use of glucose-alternative nutrients (lactate, glutamine, fatty acids) towards these pathways through cataplerosis.

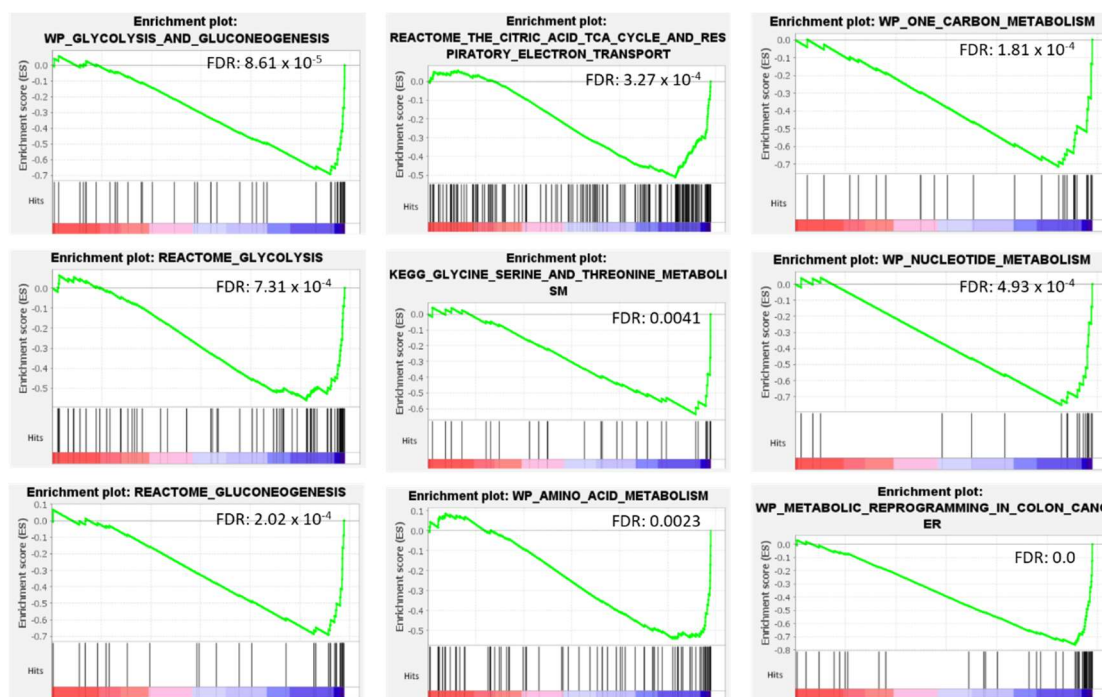


Figure R-23: Selected metabolic gene sets enriched in the DMSO treated group.

Finally, several gene sets related to cell cycle and cellular division were also enriched in the control group (Figure R-24). An increase with cell division would be consistent with increased proliferation of control cells as compared with cells treated with iPEPC-2.

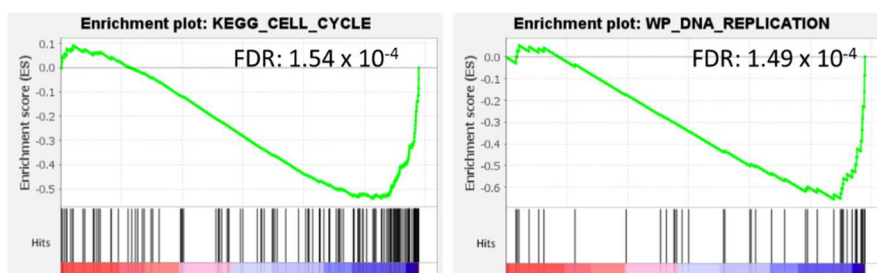


Figure R-24: Selected cell division related enriched gene sets in DMSO treated cells.

Significant results of GSEA (FDR < 0.05) were visualized using the Enrichment Map plugin available in Cytoscape (Figure R-25). This representation helps to visualize the gene sets enriched in both experimental groups and summarizes the results of this transcriptomic analysis. Overall, the control group have enriched gene sets related with several metabolic pathways branching from glycolysis/gluconeogenesis, cell cycle & division, oncogenic signaling (Ca²⁺, c-Myc, mTORC1). On the other hand, enriched gene sets in the iPEPC-2 treated group are related with oxidative stress, autophagy, and drug metabolism and detoxification.

Besides, a group of gene sets related to extracellular matrix interactions and autophagy is enriched in iPEPCK-2 treated cells. In our laboratory, we recently described that PEPCK-M contributes to cell survival in limited nutrient concentration by limiting entosis – a cell death/survival mechanism in which a cell engulfs a neighbor cell to cope with nutritional stress and glycosylation defects - (Garanina et al., 2017; Hamann et al., 2017; Hyroššová et al. publication pending). Entosis is E-cadherin-dependent, and it uses similar mechanisms than autophagy (Overholtzer et al., 2007; Sun et al., 2014). There is also a gene set enriched in the control group related with migration and the epithelial-to-mesenchymal migration.

The results of this gene set enrichment analysis could help to understand the mechanisms by which PEPCK-M inhibition limits cancer progression.

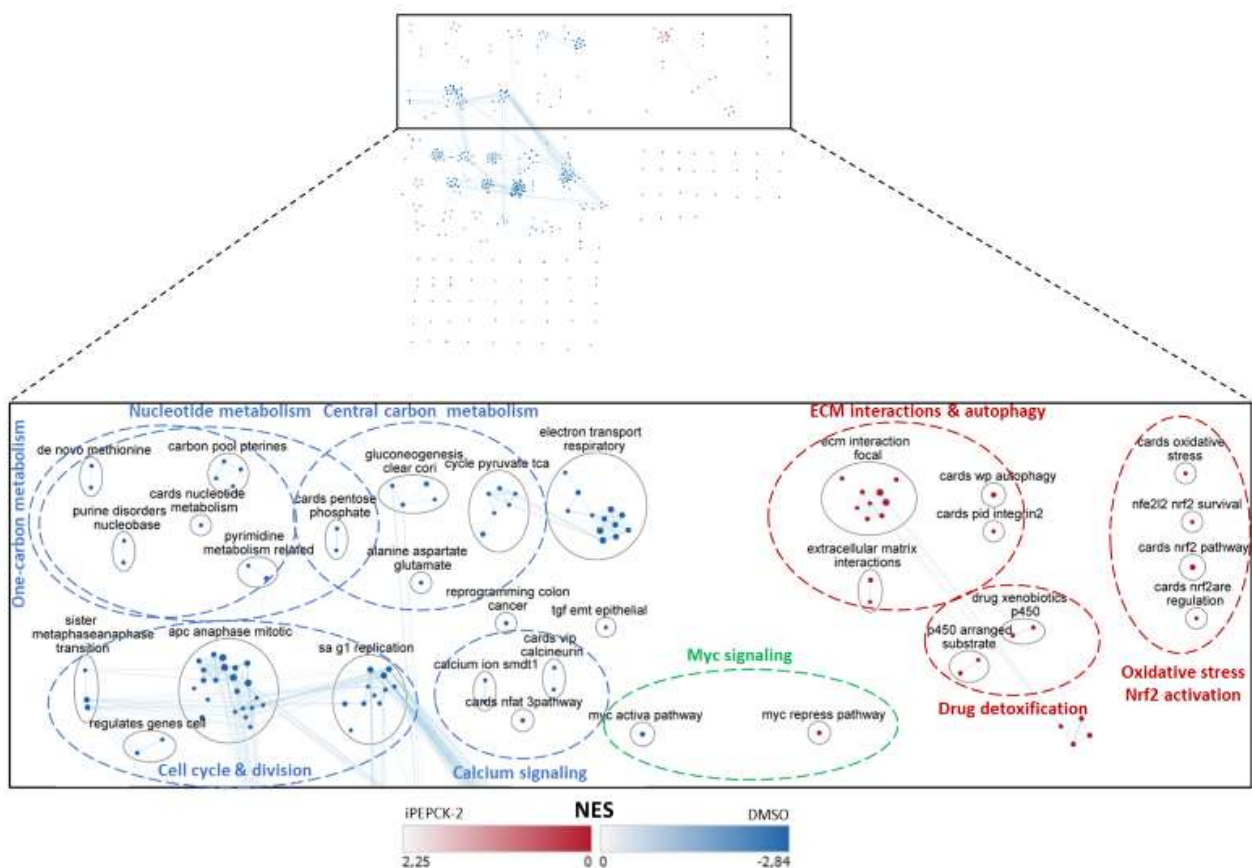


Figure R-25: Enrichment gene map of significant results from GSEA. The significant gene sets from GSEA (FDR < 0.05) were plotted using the Enrichment Map plugin available in Cytoscape. Red and blue nodes represent gene sets enriched in HCT116 treated with iPEPCK-2 or DMSO respectively. Nodes were manually laid out to form a clearer picture. Cluster of nodes were labeled using AutoAnnotate Cytoscape application. Individual node labels were removed for clarity. Cluster of nodes were grouped and manually labeled to emphasize related pathways.

Remarkably, we have collectively shown that high PEPCK-M expression in cancer cells provided a growth advantage by increasing the metabolic flexibility (which would improve cell survival and even proliferation in poor-nutrient conditions), stimulating anabolic metabolism and proteostasis, reducing oxidative stress, and activating oncogenic signaling pathways that promote cancer proliferation. Therefore, and as suggested by

the genetic silencing and overexpression models, PEPCK-M inhibition did impair cancer progression, confirming the drug and the target as valid strategy for cancer therapy.

Development of PEPCK-M selective inhibitors

After having validated PEPCK-M as a target for cancer therapy, and since PEPCK-C plays an important role in glucose homeostasis, we aimed to obtain a compound that selectively inhibits PEPCK mitochondrial isoform. The administration of a PEPCK-M selective compound would avoid the possible negative consequences of inhibiting hepatic PEPCK-C driven gluconeogenesis. As previously reported, both PEPCK isoforms have a high sequence identity and similarity (Figure R-1), and most of the amino acids of catalytic center are conserved (Figure R-3A). Although there are small differences among some amino acids close to GTP-binding site, the development of isoform-selective inhibitors would be a really complicated. Therefore, we devised a targeting strategy consisting in the incorporation of triphenylphosphonium (TPP), a mitochondrial-targeting moiety, into a 3-alkyl-2,8-dibenzylxanthine scaffold (Figure R-26).

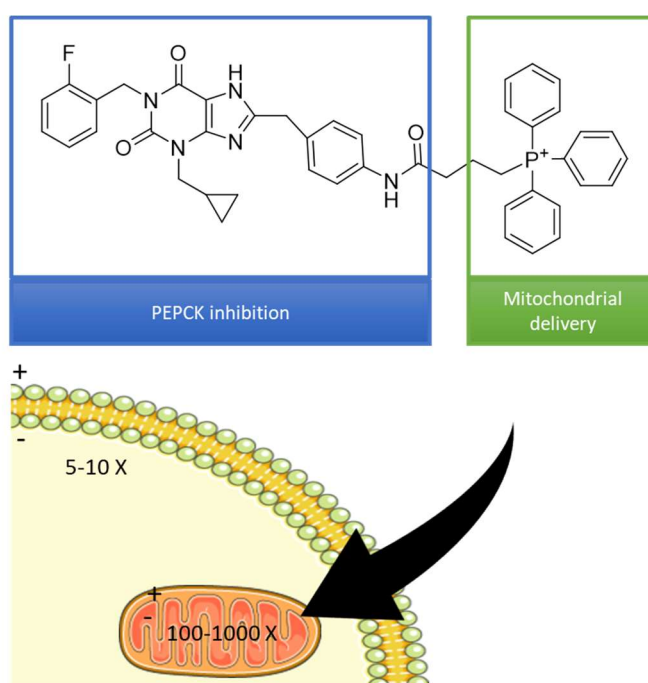


Figure R-26: Strategy followed to develop PEPCK-M selective inhibitors. The addition of a triphenylphosphonium moiety would increase the mitochondrial uptake of the PEPCK inhibitor through the membrane potential.

Nowadays, different systems of mitochondrial targeting had been described: mitochondrial targeting signal peptides, cell-penetrating peptides and lipophilic cations. These tools take advantage of the mitochondria import machinery or the high membrane potential across the inner mitochondrial membrane. Lipophilic cations such as triphenylphosphonium (TPP), can be attracted by mitochondria through electrostatic interactions and accumulated in its matrix due the negative membrane potential (Z. P. Chen et al., 2015; Zielonka et al., 2017). The conjugation of TPP to existing drugs to target the mitochondria has been a successful strategy in the development of treatments for cancer and neurodegenerative diseases. Some of these TPP-conjugated treatments are currently being tested in clinical trials. For example, TPP conjugation

to the nitrogen mustard chlorambucil had driven the compound to cancer cells mitochondria causing cell cycle arrest and inducing cell death (Millard et al., 2013). Also, Mito-DCA, which consist in a dichloroacetate-loaded compound with a TPP group had archived a potency increase of three magnitude orders compared with unconjugated dichloroacetate (Pathak et al., 2014).

Alkyltriphenylphosphonium cations easily cross lipid bilayers by non-carrier-mediated transport. They efficiently enter to the cytoplasm due the plasmatic membrane potential, and further accumulate into the mitochondria (between 100- to 1000-fold more concentrated, compared with the extracellular space) by the mitochondrial membrane potential (Smith et al., 2003). Mitochondria targeting should therefore increase the inhibitor concentration in the mitochondria, increasing the *in vivo* potency, while decreasing the inhibitor concentration at the cytosol, reducing PEPCK-C inhibition (Figure R-26).

A group of iPEPCK-2 derivates containing a TPP moiety was synthetized in Dr. M^a Carmen Escolano's laboratory. Resulting inhibitors (iPEPO-1, iPEPO-2 and iPEPO-3) differ in the number of carbons in the linker (2, 3 or 4) as shown in Figure R-27. The size of the triphenyl phosphonium group could decrease the affinity of the compound with the enzyme due steric effects. Adding carbons to the linker would increase the mobility of the triphenyl phosphonium group, allowing it to be outside of the binding pocket, and therefore maintaining the affinity.

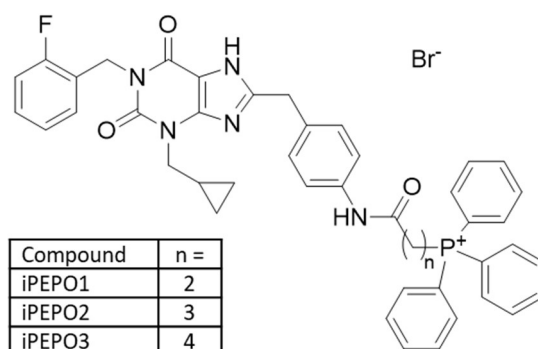


Figure R-27: Structure of the synthetized inhibitors with the tryphenylphosphonium group (iPEPO family).

iPEPOs ADME profile

Before further progressing the iPEPOs' family as on-target inhibitor of PEPCK-M *in vitro*, basic ADMET studies, including cytochrome inhibition, microsomal stability, cytotoxicity and hERG inhibition were performed by the Innopharma Screening Platform.

iPEPO-1 inhibition of recombinant human cytochrome P450 enzymes [CYP1A2, CYP2C9 and CYP2C19] was evaluated with standard substrates as fluorescent probes. The results depicted in Table R-3 showed low inhibition of the cytochromes at a concentration (10 μ M) well above its K_m for PEPCK-M (see below).

CYP1A2	CYP2C9	CYP2C19
16 ± 1	40 ± 1	46 ± 2

Table R-3: Results of % of inhibition of cytochromes by iPEPO-1 at 10 μ M.

Microsomal stability, widely used to determine the degree of primary metabolic clearance in the liver, was assessed in human, mouse and rat microsomes. The assay showed good stability of human, mouse and rat microsomes with half-lives ranging from 61 to 438 min, and from 46% to 92% of iPEPO-1 remaining after 60 min (Table R-4). However, the observed heterogeneity in microsomes from different species, should be taken further into consideration if iPEPOs compounds progress through additional preclinical studies.

Species	% remanent ¹	t1/2 (min)	Cl _{int} ²
Human	45.97	61.15	11.33
Mouse	66.02	87.84	7.89
Rat	92.01	438.21	1.58

Table R-4: Microsomal stability of iPEPO-1 in in human/mouse/rat microsomes.

¹ sampling time 60 min; ² μ L/min⁻¹ mg⁻¹ protein

No significant inhibition of cellular growth ($15 \pm 3\%$ at 100μ M) was observed using a human MRC-5 fibroblast (non-tumoral) cell viability assay, indicating very low cytotoxicity of iPEPO-1. In addition, the effect of iPEPO-1 on hERG channel activity, an important safety determinant in drug discovery, was assessed showing a small inhibition ($15 \pm 2\%$ at 10μ M), suggesting no cardiac side-effects.

Furthermore, data from in vitro PAMPA assays – performed in Dr. Belén Perez’s lab - (Pe value of 2.9 ± 1.15), indicated that iPEPO-1 can be classified to have uncertain blood brain barrier permeation as it is below the threshold established for high BBB permeation (Pe value of 5.17). However, its charge would suggest that the compound might not cross the BBB (J. Müller et al., 2015). Considering the PEPCK-M localization, the ability to cross the BBB is not an essential requirement for developing effective PEPCK-M inhibitors, on the contrary its absence from the brain would indicate a desirable lack of neurological side-effects (Nordlie & Lardy, 1963).

Evaluation of inhibitory potency in recombinant protein

The inhibitory capacity of the compounds was evaluated in human recombinant PEPCK-C and PEPCK-M produced in our laboratory (Table R-5). All compounds inhibited both PEPCK isoforms with a similar potency. iPEPO-2 proved to have the optimal length of the linker with TPP salt, since compounds with a shorter (iPEPO-1) or longer (iPEPO-3) linker decreased the potency. All three triphenylphosphonium derivatives had lower overall potency than iPEPCK-2 from which they are derived, although iPEPO-2 ($IC_{50} = 558$ nM) was in the same magnitude order.

Compound	PEPCK-C	PEPCK-M
iPEPO-1	1.179	4.752
iPEPO-2	0.157	0.558
iPEPO-3	0.771	3.090
3-MPA	10.097	17.402
iPEPCK-2	0.061	0.117

Table R-5: Evaluation of inhibitory potency in purified human recombinant PEPCK-C and PEPCK-M of iPEPO-1, iPEPO-2, iPEPO-3, and the previously described inhibitors iPEPCK-2 and 3-MPA. The table shows IC₅₀ (μM) values for both isoforms.

Target engagement

As we have previously done when evaluating iPEPCK-2, we assessed the iPEPOs capacity to inhibit GSIS as a result of a PEPCK-M inhibition in pancreatic β-cells. Specifically, GSIS was evaluated after treating mice isolated pancreatic islets with 5 μM of iPEPO-1 or iPEPO-2 (Figure R-28). iPEPCK-2 was used as a positive control. The treatment with iPEPO-2 hindered insulin secretion with a similar potency as iPEPCK-2. This confirms that iPEPO-2 could penetrate to the β-pancreatic cells, reach the mitochondria and properly inhibit PEPCK-M.

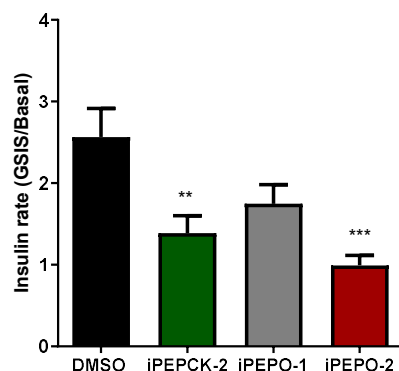


Figure R-28: Glucose stimulated insulin secretion (GSIS) inhibition. Effects of treatment with μM of iPEPO-1, iPEPO-2, or iPEPCK-2 in mice isolated pancreatic islets glucose-stimulated insulin production shown as a ratio of insulin concentration measured in the presence of 20 mM over 3 mM glucose. Data are means ± SEM. A t-test, one-way Anova and a Sidak multiple comparison test were used. Statistical significance at *p < 0.05, **p < 0.01, ***p < 0.001 vs vehicle control.

The addition of the triphenylphosphonium group should lead the molecule to the mitochondria, increasing its concentration there. Moreover, it should decrease the cytosolic concentration, potentially reducing the side effects due PEPCK-C inhibition.

To assess the mitochondrial targeting in a cellular context, a cellular thermal shift assay (CETSA) was performed using the rat hepatoma cell line FAO. FAO cells express both, mitochondrial and cytosolic, PEPCK isoforms. In this assay the most potent compound of the family (iPEPO-2) was compared to the previously described PEPCK inhibitors iPEPCK-2 and 3-MPA (Figure R-29). Since iPEPO-2 showed a slightly lower but

similar potency than iPEPCK-2 in the kinetic assay, and it inhibited GSIS with a similar potency in pancreatic β -cells, we were expecting that iPEPO-2 would have shown an improved thermal stabilization of PEPCK-M – or, at least, the same as iPEPCK-2- due the mitochondrial targeting. However, iPEPCK-2 was the better compound thermal stabilizing the two PEPCK isoforms. Furthermore, iPEPO-2 stabilized the cytosolic isoform with the same potency as the mitochondrial one.

The results of these assays couldn't demonstrate any improve on target engagement of iPEPOs when compared with iPEPCK-2, which have demonstrated a great capacity to reach the mitochondria.

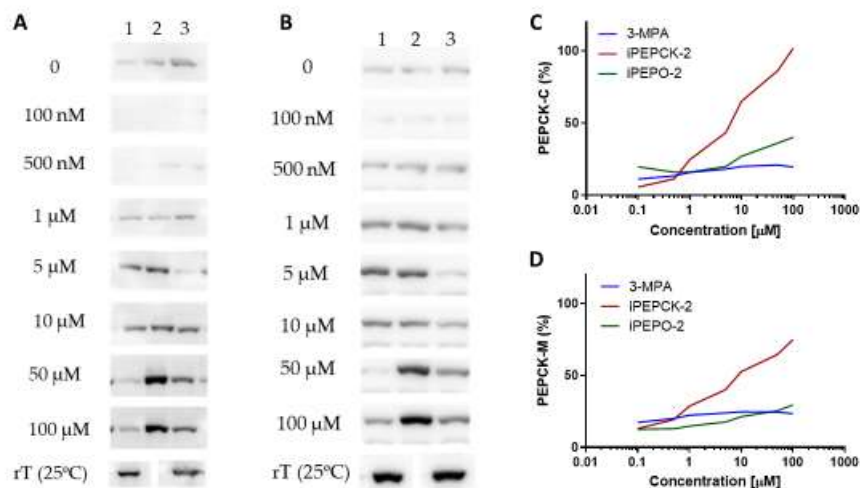


Figure R-29: Evaluation of in vitro target engagement by Cellular thermal shift assay. (A-B) Stable PEPCK-C (A) and PEPCK-M (B) in FAO cells after a thermal treatment (60°C, 3min) previously incubated with increasing doses of PEPCK inhibitors (1: 3-MPA; 2: iPEPCK-2; 3: iPEPO-2). (C-D) Smoothed curve (GraphPad Prism) of previous CETSA (PEPCK-C (C) and PEPCK-M (D)).

Antineoplastic activity

PEPCK-M inhibition by iPEPO-2 was evaluated in different cancer models to assess its antineoplastic activity. iPEPO-2 was tested with cervical cancer (HeLa), colorectal cancer (SW480) and transformed kidney embryonal (HEK-293) cell lines. As mentioned before, these cells have high expression of PEPCK-M while they don't express PEPCK-C.

Treatment with 5 μ M of iPEPO-2 reduced cell growth at 72 hours between a 32 and a 64%, depending on the cell line (Figure R-30A). They were similar values as the ones obtained when using iPEPCK-2. Interestingly, iPEPO-2 treatment up to 10 μ M did not affect cell growth and viability in HEK-293-PCK2^{del/del} cells (Figure R-30B). However, treatments with higher concentrations than 10 μ M impaired cell growth suggesting off-target toxicity at these doses. PEPCK-M inhibition by iPEPO-2 also inhibited anchorage independent growth in a similar manner than iPEPCK-2 (Figure R-30C).

Finally, treatment with iPEPO-2 decreased the viability of glucose deprived cells after 48h with the same intensity as iPEPCK-2 (Figure R-30 D-F). PEPCK-M inhibition blocks the usage of carbons from TCA cycle

(coming from glutamine, fatty acids, etc) for the obtention of necessary gluconeogenic intermediates during glucose shortage, and this leads to an increase of ER-stress-mediated apoptosis.

Despite iPEPO-2 showed a slightly lower potency in the kinetic assay and a lower thermal stabilization in CETSA compared with iPEPCK-2, it showed similar outcomes in the functional assays in pancreatic islets and cancer cells.

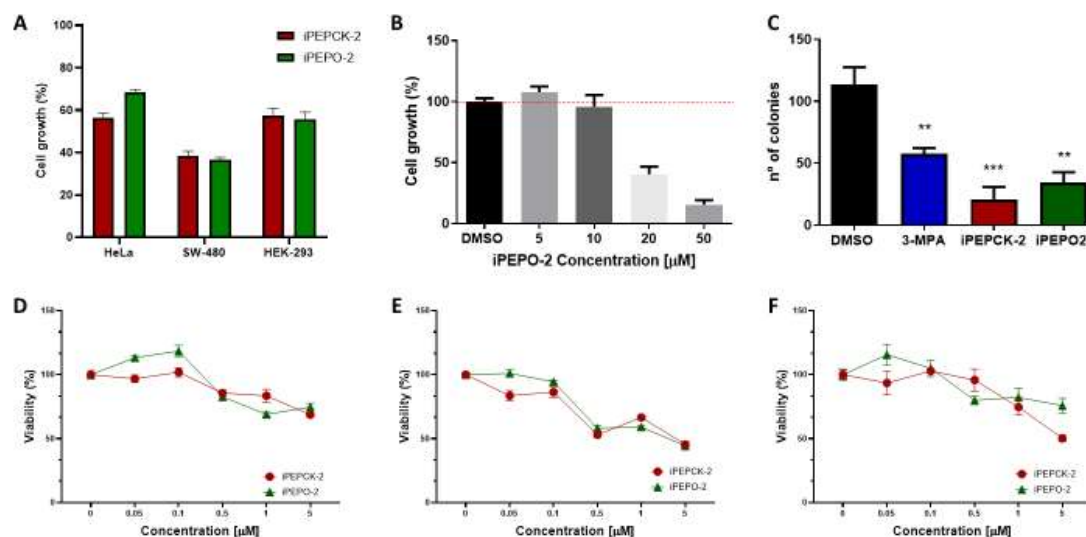


Figure R-30: iPEPO-2 activity on cancer cells. (A) Cell growth inhibition after a 5 μM treatment with iPEPCK-2 or iPEPO-2 for 72h. (B) Treatment of HEK-293-PCK2^{del/del} with increasing concentrations of Ipepo-2 (C) Colonies formed in soft agar after treatment 5 μM of different PEPCK-M inhibitors (HeLa cells) (D-F) Viability of HeLa (D), SW-480 (E), and HEK-293 (F) cells under glucose deprivation of 48h, cells were treated with different doses of iPEPCK-2 or iPEPO-2. Data are means ± SEM (3 independent experiments were performed with n=5 in for panels A, B, D, E, F; and 3 independent experiments with n=3 for panel C). A one-way Anova and a Sidak multiple comparison test was used. Statistical significance at *p < 0.05, **p < 0.01, ***p < 0.001 vs vehicle control.

Overall, we reported the first family of PEPCK-M inhibitors with a triphenylphosphonium group. Although iPEPO family has a good inhibition profile (the compounds inhibited PEPCK-M in the nanomolar range, and they could reach the mitochondria inhibiting PEPCK-M in a physiologic model), it could not demonstrate an increased efficacy respect iPEPCK family. Other strategies should be followed to find inhibitors specifically inhibit the mitochondrial isoform.

Furthermore, the search of PEPCK-M inhibitors for cancer and diabetes therapy has gained interest in the last years. Baptista et al. performed a virtual screening with ZINC's natural compounds database to identify novel PEPCK-M inhibitors (Baptista et al., 2019). And other groups identified PEPCK inhibitors from plant extracts (Femi-Olabisi et al., 2021; X. L. Ma et al., 2021).

CHAPTER 2: PYCR INHIBITORS

In silico-guided discovery of PYCR1 inhibitors for cancer therapy

Recent findings on the implication of proline metabolism derangements in iPEPCK-2 mode of action, and the overall implications of proline metabolism in metabolic reprogramming in cancer, have positioned the proline biosynthesis pathway – and specifically PYCR1 – as an emergent target for cancer therapy (Bogner et al., 2021; D’Aniello et al., 2020). PYCR1 has demonstrated to play an important role in a wide variety of cancers, and its silencing inhibited tumor growth, invasion and metastasis, and drug resistance in different genetic models (J. Ding et al., 2017; Loayza-Puch et al., 2016; Sattar Alaqbi et al., 2022; Shenoy et al., 2020; S. Xiao et al., 2020; Yan et al., 2019). Therefore, we and others postulate that its inhibition by small molecules could be useful for cancer treatment. However, as described in the introduction, few PYCR1 inhibitors have been described so far (Christensen et al., 2020; Forlani et al., 2021; Milne et al., 2019).

Since the PYCR1 crystal structure in both apo and holo forms have been already resolved (Christensen et al., 2017), we performed a computer-aided structure-based strategy to discover and design novel potent PYCR1 inhibitors.

This project was performed in collaboration with Dr. F. Javier Luque, who guided me through the computational approach, and Dr. M^a Carmen Escolano, in charge of the synthesis of the different compounds here described.

PYCR1 structural insights

The three-dimensional structures of human PYCR1 and P5CRs from different microorganism and plant species are already known (Christensen et al., 2017; Meng et al., 2006; Nocek et al., 2005; Ruszkowski et al., 2015). Regarding the human enzyme, in 2006 Meng et al. reported PYCR1 crystal structures that provided the first information about its structure. However, the low resolution of these structures (3.1 Å) was insufficient to locate the active site (Meng et al., 2006). In 2017 Christensen et al. reported high resolution structures of PYCR1 (1.85 Å) with its natural ligands (or analogs) that allowed the identification of the active site (Christensen et al., 2017). We used the structures solved by Christensen et al. (PDB IDs: 5UAV, 5UAU, 5UAT) to deploy our structure-based drug design campaign.

PYCR1 structure consists in a pentamer-of-dimers decamer. Each PYCR1 protomer has a Rossmann dinucleotide binding domain, where the cofactor NAD(P)H binds, and an α -helical domain, which mediates oligomerization and plays a role in the P5C binding. The active site is located in the dimer interface, where the P5C binding site of one protomer meets the NAD(P)H binding site of the other one (Figure R-31 A). Therefore, dimerization is essential for PYCR1 activity (Bogner et al., 2021; Christensen et al., 2017).

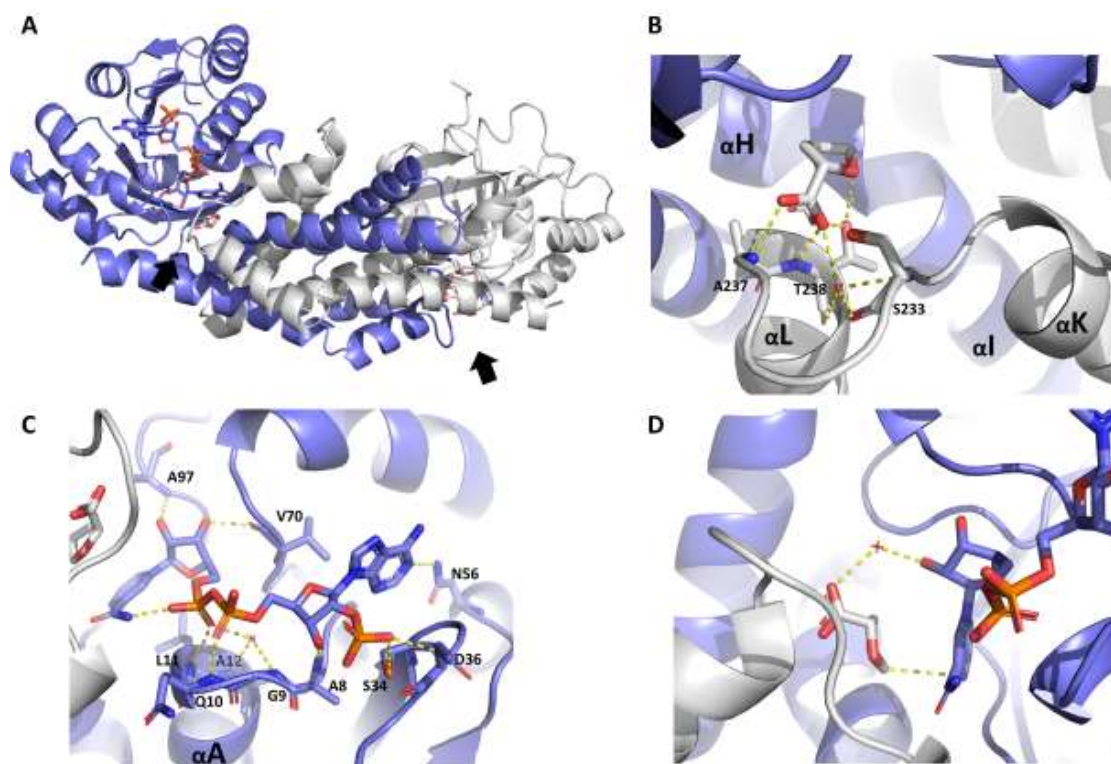


Figure R-31: PYCR1 structural insights. (A) Structure of PYCR1 (PDB ID:5UAV) homodimer each protomer is differently colored. The two binding sites are pointed by arrows. (B) P5C/proline binding site: the proline analog THFA and its interactions with the protein in its binding site. (C) NAD(P)H binding site: NADPH and its interactions with the protein in its binding site. (D) Structure of the ternary complex of PYCR1-THFA-NADPH. Amino acids that form relevant interactions are highlighted as sticks. Hydrogen bonds are represented by yellow dotted lines. α -helices are labeled according to the nomenclature used in Christensen et al. 2017.

The P5C/proline binding site is found in the pocket where the loop between the α -helices L and K from the α -helical domain of one protomer meets the α -helices H, I, and M of the other protomer (Figure R-31B). The carboxylic group of P5C/proline forms hydrogen-bonds with the residues of the α L- α K loop (mainly with the NH of the backbone), some of them mediated through a water molecule. The residues of the α H and α I provide nonpolar contacts that contribute to the catalysis (Christensen et al., 2017).

The Rossmann fold is a conserved tertiary structure that consists in six parallel β -strands, connected by α -helices, that form an extended β -sheet. The function of the Rossmann fold in enzymes is to bind nucleotide cofactors such as NADH, NADPH, and FADH₂ (Rossmann et al., 1974). Consequently, the NAD(P)H binds PYCR1 in the Rossmann fold found at the protomer's N-terminal domain. NADPH forms many non-covalent interactions with the protein, most of them with the backbone of the protein (Figure R-31C). The pyrophosphate of NADPH is positioned at the end of the first helix (α A) of the Rossmann fold forming H-bonds with the backbone's NH (residues 9-12), some of them mediated through a water (Christensen et al., 2017).

Using the proline analog THFA and NADPH, Christensen et al. reported a structure (PDB ID: 5UAV) that mimics the Michaelis complex. This structure reveals important information about the catalytic mechanism.

Importantly, the THFA ring is parallel to the nicotinamide ring of NADPH as expected for a hydride-transfer mechanism (Figure R-31D). The authors also described a group of waters that would stabilize the ternary complex. Although some authors suggested that T238 would donate a proton to the imine nitrogen of P5C, Christensen et al demonstrated that it was not essential for the catalysis.

Regarding other PYCR isoforms, a low-resolution crystal structure of PYCR2 has also been reported while the structure of PYCR3 has not been resolved yet (Escande-Beillard et al., 2020). PYCR1 and PYCR2 share 85 % of its amino acid sequence and their active sites are 97 % identical in sequence. On the other hand, PYCR3 shares 45 % of its amino acid sequence to PYCR1, and the amino acid sequence of the active site is 53 % identical and 72 % similar than PYCR1 one. The major differences between PYCR3 and PYCR1/2 active sites are found in the NADPH binding site, which may explain the differences on the cofactors used for each isoenzyme (Bogner et al., 2021).

Virtual screening protocol

As mentioned in the introduction, virtual screening (VS) protocols are used to identify compounds that would bind to a specific target from a large library of compounds. Its advantages with respect to classic high-throughput screenings are its speed (thousands of compounds could be tested in matter of hours), its reduced costs (VS significantly reduces the number of compounds that should be purchased or synthesized), and if the VS protocols are structure-based, they might provide knowledge about the molecular basis of the activity of the compounds (Gimeno et al., 2019).

To identify novel PYCR1 inhibitors, we performed a VS study using the previously resolved PYCR1 crystal structure (PDB ID: 5UAV) and the SPECS Exciting Academic Database (ExAcD). The general schema followed is described in Figure R-32.

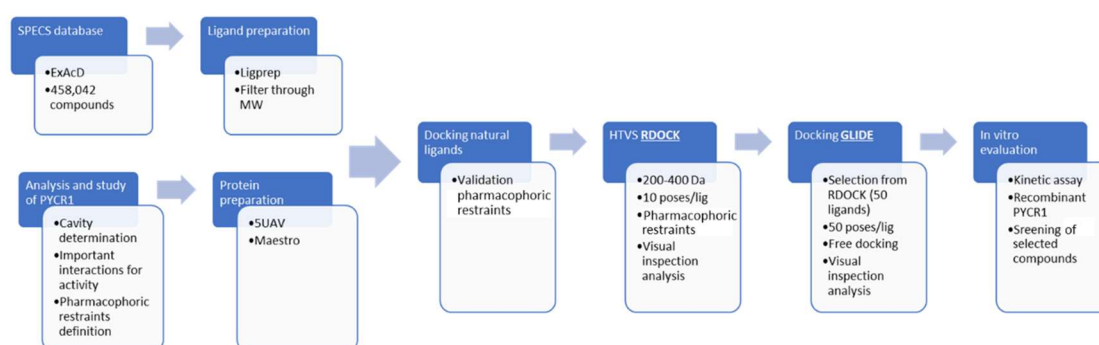


Figure R-32: Schema of the followed screening protocol.

After PYCR1 structures were studied, we defined a pocket in the active site as the cavity where the compounds were going to be docked (Figure R-33A). Interestingly, the crystal structures that did not contain P5C or a proline had a conserved sulfate molecule in the proline binding site (in the loop between α K and α L), precisely where the carboxylic group is located. Similarly, a conserved sulfate is found where the

pyrophosphate group of NADPH binds (at the end of α A) in the structures without NADPH (Figure R-33B). In both cases, hydrogen bonds are formed with the backbone amino acids and the sulfate molecules. These positions are occupied by hydrogen-bond acceptors (carboxylate from THFA/proline, pyrophosphate from NADPH, or sulfate molecules) - some of them with a negative charge - in the different structures. Therefore, we hypothesized that a molecule which could fill these positions with a hydrogen-acceptor group would increase its affinity for the enzyme. Consequently, we keep these positions as pharmacophoric restraints.

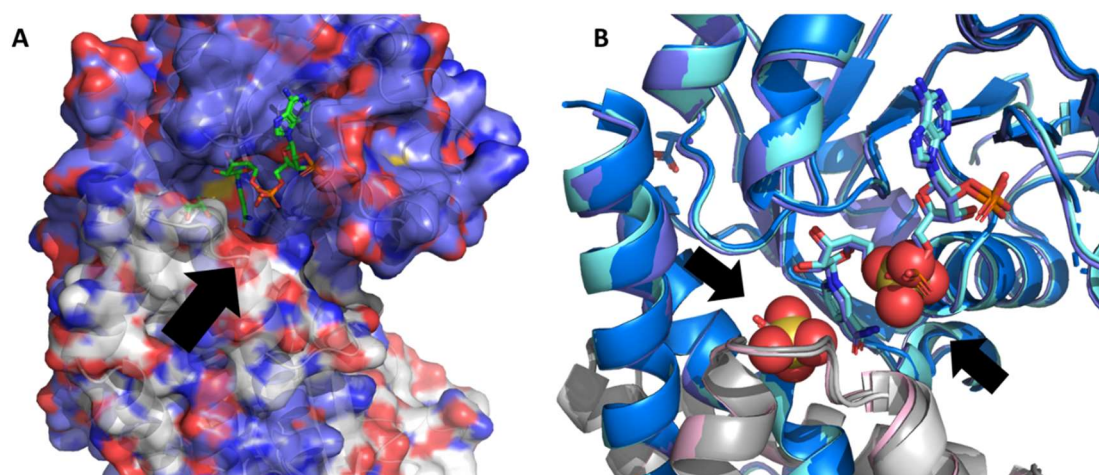


Figure R-33: PYCR1 binding site (A) The arrow indicates the pocket in the binding site where the docking was performed. **(B)** Superposition of PYCR1 structures (PDB IDs: 5UAV, 5UAU, 5UAT) where a conserved sulfate molecules (highlighted as spheres) can be observed in the P5C/proline and NAD(P)H binding sites.

The ExAcD is a library with > 450,000 structure-diverse drug-like compounds described in academia. The compounds of the library were prepared using LigPrep: the three-dimensional structures were generated forming up to 6 tautomers and 8 stereoisomer per molecule, and the ionization was defined at pH 7.4. The compounds were filtered through molecular weight (keeping those between 200 and 400 Da) and the compounds which did not have at least two hydrogen-bond acceptors were discarded.

The VS analysis consisted in two consecutive docking protocols. The first molecular docking protocol was performed using RDOCK with pharmacophoric restraints, and high-throughput VS sensitivity. The pharmacophoric restraints allowed to “guide” the docking providing information about ligand-protein interactions. In our case we defined three pharmacophoric restraints, and two of them had to be fulfilled. We defined that a H-bond acceptor should be at the position of both sulfates (showed in Figure R-33B) and in the position of the water of Figure R-31D, since it could be important for the catalytic mechanism. Ten poses were generated for each ligand. After visual inspection of the poses with better scores, 50 molecules were selected for the following docking protocol.

The second docking protocol was performed using GLIDE in a more exhaustive manner. This protocol was performed without pharmacophoric restraints to validate the positions obtained in the first protocol and to identify artifacts caused by the restraints. After visual inspection of the generated poses, 15 molecules were

selected, and nine were purchased for *in vitro* evaluation (Figure R-34). Interestingly, many poses show compounds that had a sulfonamide group placed at the end of the α A forming multiple H-bonds with the NH from the protein backbone, similarly to the pyrophosphate group of NADPH.

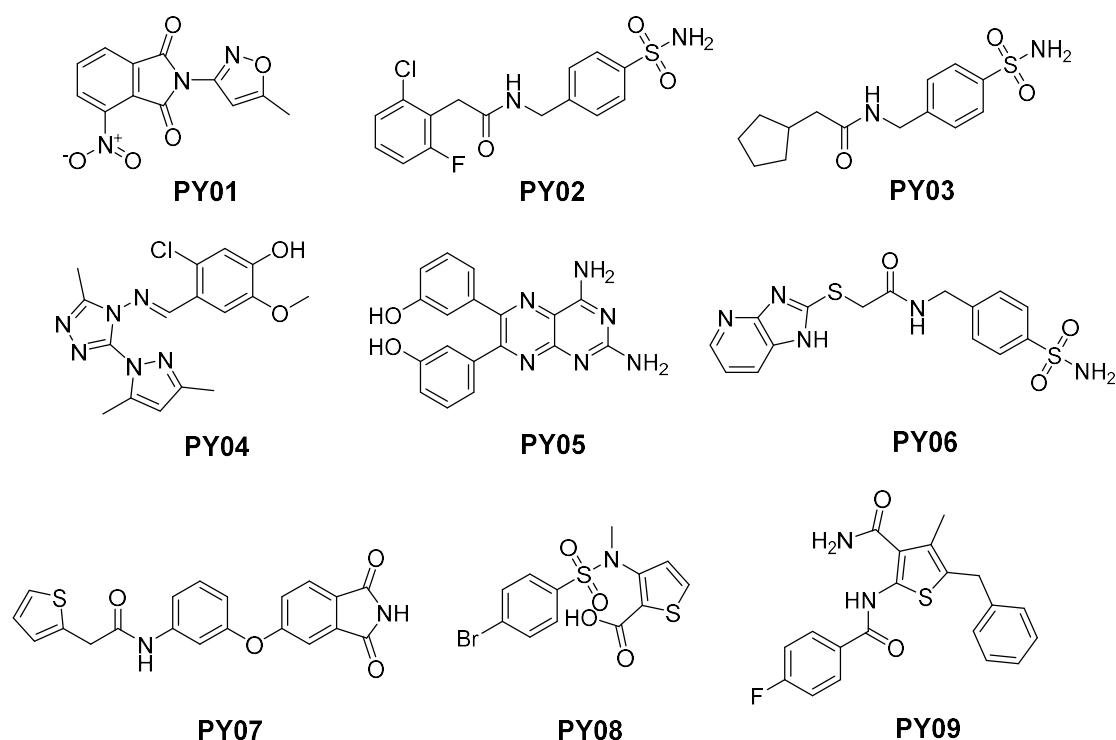


Figure R-34: Purchased compounds resulting from the virtual screening.

A kinetic assay was set up with purified recombinant human PYCR1 produced in a prokaryote system in our laboratory (Figure R-35A). In the assay we evaluated the 3,4-dehydro-L-proline (DHP) dehydrogenase activity of PYCR1 (Figure R-35B) described by Li et al. since we were not able to synthesize/purchase P5C (L. Li et al., 2017). The velocity of NAD^+ reduction was measured by fluorescence. The enzymatic assay was validated using the low-potency PYCR1 inhibitor THFA (Figure R-35C).

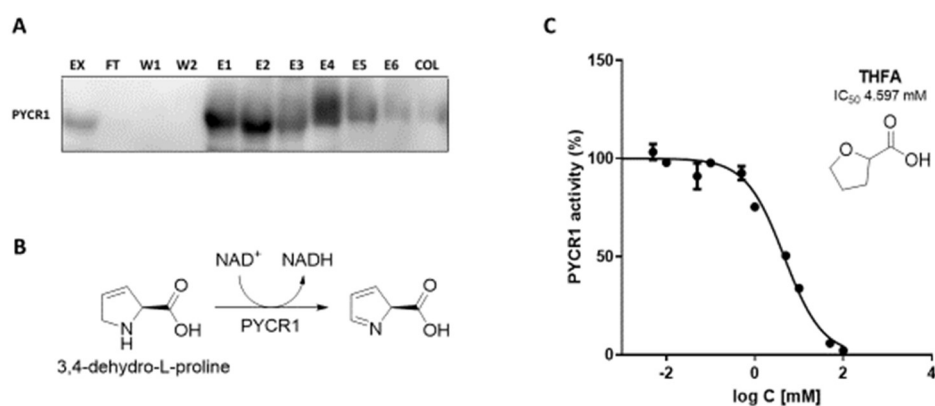


Figure R-35: Enzymatic assay set up. (A) Western blot analysis of produced PYCR1 protein during its purification. EX: extract; FT: flow through; W1-2: washes; E1-6: elution; COL: column remanent. **(B)** Reduction of 3,4-dehydro-L-proline (DHP) by the dehydrogenase activity of PYCR1. **(C)** Inhibition curve of the proline analog THFA. Data are means \pm SEM. The inhibition curve was adjusted by the nonlinear regression fit tool from GraphPad Prism.

The inhibitory capacity of the compounds (PY01-PY09) was evaluated in the aforementioned enzymatic assay (Table R-6). Results were compared with THFA, which was used as a positive control. Most of the compounds showed negligible PYCR1 inhibition, with an IC₅₀ above 1 mM. However, PY04 was identified as a hit that inhibited PYCR1 with an IC₅₀ of 123.6 μM.

Compound	Docking score [kcal/mol]	IC ₅₀	Inhibition at 1mM (%)
PY01	-6.73	>1mM	25.5
PY02	-7.33	>1mM	9.8
PY03	-6.78	>1mM	6.2
PY04	-6.59	123.6 μM	91.1
PY05	-8.04	>1mM	27.7
PY06	-7.04	>1mM	36.1
PY07	-7.19	>1mM	11.0
PY08	-6.43	>1mM	12.7
PY09	-7.09	n/a *	n/a
THFA	-	4.597 mM	24.7

Table R-6: Evaluation of purchased compounds in the enzymatic assay. The IC₅₀ was calculated by adjusting the inhibition curve with the nonlinear regression GraphPad tool.

Further kinetic studies were performed with PY04 to determine the K_i and inhibition type. The representation of Lineweaver-Burk plots demonstrated that PY04 inhibited PYCR1 in a competitive manner with both substrates, DHP and NAD⁺ (Figure R-36A-B) (Waldrop, 2009). It inhibited PYCR1 with a K_i of 521 μM for DHP and 243.5 μM for NAD⁺.

This type of inhibition is in agreement with the reported docking pose, where PY04 fills the position of both substrates (Figure R-36C). As showed in the figure, PY04 could H-bond with the backbone of αK-αL loop, the end of αA (the orientation is not perfect though), and with the carbonyl group of A69. Furthermore, it anchored the nonpolar pyrazoline ring into the hydrophobic pocket with the possibility of forming an H-bond with the lateral chain of T238, although the orientation is not optimal.

Using the chemical scaffold of PY04 as template, we searched for analogs that were subsequently screened by molecular docking. Two of them (PY04_1 and PY04_2) were purchased and showed increased potency in the kinetic assay (Figure R-37). The docking poses were similar to PY04's one and showed that the hydroxyl group could form interactions with C95 (PY04_1) or A69 (PY04_2) carbonyl groups.

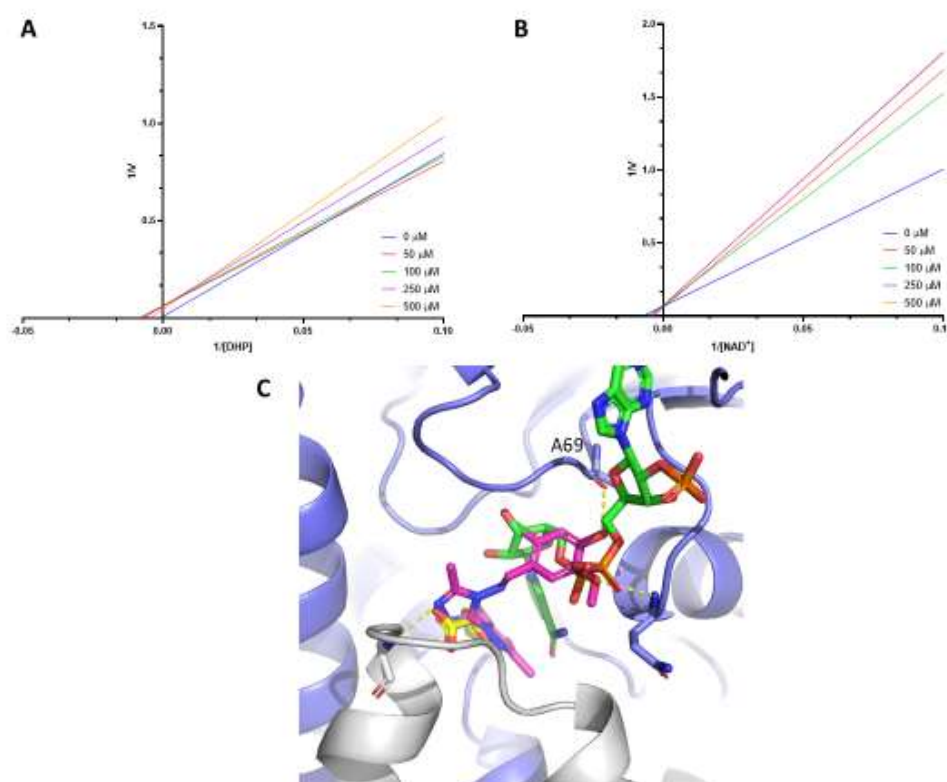


Figure R-36: PY04 inhibition mechanism. (A-B) Lineweaver-Burk plots of PY04 with different concentrations of DHP (A) and NAD^+ (B). PY04 (pink) docking pose with superposed ligands, THFA (yellow) and NADPH (green). PY04 – protein H-bonds are showed as a yellow dotted line.

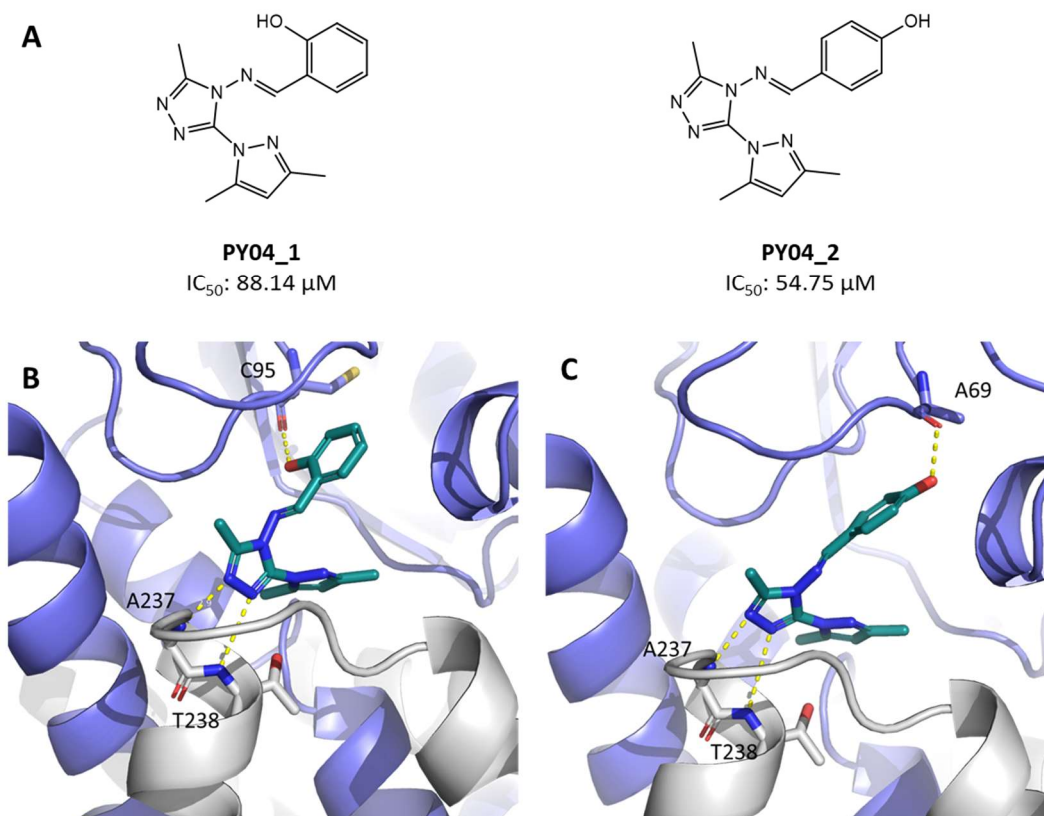


Figure R-37: PY04's analogs. (A) PY04's analogs structure and IC_{50} in the kinetic assay. (B-C) Docking poses of PY04_1 (B) and PY04_2 (C). Possible H-bonds with PYCR1 amino acids are noted as yellow dotted lines.

A molecular dynamics (MD) simulation of the most potent compound (PY04_2) was performed in order to confirm the binding mode. The H-bonds between the pyrazoline and the α K- α L loop were weak, the distance between A237 NH and the N from the pyrazoline was between 3.4 and 3.7 Å during the simulation (Figure R-38A and C). However, the H-bond formed between the carbonyl group of A69 and the hydroxyl from the phenol group was not maintained during the 50 ns of MD (Figure R-38D). Furthermore, the phenol group was mostly exposed to the solvent (Figure R-38B). Although the molecule remained in the binding site, it could not maintain the polar interactions described. Therefore, it is probable that the binding mode obtained in the dockings is not correct. Furthermore, using SwissADME we detected that PY04 and its analogs presented PAINS (pan-assay interference structures) (PAINS code: hzone_phenol) which often give false positive results in pharmacologic screens (Baell & Holloway, 2010; Daina et al., 2017).

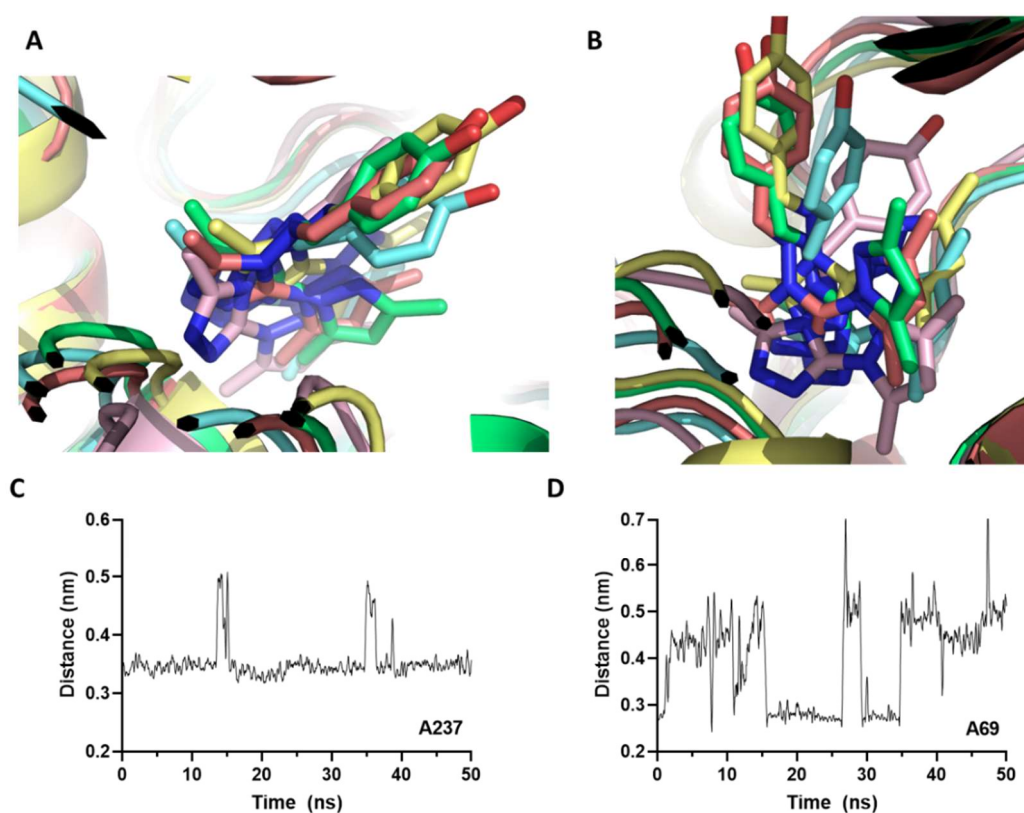


Figure R-38: PY04_2 MD simulation. (A-B) Superposition of MD simulation snapshots (every 10 ns). (C) Distance between the NH from A237 and the nitrogen from the pyrazoline ring. (D) Distance between the hydroxyl from the phenol group of PY04_1 and A69's carbonyl.

2nd Virtual screening campaign

A second VS with a different compound library (Specs_SC, with around 210,000 compounds) and a slightly different protocol summarized in Figure R-39 was performed. This protocol also consisted in a two-step docking - this time without pharmacophoric restraints - where the first docking protocol allowed us to quickly parse the whole database, and during the second one a selection of the best candidates was exhaustively analyzed. The ligands were prepared and filtered by molecular weight (150-500 Da) with LigPrep. A second

filter was applied to select the compounds that have at least one carboxylic acid or carboxylate group. Then, the resulting compounds (9813) were docked using GLIDE with a HTVS sensitivity (which is faster albeit less accurate), reporting 10 poses/ligand. The compounds with energies below -7 kcal/mol (440 compounds) were docked again using GLIDE in standard sensitivity and generating 50 poses/ligand. The poses with better score (energy < -8 kcal/mol) were visually inspected and we selected 14 compounds for further evaluation.

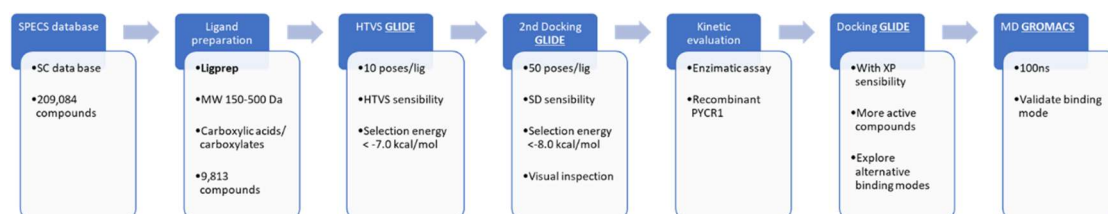


Figure R-39: Workflow diagram of the second HTVS strategy.

The selected compounds were purchased and evaluated in a kinetic assay (Figure R-40). Eight of the compounds inhibited PYCR1 with an IC_{50} below 1 mM, two of them < 100 μ M (Table R-7).

ID	Docking score [kcal/mol]	IC_{50} [μ M]	Inh 1mM (%)
PY10	-8.028	161.3	96.0
PY11	-7.023	>1mM	-3.0
PY12	-8.672	>1mM	11.6
PY13	-8.724	186.1	96.6
PY14	-8.087	>1mM	36.8
PY15	-8.739	>1mM	17.7
PY16	-8.345	67.53	*
PY17	-8.422	35.24	101.1
PY18	-8.075	>1mM	-9.5
PY19	-8.017	501.6	75.1
PY20	-8.726	>1mM	25.1
PY21	-8.22	611.9	62.1
PY22	-8.492	449.5	54.7
PY23	-8.738	216.6	88.2
THFA	-	\approx 5 mM	70.2 (10 mM)
NFLP	-	860.3	50.7

Table R-7: Evaluation of the VS selected compounds through the enzymatic assay. The IC_{50} of the different molecules were calculated by adjusting the inhibition curve with the nonlinear regression GraphPad tool.

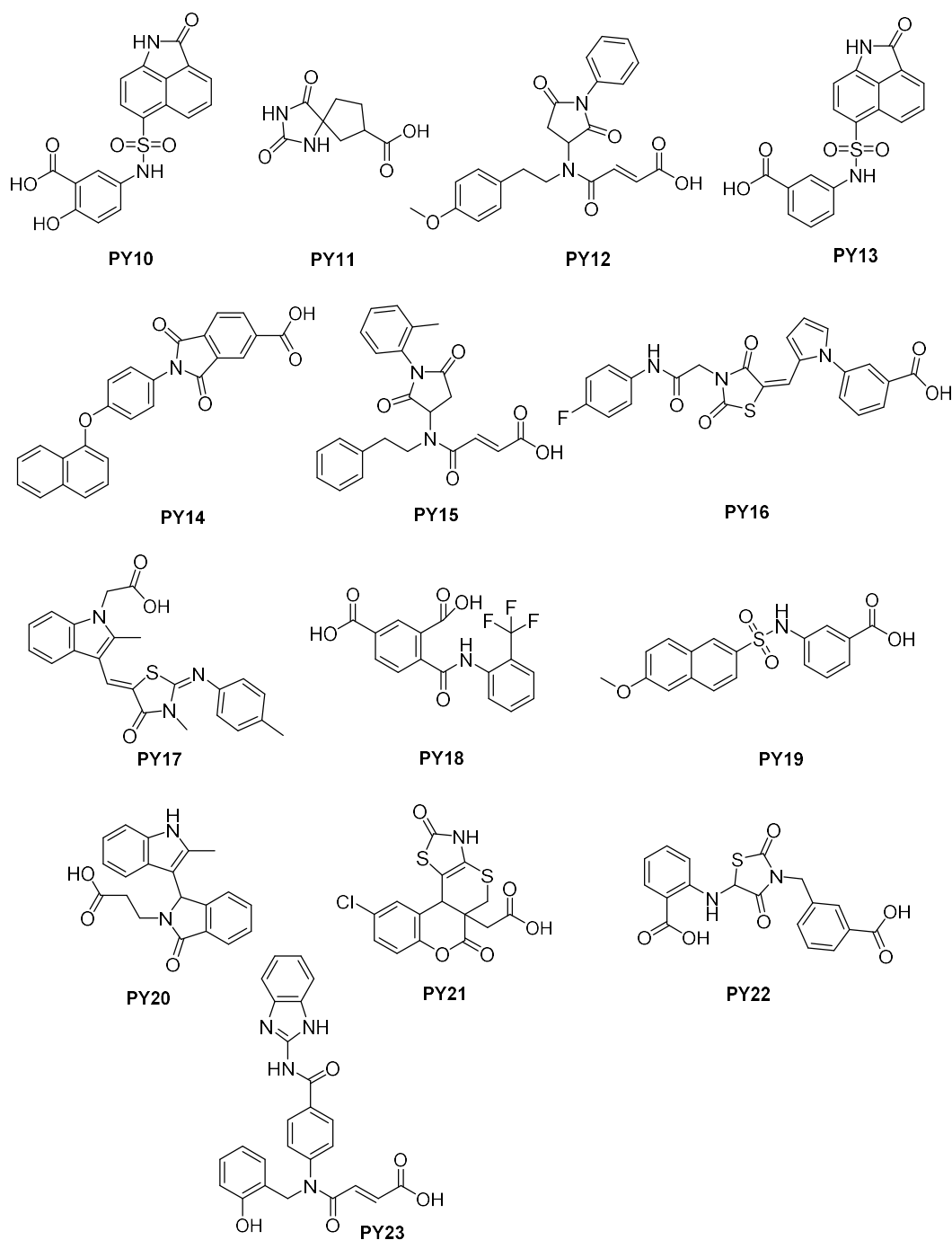


Figure R-40: Structure of the compounds selected in the second virtual screening to further in vitro evaluation.

Physicochemical descriptors and ADME parameters of hit molecules were predicted using SwissADME (Table R-8). Some of the compounds had PAINS (PY10, PY23), and therefore were discarded for further evaluation. All the compounds fulfil Lipinski's Rule-of-five showing druglike properties. Some of them (PY13, PY17, and PY19) are predicted to have high gastrointestinal absorption, while none of them are predicted to cross the blood-brain-barrier. Except PY13, all the molecules are predicted to inhibit at least one CYP isoform.

Compound	Log P	Solubility (μM)	GI absorption	BBB permeability	CYP inhibition	Lipinski
PY13	1.94	78.38	High	No	No	Yes
PY16	2.75	6.93	Low	No	CYP2C9 CYP2C19	Yes
PY17	3.77	1.35	High	No	CYP2C9 CYP2C19	Yes
PY19	2.49	2.43	High	No	CYP2C9	Yes
PY21	2.55	91.2	Low	No	CYP2C19	Yes

Table R-8: Predicted physicochemical descriptors and ADME parameters by SwissADME. Described Log P and solubility are the average of five (iLOGP, XLOGP3, WLOGP, MLOGP, SILICOS-IT) and three (ESOL, Ali, SILICOS-IT) different predictions (respectively) with different methods.

Inhibition mechanism

The inhibition of PYCR1 of the most potent hit compounds ($\text{IC}_{50} < 200 \mu\text{M}$) was evaluated in vitro with different substrates concentration in order to determine the inhibition type. PY13 and PY17 inhibited PYCR1 by a competitive mechanism with both substrates, DHP and NAD^+ . With a K_i of $21.18 \mu\text{M}$ or $14.65 \mu\text{M}$ for DHP and $27.38 \mu\text{M}$ or $15.52 \mu\text{M}$ for NAD^+ for PY13 and PY27 respectively (Figure R-41).

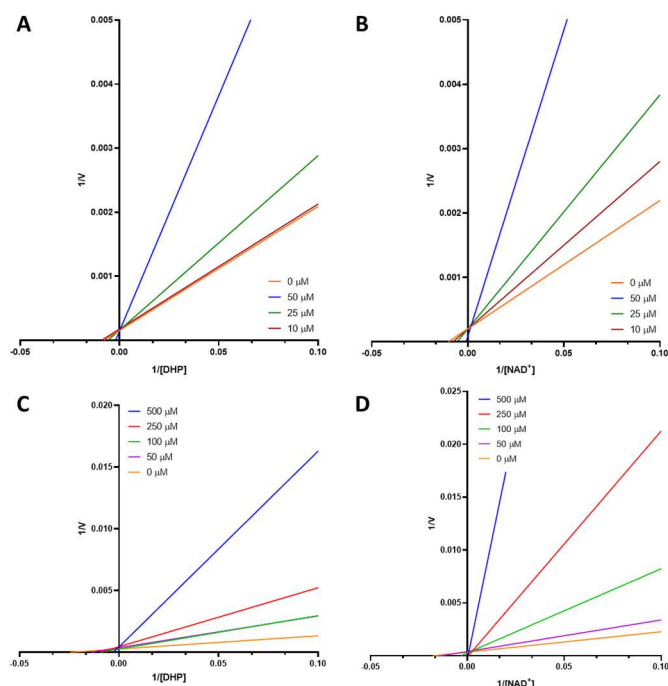


Figure R-41: Lineweaver-Burk plots of hit compounds. Lineweaver-Burk plots of PY17 (A-B) and PY13 (C-D) with different concentrations of DHP (A-C) and NAD^+ (B-D).

To precisely determine the binding mode, these compounds were docked with GLIDE using the extra precision mode (XP), and the most probable poses were selected by visual inspection to further evaluation through MD simulations (Figure R-42).

The docking analysis revealed two possible binding modes for PY13. In the first binding mode, the carboxylate group formed H-bonds with the amino acids at the end of the α A, the tricyclic ring was buried in the pocket making nonpolar interactions and forming two H-bonds with C95 and T122, and the sulfonamide was exposed to solvent (Figure R-42A). In the second binding mode, the carboxylic group of PY13 formed H-bonds with the α K- α L loop filling the position where the carboxylate group should be. The tricyclic ring was buried in the pocket in a similar manner than the other pose, and the sulfonamide was exposed to solvent with the possibility of making a H-bond with V231 (Figure R-42B).

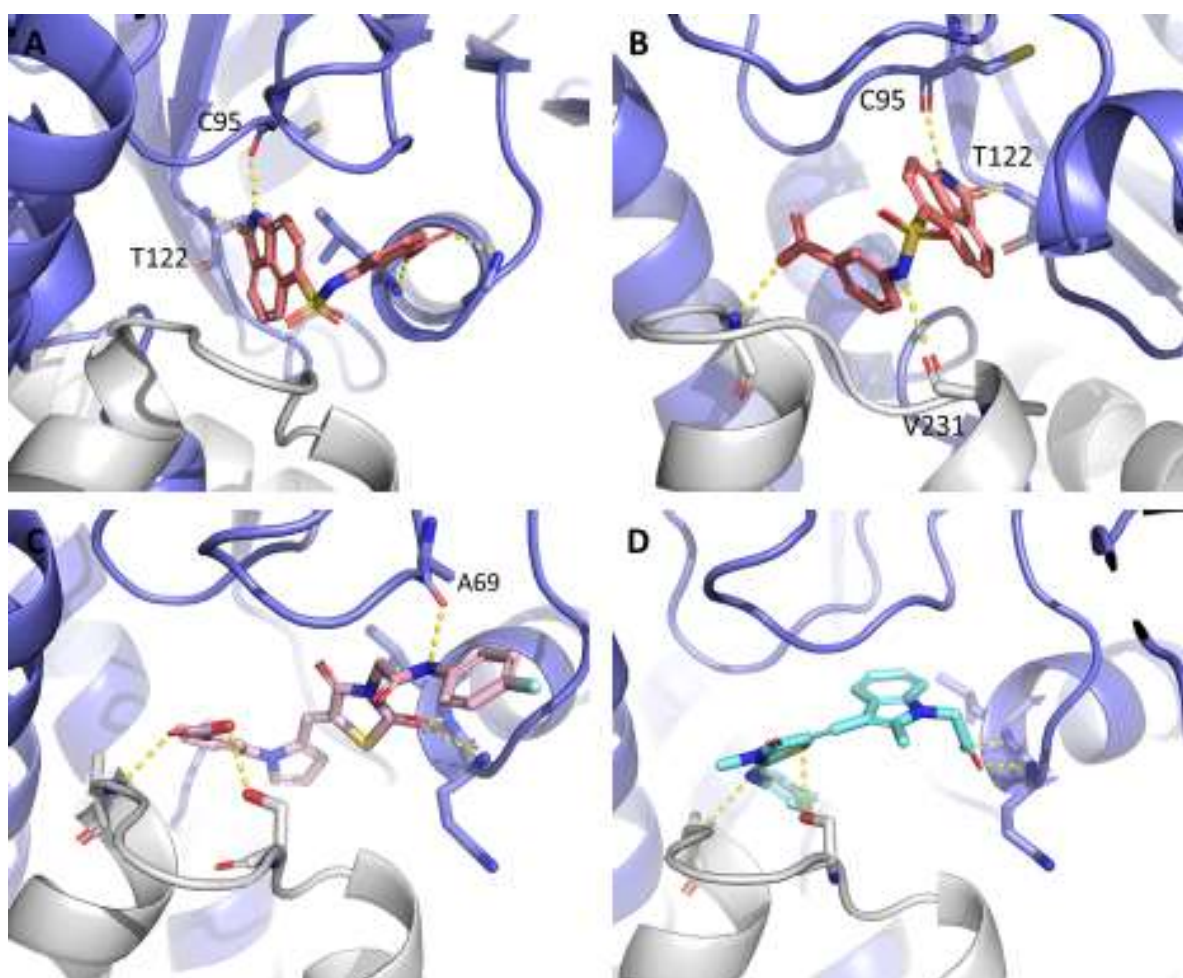


Figure R-42: Most probable binding modes of PY13, PY16, PY17. Most probable poses of PY13 (A-B), PY16 (C), and PY17 (D) in PYCR1 (PDB ID: 5UAV) binding site obtained by molecular docking with GLIDE. Possible formed hydrogen-bonds with PYCR1 residues are noted as yellow dotted lines.

The most probable binding mode of PY16 is shown in Figure R-42C. Its carboxylic group could form H-bonds with the amino acids of the α K- α L loop, while a carbonyl from the imide could interact with the residues at the end of α A. The NH from the amide could form an H-bond with A69. However, many of its polar groups

were not forming interactions which would imply a sizable desolvation cost that would reduce binding affinity.

Finally, the best pose found for PY17 shows that the carboxylic group was placed at the end of αA , where it formed interactions with the backbone of the protein. The heterocyclic ring could form interactions with the amino acids of the αK - αL loop, and the nonpolar parts of the molecule are buried in the pocket. The polar atoms of the heterocycle that could not form interactions with the αK - αL loop are exposed to solvent (Figure R-42D).

Analog search

Using the chemical scaffold of PY13, PY16, and PY17 as template, we searched for analogs that were subsequently screened by molecular docking. Docking of PY13 analogs, showed that the addition of small nonpolar substituents in *ortho* to the carboxylic group could protect the H-bonds formed between the carboxylate and the αA residues (in the first binding mode) from being disturbed by water molecules (Figure R-43B). In the other PY13 binding mode, these substituents would fill a nonpolar cavity of the pocket increasing its stability in the binding site (Figure R-43C). Three PY17 analogs showed a similar binding mode than PY17, but they seem to form a few more interactions with the protein (suggesting an increased affinity, and therefore inhibition potency). PY13 and PY17 analogs were purchased or synthesized in Dr. Escolano's laboratory and assayed *in vitro* in the kinetic assay. While PY17 analogs (PY24-26) inhibited PYCR1 with lower potency than PY17, PY13 analogs (PY27-29), they showed up to a 6-fold potency increase compared with PY13 (Table R-9).

Compound	IC ₅₀ [μ M]
PY24	157.4
PY25	229.1
PY26	135.6
PY27	30.42
PY28	46.15
PY29	58.14
PY13	186.1
PY17	35.24

Table R-9: Evaluation of PY13 & PY17 analogs by the enzymatic assay. The IC₅₀ were calculated by adjusting the inhibition curve with the nonlinear regression GraphPad tool.

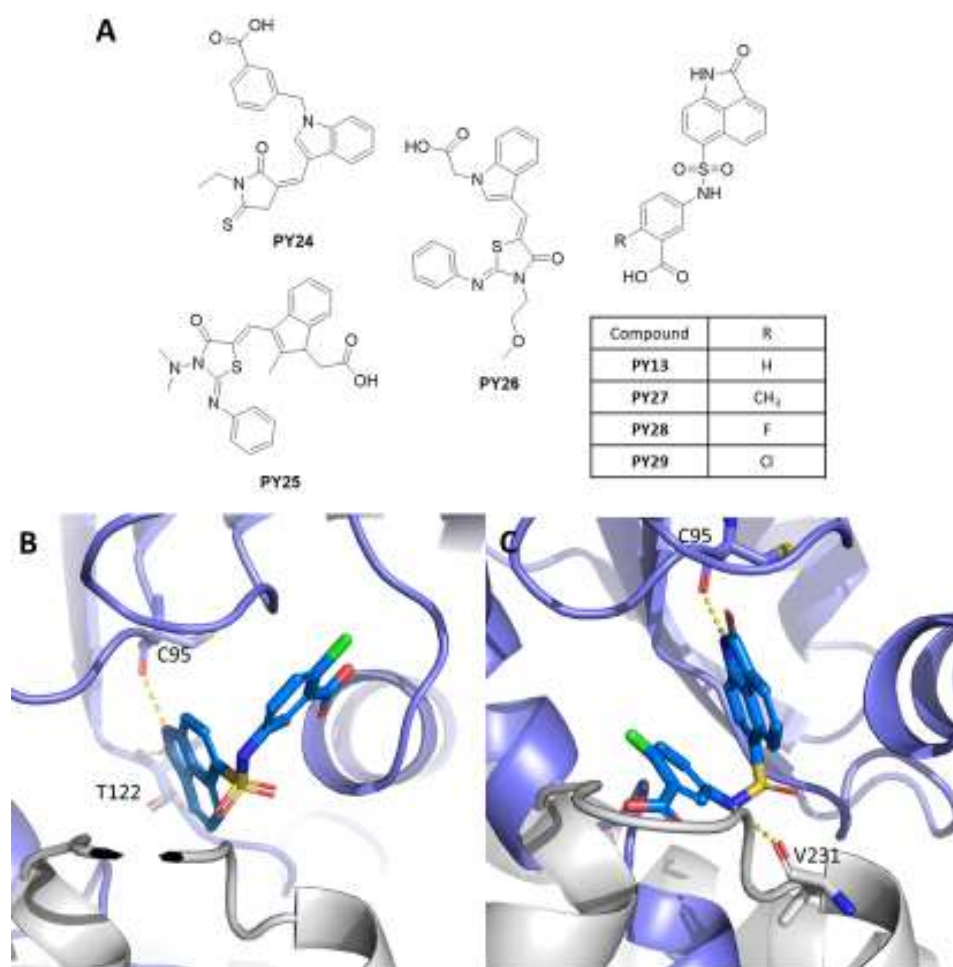


Figure R-43: PY13 and PY17 analogs. (A) Structure of PY13 (PY27-29) and PY17 (PY24-26) analogs (represented as sticks) selected for in vitro evaluation. (B-C) The two most probable binding modes of PY13 analogs found by molecular docking with GLIDE. Possible hydrogen-bonds with PYCR1 residues (resalted as sticks) are noted as yellow dotted lines.

Study of hit conformations by molecular dynamics simulations

MD simulations of the hit compounds (PY13, PY16, and PY17) were performed starting from the docked poses (**Figure R-44**) to evaluate its correctness. For PY13 both poses were used as initial conformations to check their structural stability.

Both PY13 poses were stable after 50 ns of MD simulations, although there were some changes. In the first pose, the tricyclic ring moved inside the pocket losing the H-bond of the carbonyl group, which would imply a desolvation cost. The sulfonamide could form H-bonds with S233 backbone and lateral chain, or the solvent (**Figure R-44A**). In the second pose the tricyclic ring also rotated inside the cavity leaving the polar groups exposed to solvent. K71 could form H-bonds with the carbonyl of the tricycle, and the sulfonamide could form H-bonds with V231 and T124. Nonetheless, one of the sulfonamide oxygens remains buried inside the pocket (**Figure R-44B**).

Although both docking poses seem possible for PY13 analogs with substituents in *orto* (PY27-29, Figure R-Y13 B-C), only one of the binding modes described in the MD simulations fits with the experimental values. The addition of a substituent in *orto* from the carboxylate would lead to a steric clash in the first binding mode (Figure R-45A) reducing its affinity for the enzyme. On the other hand, the addition of the same substituent in the second binding mode would fill a nonpolar cavity (Figure R-45B), stabilizing the enzyme-inhibitor complex and increasing its inhibition potency. The second predicted binding mode copes with the experimental results obtained in the kinetic assay (inhibition potency increase), and therefore is considered to be the most probable binding mode.

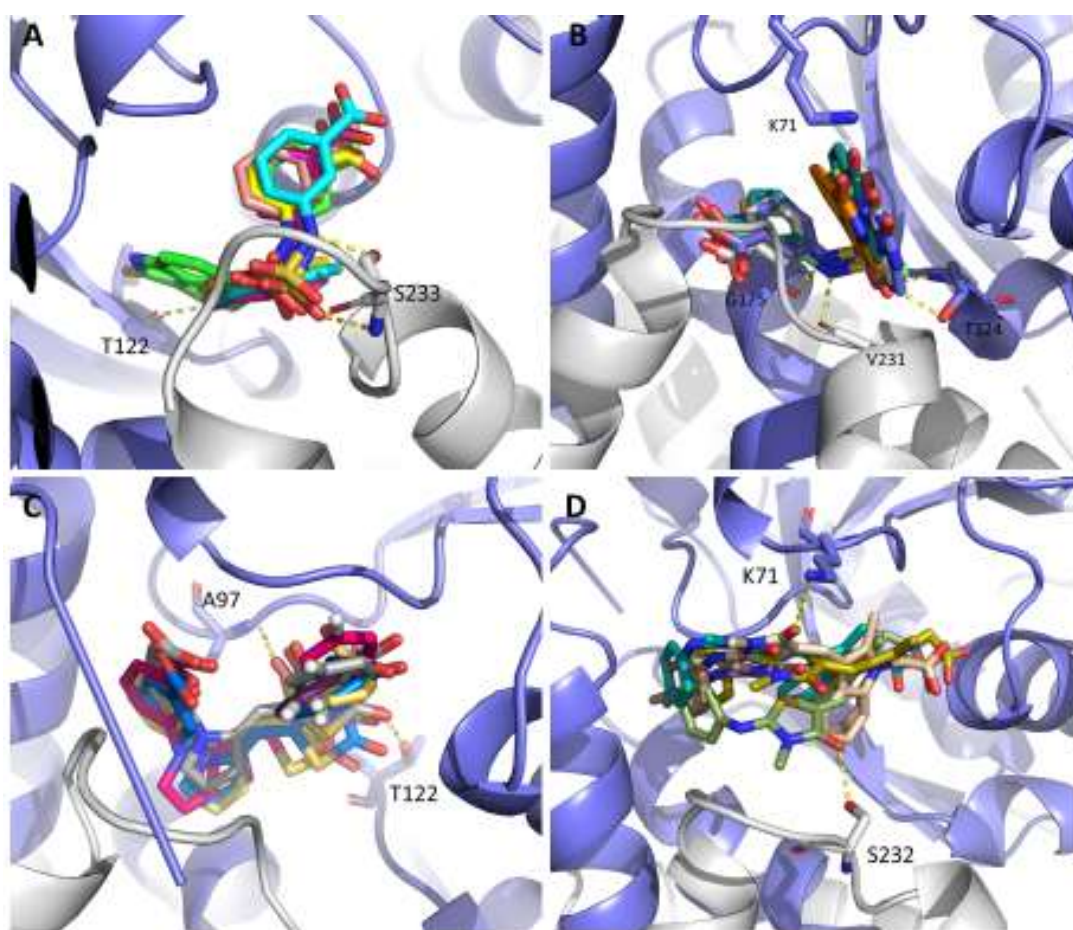


Figure R-44: Study of binding mode stability of hit compounds by MD simulation. (A-D) Superposition of PY13 (A-B), PY16 (C), and PY17 (D) snapshots (every 10 ns of simulation, represented as sticks) in the different proposed binding modes during 50 ns of molecular dynamics simulation using GROMACS. Possible hydrogen-bonds with PYCR1 residues are noted as yellow dotted lines. PYCR1 residues that could form interactions with the studied molecule are resalted as sticks and the residue name is noted.

On the other hand, most of the interactions observed for the docked poses of PY16 and PY17 are lost during the MD simulation, including the interactions of the carboxylate group of PY16 with the α K- α L loop, as well as H-bonds with A97 and T122 (Figure R-44C). PY17 only maintained the interactions between its carboxylate group and the residues at the end of the α A. It could form weak interactions with the side chains of the solvent-exposed K71 and S232 (Figure R-44D). Most PY16 and PY17 polar groups are not forming interactions

with the protein, which implies a high desolvation cost. Overall, the binding mode of both compounds do not seem correct, which presumably explains why the designed PY17 analogs were less active than PY17. Furthermore, PY17 formed few polar interactions with the protein in the proposed binding mode, causing an important desolvation cost. Overall, this pose did not cope with PY17 inhibition potency (high compared with the expected from the interactions formed in the docking pose).

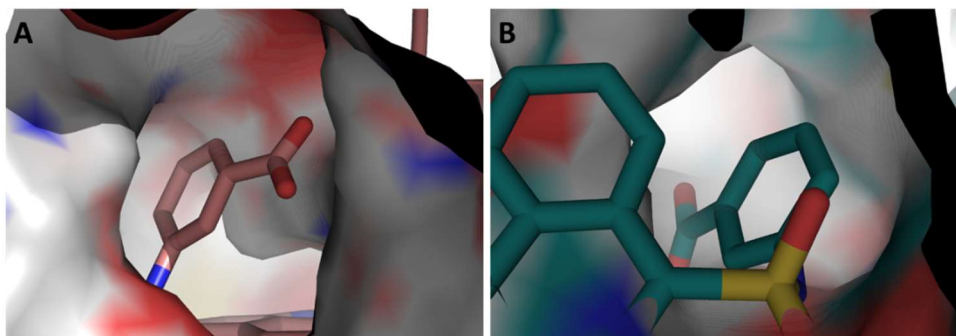


Figure R-45: Conformation of the carboxylate moiety of PY13 in both binding modes. PY13 represented as sticks in the first - carboxylate forming interactions with the end of αA – (A) and the second - carboxylate forming interactions with the residues of the αK - αL loop- (B) binding modes upon PYCR1 surface. Whilst, substituents added *ortho* from the carboxylate would collide with PYCR1 in the first binding mode (A), the same substituents would fill an hydrophobic cavity of PYCR1 in the second binding mode (B).

PY13 optimization

Data predicted through MD simulations of PY13, together with the experimental data from its analogs with nonpolar substituents in *ortho* of the carboxylate, strongly suggest a plausible binding mode for PY13. Since its chemical structure is relatively easy to modify PY13 a good candidate for an optimization campaign through rational design of its chemical structure as shown in Figure R-46. Firstly, small modifications on PY13 structure were proposed based on its predicted binding mode and the experimental data and the feasibility of their chemical synthesis. The compounds were then evaluated *in silico* by MD simulations, and those with a favorable evaluation were synthesized in Dr. M^a Carmen Escolano's lab and further evaluated *in vitro* in the enzymatic assay. The information obtained during each optimization cycle was integrated and further used in the next iteration.

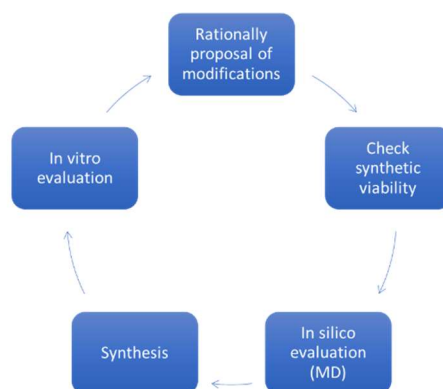


Figure R-46: Schema followed during the optimization of PY13.

The MD simulation of PY13 was extended to 300 ns. The compound remained stable forming constant interactions with the protein (Figure R-47). The carboxylate formed strong and stable H- bonds with the amino acids of the α K- α L loop. The carbonyl from the sulfonamide formed a maintained H-bond with the NH of T124, and transiently formed H-bonds with T124. The NH from the sulfonamide could form H-bond with the carbonyl from V231, it was not maintained during the whole simulation though. However, in one replica PY13 binding mode was not conserved and PY13 left the pocket at the end of the simulation.

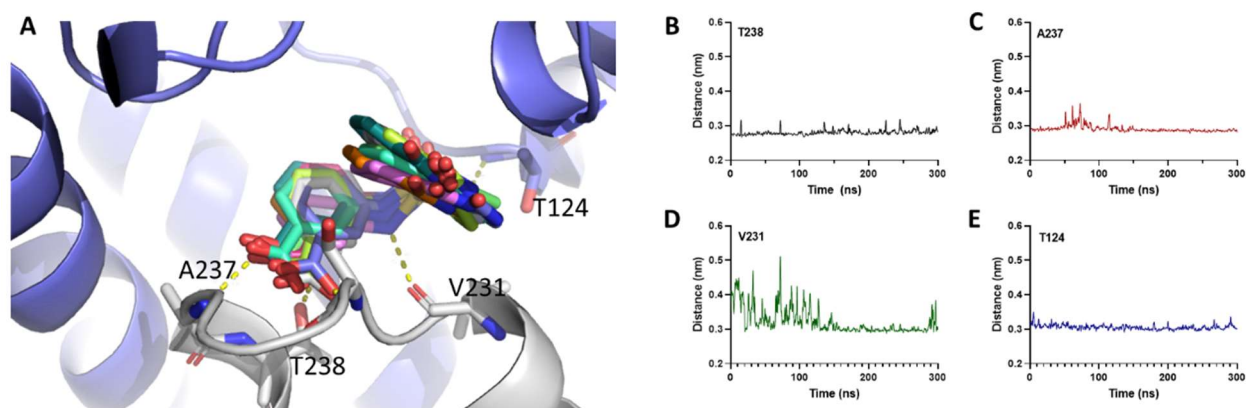


Figure R-47: Analysis of PY13 binding mode by 300 ns of molecular dynamic simulation. (A) Superposition of PY13 snapshots (sticks, every 50 ns) during the MD simulation with PYCR1. Possible hydrogen-bonds formed with PYCR1 residues are noted as yellow dotted lines. PYCR1 residues that could form interactions with PY13 are resalted as sticks and the residue name is noted. (B-E) Distances between polar atoms from PY13 and PYCR1 residues susceptible to form H-bonds during the 300 ns of MD. (B-C) Distance between the carboxylate oxygens - each oxygen is represented in a different color (black/red) – and the backbone nitrogen atoms of T238 and A237. (D) Distance between the nitrogen atom from the sulfonamide of PY13 and the oxygen form the carbonyl of V231. (E) Distance between one oxygen of the sulfonamide and the nitrogen of T124. The lines of the distance plots were smoothed using GraphPad for a clearer visualization.

The study of the pocket with the most favorable PY13 binding mode was used to suggest the modifications shown in Figure R-48. Small non-polar substituents in *ortho* and *meta* from the carboxylate could fill non-polar cavities in the protein stabilizing the conformation (Figure R-48B). Similarly, the modification of the tricycle could also fill the cavities showed in Figure R-48C. Since part of the sulfonamide group is not making interactions during the simulation (one carbonyl), its modification for an ether or amine could decrease its associated desolvation effects.

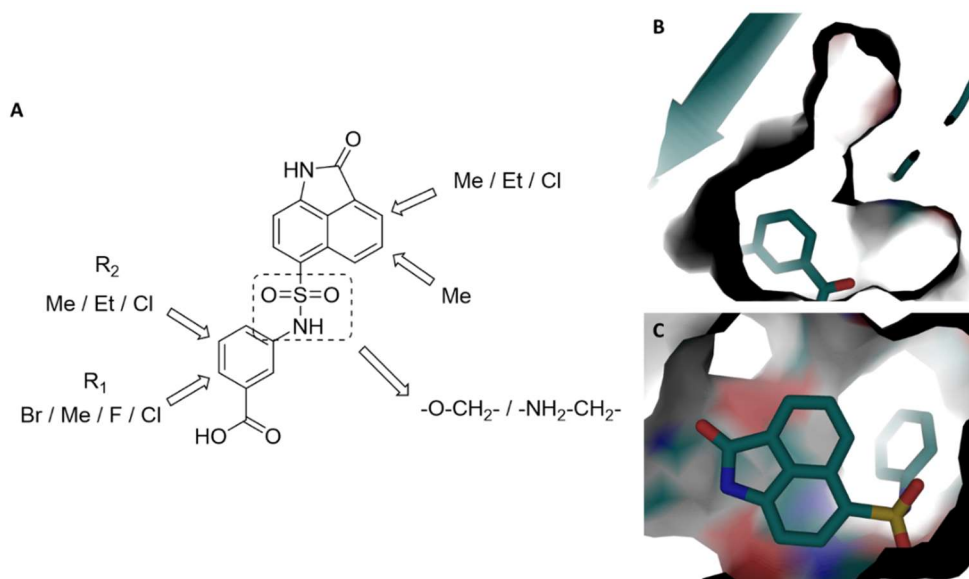


Figure R-48: First proposed PY13 modifications based on PYCR1 cavities. (A) PY13 structure with the proposed modifications. (B) Hydrophobic PYCR1 cavities observed near the carboxylate group of PY13 (shown as sticks) that could be filled by adding small non-polar substituents in R_1 and R_2 positions. (C) PYCR1 cavities near the tricyclic moiety.

Since the reagents to synthesize the compounds with non-polar substituents in *ortho* and *meta* from the carboxylate were relatively cheap and the synthesis was also easy, these compounds were synthesized without previous *in silico* evaluation. The compounds with substituents in *meta* from the carboxylate demonstrated higher inhibition potency than PY13 but were less potent than the *ortho* derivatives. In both cases (*ortho* and *meta*), the compounds with the methyl group were the most potent. In the case of the compounds with halogens, potency decreased with the atom size (Table R-10). The synthesis of molecules with modifications in the tricarboxylic ring was not viable due to the complexity of the synthesis and/or the elevated price of the reagents.

MD simulations (300 ns) were performed for PY27 and PY28 to study its binding mode and determine if there are differences with PY13.

In PY27 the carboxylate group formed stable H-bonds with amino acids of the α K- α L loop (Figure R-49), which were maintained along the whole simulation. One carbonyl from the sulfonamide formed transient H-bonds with T124 backbone and side chain (hydroxyl, more exposed to solvent and therefore less stable) while the other carbonyl was placed inside the cavity. The NH from the sulfonamide could make H-bonds with the carbonyls of V231 (most of the time) or T122. There was some mobility in the tricycle depending on the sulfonamide orientation, however its amide was oriented to solvent while the non-polar part remained inside the pocket.

Compound	IC ₅₀ [μM]
PY13	186.1
PY27 (R ₁ = CH ₃)	30.42
PY28 (R ₁ = F)	46.15
PY29 (R ₁ = Cl)	58.14
PY33 (R ₁ = Br)	134.0
PY30 (R ₂ = CH ₃)	95.5
PY31 (R ₂ = F)	109.2
PY32 (R ₂ = Cl)	149.9

Table R-10: Inhibition potency of PY13 analogs with substituents in R₁ and R₂. The IC₅₀ were calculated by adjusting the inhibition curve with the nonlinear regression GraphPad tool.

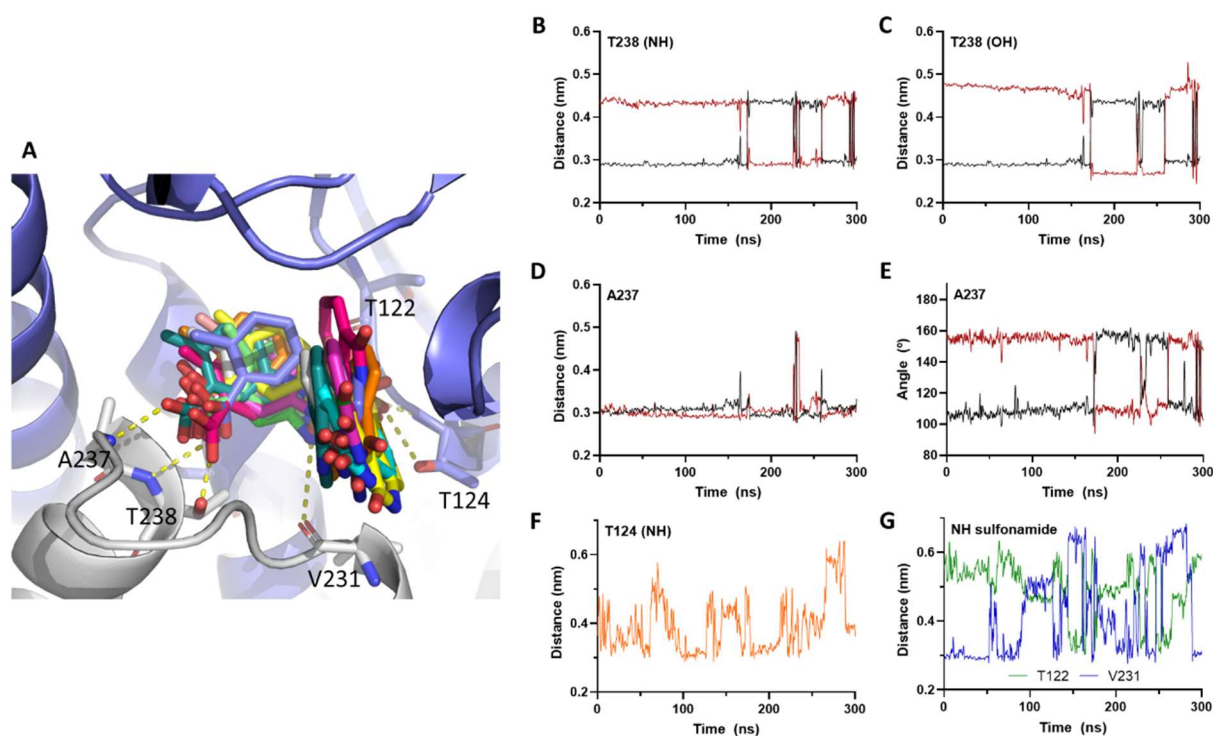


Figure R-49: Analysis of PY27 binding mode by 300 ns of molecular dynamic simulation. (A) Superposition of PY27 snapshots (sticks, every 50 ns) during the MD simulation with PYCR1. Possible hydrogen-bonds formed with PYCR1 residues are noted as yellow dotted lines. PYCR1 residues that could form interactions with PY27 are resalted as sticks and its residue name is noted. (B-D) Distance between the carboxylate oxygens - each oxygen is represented in a different color (black/red) - the backbone nitrogen atoms of T238 (B) and A237 (D), and the hydroxyl from the lateral chain of T238 (C). (D) Angle formed between the carboxylate oxygens from PY27, the nitrogen, and the hydrogen from A237. (F) Distance between one oxygen of the sulfonamide and the nitrogen of T124. (See next page)

(G) Distance between the nitrogen atom from the sulfonamide of PY27 and the oxygen from the carbonyl of T122 (blue) and V231 (green). The lines of the distance plots were smoothed using GraphPad for a clearer visualization.

The binding mode of PY28 was similar. The orientation of the benzene with the carboxylate was slightly different (Figure R-50). However, the carboxylate formed H-bonds with the amino acids of the α K- α L loop (in contrast with PY27 it formed interactions with S233 instead of with A237). During the simulations, there was a conformational change that disrupted the interactions formed by the sulfonamide (carbonyl with T124 and NH with T122). During this change of conformation, the tricyclic ring was shifted, and the amide NH formed H-bonds with N230 keeping the carbonyl exposed to solvent.

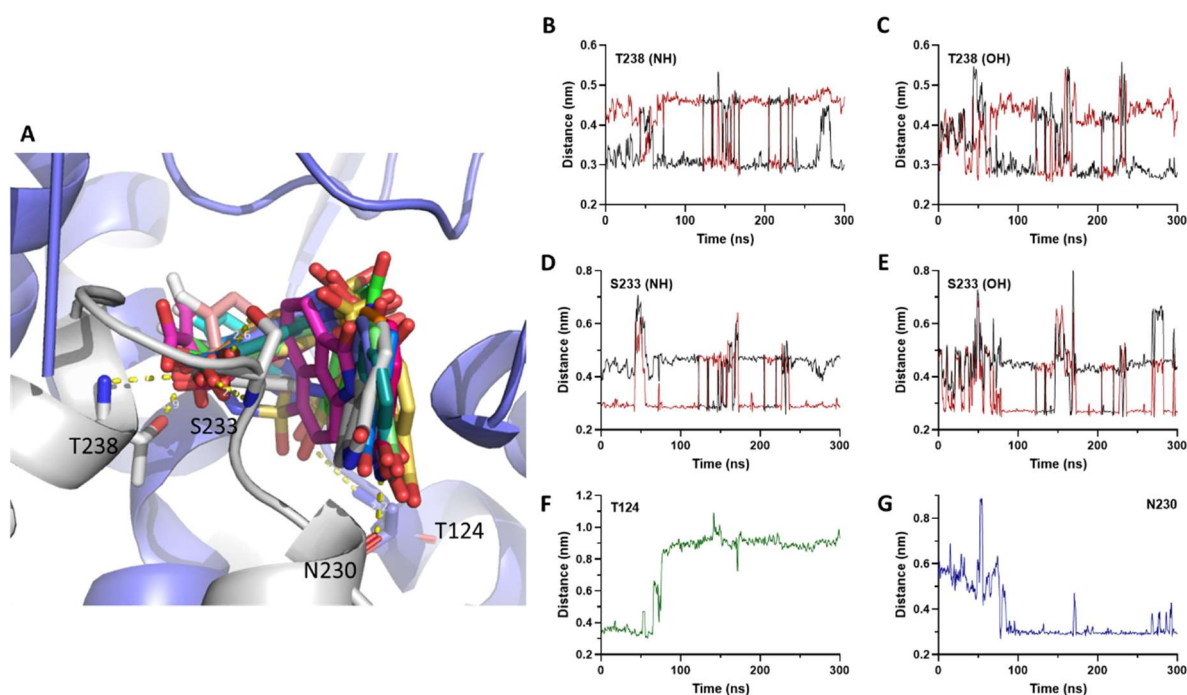


Figure R-50: Analysis of PY28 binding mode by 300 ns of molecular dynamic simulation. (A) Superposition of PY28 snapshots (sticks, every 50 ns) during the MD simulation with PYCR1. Possible hydrogen-bonds formed with PYCR1 residues are noted as yellow dotted lines. PYCR1 residues that could form interactions with PY28 are resalted as sticks and its residue name is noted. (B-E) Distance between the carboxylate oxygens - each oxygen is represented in a different color (black/red) - the backbone nitrogen atoms of T238 (B) and S233 (D), and the hydroxyl from the lateral chain of T238 (C) and S233 (D). (F) Distance between one oxygen of PY28 sulfonamide and the nitrogen of T124. (G) Distance between the nitrogen atom from the amide tricycle of PY27 and the oxygen from the carbonyl of N230. The lines of the distance plots were smoothed using GraphPad for a clearer visualization.

Overall, the PY27 binding mode was closer to PY13's. By observing PYCR1 conformations during the simulations and modeling the compounds with substituents in *meta* to the carboxylate, we realized that the cavity that these substituents should fill is too small. Therefore, the ring might rotate to accommodate these substituents in the other cavity (the one we predicted that would be filled by the substituents in *ortho*). This conformational change would leave the carboxylate with a sub-optimal orientation to the α K- α L loop, allowing the formation of H-bonds with different residues. Altogether, the increase of van der Waals

interactions upon insertion of a non-polar substituent in a hydrophobic cavity would enhance the potency compared with PY13; but the differences in the polar interactions of the carboxylate could explain the decrease in potency relative to its analogs with substituents in *ortho* to the carboxylate.

Compounds without the tricyclic moiety

We postulated that a molecule that could form H-bonds with the residues in the α K- α L loop and at the end of α A would increase its stability, and therefore, its potency (Figure R-51 A). Thus, since the modification of the tricyclic moiety was not possible, we proposed compounds which have an aromatic system and a sulfonamide (which could accept H-bonds) at the end (Figure R-51 B). We kept the substituents of the carboxylate moiety from the most potent inhibitor derived from PY13 (PY27). After being modeled, the compounds were evaluated by MD simulations.

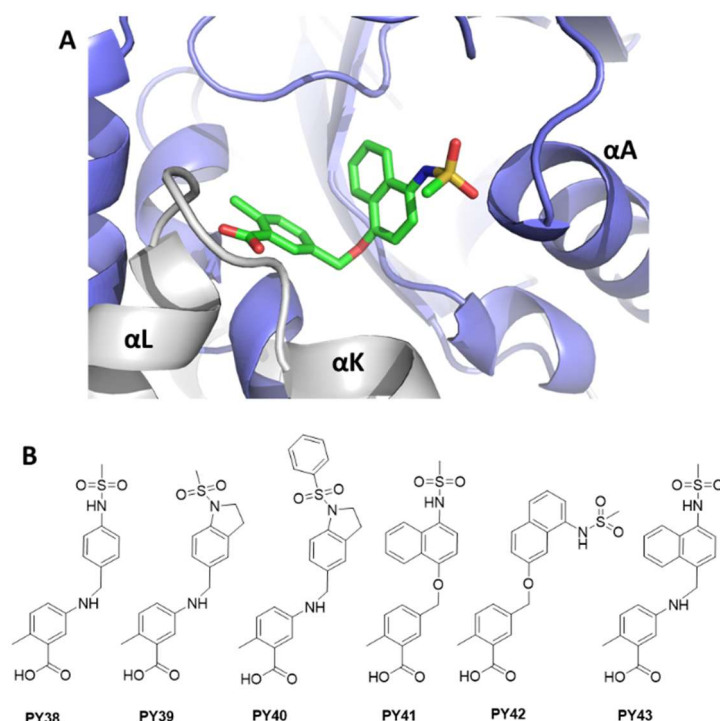


Figure R-51: Proposed PY13 modifications substituting the tricyclic moiety. (A) Proposed binding mode for the rationally designed compounds. Interestingly, the addition of a terminal sulfonamide group would allow the formation of H-bond with the residues at the end of the α A at the same time as maintaining the interactions of the carboxylate with the α K- α L loop. (B) Structure of the proposed compounds with a terminal sulfonamide.

The MD simulations of PY38 determined that the compound was not stable in the binding site. Actually, just one of the three replicas remained in its binding mode after 250 ns of simulation (Figure R-52). In the simulation where PY38 remained in the binding site, the oxygens of the carboxylic acid made H-bonds with the amino acids of the α K- α L loop (at the beginning with A237 and T238, and after 100ns also with S233). In addition, one oxygen of the sulfonamide could form H-bonds with the backbone of the α A end (G9, Q10, and L11). The other oxygen formed H-bonds with the NH from L11 during the first 100 ns of the simulation, and afterwards it was exposed to solvent or in the cavity. The linker's amine did not make interactions with the

protein. In the other replicas, the interactions between the sulfonamide and the end of the α -helix A were lost, leaving the sulfonamide exposed to solvent. At this stage the molecule was only maintained in its position by the interactions formed by the carboxylate, which would eventually break releasing the molecule (Figure R-52 BC).

The compound was synthesized and tested in the enzymatic assay. PY38 inhibited PYCR1 with an IC_{50} of 1.52 mM. The loss of potency is attributed to the replacement of the non-polar tricycle by a benzene sulfonamide, which would increase the hydrophilicity of the compound.

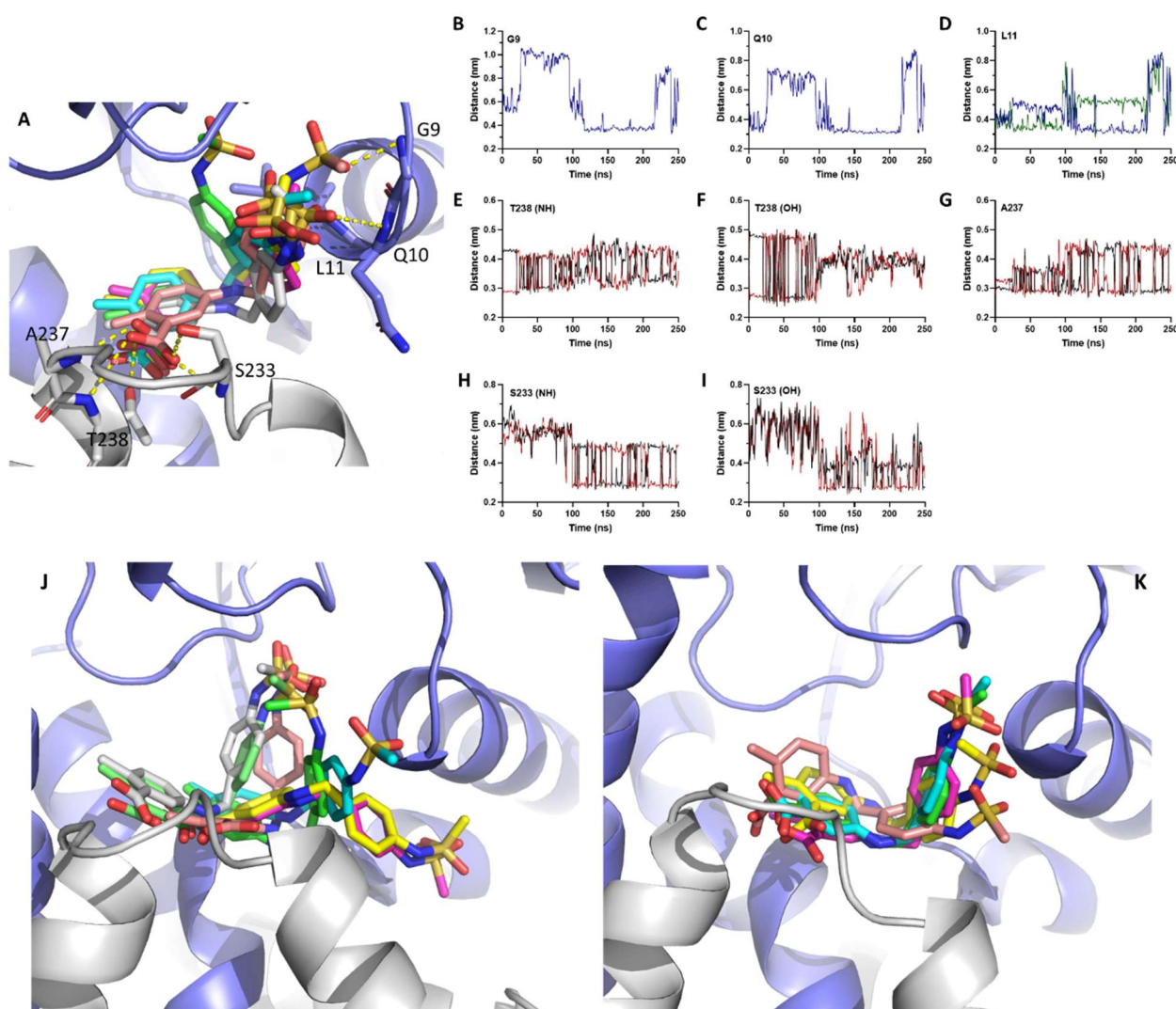


Figure R-52: Evaluation of PY38 by 250 ns of molecular dynamic simulation. (A) Superposition of PY38 snapshots (sticks) during the MD simulation with PYCR1. Possible hydrogen-bonds formed with PYCR1 residues are noted as yellow dotted lines. PYCR1 residues that could form interactions with PY38 are resalted as sticks and its residue name is noted. (B-D) Distance between the sulfonamide oxygens - each oxygen is represented in a different color (blue/green) - and the backbone nitrogen atoms of G9 (B), Q10 (D), and L11 (C). (E-I) Distance between the carboxylate oxygens - each oxygen is represented in a different color (black/red) - the backbone nitrogen atoms of T238 (E), A237 (G) and S233 (H), and the hydroxyls from the lateral chain of T238 (F) and S233 (I). (J-K) Superposition of PY38 snapshots (sticks) during the MD simulation with PYCR1. The lines of the distance plots were smoothed using GraphPad for a clearer visualization.

In contrast with PY38, PY39 was more stable in its binding mode (Figure R-53). The hydrogen bonds made by the carboxylate were maintained during most of the simulation (when one interaction was lost it was formed with the other oxygen as showed). The amine from the linker eventually formed H-bonds with the lateral chain of S233, possibly reflecting the high exposure to solvent of this interaction. The interactions formed between the sulfonamide and the end of the α A (although the interaction was weak most of the time) contributed to maintain the binding mode. The compound could not be synthesized due the lack of reagents. Instead, PY40 which had a similar structure was modeled but it was discarded. PY40's phenyl group would remain exposed to solvent, this conformation would not be favorable do phenyl's hydrophobicity.

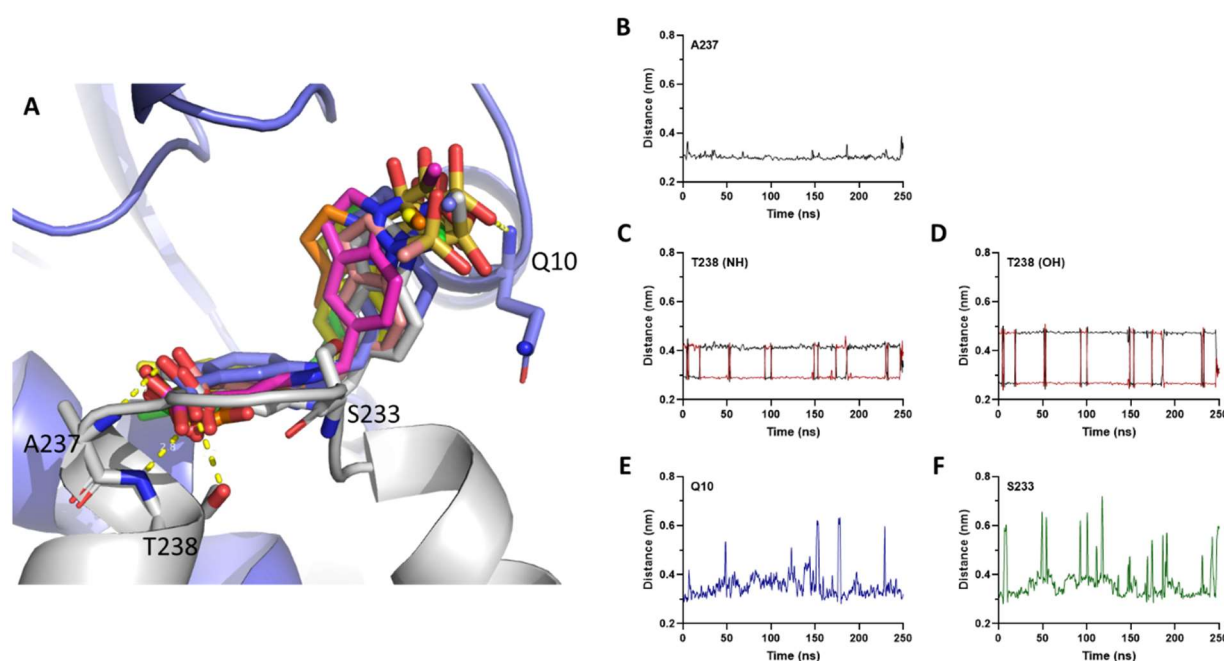


Figure R-53: Evaluation of PY39 by 250 ns of molecular dynamic simulation. (A) Superposition of PY39 snapshots (sticks) during the MD simulation with PYCR1. Possible hydrogen-bonds formed with PYCR1 residues are noted as yellow dotted lines. PYCR1 residues that could form interactions with PY39 are resalted as sticks and its residue name is noted. (B-D) Distance between the carboxylate oxygens - each oxygen is represented in a different color (black/red) – the backbone nitrogen atoms of A237 (B) and T238 (C), and the hydroxyl from the lateral chain of T238 (D). (E) Distance between an oxygen of the sulfonamide and the backbone nitrogen of Q10. (F) Distance between the nitrogen from PY39's linker and the hydroxyl of the lateral chain of S233. The lines of the distance plots were smoothed using GraphPad for a clearer visualization.

PY41 was stable bound to the pocket in the MD simulations (Figure R-54). As expected, the carboxylate formed H-bonds with the residues of the α K- α L loop. Although the carboxylate was rotating, its oxygen atoms constantly formed H-bonds with T238 and S233. The oxygen from the linker was inside the cavity without forming interactions implying a desolvation cost that is not compensated. One oxygen from the sulfonamide formed interactions with Q10 (at the end of α A), and when this interaction was broken the other oxygen took its place. Generally, the NH and the oxygen (the one that was not forming interactions with Q10) of the

sulfonamide remained exposed to solvent reducing the desolvation penalty. As predicted, the naphthalene filled the hydrophobic pocket increasing the stability by making van der Waals interactions with the protein. PY43, which differ in the linker, was synthesized instead of PY41 due problems during the synthesis. This change would maintain the desolvation penalty. Experimentally, PY43 inhibited PYCR1 with an IC_{50} of 163.1 μ M. This represents a 10-fold increase compared with PY38, confirming that decreasing the hydrophobicity of the group that substitutes the tricycle would also decrease its potency.

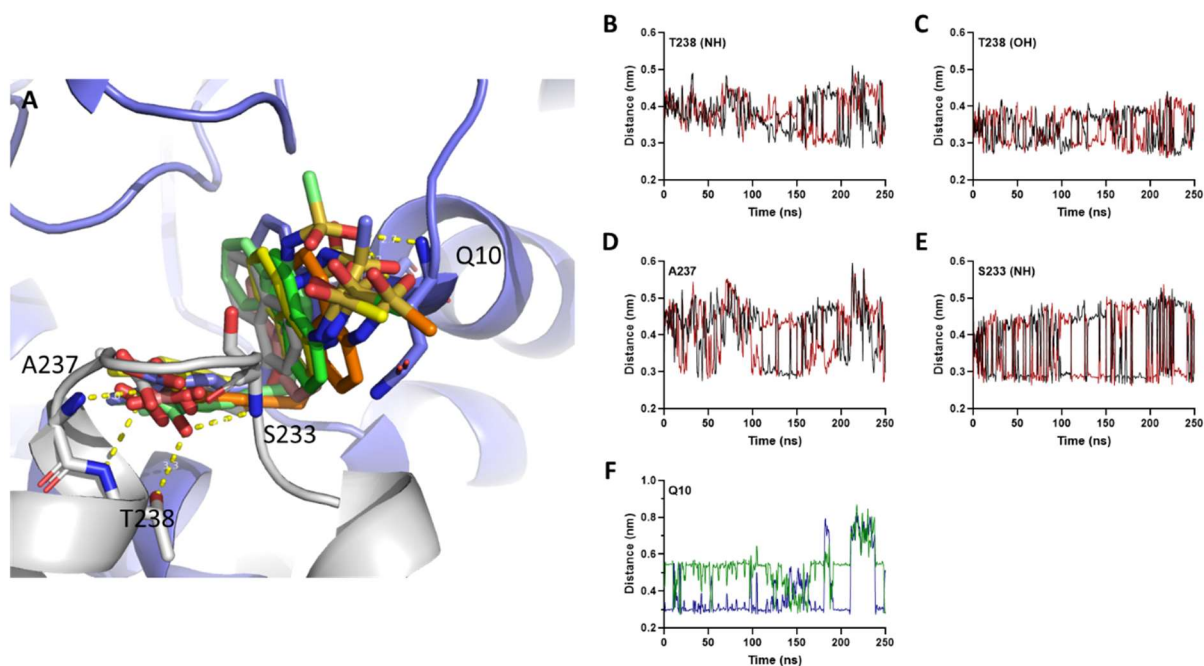


Figure R-54: Evaluation of PY41 by 250 ns of molecular dynamic simulation. (A) Superposition of PY41 snapshots (represented as sticks) during the MD simulation with PYCR1. Possible hydrogen-bonds formed with PYCR1 residues are noted as yellow dotted lines. PYCR1 residues that could form interactions with PY41 are resalted as sticks and its residue name is noted. (B-E) Distance between the carboxylate oxygens - each oxygen is represented in a different color (black/red) - the backbone nitrogen atoms of T238 (B) and S233 (D), and the hydroxyls from the lateral chain of T238 (C) and S233 (E). (F) Distance between the sulfonamide oxygens - each oxygen is represented in a different color (blue/green) - and the backbone nitrogen of Q10. The lines of the distance plots were smoothed using GraphPad for a clearer visualization.

PY42 was not stable during the MD simulations. Both the carboxylate and the sulfonamide formed H-bonds with the protein in the expected residues. However, the interactions were not maintained during the simulation. The different structure of this PY41 isomer made it difficult to maintain the interactions in both positions (α K- α L loop and the end of α A). Interestingly, the H-bonds of the carboxylate with T238 were formed when the sulfonamide with Q10 ones were broken (Figure R-55). In the other replicas the interactions were also not maintained. Therefore, this compound was discarded to further in vitro evaluation.

Another moiety that was evaluated was the linker length. Up to this moment all the PY13-derived compounds had a two-atoms linker. We modeled PY38 with linkers from 1 to 4 atoms. A linker consisting of a single unit was too small to allow the interactions of the carboxylate and sulfonamide at the same time, and the

compound with 4-atoms linker was too large to accommodate in the pocket with a rational conformation. Finally, the molecule with 3-atoms linker (PY44) could fit the pocket (Figure R-56 A), but this compound left the pocket by losing the sulfonamide interactions (Figure R-56 B) or remained folded in the pocket without maintaining the interactions (Figure R-56 C). Therefore, these results suggest that the optimal length of the linker must involve two heavy atoms.

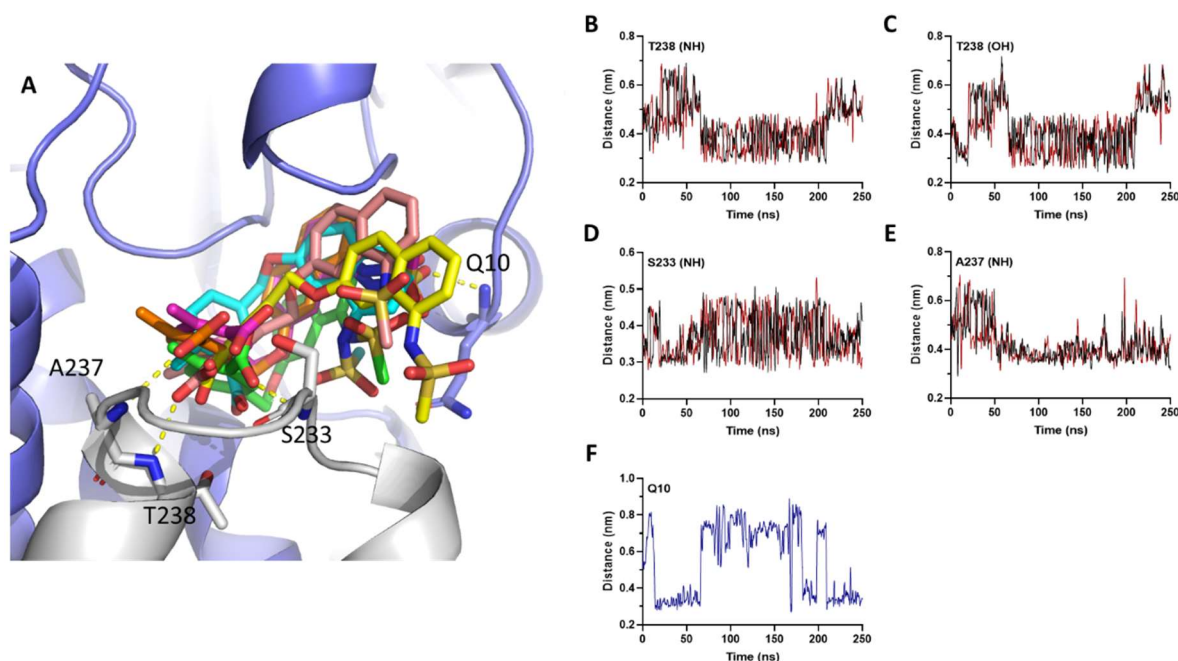


Figure R-55: Evaluation of PY42 by 250 ns of molecular dynamic simulation. (A) Superposition of PY42 snapshots (represented as sticks) during the MD simulation with PYCR1. Possible hydrogen-bonds formed with PYCR1 residues are noted as yellow dotted lines. PYCR1 residues that could form interactions with PY42 are resalted as sticks and its residue name is noted. (B-E) Distance between the carboxylate oxygens - each oxygen is represented in a different color (black/red) - the backbone nitrogen atoms of T238 (B), S233 (D), and A237 (E), and the hydroxyl from the lateral chain of T238 (C). (F) Distance between an oxygen of the sulfonamide and the backbone nitrogen of Q10. The lines of the distance plots were smoothed using GraphPad for a clearer visualization.

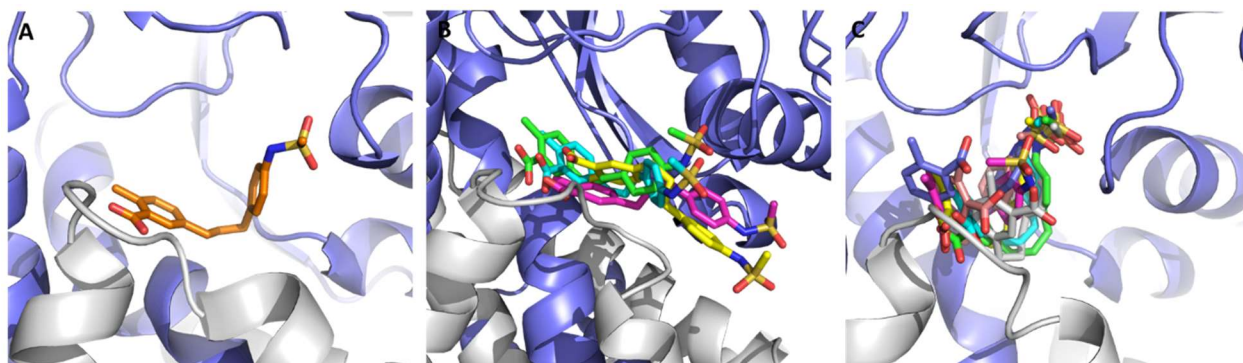


Figure R-56: Evaluation of the linker length. (A) PY44, the three-atoms linker molecule, modeled in PYCR1 binding site. (B-C) Superposition of PY44 snapshots (as stickers, every 50 ns of simulation) during up to 250 ns of MD simulation.

Preliminary evaluation in cancer cell lines

The antineoplastic activity of the most potent compounds was evaluated in breast (MCF7) and colon (HCT116) cancer cell lines. Cancer cells were treated for 72h with increasing doses of PY04_2, PY16, PY17, PY13, PY27, PY28, and PY29 (Figure R-57). All the compounds reduced cell viability, and the response was dose dependent. Interestingly, the antineoplastic potency correlated with PYCR1 inhibition potency as it could be observed in Figure R-57 C and D with PY13 analogs.

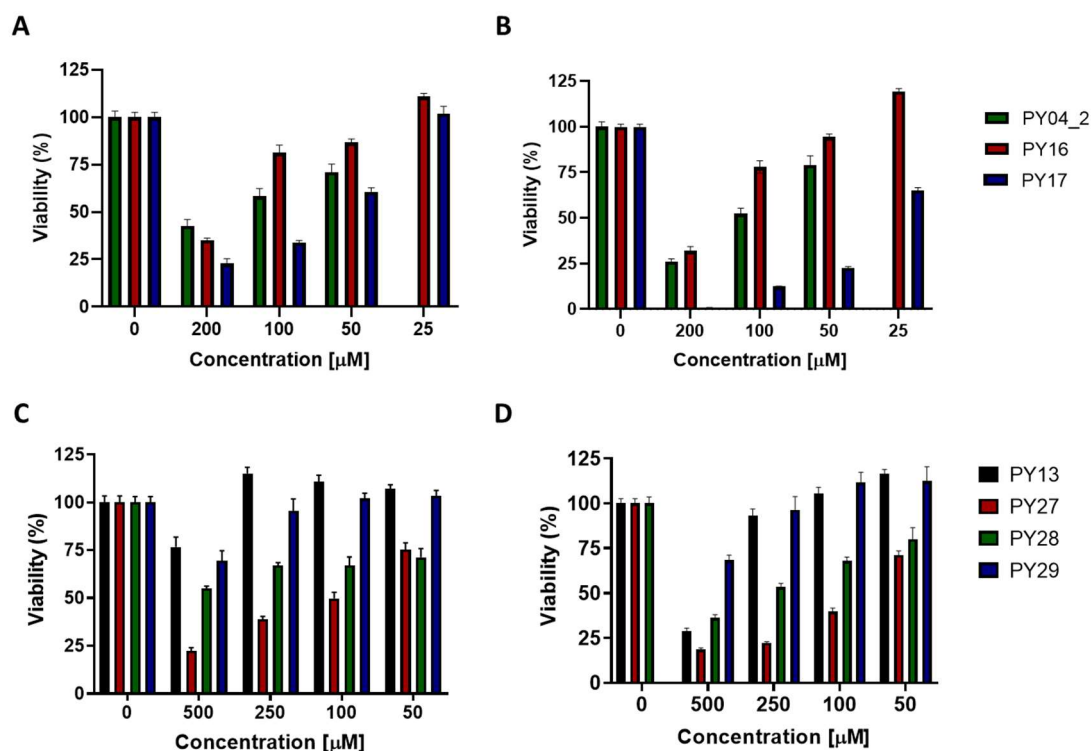


Figure R-57: Treatment with PYCR1 inhibitors reduce viability in cancer cell lines. Viability of breast cancer MCF7 (A, C) and colon cancer HCT116 (B-D) cells after 72-hours treatment with increasing concentrations of PYCR1 inhibitors in high glucose media. Viable cells were stained by MTT and quantified by spectrophotometry. Data are means \pm SEM (2 independent experiments were performed with $n=5$ in each experiment shown in panels).

Furthermore, PY27 inhibited proline biosynthesis in HCT116 cells after a short treatment (3 hours) with 500 μ M of PY27 in 10 mM glucose media (Figure R-58). Metabolite quantification by GC-MS revealed a reduction of intracellular proline concentration as well as an accumulation of glutamate suggesting that PY27 could inhibit PYCR1 in a cellular context (Figure R-58A). Moreover, there was a significant drop in citrate levels while the concentration of the other metabolites from the TCA cycle did not vary (Figure R-58C). Interestingly, there was a non-significant reduction of glycolytic metabolites (PEP and pyruvate).

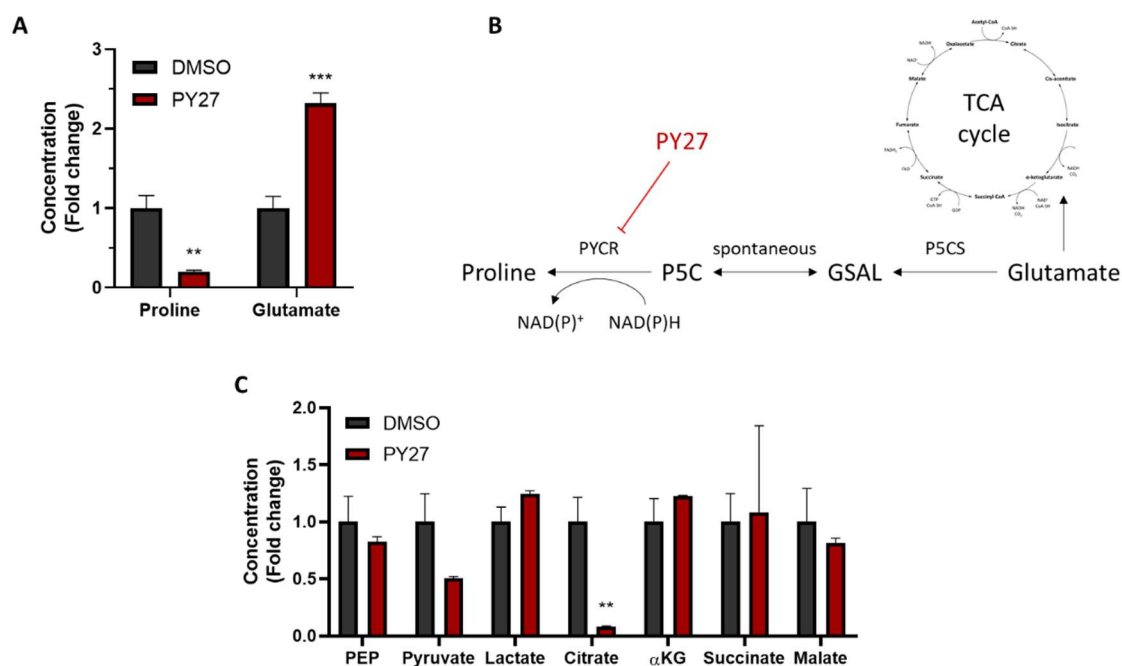


Figure R-58: Metabolites quantification by GC-MS after PY27 treatment. After a 3 hours-treatment with PY27 (500 μ M) or DMSO in DMEM supplemented with 10 % FBS, 10 mM glucose, and 2 mM glutamine the intracellular metabolites were extracted and quantified by GC-MS. **(A)** Proline (end product) and glutamate (initial substrate of proline biosynthesis pathway) intracellular concentrations. **(B)** Proline biosynthetic pathway. **(C)** Glycolytic and TCA cycle metabolites concentrations. Data are means \pm SEM of one experiment with $n=3$. Multiple t-test comparison was used. Statistical significance at * $p < 0.05$, ** $p < 0.01$, *** $p < 0.001$ vs vehicle control.

Computational approaches had become essential in drug discovery campaigns since the use of these technologies increases the evidence on how the drug is interacting with the target protein (Hassan Baig et al., 2016; X. Liu, IJerman, et al., 2021). This information allows scientists to rationally design/choose the compounds that should be screened in vitro increasing the screening coverage of the chemical space, its efficiency and reducing the costs (since less molecules had to be purchased/synthesized). Furthermore, these technologies are also useful in more advanced phases of drug discovery such as hit-to-lead optimization and pharmacokinetic evaluation.

In this work, we reported the first computational-aided inhibitor discovery strategy for PYCR1. We designed compounds which bind the active site and inhibit the enzyme by competition with the substrates (P5C and NADH). Notedly, there are other valid strategies, like the design of molecules that bind a pocket outside the active site allosterically inhibiting the enzyme (by inducing conformational changes that reduce the affinity for the substrates) (Nussinov et al., 2022). Or since the dimerization is essential for the activity, it might be possible to design molecules that impede dimerization, and therefore inhibit PYCR1 activity (H. Lu et al., 2020).

Our virtual screenings led us to the discovery of nine hits with PYCR1 activity (IC_{50} below 1 mM). Five of them had an IC_{50} lower than 200 μ M (PY04, PY10, PY13, PY16, and PY17). Using PY04's scaffold we searched for

analogs that were subsequently evaluated by molecular docking. Two of these analogs showed an increased potency compared to the original structure. Moreover, it reduced cell growth/viability in cancer cell lines. However, the structure predicted by docking was not stable during MD simulation. Furthermore, the interactions observed during the MD were not coherent with the compound potency, suggesting that our predicted binding mode was incorrect. In addition, the synthesis of similar compounds was complex and PY04 and its analogs presented PAINS (Baell & Holloway, 2010). Therefore, we put PY04 and its analogs aside and we centered in the other compounds.

The most potent inhibitors discovered in the second virtual screening were studied by molecular docking and molecular dynamics to clarify its binding mode and rationally design analogs with increased potency. Similarly to PY04_2, we could not find the correct binding mode for PY16 and PY17. Nevertheless, the binding mode predicted for PY13 seemed plausible when evaluated by MD. The carboxylic acid group of PY13 formed stable interactions with the residues in the proline binding site (α K- α L loop) in a similar manner than proline or THFA (Christensen et al., 2017). The tricycle moiety constituted a big hydrophobic group that sank in the pocket and stabilize PY13-PYCR1 complex by Van der Waals interactions. The tricycle's amide could form H-bonds with polar residues inside the cavity or could be exposed to solvent reducing the desolvation penalty. The synthetic accessibility of PY13 derivatives in addition to the binding site definition, make PY13 a good candidate for optimization.

Firstly, the benzene with the carboxylic acid was modified by adding small nonpolar substituents to fill hydrophobic cavities detected during the MD simulations. The addition of small substituents in *ortho* increased the inhibition potency up to six times (PY27) by stabilizing the carboxylate position (and interactions). Then, since the modification of the tricyclic group was synthetically challenging, we opted to substitute the whole moiety with aromatic structures with a sulfonamide at the end. We predicted that the sulfonamide group would form interactions with the residues at the end of the α A as the pyrophosphate from NADPH on the resolved structures (Christensen et al., 2017). With the substitution of the tricycle for a benzene (with the sulfonamide) the compound lost most of the tricycle hydrophobic interactions and increased its affinity for the solvent. Overall, PY38 showed a dramatic reduction of potency (with an IC_{50} around 1.5 mM) compared with PY27. PY43, which differentiates from PY38 by having a naphthalene instead of the benzene, had a modest activity (IC_{50} 163.1 μ M) but it represented a 10-fold increase when compared to PY38. This suggests that the cause for PY38 low activity was the hydrophobicity reduction. The substitution of the naphthalene for a bigger hydrophobic moiety or the addition of non-polar substituents in the naphthalene might be interesting to increase its inhibition potency.

The future obtention of crystallographic structures of PYCR1 complexed with the described inhibitors would be really useful to validate the *in silico* predicted binding mode in the case of PY13 and its analogs. It would

be also really interesting in the case of PY04, PY16, and PY17 because it would define how they bind to PYCR1 opening the door to rational optimization.

The metabolite quantification by GC-MS revealed that the intracellular proline concentration was reduced while glutamate (the initial substrate of the pathway) accumulates when the cells are treated with PY27. The reduction of the final product and the substrate accumulation are consistent with the inhibition of a metabolic pathway. Therefore, PY27 seems to successfully inhibit PYCR1 in a cellular context.

This experiment also showed that the concentration of some glycolytic intermediates could be reduced consistent with the reduction of glycolysis observed by Liu et al. (2015) and Ding et al. (2020) in PYCR1 silenced cancer cells. This reduction of glycolysis would be consequence of the reduction of NAD⁺ regeneration by PYCR1. PYCR1 has been described to regulate NAD(P)⁺/NAD(P)H ratios promoting anabolic pathways (glycolysis, pentose phosphate pathway, ...) (Chalecka et al., 2021; D'Aniello et al., 2020; Tanner et al., 2018).

The drastic reduction of citrate could be caused by an off-target inhibition of pyruvate dehydrogenase that would block the entry of Acetyl-CoA in the TCA cycle. This reduction could also be caused by an increased diversion of pyruvate to lactate in order to compensate the lost PYCR1-dependent NAD⁺ regeneration. However, more exhaustive studies with different PY27 doses, labeled metabolites, and PYCR1 silenced cells (as a positive control) need to be performed in order to fully characterize PY27 mechanism of action. In addition, some metabolites such as proline or lactate are secreted to the media, and therefore, its concentration in the media should also be quantified.

Due the structural similarity between the active site of PYCR isoforms, specially between PYCR1 and PYCR2, we hypothesized that the molecules resulting from the chosen strategy would inhibit both isoforms (Bogner et al., 2021; Escande-Beillard et al., 2020). However, it could be useful for cancer therapy since the other isoforms might also play a role in cancer progression (W. Liu et al., 2015; R. Ou et al., 2016; Sattar Alaqbi et al., 2022).

In contrast with proline analog inhibitors -such as THFA- that also inhibit PRODH (Bogner & Tanner, 2022; Elia et al., 2017), we hypothesize that the inhibitors described in this thesis would not inhibit PRODH since the catalytic center of both enzymes are not similar (Bogner & Tanner, 2022; Tanner, 2019).

Altogether, we reported various compounds (from different structural families) that inhibit PYCR1 with IC₅₀ in the low micromolar range. Furthermore, our compounds are among the most potent PYCR1 inhibitors described up to now.

CONCLUSIONS

- iPEPCK-2 inhibits both PEPCK isoforms with similar potency as predicted by molecular docking and the high structural similarity between PEPCK isoforms.
- As demonstrated by cellular thermal shift assays (CETSA) and the inhibition of glucose stimulated insulin secretion (GSIS), iPEPCK-2 and all the tested PEPCK inhibitors can reach the mitochondria and inhibit PEPCK-M in cellular and *in vivo* contexts. Consistently, GSIS inhibition was proportional to PEPCK-M inhibition potency.
- PEPCK-M inhibition by iPEPCK-2 reduces cell growth in all the tested cancer cell lines in high glucose conditions without increasing cell death. The antiproliferative effect was target specific since the same treatment in PCK2^{del/del} cells did not affect proliferation.
- PEPCK-M inhibition by iPEPCK-2 reduces cell survival capacity in glucose deprivation in all the tested cancer cell lines as previously observed in genetic models.
- PEPCK-M plays a critical role in anchorage independent cell growth, especially in low glucose conditions. Its silencing or inhibition by iPEPCK-2 drastically reduces the number of colonies formed, and its overexpression increases the number of colonies formed in low glucose conditions.
- Daily dosing of PEPCK-M inhibitor (iPEPCK-2) blunts tumor growth in subcutaneous xenograft models without apparent signs of toxicity, validating both, PEPCK-M as a target for cancer treatment, and iPEPCK-2 as a compound that could be useful for cancer therapy.
- PEPCK-M modulates the levels of glycolytic intermediates such as PEP and 3-PG even in physiological concentrations of glucose (5 mM) since PEPCK-M inhibition by iPEPCK-2 reduced the concentration of these metabolites.
- Gene set enrichment analysis revealed that PEPCK-M activity participates in maintaining oncogenic (cMyc; through PEP-SERCA-NFAT axis as previously described by Moreno-Felici et al.) and anabolic (mTORC1) signaling in physiologic concentrations of glucose.
- As revealed by the gene set enrichment analysis, PEPCK-M inhibition by iPEPCK-2 impacts the expression of metabolic (anabolic), and cell division-related gene sets and increases the expression of autophagy and oxidative stress related gene sets. Therefore, illustrating the mechanisms implicated in the iPEPCK-2-dependent reduction of proliferation in the presence of glucose.
- The family of inhibitors with a TPP moiety (iPEPOs) inhibit PEPCK-M in a similar manner than iPEPCK-2 as demonstrated by kinetic assays with recombinant protein and functional assays with cancer cell lines. However, the CETSA showed that iPEPO-2 thermally stabilizes PEPCK cytosolic isoform while it could not demonstrate an increased distribution into the mitochondria.
- Virtual screening protocols followed by *in vitro* evaluation of the selected compounds led to the identification of nine hits that inhibit recombinant PYCR1 with an IC₅₀ below 1 mM: PY04, PY10, PY13, PY16, PY17, PY19, PY21, PY22, and PY23.

CONCLUSIONS

- The activity of PY13 was increased by rational optimization using modeling and molecular dynamic simulations leading us to PY27, the most potent PYCR1 inhibitor described in this project with an IC_{50} of 30.42 μ M.
- The treatment of cancer cell lines with our PYCR1 inhibitors reduces cell viability in a dose dependent manner.
- As determined by metabolite quantification by GC-MS, treatment of HCT116 colon cancer cell line with PY27 reduces intracellular proline concentration while intracellular glutamate accumulates, confirming the PYCR1 target engagement.

MATERIALS AND METHODS

Computational procedures

Different computational methods have been used for the discovery and design of PYCR1 inhibitors. These include the use of molecular visualization (PyMol), molecular docking and virtual screening (Autodock, rDOCK, and Glide), and molecular dynamic simulation (GROMACS) programs among others.

The calculations were performed mainly using the high-performance computing facilities of the *Consorci de Serveis Universitaris de Catalunya (CSUC)* and the *Barcelona Supercomputing Center (BSC)*.

Virtual screening

Two similar virtual screening protocols have been used to discover PYCR1 inhibitors (Figures R-32 and R-39).

For both protocols the crystal structure of PYCR1 complexed to THFA and NADPH was used (PDB ID: 5UAV). Prior to docking, all the waters and ligands were removed. The binding cavity was defined in the pocket between C and D chains, specifically in the intersection of the α L- α K loop of chain C and chain D. Hydrogens were added using MAESTRO (Schrödinger) and the ionization of the susceptible residues was determined at pH 7.4.

The compound libraries were downloaded from SPECS (<https://www.specs.net>). The three-dimensional structures of the compounds from the libraries were generated using LigPrep (Schrödinger), up to 8 stereoisomers and 6 tautomers were generated for each compound and the ionization was defined at pH 7.4. LigPrep ligfilter tool was used to filter the compounds through molecular weight and hydrogen-bond acceptors.

For the virtual screening procedures, rDOCK and GLIDE (Schrödinger) were used. In both protocols, the whole filtered library was firstly docked with a “fast” but “less sensitive” protocol. The compounds with the better scores were visually inspected and a “small” subset (< 500 compounds) was selected for a second docking step with a more exhaustive protocol (higher sensitivity and generation of more poses per ligand).

Molecular dynamic simulations

The molecular dynamic simulations were performed to check the structural stability and conformational flexibility of the hit compounds bound into PYCR1 binding site using GROMACS 2019.1.

The ligands were generated using ChemDraw 18.2. Partial charges of the ligands were derived at B3LYP/6-31G(d) level of theory (Gaussian 09), after preliminary geometry optimization, by using the restrained electrostatic potential fitting procedure (Antechamber 19.0, AmberTools18). The topologies and atomic types of the ligands were produced using tleap (AmberTools18). The protein parameters without the ligand were optimized by using AMBER99SB-ILDN force field and the topology was generated using pdb2gmX (GROMACS 2019.1). The protein and ligand (coordinate and topology) files were merged as GMX input files.

The protein-ligand complexes were solvated with spc216 water molecules by using a truncated octahedron box with a layer of 15 nm, and neutralized using Na⁺ and Cl⁻ ions up to 150 mM (NaCl physiologic concentration).

The energy of the system was minimized using a two-step protocol, for the first step a steepest descent algorithm with a maximum of 5000 minimization cycles was performed. The second step consisted in a conjugate gradient, and a third steepest descent protocol can be performed if the maximum force did not converge to a $F_{\max} < 100 \text{ KJ mol}^{-1} \text{ nm}^{-1}$ after 5000 steps. Then the system was equilibrated in three steps. In the first step the system was gradually heated from 0 to 300 K during 1 ns, it was performed at constant volume (NVT). The other equilibration steps, of 10 ns each, were performed at constant temperature (NPT). To avoid artefactual alteration in the ligand pose due thermal equilibration, positional restraints were applied during the equilibration. Finally, a total MD trajectory between 50 and 300 ns at constant volume and temperature (NVT) was run using the leap-frog algorithm for integrating Newton's equations of motion. The analysis was performed for the set of snapshots saved every 3 fs along the trajectories.

Cell culture

Cell lines

Cell lines used throughout this thesis were from different origin: MCF7 are human breast adenocarcinoma cells which express estrogen receptor. These cells have an epithelial phenotype. HeLa are human cervix carcinoma cells with an epithelial phenotype. HCT116 cells are human colon carcinoma cells with an epithelial phenotype. SW480 and HT29 cells are human colon adenocarcinoma cells also with an epithelial phenotype. HEK-293 are human kidney embryonic cells with an epithelial morphology. FAO cell line is derived from rat hepatoma cells. INS-1 are rat insulinoma cells which can secrete insulin under glucose stimulation conditions. Finally, MEF cells are mouse embryonic fibroblasts.

All cell lines were cultured at 37 °C in humidified atmosphere with 5 % of CO₂. MCF7, HCT116, SW480, HT29, HeLa, HEK-293, and MEF cells were cultured with DMEM medium (Biological Industries, # 01-055-1A) supplemented with 10 % FBS (Biological Industries, # 04-001-1A), 2mM L-glutamine (Biological Industries, # 03-020-1B), and 10ml/l penicillin-streptomycin solution containing 10000 units/ml of penicillin G and 10 mg/l streptomycin sulfate (Biological Industries, # 03-031-1B). FAO cell line was cultured using RPMI 1640 (Biological Industries, # 01-104-1A) supplemented with 10 % FBS, 2 mM L-glutamine, 10 ml/l penicillin-streptomycin solution. INS-1 cells were cultured in RPMI 1640 medium supplemented with 10 % FBS, 2 mM L-glutamine, 10 ml/l penicillin-streptomycin solution, and 71 µM of β-mercaptoethanol (Merck Millipore, # 805740025).

During some experiments, cells were treated with DMEM (Biological Industries, # 01-057-1A) with different glucose concentrations (0 mM, 1 mM, 5 mM and 25 mM).

Stable PCK2-overexpressing MCF7

For overexpression of PCK2, PCK2 Human ORFeome lentiviral particles (GeneCopoeia # LP-OL06695-LX304-0200-S) were used. Transduction was performed following the protocol supplied by the manufacturer. The lentiviral vector contained blasticidin resistance gene, therefore, blasticidin (2 µg/ml; Sigma-Aldrich, # 15205) was used to select the infected cells.

Pancreatic islets culture

Islets were obtained from 12-20 weeks-old C57BL6/J male mice by collagenase (Roche) digestion and Histopaque (Sigma-Aldrich) gradient purification as previously described (Fernandez-Ruiz et al., 2020; D. S. Li et al., 2009). Isolated islets were allowed to recover overnight in RPMI-1640 media with 11 mM glucose, 10% FBS and 10 ml/l of penicillin-streptomycin before the experiments.

Gene and protein expression quantification

RT-qPCR

RT-qPCR stands for reverse transcription and quantitative PCR. The combination of these two techniques was used to analyze gene expression. Extracted mRNA is transcribed to cDNA by reverse transcription. Then cDNA is amplified in the qPCR where the measured fluorescence increases exponentially in each PCR cycle. Finally, the threshold cycle (CT) is determined and compared between every sample and gene.

RNA extraction and reverse transcription PCR

RNA of cells was extracted using TRIsure (Bioline, #BIO-38032) and following the protocol given by the manufacturer. The RNA concentration was quantified using Nanodrop One (Thermo Scientific).

High-Capacity cDNA Reverse Transcription Kit (Applied Biosystems, #4368813) was used to reversely transcribe mRNA to cDNA. The master mix was prepared as showed in the Table MM-1.

10x Buffer	2 μ l	
25x dNTP Mix (100mM)	0.8 μ l	
10x Random Primers	2 μ l	
Multiscribe Reverse transcriptase	1 μ l	
RNA	2 μ g	} 14.2 μ l
H2O endonuclease free	up to 20 μ l	

Table MM-1: Master mix for reverses transcription using High-Capacity cDNA Reverse Transcription Kit.

Spin the tubes before starting the following PCR protocol (Table MM-2). The cDNA obtained could be stored at -20 °C.

T (°C)	25	37	85	4
t (min)	10	120	5	∞

Table MM-2: RT-PCR protocol

Real-time PCR (qPCR)

For the qPCR, two mixtures were prepared separately as shown in the Table MM-3. The MicroAmp optical 384 well reaction plate (Applied Biosystems, #4309849) was loaded starting with the cDNA mixture. The plate was sealed, spined, and the qPCR reaction was performed in the *ABI PRISM HT7900 Real Time Sequence Detection System* (Applied Biosystems). The Ct were determined using SDS software (Applied Biosystems) and the $\Delta\Delta$ Ct method was used to analyze the results.

TaqMan probe	0.5 μ l	} 6 μ l
SensiFAST	5.5 μ l	

cDNA	0.5 μ l	} 5 μ l
H2O endonuclease free	4.5 μ l	
TOTAL		11 μ l

Table MM-3: Mixtures for qPCR.

Western Blot

Protein extraction of cells and tissues was performed with RIPA buffer containing protease inhibitors as shown in Table MM-4. The cells were scrapped from the plates after being frozen at -80°C. If necessary, extracts could be sonicated to ensure a proper lysis. The extracts were cleared from debris by centrifugation (10 min, 15000 g, 4°C).

RIPA buffer	Concentration
Tris/HCl pH 7.4	50 mM
NaCl	100 mM
Na ₃ VO ₄	1 mM
NaF	50 mM
EDTA	5 mM
B-Glycerophosphate	40 mM
Triton X-100	1 % (v/v)
PMSF	1 mM
Benzamidine	1 mM
Aprotinin	1 μ g/ml
Leupeptin	1 μ g/ml
Pepstatin	1 μ g/ml

Table MM-4: Composition of RIPA buffer for protein extraction.

Protein concentration was determined using Pierce BCA protein assay kit (Thermo Scientific, #23225) following manufacturer protocol. The samples were diluted to required concentration, mixed with loading buffer (Table MM-5) and boiled for 5 min at 100°C. Samples could be stored at -20°C until needed.

Western blot was performed as previously described (Mahmood & Yang, 2012). Proteins were separated on SDS-polyacrylamide gel (8-15 % acrylamide). Between 15 and 30 μ g of protein were loaded per lane. Electrophoresis was performed at constant voltage (90-130 V) in Towbin buffer with SDS (tris 25 mM, glycine 192 mM, SDS 1%, pH 8.3) for 1-2 h. Separated proteins were transferred by electroblotting to PVDF membrane (pore size 0.2 μ m, Merck Millipore, # ISEQ00010). The electroblotting was performed in Towbin

buffer with methanol (tris 25mM, glycine 192 mM, methanol 10%, pH 8.3) at constant amperage (200 mA/gel 2h) or constant voltage (20 V overnight) at 4°C.

Loading buffer 4x	Concentration
Glycerol	40 % (v/v)
Tris/HCl pH 6.8	240 mM
SDS	8 % (m/v)
β-mercaptoethanol	5 % (m/v)
Bromophenol blue	0.04 % (m/v)

Table MM-5: Composition of loading buffer for western blot sample preparation.

After blotting, membranes were blocked for 1h with 5 % nonfat dry milk in TBS-T at room temperature. After being washed with TBS-T, membranes were incubated with primary antibodies (diluted in 5 % BSA in TBS-T with sodium azide 0.02 %, Table MM-6) overnight at 4°C, or 1h at room temperature. The membranes were washed before incubation with horseradish peroxidase (HRP) conjugated secondary antibodies for 1 h at room temperature. Bands were visualized with EZ-ECL enhanced chemiluminescence detection kit (Biological Industries, #20-500-500) using Fujifilm LAS 3000 (Fujifilm) or Amersham Imager 680 (GE Healthcare Bio-Sciences AB). Relative expression of proteins was quantified by densitometry analysis using Multi Gauge v.3 (Fujifilm) software.

Primary Antibodies	Size (KDa)	Host	Dilution	Reference
PEPCK-C	71	Sp	1 : 1000	Gift from Dr. Granner
PEPCK-M	71	Rb	1 : 1000	Abcam, #ab70359
Phospho-ACC	280	Rb	1 : 1000	Cell Signaling, #3661
γ-tubulin	48	Ms	1 : 10 000	Sigma, #T-6557
β-actin	46	Ms	1 : 1000	Santa Cruz, #sc-69879
V5 tag	-	Ms	1 : 5000	Invitrogen, #46-0705
p21	21	Rb	1 : 1000	Santa Cruz, #sc-397
p53	53	Ms	1 : 1000	Abcam, #ab26
Phospho-S6	32	Rb	1 : 1000	Cell Signaling, #2211
HK-2	110	Rb	1 : 1000	Cell Signaling, #2867
PARP1	116/89	Rb	1 : 1000	Cell Signalling, #9542
Secondary antibodies		Host	Dilution	Reference
Anti-mouse		Gt	1 : 20 000	Sigma, #A9917
Anti-rabbit		Gt	1 : 10 000	Advansta, #R-05072-500

Anti-sheep	Rb	1 : 5000	Dako, #P0163
Anti-goat	Dk	1 : 5000	Santa Cruz, #sc-2056

Table MM-6: Antibodies used in western blot

RNA-seq

RNA of cells was extracted using RNeasy Mini Kit (QIAGEN, #74104) following the protocol provided by the manufacturer. The RNA concentration was quantified using Nanodrop One (Thermo Scientific) and the RNA integrity was estimated with Agilent RNA 6000 Pico Bioanalyzer 2100 (Agilent).

The RNASeq libraries were prepared with KAPA Stranded mRNA-Seq Illumina Platforms Kit (Roche) following the manufacturer's recommendations. Briefly, 500 ng of total RNA was used for the poly-A fraction enrichment with oligo-dT magnetic beads, following the mRNA fragmentation. The strand specificity was achieved during the second strand synthesis performed in the presence of dUTP instead of dTTP. The blunt-ended double stranded cDNA was 3' adenylated and Illumina platform compatible adaptors with unique dual indexes and unique molecular identifiers (Integrated DNA Technologies) were ligated. The ligation product was enriched with 15 PCR cycles. The size and quality of the libraries were assessed in a High Sensitivity DNA Bioanalyzer assay (Agilent). The libraries were sequenced on HiSeq 4000 (Illumina) with a read length of 2x76bp+8bp+8bp using HiSeq 4000 SBS kit (Illumina).

Reads were mapped against the human reference genome (GRCh38) with STAR/2.5.3a using ENCODE parameters for long RNA. Genes were quantified with RSEM/1.3.0 using the default parameters of GENCODE version 24. Quality control of the mapping and quantification steps were performed with 'gtfstats' from GEM-Tools 1.7.1. Differential expression analysis was done with DESeq2/1.18 using default parameters. Genes with FDR<5% were considered significant. Heatmap with the differentially expressed genes was performed using InstantClue software (Nolte et al., 2018). Pre-ranked gene set enrichment analysis (GSEA) was performed following the protocol described by Reimand et al., 2019. The significant gene sets from GSEA (FDR < 0.05) were plotted using the Enrichment Map plugin available in Cytoscape (Reimand et al., 2019).

Target engagement

Expression of recombinant proteins *E. coli*

To assess the target engagement of the different inhibitors, human recombinant PEPCK and PYCR1 were expressed in BL21 *E. coli* and subsequently purified. The open reading frames for human PCK1, PCK2 or PYCR1 were cloned into an expression vector (pET15b). BL21 *E. coli* strain carries a chromosomal copy of the T7 RNA polymerase gene under control of a lacUV5 promoter. The expression vector pET15b has a T7 promoter the ampicillin resistance gene. Therefore, when BL21 cells containing the expression vector (pET15b + gene) are treated with IPTG (a non-hydrolysable lactose analog), T7 RNA polymerase expression is induced and promotes the expression of the gene after the T7 promoter of the vector.

Transformation

The first step of the expression protocol consists in the transformation of competent *E. coli* (in this case of the BL21 strain) with the expression construct. The transformation can be done as follows:

- 1.- Add approximately 50 ng of DNA (in 1-5 μ l) to 50 μ l of competent bacteria* and incubate in ice for 30 min. In this step mixing with the pipet must be avoided.
- 2.- Expose the cells to a heat shock: 30 s at 42 °C and incubate on ice for 5 min.
- 3.- Add 950 μ l of SOC medium and incubate for 1 h at 37 °C under shaking (210rpm).
- 4.- Seed the cells in LB-agar plates containing selection antibiotics and incubate them overnight at 37 °C.
- 5.- Pick colonies and incubate them overnight in 3ml of LB with the selection antibiotic (in our case ampicillin at 50 μ g/ml) at 37 °C under agitation (210rpm).
- 6.- A glycerol stock could be made adding 15 % of glycerol to 500 μ l of the overnight culture. The rest of the culture could be used to extract the DNA in order to verify the plasmid.

The GenElute™ HP Plasmid Miniprep Kit (Sigma) or GenElute™ HP Plasmid Maxiprep Kit (Sigma) were used to extract the DNA from the bacteria. Manufacturer instructions were followed.

An analysis with restriction enzymes could be performed to verify if the plasmid is expressed in the picked colony, and that it is the correct one (with the gene cloned in the right place). The reagents used for restriction analysis are showed in Table MM-7; the components were mixed and incubated 2h at 37°C. After the incubation the samples were analyzed by electrophoresis on a 1,2% agarose gel with ethidium bromide at 75 V for 1 h.

Reagent	Volume (μL)
DNA	1.5
Buffer (10X)	1
Enzyme	0.2
H ₂ O	Up to 10 μl

Table MM-7: Reagents for restriction analysis. If needed 0.1 μl of BSA could be added.

* *Competent E. coli can be obtained with the following protocol:*

Procurement of competent *E. coli*

- 1.- Inoculate *E. coli* (from the desired strain) to 3mL of LB without antibiotics and incubate it overnight at 37° under shaking (180-210rpm).
- 2.- Add 2ml of the overnight culture to 100 ml of LB without antibody. Growth it at 37°C under stirring until the optical density at $\lambda=600\text{nm}$ reach 0.3-0.5.
- 3.- Chill on ice for 30 min. From this point the material should be previously refrigerated.
- 4.- Centrifuge (2500 rpm, 15 min, 4 °C) and discard the supernatant.
- 5.- Resuspend in 1ml of CaCl₂ 0.1 M and incubate in ice for 30 min.
- 6.- Centrifuge (2500 rpm, 15 min, 4 °C) and discard the supernatant.
- 7.- Resuspend the pellet in 5ml of CaCl₂ 0.1 M and incubate it overnight at 4°C. (The cells can be stored up to 1 week at this point).
- 8.- Add 125 μl of DMSO, mix it gently and incubate in ice for 5 min.
- 9.- Add 125 μl de DMSO and mix it gently.
- 10.- Split the volume in 100 μl aliquots and store at -80°C.

Each aliquot is enough for one transformation with a control (1 transformation = 50 μl).

Protein expression & purification

Once confirmed that the colony express the right expression vector (with the gene). The protein of interest can be expressed, extracted, and purified as follows:

Expression

- 1- Pick a colony from an agar plate or scratch from a glycerol stock and make a preculture in 10ml of 2xYT with selection antibiotic. Incubate it overnight at 37 °C under shacking (210 rpm).
- 2.- Add 2/8 ml of the overnight preculture to an Erlenmeyer with 50/200 ml of 2xYT with antibiotic.

3.- Incubate it at 37 °C under shaking (210rpm) until the OD₆₀₀ = 0.6-0.8.

4.- Add IPTG to a final concentration of 1 mM and incubate 5h at room temperature under soft shaking (110rpm).

5.- Centrifuge (20 min, 4000g, 4°C) and discard supernatant. The pellet can be stored at -80°C.

! For PEPCK expression with E. coli Arctic cells, during step 4 the cells were incubated during 72 h at 4 °C (Escós et al., 2016b).

Extraction

6.- Thaw and resuspend the pellet in 5 ml of *Lysis Buffer**.

7.- Add 5 mg of lysozyme and chill on ice for 30 min.

8.- Freeze/thaw with liquid N₂ three times.

9.- Sonicate the mixture: 6 cycles of 10s ON 30s OFF, output 2.

10.- Add 5 mg of DNase I and incubate on ice for 15 min.

11.- Centrifuge (18000 g, 20 min, 4 °C) and discard the pellet.

Purification

12.- Prepare the Ni-NTA agarose (QIAGEN):

a) Add 1ml of Ni-NTA slurry (500 µl of bed volume) to a 15ml tube.

b) Briefly centrifuge and discard the supernatant.

c) Wash twice with 2 ml of *Lysis Buffer**.

13.- Add the supernatant to the Ni-NTA agarose and incubate for 1 h under gently shaking at 4 °C.

14.- Prepare a column with a 2 ml syringe and glass wool. Pour the mix on the column and collect the column flow-through for further analysis.

15.- Wash twice with 2.5 ml of *Wash Buffer*. Collect the wash fractions for further analysis

16.- Eluate four times with 0.5 ml of *Elution Buffer*. Collect the eluate in four tubes.

17.- Evaluate the presence of the expressed protein in the different fractions by western blot and/or enzymatic activity.

18.- Add 10 % of glycerol to the eluates which showed activity and store at -80 °C. Add 1 mM of DTT in PEPCK samples before freeze.

*The composition of Lysis, Wash, and Elution buffer are showed in Table MM-8.

Reagent	Lysis Buffer	Wash Buffer	Elution Buffer
NaH₂PO₄	50 mM	50 mM	50 mM
NaCl	300 mM	300 mM	300 mM
Imidazole	10 mM	20 mM	250 mM

Table MM-8: Composition of Lysis, Wash, and Elution buffers.

PEPCK activity

To determine PEPCK activity, PEPCK reaction is coupled to malate dehydrogenase (MDH) reaction (Figure MM-1). MDH reversibly catalyze the oxidation of malate to oxaloacetate using the reduction of NAD⁺ to NADH. Then, oxaloacetate is converted to phosphoenolpyruvate by PEPCK (using GTP), pulling the MDH reaction through oxaloacetate formation.

NADH, unlike its oxidized form NAD⁺, absorb UV light at 340 nm. The reduction of NAD⁺ cofactor to NADH generates an increase of the absorbance at 340 nm which could be quantified using a spectrophotometer. The rate of NADH formation is used to estimate PEPCK activity.

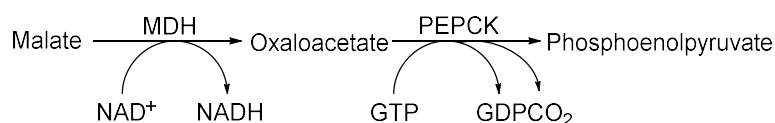


Figure MM-1: Reaction evaluated in the PEPCK assay.

1- Prepare the reaction buffer as shown in Table MM-9.

Reagent	Reaction concentration	Stock concentration	Volume for 1 reaction
HEPES pH 7.2	100 mM	1 M	100 μ l
Malic acid *	3 mM	300 mM	10 μ l
NAD⁺ *	3 mM	300 mM	10 μ l
MgCl₂	2 mM	200 mM	10 μ l
MnCl₂	0.2 mM	10 mM	10 μ l
DTT	37 mM	1 M	37 μ l
MDH	6 UI/ml	16.81 UI/ μ l	0.36 μ l
H₂O MiliQ			622.6 μ l

Table MM-9: PEPCK reaction buffer composition

2.- Add 800 μ l of the reaction buffer to a 1ml spectroscopic cuvette and add 190 μ l of a solution with recombinant PEPCK** and inhibitor in a phosphate buffer (the same as the purification but without imidazole).

3.- Read the absorbance at 340 nm with the optical spectrometer (PEPCK program: 340nm, kinetics mode, 6 min, 37 °C). Check that there are no significant variations of absorbance during this period and discard the data.

4.-Add 10 µl of GDP* 20mM (final concentration = 0.2 mM).

5.- Read the absorbance at 340 nm with the optical spectrometer (PEPCK program) and save the data.

6.- Calculate the activity using the rate at 2 min (ΔAbs) with the formula in Equation MM-1. Where $\epsilon(NADH)$ is $6220 M^{-1}cm^{-1}$, l is 1 cm, and the activity is expressed in $\mu mol/min$.

$$Activity = \frac{\Delta Abs}{\epsilon(NADH) \times l} \quad \text{(Equation MM-1)}$$

*These solutions must be prepared at the moment.

**Same buffer than used for purification without imidazole.

**The amount of PEPCK depends on the batch, a trial with different concentrations should be performed to determine it.

The activity could be evaluated as well in the other sense of the reaction. In this case NADH consumption will be observed.

1.- Prepare reaction buffer (Table MM-10). A buffer without $NaHCO_3$ could be prepared as a negative control.

Reagent	Reaction concentration	Stock concentration	Volume for 20 reactions
Tris-HCl pH 7.4	50 mM	1 M	1 ml
$NaHCO_3$	20 mM	200 mM	2 ml
$MnCl_2$	1 mM	10 mM	2 ml
MiliQ H_2O			10,46 ml

Table MM-10: PEPCK reaction buffer composition

2.- Charge the CO_2 + buffer with gas (CO_2) for 10 min

3.- Complete the buffers with the reagents in Table MM-11.

Reagent	Reaction concentration	Stock concentration	Volume for 20 reactions
PEP*	0,5 mM	50 mM	200 µl
NADH*	0,1 mM	10 mM	200 µl
MDH	2 UI/ml	16.81 UI/µl	1,2 µl
Rotenone	5 µM	1 mM	40 µl
DTT	25 mM	1 mM	500 µl

Table MM-11: Reagents to add to PEPCK reaction buffer after CO_2 charge.

4.- Proceed the same way as the other reaction but add GDP instead of GTP.

**These solutions must be prepared fresh.*

PYCR1 ACTIVITY ASSAY

Since it was not possible to obtain P5C, PYCR1 activity was evaluated by assessing 3,4-dihydro-L-proline (DHP) oxidation (Figure MM-2). Similar to PEPCK assays, during DHP oxidation NAD^+ is reduced to NADH, which formation can be tracked by absorbance at 340 nm (L. Li et al., 2017).

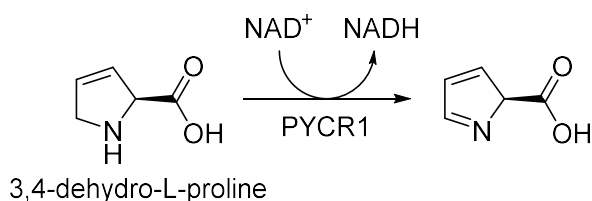


Figure MM-2: Reaction evaluated in the PYCR1 assay. Oxidation of 3,4-dihydro-L-proline.

1.- Prepare the reaction buffer (Table MM-12).

Reagent	Reaction concentration	Stock concentration	Volume for 1 reaction
Tris pH 9	300 mM	1 M	300 μl
DHP	0.4 mM	100 mM	4 μl
MiliQ H_2O			496 μl

Table MM-12: PYCR1 reaction buffer

2.- Add 800 μl of the Reaction Buffer to a 1ml spectroscopic cuvette and add 190 μl of a solution with recombinant PYCR1 and inhibitor in a phosphate buffer (the same as the purification but without imidazole).

3.- Read the absorbance at 340 nm with the optical spectrometer. Check that there are no significant variations of absorbance during this period and discard the data.

4.- Add 10 μl of NAD^{+} 100mM (to a final concentration of 1 mM).

5.- Read the absorbance at 340 nm (PYCR1 program) and save the data.

6.- Calculate the activity in the same manner than with PEPCK (Equation MM-1).

**These solutions must be prepared at the moment.*

A high throughput like assay for evaluating PYCR1 inhibitors was set up. The assay was designed for evaluating multiple compounds at the same time, as well as to reduce the amount of reagent used (since the final

volume of this assay is 100 μ l instead of 1 ml). It uses the FLUOSTAR OPTIMA (BMG LABTECH) plate reader to read the NADH fluorescence (at 360/460 nm) in 96 well/plates.

1.- Prepare reaction buffer (Table MM-13).

Reagent	Reaction concentration	Stock concentration	Volume for 1 reaction (μ l)
Tris pH 9	300 mM	1 M	30
DHP	0.4 mM	100 mM	0.4
PYCR1		10 X	7.5*
H₂O MiliQ			42.1

Table MM-13: PYCR1 reaction buffer

2.- Add 80 μ l/well of the reaction buffer into a dark 96-well plate.

3.- Add 10 μ l/well of the inhibitor at the desired concentration.

4.- Prepare a 10 mM NAD⁺ solution (10 μ l/reaction, at least prepare 1.5 ml).

5.- Charge the NAD⁺ solution to the injector.

6.- Insert the plate to the FLUOSTAR OPTIMA plate reader and read the fluorescence using the PYCR1 activity program: fluorescence 360/460 nm; duration of the protocol 8 min; after 2min, the injector adds 10 μ l of NAD⁺ 10mM (reaction concentration 1mM).

7.- Use the slope of the curve between min 2 and 4 for calculating PYCR1 activity.

Cellular thermal shift assay (CETSA)

The target engagement in a cellular context can be evaluated using a cellular thermal shift assay (CETSA). This assay is based on the ligand-induced stabilization of proteins. Proteins bounded to a ligand are more stable and can tolerate higher temperatures without denaturalizing. Higher the affinity of the ligand for the protein (lower K_d), higher the percentage of protein bounded to a ligand at a fixed concentration. Therefore, ligands with high affinity would thermically stabilize a protein with higher efficiency than ligands with lower affinity (Jafari et al., 2014).

Intact and viable mouse embryonal fibroblast (MEF) and rat hepatoma FAO cells were harvested and resuspended to a final concentration of 2×10^6 cells/ml. Different PEPCK-M inhibitors were added to this suspension, to a final concentration of 5 μ M, and incubated for 30 min at 37 °C. Cells were washed and resuspended with PBS to a final concentration of 3×10^7 cells/ml. They were split in different tubes and treated with a gradient of temperatures between 40 and 60 °C for 3 min, cells were incubated 3 min at room temperature and snap frozen with liquid nitrogen. Cells were lysed using a freeze/thaw cycle with liquid

nitrogen and centrifuged at 20000 g 20 min at 4 °C. Finally, stable PEPCK-M present in the supernatant was quantified by western blot.

The analysis was also performed treating the cells with a gradient of PEPCK-M inhibitor concentrations and a thermal treatment at a single temperature (60 °C). IsoThermal Dose-Response Fingerprint (ITDRF-CETSA) concentrations were calculated as described (Jafari et al., 2014).

Metabolites quantification

Perchloric acid extraction

This extraction removes the proteins of the sample by precipitation, and so the enzyme activities without modifying metabolites concentrations.

- 1.- Clean the cells with cold PBS.
- 2.- Add 1ml of PBS, scrap the cells and bring it to an eppendorf.
- 3.- Centrifuge 5 min 300 g rt, and discard supernatant.
- 4.- Add 200 ul of perchloric acid 1M and freeze the cells with liquid N₂.
- 5.- Freeze and thaw with liquid N₂ three times.
- 6.- Thaw, vortex and centrifugate it at 10000 g for 5 min at 4 °C. Store the pellet at -80 °C for protein quantification*.
- 7.- Bring the supernatant to a new Eppendorf and neutralize the solution with KHCO₃ 3M (until pH 7).
- 8.- Centrifuge at 10000 g 3 min at 4 °C. Store the supernatant at -80°C until using it.

**For protein quantification resuspend the pellet with 1ml of NaOH 0,1 M and quantify it by BCA.*

PEP determination

Determination of PEP concentration was performed by quantifying the ATP formed by the pyruvate kinase reaction with the StayBrite™ Highly Stable ATP Bioluminescence Assay Kit (BioVision).

- 1.- Prepare the buffer for the reaction (Table MM-14)

Reagent	Reaction concentration	Stock concentration	Volume / sample (μl)
Glycylglycine pH 7.0	50 mM	0.4 M 0	12.5
KCl	100 mM	2 M	5
MgCl₂	5 mM	200 mM	2.5
MgADP	0.1 mM	20 mM	0.5
Sample			50
MiliQ H₂O			Up to 85 μl
StayBrite Kit			10
Pyruvate kinase (PK)		9 μl/ml H ₂ O	5

Table MM-14: Reaction buffer for PEP determination

- 2.- Mix the buffer with samples/standard* in eppendorfs.
- 3.- Add the enzyme from the kit, incubate for 3 minutes and read the luminescence: background signal.
- 4.- Add Pyruvate kinase, wait 2 minutes and read the luminescence.
- 5.- Subtract the Background of each sample and interpolate the concentrations.

**Standard curve should be prepared adding 10ul of the standard solution to a buffer containing 50ul of a mix of samples. This is done to consider the matrix effect.*

G6P determination

Determination of G6P concentration was performed by quantifying the NADPH formed by the glucose-6-phosphate dehydrogenase reaction by 360/460 nm fluorescence.

- 1.- Add 100 μ l of sample or 10 μ l of standard in the wells of a black 96 well plate.
- 2.- Add the buffer (Table MM-15) up to 190 μ l.

Reagent	Reaccion concentration	Stock concentration	Volume / sample (μ l)
Glycylglycine pH 7.0	50 mM	0.4 M	25
KCl	100 mM	2 M	10
MgCl₂	5 mM	0.2 M	5
NADP⁺	2 mM	40 mM	10
Sample / Standard			100 / 10
mQ H₂O			40 / 130

Table MM-15: Reaction buffer for G6P determination.

- 3.- Measure the fluorescence at 360/460 nm.
- 4.- Add 10 μ l of G6PDH solution (18 μ l of commercial G6PDH to 1 ml of miliQ water) to each well. Incubate for 20 min.
- 5.- Measure the fluorescence again and process the data.

Glucose stimulated insulin secretion

The glucose stimulated insulin secretion (GSIS) can be assayed in animals, isolated pancreatic islets or cell lines (INS1: rat insulinoma cell line). The following protocol is designed for isolated pancreatic islets but also works for cell lines seeded in 12-well plates.

- 1.- Prepare fresh KRBH solution, adjust the pH 7.4, sterilize by filtering, and warm it at 37°C.

2.- Pick 5 islets with a similar size and put them in a 1.5 ml tube with 500 μ l KRBH 2.8 mM glucose, with or without inhibitors. Incubate them for 2 h in a water bath at 37°C with agitation (30 rpm). In the case of not testing any inhibitor 30 min would be enough.

3.- Discard the supernatant and check that the islets remain in the tube with the magnifying lens.

4.- *Insulin secretion 2.8mM glucose (basal)*: Add 500 μ l of KRBH 2.8mM glucose (+/- inhibitors), incubate the tubes in the bath for 1 h at 37 °C, under agitation (30 rpm). Save the supernatant for insulin quantification, check that the islets remain in the tube.

5.- *Insulin secretion 16.7mM glucose (GSIS)*: add 500 μ l of KRBH 16.7 mM glucose (+/- inhibitors), incubate the tubes in the bath for 1 h at 37 °C, under agitation (30 rpm). Save the supernatant for insulin quantification, check that the islets remain in the tube.

6.- Both supernatants should be saved at -20 °C.

7.- *Insulin content*: add 150 μ l of acetic-acid lysis buffer to the islets and save the tubes at -80 °C overnight.

8.- Thaw the tubes, vortex them and incubate them 10 min at 95 °C in a thermo-block.

9.- Centrifuge them at 1200 rpm 4 °C for 10 min and save the supernatant (-20 °C).

10.- Measure the insulin levels of the three supernatants by ELISA (Mercodia Kit) following the protocol provided by the manufacturer. The insulin levels should be normalized by the insulin content of the islets.

Metabolite quantification by GC-MS

Metabolite extraction from cells and derivatization of polar samples were performed as previously described (Méndez-Lucas et al., 2020).

Briefly, cells were washed with ice-cold PBS and 600 μ l of ice-cold methanol containing standards were added. Cells were scraped and transferred to an Eppendorf and 300 μ l of chloroform were added (methanol : chloroform, 2 : 1 v/v). Standards include scylloinositol (10 nmol), L-Norleucine (10 nmol), added with the methanol. After centrifugation (18000 g, 10 min, 4°C), the supernatant (SN1) was vacuum dried in rotational-vacuum-concentrator Concentrator 5301 (Eppendorf). The pellet was re-extracted with methanol : water (2:1 v/v) as described above. After centrifugation, supernatant (SN2) was vacuum dried in the SN1 tube. Phase partitioning (chloroform : methanol : water, 1:3:3 v/v) was used to separate polar and nonpolar metabolites. Fractions were vacuum dried as described above.

For GC-MS analysis of the polar metabolites, a part of the polar fraction was washed twice with methanol, derivatized by methoximation (Sigma, 20 μ l, 20 mg/ml in pyridine) and trimethylsilylation (20 μ l of N,O-bis(trimethylsilyl)trifluoroacetamide reagent (BSTFA) containing 1% trimethylchlorosilane (TMCS), Supelco),

and analysed on an Agilent 7890A-5975C GC-MS system (MacRae et al., 2013; Zamboni et al., 2009). Splitless injection (injection temperature 270°C) onto a 30 m + 10 m × 0.25 mm DB-5MS+DG column (Agilent J&W) was used, using helium as the carrier gas, in electron ionization (EI) mode. The initial oven temperature was 70°C (2 min), followed by temperature gradients to 295°C at 12.5°C/min and then to 320°C 25°C/min (held for 3 min).

Metabolite quantification and isotopologue distributions were corrected for the occurrence of natural isotopes in both the metabolite and the derivatization reagent. Data analysis and peak quantifications were performed using MassHunter Quantitative Analysis software (B.06.00 SP01, Agilent Technologies). The level of labeling of individual metabolites was corrected for natural abundance of isotopes in both the metabolite and the derivatization reagent (Chow et al., 2012). Abundance was calculated by comparison to responses of known amounts of authentic standards.

Cell biology evaluation

Viability evaluation

MTT assay

The MTT assay is a colorimetric assay used to assess cell metabolic activity, and therefore, cell viability. The yellow tetrazolium dye MTT (3-(4,5-dimethylthiazol-2-yl)-2,5-diphenyltetrazolium bromide) can be reduced to its purple insoluble formazan by metabolically active cells. The viable cells contain mitochondrial NAD(P)H-dependent oxidoreductases, which are responsible for MTT reduction. The formazan crystals are solubilized in isopropanol and the absorbance at 570 nm of the resulting solution quantified by spectrophotometry.

- 1.- Dissolve MTT powder in sterile PBS to 5 mg/ml. This solution could be stored at -20 °C up to 3 months.
- 2.- Change cell's media with complete media with 0.5 mg/ml of MTT. (For 96-well plate 100 µl, 24 and 12-well plates 500 µl).
- 3.- Incubate for 4h at 37 °C.
- 4.- Aspirate the media, add isopropanol (100 µl in 96-well plate, or 500 µl on 12/24-well plates) and incubate it for 20 min in the dark under shaking.
- 5.- If using a 12 or 24-well plate transfer 100 µl of the sample to a 96 well plate.
- 6.- Read the absorbance at 570 nm with background subtraction at 650 nm using the plate spectrophotometer. The samples can be diluted with isopropanol if the signal got saturated.

Crystal violet

Crystal violet is a dye which binds to DNA and proteins in cells. When added to adherent cells, crystal violet acts as an intercalating dye (DNA) staining the cell nuclei. Since during cell death, adherent cells tend to detach from the plate, crystal violet is used to assess proliferation and cell survival. However, crystal violet stains both, viable and dead cells. Crystal violet is also used in bacterial Gram staining.

- 1.- Prepare crystal violet solution (CV): 0.2 % of crystal violet in 2 % ethanol aqueous solution. The solution can be stored at room temperature and reused for several times.
- 2.- Aspirate cell media and wash twice with PBS.
- 3.- Add 100-500 µl of CV solution (depending on the plate used) and incubate 10 min at room temperature.
- 4.- Collect CV and wash the plates by immersion in a large beaker full of tap water. Wash it three times changing the water between washes.

5.- Let the plate dry.

6.- The crystal violet of the stained cells can be dissolved in 2 % SDS solution. Shake at room temperature until the color is uniform (1-2 h).

7.- Transfer 100 μ l to a 96 well plate (if needed) and measure the absorbance at 570nm in a plate spectrophotometer.

Annexin V

Annexin V staining assay allows us to identify the cells undergoing apoptosis. Annexin V binds to phosphatidylserine, a phospholipid that is found in the inner side of the cytoplasmic membrane. During apoptosis, phosphatidylserine is translocated to the outer side of the cytoplasmic membrane. Therefore, fluorophore (APC, FITC) conjugated annexin V stains apoptotic cells. Complementary, nucleic acid dyes (as SYTOX or propidium iodide) could be added to distinguish between viable cells (annexin negative, SYTOX negative), early apoptotic (annexin positive, SYTOX negative) and late apoptotic or dead (annexin positive, SYTOX positive).

1.- After the desired treatment, collect cell media into a tube. Wash the plates with PBS and collect it.

2.- Trypsinize cells and collect the cells together with the media and PBS.

3.- Centrifuge the tubes (400 g, 5min) and discard the supernatant.

4.- Resuspend the cells with PBS and pick 10^5 cells to another tube for annexin staining.

5.- Centrifuge the cells and resuspend with 100 μ l of Annexin V mixture (5 % annexin in binding buffer).

6.- Incubate in the dark for 15 min at room temperature.

7.- Add 200 μ l of binding buffer.

8.- Add 100 μ l of SYTOX solution (10 nM SYTOX in binding buffer).

9.- Analyze by flow cytometry.

Anchorage independent growth: soft agar

The soft agar colony formation assay is a technique widely used to evaluate cellular transformation in vitro. In this assay, cells are seeded in a semi-solid agarose over a dense agar layer. In this conditions cells can only grow in an anchorage-independent manner.

- 1.- Melt a 3% agarose solution and store it in a bath at 40 °C to avoid gelification.
- 2.- For the inferior layer, prepare a 0.6 % solution of agarose in DMEM. Gently add 2mL of the 0.6 % agarose-DMEM solution to each well of a 6-well plate.
- 3.- Store it in the fridge for 15 min until gelification, and pre-warm it in the cell incubator for 15 min before adding the upper layer.
- 4.- For the upper layer, prepare a cell suspension of 2×10^4 cells/ml in media with/without treatment and a 0.6 % solution of agarose in DMEM.
- 5.- Mix the cell suspension with the 0.6 % agarose solution one to one, and quickly add 1ml of the resultant cell suspension in each well.
- 6.- Incubate the plate at 4 °C for 5 min and incubate it at 37 °C for 2-3 weeks.
- 7.-Add 500 ul of media +/- treatment and change it every 3-4 days.

Wound healing assay

Wound healing assay is one of the first developed methods to study cell migration in vitro. This assay is based on the observation of cell migration into a wound created on a cell monolayer. The protocol is the following:

- 1.- Change the media of a 6-well plate seeded at high confluence (95-100 %) with FBS-free medium and incubate it overnight.
- 2.- Pre-incubate the cells with de desired treatment for 2h (in FBS-free medium).
- 3.- Make a wound in the cell monolayer with a pipette tip using a scraper as a ruler.
- 4.- Clean the floating cells with fresh media and add the treatment media (without FBS).
- 5.- Find the wound in the microscope and take a picture every 2 hours.
- 6.- Calculate the area of the wound at each time point using imageJ and process the results.

Cell cycle

The cell cycle is the process that take place in a cell during its division. The cell cycle in eukaryotic cells has four different phases: G₁, S, G₂, M. Cells that have left the cycle and are not dividing are in G₀ phase. During

phase G1, cells grow in size and prepare themselves to start the DNA synthesis in phase S. The phase G2 occurs between the DNA synthesis and the mitosis.

The staining of DNA with a fluorescent dye allows us to determine the cell cycle phase of the cells according to staining intensity, and therefore DNA amount.

- 1.- Collect the media, wash the cells with PBS collecting it. Collect the trypsinized cells with the floating cells of the incubation medium and the washes.
- 2.- Centrifuge the cells (400 g, 5 min, rT) and discard the supernatant. Resuspend the cells with 1 % FBS in PBS to 1 ml of $1-2 \times 10^6$ cells/ml.
- 3.- Wash twice with 1 % FBS in PBS (400 g, 5 min).
- 4.- Carefully resuspend the cells with 500 μ l of 1 % FBS in PBS. The resuspension must be complete, avoiding aggregates.
- 5.- Add 5ml of cold (-20 °C) 70 % EtOH dropwise to the resuspended cells under smooth agitation with the vortex.
- 6.- Fix the cells at -20 °C at least for 2h. The suspension could be stored up to 3 weeks.
- 7.- Centrifuge (800 g, 5 min) and wash the cells with 1% FBS in PBS.
- 8.- Resuspend the pellet with 400 μ l 1 % FBS in PBS and add 50 μ l of 0.5 mg/ml propidium iodide.
- 9.- Add 5 μ l of RNase A (10 mg/ml; DNase free) and incubate for 30-45 min at 37 °C in the dark.
- 10.- Analyze by flow cytometry.

In-vivo studies in animal models

Pharmacokinetics of iPEPCK-2 by HPLC

The pharmacokinetic study was carried on in male ICR white mice between 30 and 40 g (n = 4 per group, which is a small cohort based on the potency of the analytical and quantification techniques utilized) and all animals were randomized to either the experimental and control groups. A single intraperitoneal dose of iPEPCK-2 (dissolved in 40 % PEG 400 in physiological saline), was administered at 8 mg/kg early in the morning (between 8 and 10 a.m.) without anesthesia. Mice were monitored for signs of pain or distress during the time between injection and euthanasia (at the earliest time of 15 min and the latest at 8 h after injection) and sacrificed by cervical dislocation for blood and brain collection. Brain and plasma were immediately frozen at -80 °C for pK analysis.

iPEPCK-2 was extracted from plasma and homogenate brain in PBS with acetonitrile, in the presence of 1 M DTT and quantified by HPLC/UV.

The solid phase was C18 RP column (5 m, 20 × 0.4 cm; Kromasil 100; Teknokroma) and the mobile phase consisting in a 0.05 M KH₂PO₄ (45 %): acetonitrile (55 %). The elution time of iPEPCK-2 was 3.7 min, and it was detected at 290 nm. The assay had a range of 0.125–5 µg/ml. Calibration curves were constructed by plotting the peak area ratio of analyzed peak against known concentrations.

iPEPCK-2 plasma concentrations versus time curves for the mean of animals were analyzed by a non-compartmental model based on statistical moment theory using the *PK Solutions* computer program. The pharmacokinetic parameters calculated were the area under the concentration vs time curve (AUC), which was calculated using the trapezoidal rule in the interval 0–8 h, and the half-life ($t_{1/2\beta}$), which was determined as $\ln 2/\beta$ (β was calculated from the slope of the linear, least-squares regression line). The C_{max} and T_{max} were read directly from the mean concentration curves.

Xenograft models

Two subcutaneous tumor xenograft models were generated by injecting transformed cells in both flanks of female 5–6-week-old BALB/c nude mice (at least n = 5 per group, given the large dispersion on the size of the tumors grown in flanks of immunocompromised mice). In the first model, 1 × 10⁶ HEK-293 cells were injected per flank, whereas on the colon carcinoma model, 5 × 10⁶ SW-480 cells were utilized. Handling for the injections was in the absence of anesthesia or analgesia, and no signs of distress or pain were evident afterwards. Mice were monitored for signs of cancer disease, pain or distress during the time of the experiment and sacrificed by cervical dislocation and removed from the experiment if so advised by the veterinarian in charge of the animal facility. When the tumors grew enough to be measured, mice were randomly split in two groups, and kept in grouped cages of at least 4 animals per cage. One group received a daily (between 8 and 10 am) intra-peritoneal injection with 8 mg/kg of iPEPCK-2 without analgesia. No signs

of distress or pain resulted from the injection. The other group was treated with vehicle (5 % DMSO in 20 % PEG400 saline solution) instead, following the same therapeutic regimen. The tumors were measured, and mice weighted twice a week. After 15 days (SW-480) or 24 days (HEK-293), mice were euthanized by cervical dislocation, and the tumors and organs processed for further analysis.

Tissues were fixed twelve hours in 4 % paraformaldehyde after trimming them into appropriate size and shape and placing them in histology cassettes. They were then dehydrated following an ethanol gradient process and embedded in paraffin. Tissue sections (3–4 μM) were stained with Harris hematoxylin & eosin stain for morphological analysis.

Statistical analysis

Graphic visualization of the data and statistical analysis were performed using GraphPad Prism 8. Depending on the study, two-tailed T student test and one or two-way ANOVA were conducted for data analysis. P value ranking is specified in each figure.

Generally, experiments were independently replicated at least three times with 3-8 replicates per group. Plotted values are shown as mean \pm standard error of the mean (SEM), unless otherwise is mentioned in the figure legend.

BIBLIOGRAPHY

- Abulizi, A., Cardone, R. L., Stark, R., Lewandowski, S. L., Zhao, X., Hillion, J., Ma, L., Sehgal, R., Alves, T. C., Thomas, C., Kung, C., Wang, B., Siebel, S., Andrews, Z. B., Mason, G. F., Rinehart, J., Merrins, M. J., & Kibbey, R. G. (2020a). Multi-Tissue Acceleration of the Mitochondrial Phosphoenolpyruvate Cycle Improves Whole-Body Metabolic Health. *Cell Metabolism*, 32(5), 751-766.e11. <https://doi.org/10.1016/J.CMET.2020.10.006/ATTACHMENT/8530D86A-79D9-4EAF-8AF7-217AD9FD73E6/MMC1.PDF>
- Abulizi, A., Cardone, R. L., Stark, R., Lewandowski, S. L., Zhao, X., Hillion, J., Ma, L., Sehgal, R., Alves, T. C., Thomas, C., Kung, C., Wang, B., Siebel, S., Andrews, Z. B., Mason, G. F., Rinehart, J., Merrins, M. J., & Kibbey, R. G. (2020b). Multi-Tissue Acceleration of the Mitochondrial Phosphoenolpyruvate Cycle Improves Whole-Body Metabolic Health. *Cell Metabolism*, 32(5), 751-766.e11. <https://doi.org/10.1016/J.CMET.2020.10.006>
- Ackerman, D., & Simon, M. C. (2014). Hypoxia, lipids, and cancer: surviving the harsh tumor microenvironment. *Trends in Cell Biology*, 24(8), 472. <https://doi.org/10.1016/J.TCB.2014.06.001>
- Aggarwal, V., Tuli, H. S., Varol, A., Thakral, F., Yerer, M. B., Sak, K., Varol, M., Jain, A., Khan, M. A., & Sethi, G. (2019). Role of Reactive Oxygen Species in Cancer Progression: Molecular Mechanisms and Recent Advancements. *Biomolecules*, 9(11), 735. <https://doi.org/10.3390/BIOM9110735>
- Akincilar, S. C., Unal, B., & Tergaonkar, V. (2016). Reactivation of telomerase in cancer. *Cellular and Molecular Life Sciences* 2016 73:8, 73(8), 1659–1670. <https://doi.org/10.1007/S00018-016-2146-9>
- Akram, M. (2013a). Mini-review on Glycolysis and Cancer. *Journal of Cancer Education* 2013 28:3, 28(3), 454–457. <https://doi.org/10.1007/S13187-013-0486-9>
- Akram, M. (2013b). Citric Acid Cycle and Role of its Intermediates in Metabolism. *Cell Biochemistry and Biophysics* 2013 68:3, 68(3), 475–478. <https://doi.org/10.1007/S12013-013-9750-1>
- Alberts B, Johnson A, Lewis J, Raff M, Roberts K, & Walter P. (2002). Cancer as a microevolutionary process. In *Molecular Biology of the Cell* (pp. 1205–1256). Garland Science.
- Almuhaideb, A., Papathanasiou, N., & Bomanji, J. (2011). 18F-FDG PET/CT imaging in oncology. *Annals of Saudi Medicine*, 31(1), 3–13. <https://doi.org/10.4103/0256-4947.75771>
- Alvarez, Z., Hyrossova, P., Perales, J. C., & Alcantara, S. (2016). Neuronal Progenitor Maintenance Requires Lactate Metabolism and PEPCK-M-Directed Cataplerosis. *Cerebral Cortex (New York, N.Y. : 1991)*, 26(3), 1046–1058. <https://doi.org/10.1093/CERCOR/BHU281>
- Álvarez-García, V., Tawil, Y., Wise, H. M., & Leslie, N. R. (2019). Mechanisms of PTEN loss in cancer: It's all about diversity. *Seminars in Cancer Biology*, 59, 66–79. <https://doi.org/10.1016/J.SEMCANCER.2019.02.001>
- Anderson, A. C. (2003). The Process of Structure-Based Drug Design. *Chemistry & Biology*, 10(9), 787–797. <https://doi.org/10.1016/J.CHEMBIOL.2003.09.002>
- Anderson, D. D., & Stover, P. J. (2009). SHMT1 and SHMT2 Are Functionally Redundant in Nuclear De novo Thymidylate Biosynthesis. *PLOS ONE*, 4(6), e5839. <https://doi.org/10.1371/JOURNAL.PONE.0005839>
- Aragó, M., Moreno-Felici, J., Abás, S., Rodríguez-Arévalo, S., Hyroššová, P., Figueras, A., Viñals, F., Pérez, B., Loza, M. I., Brea, J., Latorre, P., Carrodegua, J. A., García-Rovés, P. M., Galdeano, C., Ginex, T., Luque, F. J., Escolano, C., & Perales, J. C. (2020). Pharmacology and preclinical validation of a novel anticancer compound targeting PEPCK-M. *Biomedicine & Pharmacotherapy*, 121, 109601. <https://doi.org/10.1016/j.biopha.2019.109601>

- Arinze, I. J., Garber, A. J., & Hansons, R. W. (1973). *The Regulation of Gluconeogenesis in Mammalian Liver: The role of mitochondrial phosphoenolpyruvate carboxykinase*. 18(7), 2271. [https://doi.org/10.1016/S0021-9258\(19\)44105-7](https://doi.org/10.1016/S0021-9258(19)44105-7)
- Baell, J. B., & Holloway, G. A. (2010). New substructure filters for removal of pan assay interference compounds (PAINS) from screening libraries and for their exclusion in bioassays. *Journal of Medicinal Chemistry*, 53(7), 2719–2740. https://doi.org/10.1021/JM901137J/SUPPL_FILE/JM901137J_SI_001.PDF
- Baenke, F., Peck, B., Miess, H., & Schulze, A. (2013). Hooked on fat: the role of lipid synthesis in cancer metabolism and tumour development. *Disease Models & Mechanisms*, 6(6), 1353. <https://doi.org/10.1242/DMM.011338>
- Balan, M. D., McLeod, M. J., Lotosky, W. R., Ghaly, M., & Holyoak, T. (2015). Inhibition and Allosteric Regulation of Monomeric Phosphoenolpyruvate Carboxykinase by 3-Mercaptopicolinic Acid. *Biochemistry*, 54(38), 5878–5887. <https://doi.org/10.1021/ACS.BIOCHEM.5B00822>
- Baldwin, J. E., & Krebs, H. (1981). The evolution of metabolic cycles. *Nature* 1981 291:5814, 291(5814), 381–382. <https://doi.org/10.1038/291381A0>
- Baptista, L. P. R., Sinatti, V. V. C., da Silva, J. H. M., Dardenne, L. E., & Guimarães, A. C. (2019). Computational evaluation of natural compounds as potential inhibitors of human PEPCK-M: an alternative for lung cancer therapy. *Advances and Applications in Bioinformatics and Chemistry: AABC*, 12, 15–32. <https://doi.org/10.2147/AABC.S197119>
- Batool, M., Ahmad, B., & Choi, S. (2019). A Structure-Based Drug Discovery Paradigm. *International Journal of Molecular Sciences* 2019, Vol. 20, Page 2783, 20(11), 2783. <https://doi.org/10.3390/IJMS20112783>
- Beale, E. G., Harvey, B. J., & Forest, C. (2007). PCK1 and PCK2 as candidate diabetes and obesity genes. *Cell Biochemistry and Biophysics* 2007 48:2, 48(2), 89–95. <https://doi.org/10.1007/S12013-007-0025-6>
- Benita, Y., Kikuchi, H., Smith, A. D., Zhang, M. Q., Chung, D. C., & Xavier, R. J. (2009). An integrative genomics approach identifies Hypoxia Inducible Factor-1 (HIF-1)-target genes that form the core response to hypoxia. *Nucleic Acids Research*, 37(14), 4587. <https://doi.org/10.1093/NAR/GKP425>
- Bensaad, K., Favaro, E., Lewis, C. A., Peck, B., Lord, S., Collins, J. M., Pinnick, K. E., Wigfield, S., Buffa, F. M., Li, J. L., Zhang, Q., Wakelam, M. J. O., Karpe, F., Schulze, A., & Harris, A. L. (2014). Fatty acid uptake and lipid storage induced by HIF-1 α contribute to cell growth and survival after hypoxia-reoxygenation. *Cell Reports*, 9(1), 349–365. <https://doi.org/10.1016/J.CELREP.2014.08.056>
- Bensaad, K., Tsuruta, A., Selak, M. A., Vidal, M. N. C., Nakano, K., Bartrons, R., Gottlieb, E., & Vousden, K. H. (2006). TIGAR, a p53-Inducible Regulator of Glycolysis and Apoptosis. *Cell*, 126(1), 107–120. <https://doi.org/10.1016/J.CELL.2006.05.036>
- Ben-Sahra, I., Hoxhaj, G., Ricoult, S. J. H., Asara, J. M., & Manning, B. D. (2016). mTORC1 induces purine synthesis through control of the mitochondrial tetrahydrofolate cycle. *Science*, 351(6274), 728–733. https://doi.org/10.1126/SCIENCE.AAD0489/SUPPL_FILE/BEN-SAHRA-SM.PDF
- Berendsen, H. J. C., van der Spoel, D., & van Drunen, R. (1995). GROMACS: A message-passing parallel molecular dynamics implementation. *Computer Physics Communications*, 91(1–3), 43–56. [https://doi.org/10.1016/0010-4655\(95\)00042-E](https://doi.org/10.1016/0010-4655(95)00042-E)
- Bergeron, R., Ren, J. M., Cadman, K. S., Moore, I. K., Perret, P., Pypaert, M., Young, L. H., Semenkovich, C. F., & Shulman, G. I. (2001). Chronic activation of AMP kinase results in NRF-1 activation and mitochondrial

- biogenesis. *American Journal of Physiology - Endocrinology and Metabolism*, 281(6 44-6). <https://doi.org/10.1152/AJPENDO.2001.281.6.E1340/ASSET/IMAGES/LARGE/H11210624005.JPEG>
- Bergstrom, J., Furst, P., Noree, L. O., & Vinnars, E. (1974). Intracellular free amino acid concentration in human muscle tissue. *Journal of Applied Physiology*, 36(6), 693–697. <https://doi.org/10.1152/JAPPL.1974.36.6.693>
- Bernfeld, E., & Foster, D. A. (2019). Glutamine as an Essential Amino Acid for KRas-Driven Cancer Cells. *Trends in Endocrinology & Metabolism*, 30(6), 357–368. <https://doi.org/10.1016/J.TEM.2019.03.003>
- Bhowmick, N. A., Neilson, E. G., & Moses, H. L. (2004). Stromal fibroblasts in cancer initiation and progression. *Nature 2004 432:7015*, 432(7015), 332–337. <https://doi.org/10.1038/nature03096>
- Birsoy, K., Wang, T., Chen, W. W., Freinkman, E., Abu-Remaileh, M., & Sabatini, D. M. (2015). An Essential Role of the Mitochondrial Electron Transport Chain in Cell Proliferation Is to Enable Aspartate Synthesis. *Cell*, 162(3), 540–551. <https://doi.org/10.1016/J.CELL.2015.07.016/ATTACHMENT/2B1F2CCC-E200-4EE9-9AE9-67168276839C/MMC2.XLSX>
- Bluemel, G., Planque, M., Madreiter-Sokolowski, C. T., Haitzmann, T., Hrzenjak, A., Graier, W. F., Fendt, S. M., Olschewski, H., & Leithner, K. (2021). PCK2 opposes mitochondrial respiration and maintains the redox balance in starved lung cancer cells. *Free Radical Biology and Medicine*, 176, 34–45. <https://doi.org/10.1016/J.FREERADBIOMED.2021.09.007>
- Bobrovnikova-Marjon, E., Hatzivassiliou, G., Grigoriadou, C., Romero, M., Cavener, D. R., Thompson, C. B., & Diehl, J. A. (2008). PERK-dependent regulation of lipogenesis during mouse mammary gland development and adipocyte differentiation. *Proceedings of the National Academy of Sciences of the United States of America*, 105(42), 16314. <https://doi.org/10.1073/PNAS.0808517105>
- Bogner, A. N., Stiers, K. M., & Tanner, J. J. (2021). Structure, biochemistry, and gene expression patterns of the proline biosynthetic enzyme pyrroline-5-carboxylate reductase (PYCR), an emerging cancer therapy target. *Amino Acids*, 53(12), 1817–1834. <https://doi.org/10.1007/S00726-021-02999-5/FIGURES/8>
- Bogner, A. N., & Tanner, J. J. (2022). Structure-affinity relationships of reversible proline analog inhibitors targeting proline dehydrogenase. *Organic & Biomolecular Chemistry*, 20(4), 895–905. <https://doi.org/10.1039/D1OB02328D>
- Bol, D. K., Kiguchi, K., Gimenez-Conti, I., Rupp, T., & DiGiovanni, J. (1997). Overexpression of insulin-like growth factor-1 induces hyperplasia, dermal abnormalities, and spontaneous tumor formation in transgenic mice. *Oncogene*, 14(14), 1725–1734. <https://doi.org/10.1038/SJ.ONC.1201011>
- Boppana, K., Dubey, P. K., Jagarlapudi, S. A. R. P., Vadivelan, S., & Rambabu, G. (2009). Knowledge based identification of MAO-B selective inhibitors using pharmacophore and structure based virtual screening models. *European Journal of Medicinal Chemistry*, 44(9), 3584–3590. <https://doi.org/10.1016/J.EJMECH.2009.02.031>
- Brand, A., Singer, K., Koehl, G. E., Kolitzus, M., Schoenhammer, G., Thiel, A., Matos, C., Bruss, C., Klobuch, S., Peter, K., Kastenberger, M., Bogdan, C., Schleicher, U., Mackensen, A., Ullrich, E., Fichtner-Feigl, S., Kesselring, R., Mack, M., Ritter, U., ... Kreutz, M. (2016). LDHA-Associated Lactic Acid Production Blunts Tumor Immunosurveillance by T and NK Cells. *Cell Metabolism*, 24(5), 657–671. <https://doi.org/10.1016/J.CMET.2016.08.011/ATTACHMENT/A877E863-62A2-4546-94FD-5391EBA12BF8/MMC1.PDF>

- Brand, K. A., & Hermfisse, U. (1997). Aerobic glycolysis by proliferating cells: a protective strategy against reactive oxygen species1. *The FASEB Journal*, *11*(5), 388–395. <https://doi.org/10.1096/FASEBJ.11.5.9141507>
- Brearley, M. C., Daniel, Z. C. T. R., Loughna, P. T., Parr, T., & Brameld, J. M. (2020). The phosphoenolpyruvate carboxykinase (PEPCK) inhibitor, 3-mercaptopicolinic acid (3-MPA), induces myogenic differentiation in C2C12 cells. *Scientific Reports 2020 10:1*, *10*(1), 1–10. <https://doi.org/10.1038/s41598-020-79324-9>
- Brooks, B. R., Brooks, C. L., Mackerell, A. D., Nilsson, L., Petrella, R. J., Roux, B., Won, Y., Archontis, G., Bartels, C., Boresch, S., Caflisch, A., Caves, L., Cui, Q., Dinner, A. R., Feig, M., Fischer, S., Gao, J., Hodoscek, M., Im, W., ... Karplus, M. (2009). CHARMM: The Biomolecular Simulation Program. *Journal of Computational Chemistry*, *30*(10), 1545. <https://doi.org/10.1002/JCC.21287>
- Brown, D. M., Williams, H., Ryan, K. J. P., Wilson, T. L., Daniel, Z. C. T. R., Mareko, M. H. D., Emes, R. D., Harris, D. W., Jones, S., Wattis, J. A. D., Dryden, I. L., Hodgman, T. C., Brameld, J. M., & Parr, T. (2016). Mitochondrial phosphoenolpyruvate carboxykinase (PEPCK-M) and serine biosynthetic pathway genes are co-ordinately increased during anabolic agent-induced skeletal muscle growth. *Scientific Reports 2016 6:1*, *6*(1), 1–14. <https://doi.org/10.1038/srep28693>
- Burgess, S. C., Hausler, N., Merritt, M., Jeffrey, F. M. H., Storey, C., Milde, A., Koshy, S., Lindner, J., Magnuson, M. A., Malloy, C. R., & Sherry, A. D. (2004). Impaired Tricarboxylic Acid Cycle Activity in Mouse Livers Lacking Cytosolic Phosphoenolpyruvate Carboxykinase. *Journal of Biological Chemistry*, *279*(47), 48941–48949. <https://doi.org/10.1074/JBC.M407120200>
- Cai, F., Miao, Y., Liu, C., Wu, T., Shen, S., Su, X., & Shi, Y. (2018). Pyrroline-5-carboxylate reductase 1 promotes proliferation and inhibits apoptosis in non-small cell lung cancer. *Oncology Letters*, *15*(1), 731–740. <https://doi.org/10.3892/ol.2017.7400>
- Calvo, D., Gómez-Coronado, D., Suárez, Y., Lasunción, M. A., & Vega, M. A. (1998). Human CD36 is a high affinity receptor for the native lipoproteins HDL, LDL, and VLDL. *Journal of Lipid Research*, *39*(4), 777–788. [https://doi.org/10.1016/S0022-2275\(20\)32566-9](https://doi.org/10.1016/S0022-2275(20)32566-9)
- Cantley, L. C. (2002). The Phosphoinositide 3-Kinase Pathway. *Science*, *296*(5573), 1655–1657. <https://doi.org/10.1126/SCIENCE.296.5573.1655>
- Carling, D., Zammit, V. A., & Hardie, D. G. (1987). A common bicyclic protein kinase cascade inactivates the regulatory enzymes of fatty acid and cholesterol biosynthesis. *FEBS Letters*, *223*(2), 217–222. [https://doi.org/10.1016/0014-5793\(87\)80292-2](https://doi.org/10.1016/0014-5793(87)80292-2)
- Caro, P., Kishan, A. U., Norberg, E., Stanley, I. A., Chapuy, B., Ficarro, S. B., Polak, K., Tondera, D., Gounarides, J., Yin, H., Zhou, F., Green, M. R., Chen, L., Monti, S., Marto, J. A., Shipp, M. A., & Danial, N. N. (2012). Metabolic Signatures Uncover Distinct Targets in Molecular Subsets of Diffuse Large B Cell Lymphoma. *Cancer Cell*, *22*(4), 547–560. <https://doi.org/10.1016/J.CCR.2012.08.014/ATTACHMENT/6DF6AD2B-1FDF-4265-A315-08DE405519FA/MMC4.XLSX>
- Case, D. A., Cheatham, T. E., Darden, T., Gohlke, H., Luo, R., Merz, K. M., Onufriev, A., Simmerling, C., Wang, B., & Woods, R. J. (2005). The Amber biomolecular simulation programs. *Journal of Computational Chemistry*, *26*(16), 1668–1688. <https://doi.org/10.1002/JCC.20290>
- Cassim, S., & Pouyssegur, J. (2020). Tumor Microenvironment: A Metabolic Player that Shapes the Immune Response. *International Journal of Molecular Sciences*, *21*(1). <https://doi.org/10.3390/IJMS21010157>
- Chabner, B. A., & Roberts, T. G. (2005). Chemotherapy and the war on cancer. *Nature Reviews Cancer 2005 5:1*, *5*(1), 65–72. <https://doi.org/10.1038/NRC1529>

- Chaika, N. v., Yu, F., Purohit, V., Mehla, K., Lazenby, A. J., DiMaio, D., Anderson, J. M., Yeh, J. J., Johnson, K. R., Hollingsworth, M. A., & Singh, P. K. (2012). Differential Expression of Metabolic Genes in Tumor and Stromal Components of Primary and Metastatic Loci in Pancreatic Adenocarcinoma. *PLoS ONE*, *7*(3). <https://doi.org/10.1371/JOURNAL.PONE.0032996>
- Chakravarty, K., Wu, S. Y., Chiang, C. M., Samols, D., & Hanson, R. W. (2004). SREBP-1c and Sp1 interact to regulate transcription of the gene for phosphoenolpyruvate carboxykinase (GTP) in the liver. *The Journal of Biological Chemistry*, *279*(15), 15385–15395. <https://doi.org/10.1074/JBC.M309905200>
- Chalecka, M., Kazberuk, A., Palka, J., & Surazynski, A. (2021). P5C as an Interface of Proline Interconvertible Amino Acids and Its Role in Regulation of Cell Survival and Apoptosis. *International Journal of Molecular Sciences*, *22*(21), 11763. <https://doi.org/10.3390/IJMS222111763>
- Chaneton, B., & Gottlieb, E. (2012). PGAMgnam Style: A Glycolytic Switch Controls Biosynthesis. *Cancer Cell*, *22*(5), 565–566. <https://doi.org/10.1016/J.CCR.2012.10.014>
- Chaneton, B., Hillmann, P., Zheng, L., Martin, A. C. L., Maddocks, O. D. K., Chokkathukalam, A., Coyle, J. E., Jankevics, A., Holding, F. P., Vousden, K. H., Frezza, C., O'Reilly, M., & Gottlieb, E. (2012). Serine is a natural ligand and allosteric activator of pyruvate kinase M2. *Nature* *2012* *491*:7424, *491*(7424), 458–462. <https://doi.org/10.1038/NATURE11540>
- Chang, C. H., Qiu, J., O'Sullivan, D., Buck, M. D., Noguchi, T., Curtis, J. D., Chen, Q., Gindin, M., Gubin, M. M., van der Windt, G. J. W., Tonc, E., Schreiber, R. D., Pearce, E. J., & Pearce, E. L. (2015). Metabolic Competition in the Tumor Microenvironment Is a Driver of Cancer Progression. *Cell*, *162*(6), 1229–1241. <https://doi.org/10.1016/J.CELL.2015.08.016>
- Chang, H. C., & Lane, M. D. (1966). The Enzymatic Carboxylation of Phosphoenolpyruvate: II. PURIFICATION AND PROPERTIES OF LIVER MITOCHONDRIAL PHOSPHOENOLPYRUVATE CARBOXYKINASE. *Journal of Biological Chemistry*, *241*(10), 2413–2420. [https://doi.org/10.1016/S0021-9258\(18\)96635-4](https://doi.org/10.1016/S0021-9258(18)96635-4)
- Chen, E. I., Hewel, J., Krueger, J. S., Tiraby, C., Weber, M. R., Kralli, A., Becker, K., Yates, J. R., & Felding-Habermann, B. (2007). Adaptation of energy metabolism in breast cancer brain metastases. *Cancer Research*, *67*(4), 1472–1486. <https://doi.org/10.1158/0008-5472.CAN-06-3137>
- Chen, J. (2016). The Cell-Cycle Arrest and Apoptotic Functions of p53 in Tumor Initiation and Progression. *Cold Spring Harbor Perspectives in Medicine*, *6*(3), a026104. <https://doi.org/10.1101/CSHPERSPECT.A026104>
- Chen, J., Chung, F., Yang, G. G., Pu, M., Gao, H., Jiang, W., Yin, H., Capka, V., Kasibhatla, S., Laffitte, B., Jaeger, S., Pagliarini, R., Chen, Y., & Zhou, W. (2013). Phosphoglycerate dehydrogenase is dispensable for breast tumor maintenance and growth. *Oncotarget*, *4*(12), 2502–2511. <https://doi.org/10.18632/ONCOTARGET.1540>
- Chen, S., Yang, X., Yu, M., Wang, Z., Liu, B., Liu, M., Liu, L., Ren, M., Qi, H., Zou, J., Vucenik, I., Zhu, W. G., & Luo, J. (2019). SIRT3 regulates cancer cell proliferation through deacetylation of PYCR1 in proline metabolism. *Neoplasia*, *21*(7), 665–675. <https://doi.org/10.1016/J.NEO.2019.04.008>
- Chen, Z. H., Walker, R. P., Acheson, R. M., & Leegood, R. C. (2002). Phosphoenolpyruvate carboxykinase assayed at physiological concentrations of metal ions has a high affinity for CO₂. *Plant Physiology*, *128*(1), 160–164. <https://doi.org/10.1104/PP.010431>
- Chen, Z. P., Li, M., Zhang, L. J., He, J. Y., Wu, L., Xiao, Y. Y., Duan, J. A., Cai, T., & Li, W. D. (2015). Mitochondria-targeted drug delivery system for cancer treatment.

- [Http://Dx.Doi.Org/10.3109/1061186X.2015.1108325](http://Dx.Doi.Org/10.3109/1061186X.2015.1108325), 24(6), 492–502.
<https://doi.org/10.3109/1061186X.2015.1108325>
- Chiche, J., Reverso-Meinietti, J., Mouchotte, A., Rubio-Patiño, C., Mhaidly, R., Villa, E., Bossowski, J. P., Proics, E., Grima-Reyes, M., Paquet, A., Fragaki, K., Marchetti, S., Briere, J., Ambrosetti, D., Michiels, J. F., Molina, T. J., Copie-Bergman, C., Lehmann-Che, J., Peyrottes, I., ... Ricci, J. E. (2019). GAPDH Expression Predicts the Response to R-CHOP, the Tumor Metabolic Status, and the Response of DLBCL Patients to Metabolic Inhibitors. *Cell Metabolism*, 29(6), 1243-1257.e10. <https://doi.org/10.1016/J.CMET.2019.02.002/ATTACHMENT/C5988D2C-ABCE-4AD9-ABD5-3C925CC8771B/MMC2.XLSX>
- Chowdhury, R., Yeoh, K. K., Tian, Y. M., Hillringhaus, L., Bagg, E. A., Rose, N. R., Leung, I. K. H., Li, X. S., Woon, E. C. Y., Yang, M., McDonough, M. A., King, O. N., Clifton, I. J., Klose, R. J., Claridge, T. D. W., Ratcliffe, P. J., Schofield, C. J., & Kawamura, A. (2011). The oncometabolite 2-hydroxyglutarate inhibits histone lysine demethylases. *EMBO Reports*, 12(5), 463–469. <https://doi.org/10.1038/EMBOR.2011.43>
- Christensen, E. M., Bogner, A. N., Vandekerke, A., Tam, G. S., Patel, S. M., Becker, D. F., Fendt, S.-M., & Tanner, J. J. (2020). *In Crystallo* Screening for Proline Analog Inhibitors of the Proline Cycle Enzyme PYCR1. *Journal of Biological Chemistry*, jbc.RA120.016106. <https://doi.org/10.1074/jbc.RA120.016106>
- Christensen, E. M., Patel, S. M., Korasick, D. A., Campbell, A. C., Krause, K. L., Becker, D. F., & Tanner, J. J. (2017). Resolving the cofactor-binding site in the proline biosynthetic enzyme human pyrroline-5-carboxylate reductase 1. *Journal of Biological Chemistry*, 292(17), 7233–7243. <https://doi.org/10.1074/jbc.M117.780288>
- Chu, P. Y., Jiang, S. S., Shan, Y. S., Hung, W. C., Chen, M. H., Lin, H. Y., Chen, Y. L., Tsai, H. J., & Chen, L. T. (2017). Mitochondrial phosphoenolpyruvate carboxykinase (PEPCK-M) regulates the cell metabolism of pancreatic neuroendocrine tumors (pNET) and de-sensitizes pNET to mTOR inhibitors. *Oncotarget*, 8(61), 103613–103625. <https://doi.org/10.18632/ONCOTARGET.21665>
- Chun, S. Y., Johnson, C., Washburn, J. G., Cruz-Correa, M. R., Dang, D. T., & Dang, L. H. (2010). Oncogenic KRAS modulates mitochondrial metabolism in human colon cancer cells by inducing HIF-1 α and HIF-2 α target genes. *Molecular Cancer*, 9. <https://doi.org/10.1186/1476-4598-9-293>
- Colegio, O. R., Chu, N. Q., Szabo, A. L., Chu, T., Rhebergen, A. M., Jairam, V., Cyrus, N., Brokowski, C. E., Eisenbarth, S. C., Phillips, G. M., Cline, G. W., Phillips, A. J., & Medzhitov, R. (2014). Functional polarization of tumour-associated macrophages by tumour-derived lactic acid. *Nature* 2014 513:7519, 513(7519), 559–563. <https://doi.org/10.1038/NATURE13490>
- Commisso, C., Davidson, S. M., Soydaner-Azeloglu, R. G., Parker, S. J., Kamphorst, J. J., Hackett, S., Grabocka, E., Nofal, M., Drebin, J. A., Thompson, C. B., Rabinowitz, J. D., Metallo, C. M., vander Heiden, M. G., & Bar-Sagi, D. (2013). Macropinocytosis of protein is an amino acid supply route in Ras-transformed cells. *Nature* 2013 497:7451, 497(7451), 633–637. <https://doi.org/10.1038/NATURE12138>
- Cooper, G. M. (2000). *Cell Proliferation in Development and Differentiation*. <https://www.ncbi.nlm.nih.gov/books/NBK9906/>
- Cournia, Z., Allen, B., & Sherman, W. (2017). Relative Binding Free Energy Calculations in Drug Discovery: Recent Advances and Practical Considerations. *Journal of Chemical Information and Modeling*, 57(12), 2911–2937. <https://doi.org/10.1021/ACS.JCIM.7B00564>
- Craze, M. L., Cheung, H., Jewa, N., Coimbra, N. D. M., Soria, D., El-Ansari, R., Aleskandarany, M. A., Wai Cheng, K., Diez-Rodriguez, M., Nolan, C. C., Ellis, I. O., Rakha, E. A., & Green, A. R. (2017). MYC regulation of

- glutamine–proline regulatory axis is key in luminal B breast cancer. *British Journal of Cancer* 2018 118:2, 118(2), 258–265. <https://doi.org/10.1038/bjc.2017.387>
- Crouwel, F., Buitter, H. J. C., & de Boer, N. K. (2022). The thiopurine tale: an unexpected journey. *Journal of Crohn's & Colitis*. <https://doi.org/10.1093/ECCO-JCC/JJAC004>
- Cruz-Bermúdez, A., Laza-Briviesca, R., Vicente-Blanco, R. J., García-Grande, A., Coronado, M. J., Laine-Menéndez, S., Palacios-Zambrano, S., Moreno-Villa, M. R., Ruiz-Valdepeñas, A. M., Lendinez, C., Romero, A., Franco, F., Calvo, V., Alfaro, C., Acosta, P. M., Salas, C., Garcia, J. M., & Provencio, M. (2019). Cisplatin resistance involves a metabolic reprogramming through ROS and PGC-1 α in NSCLC which can be overcome by OXPHOS inhibition. *Free Radical Biology & Medicine*, 135, 167–181. <https://doi.org/10.1016/J.FREERADBIOMED.2019.03.009>
- Curto, M., Cole, B. K., Lallemand, D., Liu, C. H., & McClatchey, A. I. (2007). Contact-dependent inhibition of EGFR signaling by Nf2/Merlin. *Journal of Cell Biology*, 177(5), 893–903. <https://doi.org/10.1083/JCB.200703010>
- Cynober, L. A. (2002). Plasma amino acid levels with a note on membrane transport: characteristics, regulation, and metabolic significance. *Nutrition*, 18(9), 761–766. [https://doi.org/10.1016/S0899-9007\(02\)00780-3](https://doi.org/10.1016/S0899-9007(02)00780-3)
- Daidone, F., Florio, R., Rinaldo, S., Contestabile, R., di Salvo, M. L., Cutruzzolà, F., Bossa, F., & Paiardini, A. (2011). In silico and in vitro validation of serine hydroxymethyltransferase as a chemotherapeutic target of the antifolate drug pemetrexed. *European Journal of Medicinal Chemistry*, 46(5), 1616–1621. <https://doi.org/10.1016/J.EJMECH.2011.02.009>
- Daina, A., Michielin, O., & Zoete, V. (2017). SwissADME: a free web tool to evaluate pharmacokinetics, drug-likeness and medicinal chemistry friendliness of small molecules. *Scientific Reports*, 7. <https://doi.org/10.1038/SREP42717>
- Dalla Pozza, E., Dando, I., Pacchiana, R., Liboi, E., Scupoli, M. T., Donadelli, M., & Palmieri, M. (2020). Regulation of succinate dehydrogenase and role of succinate in cancer. *Seminars in Cell & Developmental Biology*, 98, 4–14. <https://doi.org/10.1016/J.SEMCDB.2019.04.013>
- Dang, L., Yen, K., & Attar, E. C. (2016). IDH mutations in cancer and progress toward development of targeted therapeutics. *Annals of Oncology*, 27(4), 599–608. <https://doi.org/10.1093/ANNONC/MDW013>
- D'aniello, C., Fico, A., Casalino, L., Guardiola, O., di Napoli, G., Cermola, F., de Cesare, D., Tatè, R., Cobellis, G., Patriarca, E. J., & Minchiotti, G. (2015). A novel autoregulatory loop between the Gcn2-Atf4 pathway and L-Proline metabolism controls stem cell identity. *Cell Death and Differentiation*, 22, 1094–1105. <https://doi.org/10.1038/cdd.2015.24>
- D'Aniello, C., Patriarca, E. J., Phang, J. M., & Minchiotti, G. (2020). Proline Metabolism in Tumor Growth and Metastatic Progression. *Frontiers in Oncology*, 10, 776. <https://doi.org/10.3389/fonc.2020.00776>
- Dayton, T. L., Jacks, T., & vander Heiden, M. G. (2016). PKM2, cancer metabolism, and the road ahead. *EMBO Reports*, 17(12), 1721–1730. <https://doi.org/10.15252/EMBR.201643300>
- de Ingeniis, J., Ratnikov, B., Richardson, A. D., Scott, D. A., Aza-Blanc, P., De, S. K., Kazanov, M., Pellicchia, M., Ronai, Z., Osterman, A. L., & Smith, J. W. (2012). Functional Specialization in Proline Biosynthesis of Melanoma. *PLOS ONE*, 7(9), e45190. <https://doi.org/10.1371/JOURNAL.PONE.0045190>
- de Vitto, H., Pérez-Valencia, J., & Radosevich, J. A. (2015). Glutamine at focus: versatile roles in cancer. *Tumor Biology* 2015 37:2, 37(2), 1541–1558. <https://doi.org/10.1007/S13277-015-4671-9>

- DeBerardinis, R. J., & Chandel, N. S. (2016). Fundamentals of cancer metabolism. *Science Advances*, 2(5). <https://doi.org/10.1126/SCIADV.1600200>
- Deberardinis, R. J., & Cheng, T. (2009). Q's next: the diverse functions of glutamine in metabolism, cell biology and cancer. *Oncogene* 29:3, 29(3), 313–324. <https://doi.org/10.1038/onc.2009.358>
- DeBerardinis, R. J., Lum, J. J., Hatzivassiliou, G., & Thompson, C. B. (2008). The Biology of Cancer: Metabolic Reprogramming Fuels Cell Growth and Proliferation. *Cell Metabolism*, 7(1), 11–20. <https://doi.org/10.1016/J.CMET.2007.10.002>
- DeBerardinis, R. J., Sayed, N., Ditsworth, D., & Thompson, C. B. (2008). Brick by brick: metabolism and tumor cell growth. *Current Opinion in Genetics & Development*, 18(1), 54. <https://doi.org/10.1016/J.GDE.2008.02.003>
- Dejure, F. R., & Eilers, M. (2017). MYC and tumor metabolism: chicken and egg. *The EMBO Journal*, 36(23), 3409–3420. <https://doi.org/10.15252/EMBJ.201796438>
- DeNicola, G. M., Chen, P. H., Mullarky, E., Sudderth, J. A., Hu, Z., Wu, D., Tang, H., Xie, Y., Asara, J. M., Huffman, K. E., Wistuba, I. I., Minna, J. D., DeBerardinis, R. J., & Cantley, L. C. (2015). NRF2 regulates serine biosynthesis in non-small cell lung cancer. *Nature Genetics* 2015 47:12, 47(12), 1475–1481. <https://doi.org/10.1038/NG.3421>
- Devine, J. H., Eubank, D. W., Clouthier, D. E., Tontonoz, P., Spiegelman, B. M., Hammer, R. E., & Beale, E. G. (1999). Adipose expression of the phosphoenolpyruvate carboxykinase promoter requires peroxisome proliferator-activated receptor gamma and 9-cis-retinoic acid receptor binding to an adipocyte-specific enhancer in vivo. *The Journal of Biological Chemistry*, 274(19), 13604–13612. <https://doi.org/10.1074/JBC.274.19.13604>
- Dick, F. A., & Rubin, S. M. (2013). Molecular mechanisms underlying RB protein function. *Nature Reviews Molecular Cell Biology* 2013 14:5, 14(5), 297–306. <https://doi.org/10.1038/NRM3567>
- Ding, J., Kuo, M. L., Su, L., Xue, L., Luh, F., Zhang, H., Wang, J., Lin, T. G., Zhang, K., Chu, P., Zheng, S., Liu, X., & Yen, Y. (2017). Human mitochondrial pyrroline-5-carboxylate reductase 1 promotes invasiveness and impacts survival in breast cancers. *Carcinogenesis*, 38(5), 519–531. <https://doi.org/10.1093/CARCIN/BGX022>
- Ding, Z., Ericksen, R. E., Escande-Beillard, N., Lee, Q. Y., Loh, A., Denil, S., Steckel, M., Haegebarth, A., Wai Ho, T. S., Chow, P., Toh, H. C., Reversade, B., Gruenewald, S., & Han, W. (2020). Metabolic pathway analyses identify proline biosynthesis pathway as a promoter of liver tumorigenesis. *Journal of Hepatology*, 72(4), 725–735. <https://doi.org/10.1016/J.JHEP.2019.10.026>
- DiTullio, N. W., Berkoff, C. E., Blank, B., Kostos, V., Stack, E. J., & Saunders, H. L. (1974). 3-Mercaptopicolinic acid, an inhibitor of gluconeogenesis. *Biochemical Journal*, 138(3), 387–394. <https://doi.org/10.1042/BJ1380387>
- Donald, S. P., Sun, X.-Y., Hu, C.-A. A., Yu, J., Mei, J. M., Valle, D., & Phang, J. M. (2001). Proline Oxidase, Encoded by p53-induced Gene-6, Catalyzes the Generation of Proline-dependent Reactive Oxygen Species. *CANCER RESEARCH*, 61, 1810–1815. <http://aacrjournals.org/cancerres/article-pdf/61/5/1810/2492617/ch050101810.pdf>
- Doubleday, P. F., Fornelli, L., Ntai, I., & Kelleher, N. L. (2021). Oncogenic KRAS creates an aspartate metabolism signature in colorectal cancer cells. *The FEBS Journal*, 288(23), 6683–6699. <https://doi.org/10.1111/FEBS.16111>

- Drahota, Z., Rauchová, H., Miková, M., Kaul, P., & Bass, A. (1983). Phosphoenolpyruvate shuttle--transport of energy from mitochondria to cytosol. *FEBS Letters*, *157*(2), 347–349. [https://doi.org/10.1016/0014-5793\(83\)80573-0](https://doi.org/10.1016/0014-5793(83)80573-0)
- Du, S., Sui, Y., Ren, W., Zhou, J., & Du, C. (2021). PYCR1 promotes bladder cancer by affecting the Akt/Wnt/ β -catenin signaling. *Journal of Bioenergetics and Biomembranes*, *53*(2), 247–258. <https://doi.org/10.1007/S10863-021-09887-3/FIGURES/7>
- Du, X., Li, Y., Xia, Y. L., Ai, S. M., Liang, J., Sang, P., Ji, X. L., & Liu, S. Q. (2016). Insights into Protein–Ligand Interactions: Mechanisms, Models, and Methods. *International Journal of Molecular Sciences*, *17*(2). <https://doi.org/10.3390/IJMS17020144>
- Durgan, J., & Florey, O. (2018). Cancer cell cannibalism: Multiple triggers emerge for entosis. *Biochimica et Biophysica Acta. Molecular Cell Research*, *1865*(6), 831–841. <https://doi.org/10.1016/J.BBAMCR.2018.03.004>
- E. Costa, R. K., Rodrigues, C. T., H. Campos, J. C., Paradela, L. S., Dias, M. M., Novaes da Silva, B., de Valega Negrao, C. von Z., Gonçalves, K. de A., Ascensão, C. F. R., Adamoski, D., Mercaldi, G. F., Bastos, A. C. S., Batista, F. A. H., Figueira, A. C., Cordeiro, A. T., Ambrosio, A. L. B., Guido, R. V. C., & Dias, S. M. G. (2021). High-Throughput Screening Reveals New Glutaminase Inhibitor Molecules. *ACS Pharmacology & Translational Science*, *4*(6), 1849–1866. https://doi.org/10.1021/ACSPTSCI.1C00226/SUPPL_FILE/PT1C00226_SI_002.XLSX
- Ebert, B. L., Firth, J. D., & Ratcliffe, P. J. (1995). Hypoxia and Mitochondrial Inhibitors Regulate Expression of Glucose Transporter-1 via Distinct Cis-acting Sequences (*). *Journal of Biological Chemistry*, *270*(49), 29083–29089. <https://doi.org/10.1074/JBC.270.49.29083>
- Eggleston, L. v., & Krebs, H. A. (1974). Regulation of the pentose phosphate cycle. *Biochemical Journal*, *138*(3), 425. <https://doi.org/10.1042/BJ1380425>
- Elia, I., Broekaert, D., Christen, S., Boon, R., Radaelli, E., Orth, M. F., Verfaillie, C., Grünewald, T. G. P., & Fendt, S. M. (2017). Proline metabolism supports metastasis formation and could be inhibited to selectively target metastasizing cancer cells. *Nature Communications* 2017 8:1, *8*(1), 1–11. <https://doi.org/10.1038/NCOMMS15267>
- Elinav, E., Nowarski, R., Thaïss, C. A., Hu, B., Jin, C., & Flavell, R. A. (2013). Inflammation-induced cancer: crosstalk between tumours, immune cells and microorganisms. *Nature Reviews Cancer* 2013 13:11, *13*(11), 759–771. <https://doi.org/10.1038/NRC3611>
- Elion, G. B. (1989). The Purine Path to Chemotherapy. *Science*, *244*(4900), 41–47. <https://doi.org/10.1126/SCIENCE.2649979>
- Elstrom, R. L., Bauer, D. E., Buzzai, M., Karnauskas, R., Harris, M. H., Plas, D. R., Zhuang, H., Cinalli, R. M., Alavi, A., Rudin, C. M., & Thompson, C. B. (2004). Akt Stimulates Aerobic Glycolysis in Cancer Cells. *Cancer Research*, *64*(11), 3892–3899. <https://doi.org/10.1158/0008-5472.CAN-03-2904>
- Englebienne, P., & Moitessier, N. (2009). Docking ligands into flexible and solvated macromolecules. 5. Force-field-based prediction of binding affinities of ligands to proteins. *Journal of Chemical Information and Modeling*, *49*(11), 2564–2571. <https://doi.org/10.1021/CI900251K>
- Escande-Beillard, N., Loh, A., Saleem, S. N., Kanata, K., Hashimoto, Y., Altunoglu, U., Metoska, A., Grandjean, J., Ng, F. M., Pomp, O., Baburajendran, N., Wong, J., Hill, J., Beillard, E., Cozzone, P., Zaki, M., Kayserili, H., Hamada, H., Shiratori, H., & Reversade, B. (2020). Loss of PYCR2 Causes Neurodegeneration by

- Increasing Cerebral Glycine Levels via SHMT2. *Neuron*, 107(1), 82-94.e6. <https://doi.org/10.1016/J.NEURON.2020.03.028>
- Escós, M., Latorre, P., Hidalgo, J., Hurtado-Guerrero, R., Carrodeguas, J. A., & López-Buesa, P. (2016a). Kinetic and functional properties of human mitochondrial phosphoenolpyruvate carboxykinase. *Biochemistry and Biophysics Reports*, 7, 124–129. <https://doi.org/10.1016/J.BBREP.2016.06.007>
- Escós, M., Latorre, P., Hidalgo, J., Hurtado-Guerrero, R., Carrodeguas, J. A., & López-Buesa, P. (2016b). Kinetic and functional properties of human mitochondrial phosphoenolpyruvate carboxykinase. *Biochemistry and Biophysics Reports*, 7, 124–129. <https://doi.org/10.1016/j.bbrep.2016.06.007>
- Esteller, M. (2009). Epigenetics in Cancer. [Http://Dx.Doi.Org.Sire.Ub.Edu/10.1056/NEJMra072067](http://Dx.Doi.Org.Sire.Ub.Edu/10.1056/NEJMra072067), 358(11), 1148–1159. <https://doi.org/10.1056/NEJMRA072067>
- Fan, J., Kamphorst, J. J., Mathew, R., Chung, M. K., White, E., Shlomi, T., & Rabinowitz, J. D. (2013). Glutamine-driven oxidative phosphorylation is a major ATP source in transformed mammalian cells in both normoxia and hypoxia. *Molecular Systems Biology*, 9(1), 712. <https://doi.org/10.1038/MSB.2013.65>
- Fang, E., Wang, X., Yang, F., Hu, A., Wang, J., Li, D., Song, H., Hong, M., Guo, Y., Liu, Y., Li, H., Huang, K., Zheng, L., Tong, Q., Fang, E., Yang, F., Hu, A., Wang, J., Li, D., ... Li, H. (2019). Therapeutic Targeting of MZF1-AS1/PARP1/E2F1 Axis Inhibits Proline Synthesis and Neuroblastoma Progression. *Advanced Science*, 6(19), 1900581. <https://doi.org/10.1002/ADVS.201900581>
- Fares, J., Fares, M. Y., Khachfe, H. H., Salhab, H. A., & Fares, Y. (2020). Molecular principles of metastasis: a hallmark of cancer revisited. *Signal Transduction and Targeted Therapy* 2020 5:1, 5(1), 1–17. <https://doi.org/10.1038/s41392-020-0134-x>
- Farrell, A. S., & Sears, R. C. (2014). MYC Degradation. *Cold Spring Harbor Perspectives in Medicine*, 4(3), a014365. <https://doi.org/10.1101/CSHPERSPECT.A014365>
- Faubert, B., Li, K. Y., Cai, L., Young, J. D., Kernstine, K., & Deberardinis Correspondence, R. J. (2017). Lactate Metabolism in Human Lung Tumors. *Cell*, 171, 358–371. <https://doi.org/10.1016/j.cell.2017.09.019>
- Favia, A. D. (2011). Theoretical and computational approaches to ligand-based drug discovery. *Frontiers in Bioscience (Landmark Edition)*, 16(4), 1276–1290. <https://doi.org/10.2741/3788>
- Femi-Olabisi, F. J., Ishola, A. A., Faokunla, O., Agboola, A. O., & Babalola, B. A. (2021). Evaluation of the inhibitory potentials of selected compounds from *Costus spicatus* (Jacq.) rhizome towards enzymes associated with insulin resistance in polycystic ovarian syndrome: an in silico study. *Journal of Genetic Engineering & Biotechnology*, 19(1), 176. <https://doi.org/10.1186/S43141-021-00276-2>
- Ferlay, J., Colombet, M., Soerjomataram, I., Dyba, T., Randi, G., Bettio, M., Gavin, A., Visser, O., & Bray, F. (2018). Cancer incidence and mortality patterns in Europe: Estimates for 40 countries and 25 major cancers in 2018. *European Journal of Cancer*, 103, 356–387. <https://doi.org/10.1016/J.EJCA.2018.07.005>
- Ferlay, J., Ervik, M., Lam, F., Colombet, M., Mery, L., & Piñeros, M. (2020). *Global Cancer Observatory: Cancer Today*. International Agency for Research on Cancer. <https://gco.iarc.fr/today>
- Fernández-Coto, D. L., Gil, J., Hernández, A., Herrera-Goepfert, R., Castro-Romero, I., Hernández-Márquez, E., Arenas-Linares, A. S., Calderon-Sosa, V. T., Sanchez-Aleman, M. Á., Mendez-Tenorio, A., Encarnación-Guevara, S., & Ayala, G. (2018a). Quantitative proteomics reveals proteins involved in the progression from non-cancerous lesions to gastric cancer. *Journal of Proteomics*, 186, 15–27. <https://doi.org/10.1016/J.JPROT.2018.07.013>

- Fernández-Coto, D. L., Gil, J., Hernández, A., Herrera-Goepfert, R., Castro-Romero, I., Hernández-Márquez, E., Arenas-Linares, A. S., Calderon-Sosa, V. T., Sanchez-Aleman, M. Á., Mendez-Tenorio, A., Encarnación-Guevara, S., & Ayala, G. (2018b). Quantitative proteomics reveals proteins involved in the progression from non-cancerous lesions to gastric cancer. *Journal of Proteomics*, *186*, 15–27. <https://doi.org/10.1016/J.JPROT.2018.07.013>
- Fernandez-Ruiz, R., García-Alamán, A., Esteban, Y., Mir-Coll, J., Serra-Navarro, B., Fontcuberta-PiSunyer, M., Broca, C., Armanet, M., Wojtuszczyński, A., Kram, V., Young, M. F., Vidal, J., Gomis, R., & Gasa, R. (2020). Wisp1 is a circulating factor that stimulates proliferation of adult mouse and human beta cells. *Nature Communications*, *11*(1). <https://doi.org/10.1038/s41467-020-19657-1>
- Feron, O. (2009). Pyruvate into lactate and back: From the Warburg effect to symbiotic energy fuel exchange in cancer cells. *Radiotherapy and Oncology*, *92*(3), 329–333. <https://doi.org/10.1016/J.RADONC.2009.06.025>
- Ferrara, N. (2009). Vascular endothelial growth factor. *Arteriosclerosis, Thrombosis, and Vascular Biology*, *29*(6), 789–791. <https://doi.org/10.1161/ATVBAHA.108.179663>
- Ferreira, L. G., dos Santos, R. N., Oliva, G., & Andricopulo, A. D. (2015). Molecular Docking and Structure-Based Drug Design Strategies. *Molecules*, *20*(7), 13384. <https://doi.org/10.3390/MOLECULES200713384>
- Ferrer, M., Chernikova, T. N., Yakimov, M. M., Golyshin, P. N., & Timmis, K. N. (2003). Chaperonins govern growth of *Escherichia coli* at low temperatures. *Nature Biotechnology* *2003* *21*:11, *21*(11), 1266–1267. <https://doi.org/10.1038/NBT1103-1266>
- Foley, L. H., Wang, P., Dunten, P., Ramsey, G., Gubler, M. lou, & Wertheimer, S. J. (2003a). Modified 3-Alkyl-1,8-dibenzylxanthines as GTP-Competitive inhibitors of phosphoenolpyruvate carboxykinase. *Bioorganic & Medicinal Chemistry Letters*, *13*(20), 3607–3610. [https://doi.org/10.1016/S0960-894X\(03\)00722-4](https://doi.org/10.1016/S0960-894X(03)00722-4)
- Foley, L. H., Wang, P., Dunten, P., Ramsey, G., Gubler, M. lou, & Wertheimer, S. J. (2003b). X-ray Structures of two xanthine inhibitors bound to PEPCK and N-3 modifications of substituted 1,8-Dibenzylxanthines. *Bioorganic & Medicinal Chemistry Letters*, *13*(21), 3871–3874. [https://doi.org/10.1016/S0960-894X\(03\)00723-6](https://doi.org/10.1016/S0960-894X(03)00723-6)
- Forlani, G., Berlicki, Ł., Duò, M., Dzièdziola, G., Giberti, S., Bertazzini, M., & Kafarski, P. (2013). Synthesis and Evaluation of Effective Inhibitors of Plant δ 1-Pyrroline-5-carboxylate Reductase. *Journal of Agricultural and Food Chemistry*, *61*(28), 6792–6798. <https://doi.org/10.1021/JF401234S>
- Forlani, G., Giberti, S., Berlicki, Ł., Petrollino, D., & Kafarski, P. (2007). Plant P5C Reductase as a New Target for Aminomethylenebisphosphonates. *Journal of Agricultural and Food Chemistry*, *55*(11), 4340–4347. <https://doi.org/10.1021/JF0701032>
- Forlani, G., Occhipinti, A., Berlicki, Ł., Dzièdziola, G., Wieczorek, A., & Kafarski, P. (2008). Tailoring the structure of aminobisphosphonates to target plant P5C reductase. *Journal of Agricultural and Food Chemistry*, *56*(9), 3193–3199. https://doi.org/10.1021/JF800029T/SUPPL_FILE/JF800029T-FILE002.PDF
- Forlani, G., Sabbioni, G., Ragno, D., Petrollino, D., & Borgatti, M. (2021). Phenyl-substituted aminomethylenebisphosphonates inhibit human P5C reductase and show antiproliferative activity against proline-hyperproducing tumour cells. *Journal of Enzyme Inhibition and Medicinal Chemistry*, *36*(1), 1248–1257. <https://doi.org/10.1080/14756366.2021.1919890>

- Fos, B., Gurney, A. L., Park, E. A., Giralt, M., Liu, J., & Hanson, R. W. (1992). Opposing Actions of Fos and Jun on Transcription of the Phosphoenolpyruvate Carboxykinase (GTP) Gene DOMINANT NEGATIVE REGULATION. *Journal of Biological Chemistry*, *267*(25), 18133–18139. [https://doi.org/10.1016/S0021-9258\(19\)37163-7](https://doi.org/10.1016/S0021-9258(19)37163-7)
- Foster, J. D., Bode, A. M., & Nordlie, R. C. (1994). Time-dependent inhibition of glucose 6-phosphatase by 3-mercaptopicolinic acid. *Biochimica et Biophysica Acta (BBA) - Protein Structure and Molecular Enzymology*, *1208*(2), 222–228. [https://doi.org/10.1016/0167-4838\(94\)90107-4](https://doi.org/10.1016/0167-4838(94)90107-4)
- Fox, S., Farr-Jones, S., Sopchak, L., Boggs, A., Nicely, H. W., Khoury, R., & Biro, M. (2006). High-throughput screening: Update on practices and success. *Journal of Biomolecular Screening*, *11*(7), 864–869. <https://doi.org/10.1177/1087057106292473>
- Franckhauser, S., Muñoz, S., Elias, I., Ferre, T., & Bosch, F. (2006). Adipose Overexpression of Phosphoenolpyruvate Carboxykinase Leads to High Susceptibility to Diet-Induced Insulin Resistance and Obesity. *Diabetes*, *55*(2), 273–280. <https://doi.org/10.2337/DIABETES.55.02.06.DB05-0482>
- Franckhauser, S., Muñoz, S., Pujol, A., Casellas, A., Riu, E., Otaegui, P., Su, B., & Bosch, F. (2002). Increased Fatty Acid Re-esterification by PEPCK Overexpression in Adipose Tissue Leads to Obesity Without Insulin Resistance. *Diabetes*, *51*(3), 624–630. <https://doi.org/10.2337/DIABETES.51.3.624>
- Franklin, D. A., He, Y., Leslie, P. L., Tikunov, A. P., Fenger, N., MacDonald, J. M., & Zhang, Y. (2016). p53 coordinates DNA repair with nucleotide synthesis by suppressing PFKFB3 expression and promoting the pentose phosphate pathway. *Scientific Reports 2016* *6*:1, 6(1), 1–13. <https://doi.org/10.1038/srep38067>
- Freitas, J. T., Jozic, I., & Bedogni, B. (2021). Wound Healing Assay for Melanoma Cell Migration. *Methods in Molecular Biology*, *2265*, 65–71. https://doi.org/10.1007/978-1-0716-1205-7_4
- Friesner, R. A., Murphy, R. B., Repasky, M. P., Frye, L. L., Greenwood, J. R., Halgren, T. A., Sanschagrin, P. C., & Mainz, D. T. (2006). Extra precision glide: Docking and scoring incorporating a model of hydrophobic enclosure for protein-ligand complexes. *Journal of Medicinal Chemistry*, *49*(21), 6177–6196. https://doi.org/10.1021/JM051256O/SUPPL_FILE/JM051256OSI20060602_023733.PDF
- Fritz, V., & Fajas, L. (2010). Metabolism and proliferation share common regulatory pathways in cancer cells. *Oncogene 2010* *29*:31, 29(31), 4369–4377. <https://doi.org/10.1038/onc.2010.182>
- Fulda, S. (2009). Tumor resistance to apoptosis. *International Journal of Cancer*, *124*(3), 511–515. <https://doi.org/10.1002/IJC.24064>
- Gamble, J. L., & Mazur, J. A. (1967). Intramitochondrial Metabolism of Phosphoenolpyruvate. *THE JOURNAL OF BIOLOGICAL CHEMISTRY*, *242*(1), 67–72. [https://doi.org/10.1016/S0021-9258\(18\)96319-2](https://doi.org/10.1016/S0021-9258(18)96319-2)
- Ganesh, K., & Massagué, J. (2021). Targeting metastatic cancer. *Nature Medicine 2021* *27*:1, 27(1), 34–44. <https://doi.org/10.1038/S41591-020-01195-4>
- Gao, Y., Luo, L., Xie, Y., Zhao, Y., Yao, J., & Liu, X. (2020). PYCR1 knockdown inhibits the proliferation, migration, and invasion by affecting JAK/STAT signaling pathway in lung adenocarcinoma. *Molecular Carcinogenesis*, *59*(5), 503–511. <https://doi.org/10.1002/MC.23174>
- Garanina, A. S., Kisurina-Evgenieva, O. P., Erokhina, M. v., Smirnova, E. A., Factor, V. M., & Onishchenko, G. E. (2017). Consecutive entosis stages in human substrate-dependent cultured cells. *Scientific Reports 2017* *7*:1, 7(1), 1–12. <https://doi.org/10.1038/s41598-017-12867-6>

- Geng, P., Qin, W., & Xu, G. (2021). Proline metabolism in cancer. *Amino Acids*, 53(12), 1769–1777. <https://doi.org/10.1007/S00726-021-03060-1/FIGURES/3>
- George, K. S., & Wu, S. (2012). Lipid Raft: A Floating Island Of Death or Survival. *Toxicology and Applied Pharmacology*, 259(3), 311. <https://doi.org/10.1016/J.TAAP.2012.01.007>
- Gilkes, D. M., Chaturvedi, P., Bajpai, S., Wong, C. C., Wei, H., Pitcairn, S., Hubbi, M. E., Wirtz, D., & Semenza, G. L. (2013). Collagen Prolyl Hydroxylases Are Essential for Breast Cancer Metastasis. *Cancer Research*, 73(11), 3285–3296. <https://doi.org/10.1158/0008-5472.CAN-12-3963>
- Gimeno, A., Ojeda-Montes, M. J., Tomás-Hernández, S., Cereto-Massagué, A., Beltrán-Debón, R., Mulero, M., Pujadas, G., & Garcia-Vallvé, S. (2019). The Light and Dark Sides of Virtual Screening: What Is There to Know? *International Journal of Molecular Sciences* 2019, Vol. 20, Page 1375, 20(6), 1375. <https://doi.org/10.3390/IJMS20061375>
- Gnaiger, E., & MitoEAGLE Task Group. (2020). Mitochondrial physiology. *Bioenergetics Communications*, 2020(1), 1–1. <https://doi.org/10.26124/BEC:2020-0001.V1>
- Goetzman, E. S., & Prochownik, E. v. (2018). The role for myc in coordinating glycolysis, oxidative phosphorylation, glutaminolysis, and fatty acid metabolism in normal and neoplastic tissues. *Frontiers in Endocrinology*, 9(APR), 129. <https://doi.org/10.3389/FENDO.2018.00129/BIBTEX>
- Gohlke, H., Hendlich, M., & Klebe, G. (2000). Knowledge-based scoring function to predict protein-ligand interactions. *Journal of Molecular Biology*, 295(2), 337–356. <https://doi.org/10.1006/JMBI.1999.3371>
- Gómez-Valadés, A. G., Méndez-Lucas, A., Vidal-Alabro, A., Blasco, F. X., Chillón, M., Bartrons, R., Bermúdez, J., & Perales, J. C. (2008). Pck1 gene silencing in the liver improves glycemia control, insulin sensitivity, and dyslipidemia in db/db mice. *Diabetes*, 57(8), 2199–2210. <https://doi.org/10.2337/DB07-1087>
- Goodsell, D. S., & Olson, A. J. (1990). Automated docking of substrates to proteins by simulated annealing. *Proteins: Structure, Function, and Bioinformatics*, 8(3), 195–202. <https://doi.org/10.1002/PROT.340080302>
- Grabiner, B. C., Nardi, V., Birsoy, K., Possemato, R., Shen, K., Sinha, S., Jordan, A., Beck, A. H., & Sabatini, D. M. (2014). A diverse array of cancer-associated MTOR mutations are hyperactivating and can predict rapamycin sensitivity. *Cancer Discovery*, 4(5), 554–563. <https://doi.org/10.1158/2159-8290.CD-13-0929>
- Grasmann, G., Smolle, E., Olschewski, H., & Leithner, K. (2019). Gluconeogenesis in cancer cells – Repurposing of a starvation-induced metabolic pathway? In *Biochimica et Biophysica Acta - Reviews on Cancer* (Vol. 1872, Issue 1, pp. 24–36). Elsevier B.V. <https://doi.org/10.1016/j.bbcan.2019.05.006>
- Gravel, S. P., Hulea, L., Toban, N., Birman, E., Blouin, M. J., Zakikhani, M., Zhao, Y., Topisirovic, I., St-Pierre, J., & Pollak, M. (2014). Serine Deprivation Enhances Antineoplastic Activity of Biguanides. *Cancer Research*, 74(24), 7521–7533. <https://doi.org/10.1158/0008-5472.CAN-14-2643-T>
- Greger, V., Passarge, E., Höpping, W., Messmer, E., & Horsthemke, B. (1989). Epigenetic changes may contribute to the formation and spontaneous regression of retinoblastoma. *Human Genetics*, 83(2), 155–158. <https://doi.org/10.1007/BF00286709>
- Gross, M. I., Demo, S. D., Dennison, J. B., Chen, L., Chernov-Rogan, T., Goyal, B., Janes, J. R., Laidig, G. J., Lewis, E. R., Li, J., MacKinnon, A. L., Parlati, F., Rodriguez, M. L. M., Shwonek, P. J., Sjogren, E. B., Stanton, T. F., Wang, T., Yang, J., Zhao, F., & Bennett, M. K. (2014). Antitumor Activity of the Glutaminase Inhibitor CB-

- 839 in Triple-Negative Breast Cancer. *Molecular Cancer Therapeutics*, 13(4), 890–901. <https://doi.org/10.1158/1535-7163.MCT-13-0870>
- Gu, Y., Zhang, J., Ma, X., Kim, B. wook, Wang, H., Li, J., Pan, Y., Xu, Y., Ding, L., Yang, L., Guo, C., Wu, X., Wu, J., Wu, K., Gan, X., Li, G., Li, L., Forman, S. J., Chan, W. C., ... Huang, W. (2017). Stabilization of the c-Myc Protein by CAMKII γ Promotes T Cell Lymphoma. *Cancer Cell*, 32(1), 115-128.e7. <https://doi.org/10.1016/J.CCELL.2017.06.001>
- Gui, D. Y., Sullivan, L. B., Luengo, A., Hosios, A. M., Bush, L. N., Gitego, N., Davidson, S. M., Freinkman, E., Thomas, C. J., & vander Heiden, M. G. (2016). Environment Dictates Dependence on Mitochondrial Complex I for NAD⁺ and Aspartate Production and Determines Cancer Cell Sensitivity to Metformin. *Cell Metabolism*, 24(5), 716–727. <https://doi.org/10.1016/J.CMET.2016.09.006/ATTACHMENT/0705F8AD-3E01-491E-97DE-EA0D25A8D354/MMC1.PDF>
- Guillaumond, F., Leca, J., Olivares, O., Lavaut, M. N., Vidal, N., Berthezène, P., Dusetti, N. J., Loncle, C., Calvo, E., Turrini, O., Iovanna, J. L., Tomasini, R., & Vasseur, S. (2013). Strengthened glycolysis under hypoxia supports tumor symbiosis and hexosamine biosynthesis in pancreatic adenocarcinoma. *Proceedings of the National Academy of Sciences of the United States of America*, 110(10), 3919–3924. <https://doi.org/10.1073/PNAS.1219555110/-/DCSUPPLEMENTAL>
- Guo, L., Cui, C., Wang, J., Yuan, J., Yang, Q., Zhang, P., Su, W., Bao, R., Ran, J., & Wu, C. (2020). PINCH-1 regulates mitochondrial dynamics to promote proline synthesis and tumor growth. *Nature Communications* 2020 11:1, 11(1), 1–20. <https://doi.org/10.1038/S41467-020-18753-6>
- Guo, L., Cui, C., Zhang, K., Wang, J., Wang, Y., Lu, Y., Chen, K., Yuan, J., Xiao, G., Tang, B., Sun, Y., & Wu, C. (2019). Kindlin-2 links mechano-environment to proline synthesis and tumor growth. *Nature Communications* 2019 10:1, 10(1), 1–20. <https://doi.org/10.1038/S41467-019-08772-3>
- Hakimi, P., Johnson, M. T., Yang, J., Lepage, D. F., Conlon, R. A., Kalhan, S. C., Reshef, L., Tilghman, S. M., & Hanson, R. W. (2005). Phosphoenolpyruvate carboxykinase and the critical role of cataplerosis in the control of hepatic metabolism. *Nutrition & Metabolism*, 2, 33. <https://doi.org/10.1186/1743-7075-2-33>
- Hall, R. K., Scott, D. K., Noisin, E. L., Lucas, P. C., & Granner, D. K. (1992). Activation of the phosphoenolpyruvate carboxykinase gene retinoic acid response element is dependent on a retinoic acid receptor/coregulator complex. *Molecular and Cellular Biology*, 12(12), 5527–5535. <https://doi.org/10.1128/MCB.12.12.5527-5535.1992>
- Hamann, J. C., Surcel, A., Chen, R., Teragawa, C., Albeck, J. G., Robinson, D. N., & Overholtzer, M. (2017). Entosis Is Induced by Glucose Starvation. *Cell Reports*, 20(1), 201–210. <https://doi.org/10.1016/j.celrep.2017.06.037>
- Hanahan, D. (2022). Hallmarks of Cancer: New Dimensions. *Cancer Discovery*, 12(1), 31–46. <https://doi.org/10.1158/2159-8290.CD-21-1059>
- Hanahan, D., & Weinberg, R. A. (2000). The Hallmarks of Cancer. *Cell*, 100(1), 57–70. [https://doi.org/10.1016/S0092-8674\(00\)81683-9](https://doi.org/10.1016/S0092-8674(00)81683-9)
- Hanahan, D., & Weinberg, R. A. (2011). Hallmarks of Cancer: The Next Generation. *Cell*, 144(5), 646–674. <https://doi.org/10.1016/J.CELL.2011.02.013>
- Hanson, R. W., & Hakimi, P. (2008). Born to run; the story of the PEPCK-Cmus mouse. *Biochimie*, 90(6), 838. <https://doi.org/10.1016/J.BIOCHI.2008.03.009>

- Hanson, R. W., & Patel, Y. M. (1994). Phosphoenolpyruvate Carboxykinase (GTP): the Gene and the Enzyme. *Advances in Enzymology and Related Areas of Molecular Biology*, 69, 203–281. <https://doi.org/10.1002/9780470123157.CH6>
- Hanson, R. W., & Reshef, L. (1997). Regulation of phosphoenolpyruvate carboxykinase (GTP) gene expression. *Annual Review of Biochemistry*, 66, 581–611. <https://doi.org/10.1146/ANNUREV.BIOCHEM.66.1.581>
- Hara, K., Yonezawa, K., Weng, Q. P., Kozlowski, M. T., Belham, C., & Avruch, J. (1998). Amino acid sufficiency and mTOR regulate p70 S6 kinase and eIF-4E BP1 through a common effector mechanism. *The Journal of Biological Chemistry*, 273(23), 14484–14494. <https://doi.org/10.1074/JBC.273.23.14484>
- Hassan Baig, M., Ahmad, K., Roy, S., Mohammad Ashraf, J., Adil, M., Haris Siddiqui, M., Khan, S., Amjad Kamal, M., Provaznik, I., & Choi, I. (2016). Computer Aided Drug Design: Success and Limitations. *Current Pharmaceutical Design*, 22(5), 572–581. <https://doi.org/10.2174/1381612822666151125000550>
- Havas, K. M., Milchevskaya, V., Radic, K., Alladin, A., Kafkia, E., Garcia, M., Stolte, J., Klaus, B., Rotmensz, N., Gibson, T. J., Burwinkel, B., Schneeweiss, A., Pruner, G., Patil, K. R., Sotillo, R., & Jechlinger, M. (2017). Metabolic shifts in residual breast cancer drive tumor recurrence. *The Journal of Clinical Investigation*, 127(6), 2091. <https://doi.org/10.1172/JCI89914>
- He, F., Antonucci, L., & Karin, M. (2020). NRF2 as a regulator of cell metabolism and inflammation in cancer. *Carcinogenesis*, 41(4), 405–416. <https://doi.org/10.1093/CARCIN/BGAA039>
- He, F., Antonucci, L., Yamachika, S., Zhang, Z., Taniguchi, K., Umemura, A., Hatzivassiliou, G., Roose-Girma, M., Reina-Campos, M., Duran, A., Diaz-Meco, M. T., Moscat, J., Sun, B., & Karin, M. (2020). NRF2 activates growth factor genes and downstream AKT signaling to induce mouse and human hepatomegaly. *Journal of Hepatology*, 72(6), 1182. <https://doi.org/10.1016/J.JHEP.2020.01.023>
- Heidelberger, C., Chaudhuri, N. K., Danneberg, P., Mooren, D., Griesbach, L., Duschinsky, R., Schnitzer, R. J., Plevin, E., & Scheiner, J. (1957). Fluorinated Pyrimidines, A New Class of Tumour-Inhibitory Compounds. *Nature* 1957 179:4561, 179(4561), 663–666. <https://doi.org/10.1038/179663a0>
- Heiden, M. G. vander, Cantley, L. C., & Thompson, C. B. (2009). Understanding the Warburg Effect: The Metabolic Requirements of Cell Proliferation. *Science*, 324(5930), 1029–1033. <https://doi.org/10.1126/SCIENCE.1160809>
- Heiden Vander, M. G., Lunt, S. Y., Dayton, T. L., Fiske, B. P., Israelsen, W. J., Mattaini, K. R., Vokes, N. I., Stephanopoulos, G., Cantley, L. C., Metallo, C. M., & Locasale, J. W. (2011). Metabolic Pathway Alterations that Support Cell Proliferation. *Cold Spring Harbor Symposia on Quantitative Biology*, 76, 325–334. <https://doi.org/10.1101/SQB.2012.76.010900>
- Heilos, D., Röhr, C., Pirker, C., Englinger, B., Baier, D., Mohr, T., Schwaiger, M., Iqbal, S. M., van Schoonhoven, S., Klavins, K., Eberhart, T., Windberger, U., Taibon, J., Sturm, S., Stuppner, H., Koellensperger, G., Dornetshuber-Fleiss, R., Jäger, W., Lemmens-Gruber, R., & Berger, W. (2018). Altered membrane rigidity via enhanced endogenous cholesterol synthesis drives cancer cell resistance to destruxins. *Oncotarget*, 9(39), 25661–25680. <https://doi.org/10.18632/ONCOTARGET.25432>
- Herzig, S., & Shaw, R. J. (2017). AMPK: guardian of metabolism and mitochondrial homeostasis. *Nature Reviews Molecular Cell Biology* 2017 19:2, 19(2), 121–135. <https://doi.org/10.1038/NRM.2017.95>
- Hess, D., Yang, T., & Stavrakis, S. (2019). Droplet-based optofluidic systems for measuring enzyme kinetics. *Analytical and Bioanalytical Chemistry* 2019 412:14, 412(14), 3265–3283. <https://doi.org/10.1007/S00216-019-02294-Z>

- Hidalgo, J., Latorre, P., Carrodeguas, J. A., Velázquez-Campoy, A., Sancho, J., & López-Buesa, P. (2016). Inhibition of Pig Phosphoenolpyruvate Carboxykinase Isoenzymes by 3-Mercaptopicolinic Acid and Novel Inhibitors. *PLOS ONE*, *11*(7), e0159002. <https://doi.org/10.1371/journal.pone.0159002>
- Ho, P. C., Bihuniak, J. D., MacIntyre, A. N., Staron, M., Liu, X., Amezcua, R., Tsui, Y. C., Cui, G., Micevic, G., Perales, J. C., Kleinstein, S. H., Abel, E. D., Insogna, K. L., Feske, S., Locasale, J. W., Bosenberg, M. W., Rathmell, J. C., & Kaech, S. M. (2015). Phosphoenolpyruvate Is a Metabolic Checkpoint of Anti-tumor T Cell Responses. *Cell*, *162*(6), 1217–1228. <https://doi.org/10.1016/J.CELL.2015.08.012>
- Hoffer, L., Muller, C., Roche, P., & Morelli, X. (2018). Chemistry-driven Hit-to-lead Optimization Guided by Structure-based Approaches. *Molecular Informatics*, *37*(9–10), 1800059. <https://doi.org/10.1002/MINF.201800059>
- Hofmarcher, T., Lindgren, P., Wilking, N., & Jö, B. (2020). The cost of cancer in Europe 2018. *European Journal of Cancer*, *129*, 41–49. <https://doi.org/10.1016/j.ejca.2020.01.011>
- Hopgood, M. F., Ballard, F. J., Reshef, L., & Hanson, R. W. (1973). Synthesis and degradation of phosphoenolpyruvate carboxylase in rat liver and adipose tissue. Changes during a starvation-re-feeding cycle. *The Biochemical Journal*, *134*(2), 445–453. <https://doi.org/10.1042/BJ1340445>
- Hosios, A. M., & vander Heiden, M. G. (2018). The redox requirements of proliferating mammalian cells. *Journal of Biological Chemistry*, *293*(20), 7490–7498. <https://doi.org/10.1074/JBC.TM117.000239>
- Hsieh, C. W., Millward, C. A., DeSantis, D., Pisano, S., Machova, J., Perales, J. C., & Croniger, C. M. (2009). Reduced Milk Triglycerides in Mice Lacking Phosphoenolpyruvate Carboxykinase in Mammary Gland Adipocytes and White Adipose Tissue Contribute to the Development of Insulin Resistance in Pups. *The Journal of Nutrition*, *139*(12), 2257. <https://doi.org/10.3945/JN.109.113092>
- Hu, C. A. A. (2021). Isozymes of P5C reductase (PYCR) in human diseases: focus on cancer. *Amino Acids*, *53*(12), 1835–1840. <https://doi.org/10.1007/S00726-021-03048-X/FIGURES/2>
- Hu, Y., Deng, K., Pan, M., Liu, S., Li, W., Huang, J., Yao, J., & Zuo, J. (2020). Down-regulation of PCK2 inhibits the invasion and metastasis of laryngeal carcinoma cells. *American Journal of Translational Research*, *12*(7), 3842. [/pmc/articles/PMC7407686/](https://pubmed.ncbi.nlm.nih.gov/3407686/)
- Huang, J., & Manning, B. D. (2009). A complex interplay between Akt, TSC2, and the two mTOR complexes. *Biochemical Society Transactions*, *37*(Pt 1), 217. <https://doi.org/10.1042/BST0370217>
- Hughes, J. P., Rees, S. S., Kalindjian, S. B., & Philpott, K. L. (2011). Principles of early drug discovery. *British Journal of Pharmacology*, *162*(6), 1239–1249. <https://doi.org/10.1111/J.1476-5381.2010.01127.X>
- Hulvat, M. C. (2020). Cancer Incidence and Trends. *Surgical Clinics of North America*, *100*(3), 469–481. <https://doi.org/10.1016/J.SUC.2020.01.002>
- Husain, Z., Huang, Y., Seth, P., & Sukhatme, V. P. (2013). Tumor-Derived Lactate Modifies Antitumor Immune Response: Effect on Myeloid-Derived Suppressor Cells and NK Cells. *The Journal of Immunology*, *191*(3), 1486–1495. <https://doi.org/10.4049/JIMMUNOL.1202702>
- Huynh, T. Y. L., Zareba, I., Baszanowska, W., Lewoniewska, S., & Palka, J. (2020). Understanding the role of key amino acids in regulation of proline dehydrogenase/proline oxidase (prodh/pox)-dependent apoptosis/autophagy as an approach to targeted cancer therapy. *Molecular and Cellular Biochemistry*, *466*(1–2), 35–44. <https://doi.org/10.1007/S11010-020-03685-Y/FIGURES/1>

- Hyroššová, P., Aragón, M., Moreno-Felici, J., Fu, X., Mendez-Lucas, A., García-Rovés, P. M., Burgess, S., Figueras, A., Viñals, F., & Perales, J. C. (2021). PEPCK-M recoups tumor cell anabolic potential in a PKC- ζ -dependent manner. *Cancer & Metabolism*, 9(1), 1. <https://doi.org/10.1186/s40170-020-00236-3>
- Isaacs, J. S., Yun, J. J., Mole, D. R., Lee, S., Torres-Cabala, C., Chung, Y. L., Merino, M., Trepel, J., Zbar, B., Toro, J., Ratcliffe, P. J., Linehan, W. M., & Neckers, L. (2005). HIF overexpression correlates with biallelic loss of fumarate hydratase in renal cancer: novel role of fumarate in regulation of HIF stability. *Cancer Cell*, 8(2), 143–153. <https://doi.org/10.1016/J.CCR.2005.06.017>
- Itoh, S. G., & Okumura, H. (2022). All-Atom Molecular Dynamics Simulation Methods for the Aggregation of Protein and Peptides: Replica Exchange/Permutation and Nonequilibrium Simulations. *Methods in Molecular Biology (Clifton, N.J.)*, 2340, 197–220. https://doi.org/10.1007/978-1-0716-1546-1_10
- Iurlaro, R., León-Annicchiarico, C. L., & Muñoz-Pinedo, C. (2014). Regulation of Cancer Metabolism by Oncogenes and Tumor Suppressors. *Methods in Enzymology*, 542, 59–80. <https://doi.org/10.1016/B978-0-12-416618-9.00003-0>
- Jafari, R., Almqvist, H., Axelsson, H., Ignatushchenko, M., Lundbäck, T., Nordlund, P., & Molina, D. M. (2014). The cellular thermal shift assay for evaluating drug target interactions in cells. *Nature Protocols*, 9(9), 2100–2122. <https://doi.org/10.1038/nprot.2014.138>
- Jariwala, U., Prescott, J., Jia, L., Barski, A., Pregizer, S., Cogan, J. P., Arasheben, A., Tilley, W. D., Scher, H. I., Gerald, W. L., Buchanan, G., Coetzee, G. A., & Frenkel, B. (2007). Identification of novel androgen receptor target genes in prostate cancer. *Molecular Cancer*, 6(1), 1–15. <https://doi.org/10.1186/1476-4598-6-39/FIGURES/5>
- Jayasingam, S. D., Citartan, M., Thang, T. H., Mat Zin, A. A., Ang, K. C., & Ch'ng, E. S. (2019). Evaluating the Polarization of Tumor-Associated Macrophages Into M1 and M2 Phenotypes in Human Cancer Tissue: Technicalities and Challenges in Routine Clinical Practice. *Frontiers in Oncology*, 9. <https://doi.org/10.3389/FONC.2019.01512>
- Jiang, P., Du, W., Wang, X., Mancuso, A., Gao, X., Wu, M., & Yang, X. (2011). p53 regulates biosynthesis through direct inactivation of glucose-6-phosphate dehydrogenase. *Nature Cell Biology* 2011 13:3, 13(3), 310–316. <https://doi.org/10.1038/NCB2172>
- Jiang, W., Wang, S., Xiao, M., Lin, Y., Zhou, L., Lei, Q., Xiong, Y., Guan, K. L., & Zhao, S. (2011). Acetylation Regulates Gluconeogenesis by Promoting PEPCK1 Degradation via Recruiting the UBR5 Ubiquitin Ligase. *Molecular Cell*, 43(1), 33–44. <https://doi.org/10.1016/J.MOLCEL.2011.04.028>
- Jiang, W., Zhou, X., Li, Z., Liu, K., Wang, W., Tan, R., Cong, X., Shan, J., Zhan, Y., Cui, Z., Jiang, L., Li, Q., Shen, S., Bai, M., Cheng, Y., Li, B., Tan, M., Ma, D. K., Liu, J. O., & Dang, Y. (2018). Prolyl 4-hydroxylase 2 promotes B-cell lymphoma progression via hydroxylation of Carabin. *Blood*, 131(12), 1325–1336. <https://doi.org/10.1182/BLOOD-2017-07-794875>
- Jomain-Baum, M., Schramm, V. L., & Hanson, R. W. (1976). Mechanism of 3-Mercaptopicolinic Acid Inhibition of Hepatic Phosphoenolpyruvate Carboxykinase (GTP) *. *THE JOURNAL OF BIOLOGICAL CHEMISTRY*, 251(1), 37–44. [https://doi.org/10.1016/S0021-9258\(17\)33923-6](https://doi.org/10.1016/S0021-9258(17)33923-6)
- Jones, G., Willett, P., Glen, R. C., Leach, A. R., & Taylor, R. (1997). Development and validation of a genetic algorithm for flexible docking. *Journal of Molecular Biology*, 267(3), 727–748. <https://doi.org/10.1006/JMBI.1996.0897>
- Judge, A., & Dodd, M. S. (2020). Metabolism. *Essays in Biochemistry*, 64(4), 607. <https://doi.org/10.1042/EBC20190041>

- Junttila, M. R., & Evan, G. I. (2009). p53 — a Jack of all trades but master of none. *Nature Reviews Cancer* 2009 9:11, 9(11), 821–829. <https://doi.org/10.1038/nrc2728>
- Kalhan, S. C., Mahajan, S., Burkett, E., Reshef, L., & Hanson, R. W. (2001). Glyceroneogenesis and the Source of Glycerol for Hepatic Triacylglycerol Synthesis in Humans *. *Journal of Biological Chemistry*, 276(16), 12928–12931. <https://doi.org/10.1074/JBC.M006186200>
- Kalish, B. T., Fallon, E. M., & Puder, M. (2012). A Tutorial on Fatty Acid Biology. *Journal of Parenteral and Enteral Nutrition*, 36(4), 380–388. <https://doi.org/10.1177/0148607112449650>
- Kamarajugadda, S., Stemboroski, L., Cai, Q., Simpson, N. E., Nayak, S., Tan, M., & Lu, J. (2012). Glucose Oxidation Modulates Anoikis and Tumor Metastasis. *Molecular and Cellular Biology*, 32(10), 1893–1907. <https://doi.org/10.1128/MCB.06248-11/ASSET/60A9F2AD-51A4-46BA-B7DE-AE0200E8207C/ASSETS/GRAPHIC/ZMB9991094910010.JPEG>
- Kamphorst, J. J., Nofal, M., Commisso, C., Hackett, S. R., Lu, W., Grabocka, E., vander Heiden, M. G., Miller, G., Drebin, J. A., Bar-Sagi, D., Thompson, C. B., & Rabinowitz, J. D. (2015). Human pancreatic cancer tumors are nutrient poor and tumor cells actively scavenge extracellular protein. *Cancer Research*, 75(3), 544. <https://doi.org/10.1158/0008-5472.CAN-14-2211>
- Kardos, G. R., Wastyk, H. C., & Robertson, G. P. (2015). Disruption of proline synthesis in melanoma inhibits protein production mediated by the GCN2 pathway. *Molecular Cancer Research*, 13(10), 1408–1420. <https://doi.org/10.1158/1541-7786.MCR-15-0048>
- Kattan, W. E., & Hancock, J. F. (2020). RAS Function in cancer cells: translating membrane biology and biochemistry into new therapeutics. *Biochemical Journal*, 477(15), 2893–2919. <https://doi.org/10.1042/BCJ20190839>
- Kazerounian, S., Yee, K. O., & Lawler, J. (2008). Thrombospondins in cancer. *Cellular and Molecular Life Sciences : CMLS*, 65(5), 700. <https://doi.org/10.1007/S00018-007-7486-Z>
- Keum, N. N., & Giovannucci, E. (2019). Global burden of colorectal cancer: emerging trends, risk factors and prevention strategies. *Nature Reviews Gastroenterology & Hepatology* 2019 16:12, 16(12), 713–732. <https://doi.org/10.1038/S41575-019-0189-8>
- Khwairakpam, A., Shyamananda, M., Sailo, B., Rathnakaram, S., Padmavathi, G., Kotoky, J., & Kunnumakkara, A. (2015). ATP citrate lyase (ACLY): a promising target for cancer prevention and treatment. *Current Drug Targets*, 16(2), 156–163. <https://doi.org/10.2174/1389450115666141224125117>
- Kibbey, R. G. (2016). PEPCK-M. *Encyclopedia of Signaling Molecules*, 1–9. https://doi.org/10.1007/978-1-4614-6438-9_101756-1
- Kibbey, R. G., Pongratz, R. L., Romanelli, A. J., Wollheim, C. B., Cline, G. W., & Shulman, G. I. (2007). Mitochondrial GTP Regulates Glucose-Stimulated Insulin Secretion. *Cell Metabolism*, 5(4), 253–264. <https://doi.org/10.1016/J.CMET.2007.02.008>
- Kim, J. W., Tchernyshyov, I., Semenza, G. L., & Dang, C. v. (2006). HIF-1-mediated expression of pyruvate dehydrogenase kinase: A metabolic switch required for cellular adaptation to hypoxia. *Cell Metabolism*, 3(3), 177–185. <https://doi.org/10.1016/J.CMET.2006.02.002>
- Kim, J., Zeller, K. I., Wang, Y., Jegga, A. G., Aronow, B. J., O'Donnell, K. A., & Dang, C. v. (2004). Evaluation of Myc E-Box Phylogenetic Footprints in Glycolytic Genes by Chromatin Immunoprecipitation Assays. *Molecular and Cellular Biology*, 24(13), 5923–5936. https://doi.org/10.1128/MCB.24.13.5923-5936.2004/SUPPL_FILE/SUPPLEMENTARY_TABLE_S2.DOC

- Kimmelman, A. C., & White, E. (2017). Autophagy and Tumor Metabolism. *Cell Metabolism*, 25(5), 1037–1043. <https://doi.org/10.1016/J.CMET.2017.04.004>
- Kitchen, D. B., Decornez, H., Furr, J. R., & Bajorath, J. (2004). Docking and scoring in virtual screening for drug discovery: methods and applications. *Nature Reviews Drug Discovery* 2004 3:11, 3(11), 935–949. <https://doi.org/10.1038/NRD1549>
- Knight, S., Gianni, D., & Hendricks, A. (2022). Fragment-based screening: A new paradigm for ligand and target discovery. *SLAS Discovery*, 27(1), 3–7. <https://doi.org/10.1016/J.SLASD.2021.10.011>
- Kottakis, F., Nicolay, B. N., Roumane, A., Karnik, R., Gu, H., Nagle, J. M., Boukhali, M., Hayward, M. C., Li, Y., Y., Chen, T., Liesa, M., Hammerman, P. S., Wong, K. K., Hayes, D. N., Shirihai, O. S., Dyson, N. J., Haas, W., Meissner, A., & Bardeesy, N. (2016). LKB1 loss links serine metabolism to DNA methylation and tumorigenesis. *Nature* 2016 539:7629, 539(7629), 390–395. <https://doi.org/10.1038/NATURE20132>
- Koundouros, N., & Poulogiannis, G. (2019). Reprogramming of fatty acid metabolism in cancer. *British Journal of Cancer* 2019 122:1, 122(1), 4–22. <https://doi.org/10.1038/s41416-019-0650-z>
- Kovářová, J., & Barrett, M. P. (2016). The Pentose Phosphate Pathway in Parasitic Trypanosomatids. *Trends in Parasitology*, 32(8), 622–634. <https://doi.org/10.1016/J.PT.2016.04.010>
- Krishnan, N., Dickman, M. B., & Becker, D. F. (2008). Proline modulates the intracellular redox environment and protects mammalian cells against oxidative stress. *Free Radical Biology & Medicine*, 44(4), 671. <https://doi.org/10.1016/J.FREERADBIOMED.2007.10.054>
- Kulis, M., & Esteller, M. (2010). DNA Methylation and Cancer. *Advances in Genetics*, 70(C), 27–56. <https://doi.org/10.1016/B978-0-12-380866-0.60002-2>
- Kuo, M. L., Lee, M. B. E., Tang, M., den Besten, W., Hu, S., Sweredoski, M. J., Hess, S., Chou, C. M., Changou, C. A., Su, M., Jia, W., Su, L., & Yen, Y. (2016). PYCR1 and PYCR2 Interact and Collaborate with RRM2B to Protect Cells from Overt Oxidative Stress. *Scientific Reports* 2016 6:1, 6(1), 1–15. <https://doi.org/10.1038/srep18846>
- Kurmi, K., & Haigis, M. C. (2020). Nitrogen Metabolism in Cancer and Immunity. *Trends in Cell Biology*, 30(5), 408–424. <https://doi.org/10.1016/J.TCB.2020.02.005>
- Labuschagne, C. F., van den Broek, N. J. F., Mackay, G. M., Vousden, K. H., & Maddocks, O. D. K. (2014). Serine, but Not Glycine, Supports One-Carbon Metabolism and Proliferation of Cancer Cells. *Cell Reports*, 7(4), 1248–1258. <https://doi.org/10.1016/J.CELREP.2014.04.045>
- Lacey, J. M., & Wilmore, D. W. (1990). Is Glutamine a Conditionally Essential Amino Acid? *Nutrition Reviews*, 48(8), 297–309. <https://doi.org/10.1111/J.1753-4887.1990.TB02967.X>
- Ladanyi, A., Mukherjee, A., Kenny, H. A., Johnson, A., Mitra, A. K., Sundaresan, S., Nieman, K. M., Pascual, G., Benitah, S. A., Montag, A., Yamada, S. D., Abumrad, N. A., & Lengyel, E. (2018). Adipocyte-induced CD36 expression drives ovarian cancer progression and metastasis. *Oncogene* 2018 37:17, 37(17), 2285–2301. <https://doi.org/10.1038/S41388-017-0093-Z>
- Lahiguera, Á., Hyroššová, P., Figueras, A., Garzón, D., Moreno, R., Soto-Cerrato, V., McNeish, I., Serra, V., Lazaro, C., Barretina, P., Brunet, J., Menéndez, J., Matias-Guiu, X., Vidal, A., Villanueva, A., Taylor-Harding, B., Tanaka, H., Orsulic, S., Junza, A., ... Viñals, F. (2020). Tumors defective in homologous recombination rely on oxidative metabolism: relevance to treatments with PARP inhibitors. *EMBO Molecular Medicine*, 1–23. <https://doi.org/10.15252/emmm.201911217>

- Lampa, M., Arlt, H., He, T., Ospina, B., Reeves, J., Zhang, B., Murtie, J., Deng, G., Barberis, C., Hoffmann, D., Cheng, H., Pollard, J., Winter, C., Richon, V., Garcia-Escheverria, C., Adrian, F., Wiederschain, D., & Srinivasan, L. (2017). Glutaminase is essential for the growth of triple-negative breast cancer cells with a deregulated glutamine metabolism pathway and its suppression synergizes with mTOR inhibition. *PLoS ONE*, *12*(9). <https://doi.org/10.1371/JOURNAL.PONE.0185092>
- Laplante, M., & Sabatini, D. M. (2012). mTOR Signaling in Growth Control and Disease. *Cell*, *149*(2), 274–293. <https://doi.org/10.1016/J.CELL.2012.03.017>
- Leahy, P., Crawford, D. R., Grossman, G., Gronostajski, R. M., & Hanson, R. W. (1999). CREB binding protein coordinates the function of multiple transcription factors including nuclear factor I to regulate phosphoenolpyruvate carboxykinase (GTP) gene transcription. *The Journal of Biological Chemistry*, *274*(13), 8813–8822. <https://doi.org/10.1074/JBC.274.13.8813>
- Lee, M. H., Hebda, C. A., & Nowak, T. (1981). The role of cations in avian liver phosphoenolpyruvate carboxykinase catalysis. Activation and regulation. *Journal of Biological Chemistry*, *256*(24), 12793–12801. [https://doi.org/10.1016/S0021-9258\(18\)42965-1](https://doi.org/10.1016/S0021-9258(18)42965-1)
- Leithner, K., Hrzenjak, A., Trötz Müller, M., Moustafa, T., Köfeler, H. C., Wohlkoenig, C., Stacher, E., Lindenmann, J., Harris, A. L., Olschewski, A., & Olschewski, H. (2014). PCK2 activation mediates an adaptive response to glucose depletion in lung cancer. *Oncogene* *2015* *34*:8, *34*(8), 1044–1050. <https://doi.org/10.1038/onc.2014.47>
- Leithner, K., Hrzenjak, A., Trötz Müller, M., Moustafa, T., Köfeler, H. C., Wohlkoenig, C., Stacher, E., Lindenmann, J., Harris, A. L., Olschewski, A., & Olschewski, H. (2015). PCK2 activation mediates an adaptive response to glucose depletion in lung cancer. *Oncogene*, *34*(8), 1044–1050. <https://doi.org/10.1038/ONC.2014.47>
- Leithner, K., Triebel, A., Trötz Müller, M., Hinteregger, B., Leko, P., Wieser, B. I., Grasmann, G., Bertsch, A. L., Züllig, T., Stacher, E., Valli, A., Prassl, R., Olschewski, A., Harris, A. L., Köfeler, H. C., Olschewski, H., & Hrzenjak, A. (2018). The glycerol backbone of phospholipids derives from noncarbohydrate precursors in starved lung cancer cells. *Proceedings of the National Academy of Sciences of the United States of America*, *115*(24), 6225–6230. <https://doi.org/10.1073/PNAS.1719871115/-/DCSUPPLEMENTAL>
- Lemmon, M. A., & Schlessinger, J. (2010). Cell signaling by receptor tyrosine kinases. *Cell*, *141*(7), 1117–1134. <https://doi.org/10.1016/J.CELL.2010.06.011/ATTACHMENT/B383EB98-F844-43F4-878F-A14D3681EED4/MMC1.PDF>
- Li, C. F., Fang, F. M., Chen, Y. Y., Liu, T. T., Chan, T. C., Yu, S. C., Chen, L. T., & Huang, H. Y. (2017). Overexpressed Fatty Acid Synthase in Gastrointestinal Stromal Tumors: Targeting a Progression-Associated Metabolic Driver Enhances the Antitumor Effect of Imatinib. *Clinical Cancer Research : An Official Journal of the American Association for Cancer Research*, *23*(16), 4908–4918. <https://doi.org/10.1158/1078-0432.CCR-16-2770>
- Li, D. S., Yuan, Y. H., Tu, H. J., Liang, Q. le, & Dail, L. J. (2009). A protocol for islet isolation from mouse pancreas. *Nature Protocols*, *4*(11), 1649–1652. <https://doi.org/10.1038/nprot.2009.150>
- Li, L., Ye, Y., Sang, P., Yin, Y., Hu, W., Wang, J., Zhang, C., Li, D., Wan, W., Li, R., Li, L., Ma, L., Xie, Y., & Meng, Z. (2017). Effect of R119G Mutation on Human P5CR1 Dynamic Property and Enzymatic Activity. *BioMed Research International*, *2017*. <https://doi.org/10.1155/2017/4184106>
- Li, N., Li, H., Cao, L., & Zhan, X. (2018). Quantitative analysis of the mitochondrial proteome in human ovarian carcinomas. *Endocrine-Related Cancer*, *25*(10), 909–931. <https://doi.org/10.1530/ERC-18-0243>

- Li, Q., Wang, Q., Zhang, Q., Zhang, J., & Zhang, J. (2019). Collagen prolyl 4-hydroxylase 2 predicts worse prognosis and promotes glycolysis in cervical cancer. *American Journal of Translational Research*, *11*(11), 6938. /pmc/articles/PMC6895525/
- Li, Y., Bie, J., Song, C., Liu, M., & Luo, J. (2021). PYCR, a key enzyme in proline metabolism, functions in tumorigenesis. *Amino Acids*, *53*(12), 1841–1850. <https://doi.org/10.1007/S00726-021-03047-Y/FIGURES/2>
- Li, Y. C., Park, M. J., Ye, S. K., Kim, C. W., & Kim, Y. N. (2006). Elevated levels of cholesterol-rich lipid rafts in cancer cells are correlated with apoptosis sensitivity induced by cholesterol-depleting agents. *The American Journal of Pathology*, *168*(4), 1107–1118. <https://doi.org/10.2353/AJPATH.2006.050959>
- Li, Y., Luo, S., Ma, R., Liu, J., Xu, P., Zhang, H., Tang, K., Ma, J., Zhang, Y., Liang, X., Sun, Y., Ji, T., Wang, N., & Huang, B. (2015). Upregulation of cytosolic phosphoenolpyruvate carboxykinase is a critical metabolic event in melanoma cells that repopulate tumors. *Cancer Research*, *75*(7), 1191. <https://doi.org/10.1158/0008-5472.CAN-14-2615>
- Li, Y., Xu, S., Mihaylova, M. M., Zheng, B., Hou, X., Jiang, B., Park, O., Luo, Z., Lefai, E., Shyy, J. Y. J., Gao, B., Wierzbicki, M., Verbeuren, T. J., Shaw, R. J., Cohen, R. A., & Zang, M. (2011). AMPK Phosphorylates and Inhibits SREBP Activity to Attenuate Hepatic Steatosis and Atherosclerosis in Diet-induced Insulin Resistant Mice. *Cell Metabolism*, *13*(4), 376. <https://doi.org/10.1016/J.CMET.2011.03.009>
- Li, Y., Zhang, M., Dorfman, R. G., Pan, Y., Tang, D., Xu, L., Zhao, Z., Zhou, Q., Zhou, L., Wang, Y., Yin, Y., Shen, S., Kong, B., Friess, H., Zhao, S., Wang, L., & Zou, X. (2018). SIRT2 Promotes the Migration and Invasion of Gastric Cancer through RAS/ERK/JNK/MMP-9 Pathway by Increasing PEPCK1-Related Metabolism. *Neoplasia (New York, N.Y.)*, *20*(7), 745. <https://doi.org/10.1016/J.NEO.2018.03.008>
- Li, Z., Liu, X., Zhu, Y., Du, Y., Liu, X., Lv, L., Zhang, X., Liu, Y., Zhang, P., & Zhou, Y. (2019). Mitochondrial Phosphoenolpyruvate Carboxykinase Regulates Osteogenic Differentiation by Modulating AMPK/ULK1-Dependent Autophagy. *Stem Cells (Dayton, Ohio)*, *37*(12), 1542. <https://doi.org/10.1002/STEM.3091>
- Liao, L., Ge, M., Zhan, Q., Huang, R., Ji, X., Liang, X., & Zhou, X. (2019). PSPH Mediates the Metastasis and Proliferation of Non-small Cell Lung Cancer through MAPK Signaling Pathways. *International Journal of Biological Sciences*, *15*(1), 183–194. <https://doi.org/10.7150/IJBS.29203>
- Ligresti, G., Militello, L., Steelman, L. S., Cavallaro, A., Basile, F., Nicoletti, F., Stivala, F., McCubrey, J. A., & Libra, M. (2009). PIK3CA mutations in human solid tumors: Role in sensitivity to various therapeutic approaches. *Cell Cycle*, *8*(9), 1352. <https://doi.org/10.4161/CC.8.9.8255>
- Lin, J., Wu, X.-J., Wei, W.-X., Gao, X.-C., Jin, M.-Z., Cui, Y., Jin, W.-L., & Qiu, G.-Z. (2020). P4HA2 is associated with prognosis, promotes proliferation, invasion, migration and EMT in glioma. *BioRxiv*, 2020.02.05.935221. <https://doi.org/10.1101/2020.02.05.935221>
- Lin, J.-H. (2012). Accommodating Protein Flexibility for Structure-Based Drug Design. *Current Topics in Medicinal Chemistry*, *11*(2), 171–178. <https://doi.org/10.2174/156802611794863580>
- Lin, Y. yi, Lu, J. ying, Zhang, J., Walter, W., Dang, W., Wan, J., Tao, S. C., Qian, J., Zhao, Y., Boeke, J. D., Berger, S. L., & Zhu, H. (2009). Protein Acetylation Microarray Reveals that NuA4 Controls Key Metabolic Target Regulating Gluconeogenesis. *Cell*, *136*(6), 1073–1084. <https://doi.org/10.1016/J.CELL.2009.01.033>
- Lipinski, C. A., Lombardo, F., Dominy, B. W., & Feeney, P. J. (2001). Experimental and computational approaches to estimate solubility and permeability in drug discovery and development settings. *Advanced Drug Delivery Reviews*, *46*(1–3), 3–26. [https://doi.org/10.1016/S0169-409X\(00\)00129-0](https://doi.org/10.1016/S0169-409X(00)00129-0)

- Liu, H. Y., Zhang, H. S., Liu, M. Y., Li, H. M., Wang, X. Y., & Wang, M. (2021). GLS1 depletion inhibited colorectal cancer proliferation and migration via redox/Nrf2/autophagy-dependent pathway. *Archives of Biochemistry and Biophysics*, *708*. <https://doi.org/10.1016/J.ABB.2021.108964>
- Liu, J., Zhang, C., Hu, W., & Feng, Z. (2019). Tumor suppressor p53 and metabolism. *Journal of Molecular Cell Biology*, *11*(4), 284. <https://doi.org/10.1093/JMCB/MJY070>
- Liu, M., Wang, Y., Yang, C., Ruan, Y., Bai, C., Chu, Q., Cui, Y., Chen, C., Ying, G., & Li, B. (2020). Inhibiting both proline biosynthesis and lipogenesis synergistically suppresses tumor growth. *Journal of Experimental Medicine*, *217*(3). <https://doi.org/10.1084/JEM.20191226/133620>
- Liu, M. X., Jin, L., Sun, S. J., Liu, P., Feng, X., Cheng, Z. L., Liu, W. R., Guan, K. L., Shi, Y. H., Yuan, H. X., & Xiong, Y. (2018). Metabolic reprogramming by PCK1 promotes TCA cataplerosis, oxidative stress and apoptosis in liver cancer cells and suppresses hepatocellular carcinoma. *Oncogene*, *37*(12), 1637–1653. <https://doi.org/10.1038/S41388-017-0070-6>
- Liu, P., Ge, M., Hu, J., Li, X., Che, L., Sun, K., Cheng, L., Huang, Y., Pilo, M. G., Cigliano, A., Pes, G. M., Pascale, R. M., Brozzetti, S., Vidili, G., Porcu, A., Cossu, A., Palmieri, G., Sini, M. C., Ribback, S., ... Chen, X. (2017). A functional mammalian target of rapamycin complex 1 signaling is indispensable for c-Myc-driven hepatocarcinogenesis. *Hepatology*, *66*(1), 167–181. <https://doi.org/10.1002/hep.29183>
- Liu, S.-Q., Ji, X.-L., Tao, Y., Tan, D.-Y., Zhang, K.-Q., & Fu, Y.-X. (2012). Protein Folding, Binding and Energy Landscape: A Synthesis. *Protein Engineering*. <https://doi.org/10.5772/30440>
- Liu, W., Glunde, K., Bhujwala, Z. M., Raman, V., Sharma, A., & Phang, J. M. (2012). Proline oxidase promotes tumor cell survival in hypoxic tumor microenvironments. *Cancer Research*, *72*(14), 3677–3686. <https://doi.org/10.1158/0008-5472.CAN-12-0080/650367/AM/PROLINE-OXIDASE-PROMOTES-TUMOR-CELL-SURVIVAL-IN>
- Liu, W., Hancock, C. N., Fischer, J. W., Harman, M., & Phang, J. M. (2015). Proline biosynthesis augments tumor cell growth and aerobic glycolysis: Involvement of pyridine nucleotides. *Scientific Reports*, *5*(1), 1–13. <https://doi.org/10.1038/srep17206>
- Liu, W., Le, A., Hancock, C., Lane, A. N., Dang, C. v., Fan, T. W. M., & Phang, J. M. (2012). Reprogramming of proline and glutamine metabolism contributes to the proliferative and metabolic responses regulated by oncogenic transcription factor c-MYC. *Proceedings of the National Academy of Sciences of the United States of America*, *109*(23), 8983–8988. <https://doi.org/10.1073/PNAS.1203244109/-/DCSUPPLEMENTAL>
- Liu, X., Blaženović, I., Contreras, A. J., Pham, T. M., Tabuloc, C. A., Li, Y. H., Ji, J., Fiehn, O., & Chiu, J. C. (2021). Hexosamine biosynthetic pathway and O-GlcNAc-processing enzymes regulate daily rhythms in protein O-GlcNAcylation. *Nature Communications* *2021 12:1*, *12*(1), 1–16. <https://doi.org/10.1038/s41467-021-24301-7>
- Liu, X., IJzerman, A. P., & van Westen, G. J. P. (2021). Computational Approaches for De Novo Drug Design: Past, Present, and Future. *Methods in Molecular Biology (Clifton, N.J.)*, *2190*, 139–165. https://doi.org/10.1007/978-1-0716-0826-5_6
- Liu, Y., Borchert, G. L., Donald, S. P., Diwan, B. A., Anver, M., & Phang, J. M. (2009). Proline oxidase functions as a mitochondrial tumor suppressor in human cancers. *Cancer Research*, *69*(16), 6414–6422. <https://doi.org/10.1158/0008-5472.CAN-09-1223/655394/P/PROLINE-OXIDASE-FUNCTIONS-AS-A-MITOCHONDRIAL-TUMOR>

- Liu, Y., Borchert, G. L., Donald, S. P., Surazynski, A., Hu, C. A., Weydert, C. J., Oberley, L. W., & Phang, J. M. (2005). MnSOD inhibits proline oxidase-induced apoptosis in colorectal cancer cells. *Carcinogenesis*, *26*(8), 1335–1342. <https://doi.org/10.1093/CARCIN/BGI083>
- Liu, Y., Borchert, G. L., Surazynski, A., Hu, C. A., & Phang, J. M. (2006). Proline oxidase activates both intrinsic and extrinsic pathways for apoptosis: the role of ROS/superoxides, NFAT and MEK/ERK signaling. *Oncogene* *2006 25:41*, *25*(41), 5640–5647. <https://doi.org/10.1038/SJ.ONC.1209564>
- Liu, Y., Borchert, G. L., Surazynski, A., & Phang, J. M. (2008). Proline oxidase, a p53-induced gene, targets COX-2/PGE2 signaling to induce apoptosis and inhibit tumor growth in colorectal cancers. *Oncogene* *2008 27:53*, *27*(53), 6729–6737. <https://doi.org/10.1038/ONC.2008.322>
- Liu, Y., Mao, C., Wang, M., Liu, N., Ouyang, L., Liu, S., Tang, H., Cao, Y., Liu, S., Wang, X., Xiao, D., Chen, C., Shi, Y., Yan, Q., & Tao, Y. (2020). Cancer progression is mediated by proline catabolism in non-small cell lung cancer. *Oncogene* *2020 39:11*, *39*(11), 2358–2376. <https://doi.org/10.1038/S41388-019-1151-5>
- Loayza-Puch, F., Rooijers, K., Buil, L. C. M., Zijlstra, J., Oude Vrielink, J. F., Lopes, R., Ugalde, A. P., van Breugel, P., Hofland, I., Wesseling, J., van Tellingen, O., Bex, A., & Agami, R. (2016). Tumour-specific proline vulnerability uncovered by differential ribosome codon reading. *Nature* *2016 530:7591*, *530*(7591), 490–494. <https://doi.org/10.1038/NATURE16982>
- Lobo, C., Ruiz-Bellido, M. A., Aledo, J. C., Márquez, J., Núñez De Castro, I., & Alonso, F. J. (2000). Inhibition of glutaminase expression by antisense mRNA decreases growth and tumorigenicity of tumour cells. *Biochemical Journal*, *348*(Pt 2), 257. <https://doi.org/10.1042/0264-6021:3480257>
- Locasale, J. W. (2013). Serine, glycine and one-carbon units: cancer metabolism in full circle. *Nature Reviews Cancer* *2013 13:8*, *13*(8), 572–583. <https://doi.org/10.1038/NRC3557>
- Lu, H., Zhou, Q., He, J., Jiang, Z., Peng, C., Tong, R., & Shi, J. (2020). Recent advances in the development of protein–protein interactions modulators: mechanisms and clinical trials. *Signal Transduction and Targeted Therapy* *2020 5:1*, *5*(1), 1–23. <https://doi.org/10.1038/s41392-020-00315-3>
- Lu, J. (2019). The Warburg metabolism fuels tumor metastasis. *Cancer and Metastasis Reviews*, *38*(1–2), 157–164. <https://doi.org/10.1007/S10555-019-09794-5/FIGURES/1>
- Lu, J., Lin, J., Zhou, Y., Ye, K., & Fang, C. (2021). MiR-328–3p inhibits lung adenocarcinoma-genes by downregulation PYCR1. *Biochemical and Biophysical Research Communications*, *550*, 99–106. <https://doi.org/10.1016/J.BBRC.2021.02.029>
- Lu, J., Tan, M., & Cai, Q. (2015). The Warburg effect in tumor progression: Mitochondrial oxidative metabolism as an anti-metastasis mechanism. *Cancer Letters*, *356*(2), 156–164. <https://doi.org/10.1016/J.CANLET.2014.04.001>
- Luengo, A., Gui, D. Y., & vander Heiden, M. G. (2017). Targeting Metabolism for Cancer Therapy. *Cell Chemical Biology*, *24*(9), 1161–1180. <https://doi.org/10.1016/J.CHEMBIOL.2017.08.028>
- Luengo, A., Li, Z., Gui, D. Y., Sullivan, L. B., Zagorulya, M., Do, B. T., Ferreira, R., Naamati, A., Ali, A., Lewis, C. A., Thomas, C. J., Spranger, S., Matheson, N. J., & vander Heiden, M. G. (2021). Increased demand for NAD⁺ relative to ATP drives aerobic glycolysis. *Molecular Cell*, *81*(4), 691-707.e6. <https://doi.org/10.1016/J.MOLCEL.2020.12.012/ATTACHMENT/A7FC561E-A203-4D0B-B82A-1BED6881F984/MMC1.PDF>

- Lugano, R., Ramachandran, M., & Dimberg, A. (2020). Tumor angiogenesis: causes, consequences, challenges and opportunities. *Cellular and Molecular Life Sciences*, 77(9), 1745–1770. <https://doi.org/10.1007/S00018-019-03351-7/FIGURES/3>
- Lunt, S. Y., & vander Heiden, M. G. (2011). Aerobic Glycolysis: Meeting the Metabolic Requirements of Cell Proliferation. <Http://Dx.Doi.Org/10.1146/Annurev-Cellbio-092910-154237>, 27, 441–464. <https://doi.org/10.1146/ANNUREV-CELLBIO-092910-154237>
- Luo, S., Li, Y., Ma, R., Liu, J., Xu, P., Zhang, H., Tang, K., Ma, J., Liu, N., Zhang, Y., Sun, Y., Ji, T., Liang, X., Yin, X., Liu, Y., Tong, W., Niu, Y., Wang, N., Wang, X., & Huang, B. (2017). Downregulation of PCK2 remodels tricarboxylic acid cycle in tumor-repopulating cells of melanoma. *Oncogene* 2017 36:25, 36(25), 3609–3617. <https://doi.org/10.1038/onc.2016.520>
- Luo, W., Hu, H., Chang, R., Zhong, J., Knabel, M., O’Meally, R., Cole, R. N., Pandey, A., & Semenza, G. L. (2011). Pyruvate kinase M2 is a PHD3-stimulated coactivator for hypoxia-inducible factor 1. *Cell*, 145(5), 732–744. <https://doi.org/10.1016/J.CELL.2011.03.054/ATTACHMENT/60AE52E7-6E49-4376-8719-B9A2966D0983/MMC8.MP3>
- Ma, H., Yu, S., Liu, X., Zhang, Y., Fakadej, T., Liu, Z., Yin, C., Shen, W., Locasale, J. W., Taylor, J. M., Qian, L., & Liu, J. (2019). Lin28a Regulates Pathological Cardiac Hypertrophic Growth Through Pck2-Mediated Enhancement of Anabolic Synthesis. *Circulation*, 139(14), 1725–1740. <https://doi.org/10.1161/CIRCULATIONAHA.118.037803>
- Ma, X. L., Zhu, S. S., Liu, Y., Chen, H. W., Shi, Y. T., Zeng, K. W., Tu, P. F., & Jiang, Y. (2021). Carbazole alkaloids with potential cytotoxic activities targeted on PCK2 protein from *Murraya microphylla*. *Bioorganic Chemistry*, 114, 105113. <https://doi.org/10.1016/J.BIOORG.2021.105113>
- Maddocks, O. D. K., Athineos, D., Cheung, E. C., Lee, P., Zhang, T., van den Broek, N. J. F., Mackay, G. M., Labuschagne, C. F., Gay, D., Kruiswijk, F., Blagih, J., Vincent, D. F., Campbell, K. J., Ceteci, F., Sansom, O. J., Blyth, K., & Vousden, K. H. (2017). Modulating the therapeutic response of tumours to dietary serine and glycine starvation. *Nature* 2017 544:7650, 544(7650), 372–376. <https://doi.org/10.1038/NATURE22056>
- Maddocks, O. D. K., Berkers, C. R., Mason, S. M., Zheng, L., Blyth, K., Gottlieb, E., & Vousden, K. H. (2012). Serine starvation induces stress and p53-dependent metabolic remodelling in cancer cells. *Nature* 2012 493:7433, 493(7433), 542–546. <https://doi.org/10.1038/NATURE11743>
- Mahmood, T., & Yang, P. C. (2012). Western blot: Technique, theory, and trouble shooting. *North American Journal of Medical Sciences*, 4(9), 429–434. <https://doi.org/10.4103/1947-2714.100998>
- Martin, J. D., Fukumura, D., Duda, D. G., Boucher, Y., & Jain, R. K. (2016). Reengineering the Tumor Microenvironment to Alleviate Hypoxia and Overcome Cancer Heterogeneity. *Cold Spring Harbor Perspectives in Medicine*, 6(12). <https://doi.org/10.1101/CSHPERSPECT.A027094>
- Martínez-Reyes, I., & Chandel, N. S. (2020). Mitochondrial TCA cycle metabolites control physiology and disease. *Nature Communications* 2020 11:1, 11(1), 1–11. <https://doi.org/10.1038/s41467-019-13668-3>
- Masoud, G. N., & Li, W. (2015). HIF-1 α pathway: role, regulation and intervention for cancer therapy. *Acta Pharmaceutica Sinica. B*, 5(5), 378. <https://doi.org/10.1016/J.APSB.2015.05.007>
- Massagué, J., & Obenauf, A. C. (2016). Metastatic colonization by circulating tumour cells. *Nature* 2016 529:7586, 529(7586), 298–306. <https://doi.org/10.1038/NATURE17038>

- Matoba, S., Kang, J. G., Patino, W. D., Wragg, A., Boehm, M., Gavrillova, O., Hurley, P. J., Bunz, F., & Hwang, P. M. (2006). p53 regulates mitochondrial respiration. *Science*, *312*(5780), 1650–1653. https://doi.org/10.1126/SCIENCE.1126863/SUPPL_FILE/PAP.PDF
- Mattaini, K. R., Sullivan, M. R., & vander Heiden, M. G. (2016). The importance of serine metabolism in cancer. *Journal of Cell Biology*, *214*(3), 249–257. <https://doi.org/10.1083/JCB.201604085>
- Mayers, J. R., & vander Heiden, M. G. (2015). Famine versus feast: Understanding the metabolism of tumors in vivo. *Trends in Biochemical Sciences*, *40*(3), 130–140. <https://doi.org/10.1016/J.TIBS.2015.01.004/ATTACHMENT/8D82F0F2-A52B-411F-B118-E505F2EBE184/MMC1.XLSX>
- Mayers, J. R., & vander Heiden, M. G. (2017). Nature and Nurture: What Determines Tumor Metabolic Phenotypes? *Cancer Research*, *77*(12), 3131–3134. <https://doi.org/10.1158/0008-5472.CAN-17-0165>
- Méndez-Lucas, A., Duarte, J. A. G., Sunny, N. E., Satapati, S., He, T., Fu, X., Bermúdez, J., Burgess, S. C., & Perales, J. C. (2013). PEPCK-M expression in mouse liver potentiates, not replaces, PEPCK-C mediated gluconeogenesis. *Journal of Hepatology*, *59*(1), 105. <https://doi.org/10.1016/J.JHEP.2013.02.020>
- Méndez-Lucas, A., Hyroššová, P., Novellasdemunt, L., Viñals, F., & Perales, J. C. (2014a). Mitochondrial phosphoenolpyruvate carboxykinase (PEPCK-M) is a pro-survival, endoplasmic reticulum (ER) stress response gene involved in tumor cell adaptation to nutrient availability. *The Journal of Biological Chemistry*, *289*(32), 22090–22102. <https://doi.org/10.1074/JBC.M114.566927>
- Méndez-Lucas, A., Hyroššová, P., Novellasdemunt, L., Viñals, F., & Perales, J. C. (2014b). Mitochondrial phosphoenolpyruvate carboxykinase (PEPCK-M) is a pro-survival, endoplasmic reticulum (ER) stress response gene involved in tumor cell adaptation to nutrient availability. *Journal of Biological Chemistry*, *289*(32), 22090–22102. <https://doi.org/10.1074/jbc.M114.566927>
- Méndez-Lucas, A., Lin, W., Driscoll, P. C., Legrave, N., Novellasdemunt, L., Xie, C., Charles, M., Wilson, Z., Jones, N. P., Rayport, S., Rodríguez-Justo, M., Li, V., MacRae, J. I., Hay, N., Chen, X., & Yuneva, M. (2020). Identifying strategies to target the metabolic flexibility of tumours. *Nature Metabolism* *2*:4, *2*(4), 335–350. <https://doi.org/10.1038/S42255-020-0195-8>
- Mendonsa, A. M., Na, T. Y., & Gumbiner, B. M. (2018). E-cadherin in contact inhibition and cancer. *Oncogene*, *37*(35), 4769–4780. <https://doi.org/10.1038/S41388-018-0304-2>
- Meng, Z., Lou, Z., Liu, Z., Li, M., Zhao, X., Bartlam, M., & Rao, Z. (2006). Crystal Structure of Human Pyrroline-5-carboxylate Reductase. *Journal of Molecular Biology*, *359*(5), 1364–1377. <https://doi.org/10.1016/J.JMB.2006.04.053>
- Meric-Bernstam, F., Lee, R. J., Carthon, B. C., Iliopoulos, O., Mier, J. W., Patel, M. R., Tannir, N. M., Owonikoko, T. K., Haas, N. B., Voss, M. H., Harding, J. J., Srinivasan, R., Shapiro, G., Telli, M. L., Munster, P. N., Carvajal, R. D., Jenkins, Y., Whiting, S. H., Bendell, J. C., & Bauer, T. M. (2019). CB-839, a glutaminase inhibitor, in combination with cabozantinib in patients with clear cell and papillary metastatic renal cell cancer (mRCC): Results of a phase I study. https://doi.org/10.1200/JCO.2019.37.7_suppl.549, *37*(7_suppl), 549–549. https://doi.org/10.1200/JCO.2019.37.7_SUPPL.549
- Merrill, M. J., Yeh, G. C., & Phang, J. M. (1989). Purified Human Erythrocyte Pyrroline-5-carboxylate Reductase: Preferential Oxidation of NADPH. *Journal of Biological Chemistry*, *264*(16), 9352–9358. [https://doi.org/10.1016/S0021-9258\(18\)60538-1](https://doi.org/10.1016/S0021-9258(18)60538-1)

- Millard, M., Gallagher, J. D., Olenyuk, B. Z., & Neamati, N. (2013). A selective mitochondrial-targeted chlorambucil with remarkable cytotoxicity in breast and pancreatic cancers. *Journal of Medicinal Chemistry*, 56(22), 9170–9179. https://doi.org/10.1021/JM4012438/SUPPL_FILE/JM4012438_SI_001.PDF
- Milne, K., Sun, J., Zaal, E. A., Mowat, J., Celie, P. H. N., Fish, A., Berkers, C. R., Forlani, G., Loayza-Puch, F., Jamieson, C., & Agami, R. (2019). A fragment-like approach to PYCR1 inhibition. *Bioorganic & Medicinal Chemistry Letters*, 29(18), 2626–2631. <https://doi.org/10.1016/j.bmcl.2019.07.047>
- Mithieux, G., Bady, I., Gautier, A., Croset, M., Rajas, F., & Zitoun, C. (2004). Induction of control genes in intestinal gluconeogenesis is sequential during fasting and maximal in diabetes. *American Journal of Physiology - Endocrinology and Metabolism*, 286(3), 49-3. <https://doi.org/10.1152/AJPENDO.00299.2003/ASSET/IMAGES/LARGE/ZH10030415770004.JPEG>
- Mitsuishi, Y., Taguchi, K., Kawatani, Y., Shibata, T., Nukiwa, T., Aburatani, H., Yamamoto, M., & Motohashi, H. (2012). Nrf2 Redirects Glucose and Glutamine into Anabolic Pathways in Metabolic Reprogramming. *Cancer Cell*, 22(1), 66–79. <https://doi.org/10.1016/J.CCR.2012.05.016/ATTACHMENT/E80F4DAB-A308-4B5C-8014-EC7D59CBB805/MMC8.XLS>
- Modaressi, S., Brechtel, K., Christ, B., & Jungermann, K. (1998). Human mitochondrial phosphoenolpyruvate carboxykinase 2 gene. Structure, chromosomal localization and tissue-specific expression. *The Biochemical Journal*, 333 (Pt 2)(Pt 2), 359–366. <https://doi.org/10.1042/BJ3330359>
- Mohamed Yusoff, A. A. (2015). Role of mitochondrial DNA mutations in brain tumors: A mini-review. *Journal of Cancer Research and Therapeutics*, 11(3), 535. <https://doi.org/10.4103/0973-1482.161925>
- Montal, E. D., Bhalla, K., Dewi, R. E., Ruiz, C. F., Haley, J. A., Ropell, A. E., Gordon, C., Haley, J. D., & Girnun, G. D. (2019a). Inhibition of phosphoenolpyruvate carboxykinase blocks lactate utilization and impairs tumor growth in colorectal cancer. *Cancer & Metabolism*, 7(1). <https://doi.org/10.1186/s40170-019-0199-6>
- Montal, E. D., Bhalla, K., Dewi, R. E., Ruiz, C. F., Haley, J. A., Ropell, A. E., Gordon, C., Haley, J. D., & Girnun, G. D. (2019b). Inhibition of phosphoenolpyruvate carboxykinase blocks lactate utilization and impairs tumor growth in colorectal cancer. *Cancer & Metabolism*, 7(1). <https://doi.org/10.1186/s40170-019-0199-6>
- Montal, E. D., Dewi, R., Bhalla, K., Ou, L., Hwang, B. J., Ropell, A. E., Gordon, C., Liu, W. J., DeBerardinis, R. J., Sudderth, J., Twaddel, W., Boros, L. G., Shroyer, K. R., Duraisamy, S., Drapkin, R., Powers, R. S., Rohde, J. M., Boxer, M. B., Wong, K. K., & Girnun, G. D. (2015). PEPCK Coordinates the Regulation of Central Carbon Metabolism to Promote Cancer Cell Growth. *Molecular Cell*, 60(4), 571–583. <https://doi.org/10.1016/J.MOLCEL.2015.09.025>
- Moreno-Felici, J., Hyroššová, P., Aragón, M., Rodríguez-Arévalo, S., García-Rovés, P. M., Escolano, C., & Perales, J. C. (2019). Phosphoenolpyruvate from Glycolysis and PEPCK Regulate Cancer Cell Fate by Altering Cytosolic Ca²⁺. *Cells*, 9(1), 18. <https://doi.org/10.3390/cells9010018>
- Mori, S., Chang, J. T., Andrechek, E. R., Matsumura, N., Baba, T., Yao, G., Kim, J. W., Gatzka, M., Murphy, S., & Nevins, J. R. (2009). Anchorage-independent cell growth signature identifies tumors with metastatic potential. *Oncogene* 2009 28:31, 28(31), 2796–2805. <https://doi.org/10.1038/onc.2009.139>
- Mostafa, T. M., El-Din, M. A. A., & Rashdan, A. R. (2022). Celecoxib as an adjuvant to chemotherapy for patients with metastatic colorectal cancer. *Saudi Medical Journal*, 43(1), 37–44. <https://doi.org/10.15537/SMJ.2022.43.1.20210574>

- Muenst, S., Läubli, H., Soysal, S. D., Zippelius, A., Tzankov, A., & Hoeller, S. (2016). The immune system and cancer evasion strategies: therapeutic concepts. *Journal of Internal Medicine*, 279(6), 541–562. <https://doi.org/10.1111/JOIM.12470>
- Mullarky, E., Lucki, N. C., Zavareh, R. B., Anglin, J. L., Gomes, A. P., Nicolay, B. N., Wong, J. C. Y., Christen, S., Takahashi, H., Singh, P. K., Blenis, J., Warren, J. D., Fendt, S. M., Asara, J. M., DeNicola, G. M., Lyssiotis, C. A., Lairson, L. L., & Cantley, L. C. (2016). Identification of a small molecule inhibitor of 3-phosphoglycerate dehydrogenase to target serine biosynthesis in cancers. *Proceedings of the National Academy of Sciences of the United States of America*, 113(7), 1778–1783. <https://doi.org/10.1073/PNAS.1521548113/-/DCSUPPLEMENTAL>
- Müller, J., Esso, K., Dargó, G., Könczöl, Á., & Balogh, G. T. (2015). Tuning the predictive capacity of the PAMPA-BBB model. *European Journal of Pharmaceutical Sciences*, 79, 53–60. <https://doi.org/10.1016/J.EJPS.2015.08.019>
- Müller, M., Mentel, M., Hellemond, J. J. van, Henze, K., Woehle, C., Gould, S. B., Yu, R.-Y., Giezen, M. van der, Tielens, A. G. M., & Martin, W. F. (2012). Biochemistry and Evolution of Anaerobic Energy Metabolism in Eukaryotes. *Microbiology and Molecular Biology Reviews: MMBR*, 76(2), 444. <https://doi.org/10.1128/MMBR.05024-11>
- Munir, R., Lisec, J., Swinnen, J. v., & Zaidi, N. (2019). Lipid metabolism in cancer cells under metabolic stress. *British Journal of Cancer* 2019 120:12, 120(12), 1090–1098. <https://doi.org/10.1038/s41416-019-0451-4>
- Murray, C. W., Auton, T. R., & Eldridge, M. D. (1998). Empirical scoring functions. II. The testing of an empirical scoring function for the prediction of ligand-receptor binding affinities and the use of Bayesian regression to improve the quality of the model. *Journal of Computer-Aided Molecular Design*, 12(5), 503–519. <https://doi.org/10.1023/A:1008040323669>
- Muthusamy, T., Cordes, T., Handzlik, M. K., You, L., Lim, E. W., Gengatharan, J., Pinto, A. F. M., Badur, M. G., Kolar, M. J., Wallace, M., Saghatelian, A., & Metallo, C. M. (2020). Serine restriction alters sphingolipid diversity to constrain tumour growth. *Nature* 2020 586:7831, 586(7831), 790–795. <https://doi.org/10.1038/S41586-020-2609-X>
- Nagao, A., Kobayashi, M., Koyasu, S., Chow, C. C. T., & Harada, H. (2019). HIF-1-Dependent Reprogramming of Glucose Metabolic Pathway of Cancer Cells and Its Therapeutic Significance. *International Journal of Molecular Sciences*, 20(2). <https://doi.org/10.3390/IJMS20020238>
- Nagy, J. A., Chang, S. H., Shih, S. C., Dvorak, A. M., & Dvorak, H. F. (2010). Heterogeneity of the Tumor Vasculature. *Seminars in Thrombosis and Hemostasis*, 36(3), 321. <https://doi.org/10.1055/S-0030-1253454>
- Nam, K. H. (2021). Molecular Dynamics—From Small Molecules to Macromolecules. *International Journal of Molecular Sciences* 2021, Vol. 22, Page 3761, 22(7), 3761. <https://doi.org/10.3390/IJMS22073761>
- Natarajan, S. K., Zhu, W., Liang, X., Zhang, L., Demers, A. J., Zimmerman, M. C., Simpson, M. A., & Becker, D. F. (2012). Proline dehydrogenase is essential for proline protection against hydrogen peroxide induced cell death. *Free Radical Biology & Medicine*, 53(5), 1181. <https://doi.org/10.1016/J.FREERADBIOMED.2012.07.002>
- Nathan Entner, B., & Doudoroff, M. (1952). *Glucose and gluconic acid oxidation of Pseudomonas Saccharophila**. [https://doi.org/10.1016/S0021-9258\(19\)52415-2](https://doi.org/10.1016/S0021-9258(19)52415-2)

- Nedelcu, A. M. (2020). The evolution of multicellularity and cancer: views and paradigms. *Biochemical Society Transactions*, 48(4), 1505–1518. <https://doi.org/10.1042/BST20190992>
- Negrini, S., Gorgoulis, V. G., & Halazonetis, T. D. (2010). Genomic instability — an evolving hallmark of cancer. *Nature Reviews Molecular Cell Biology* 2010 11:3, 11(3), 220–228. <https://doi.org/10.1038/NRM2858>
- Nelson, D. L., & Cox, M. M. (2000). Bioenergetics and metabolism. In *Lehninger Principles of Biochemistry* (Third). Worth Publishers.
- Newman, A. C., & Maddocks, O. D. K. (2017). One-carbon metabolism in cancer. *British Journal of Cancer* 2017 116:12, 116(12), 1499–1504. <https://doi.org/10.1038/bjc.2017.118>
- Nilsson, L. M., Plym Forshell, T. Z., Rimpi, S., Kreutzer, C., Pretsch, W., Bornkamm, G. W., & Nilsson, J. A. (2012). Mouse Genetics Suggests Cell-Context Dependency for Myc-Regulated Metabolic Enzymes during Tumorigenesis. *PLOS Genetics*, 8(3), e1002573. <https://doi.org/10.1371/JOURNAL.PGEN.1002573>
- Nocek, B., Chang, C., Li, H., Lezondra, L., Holzle, D., Collart, F., & Joachimiak, A. (2005). Crystal structures of delta1-pyrroline-5-carboxylate reductase from human pathogens *Neisseria meningitidis* and *Streptococcus pyogenes*. *Journal of Molecular Biology*, 354(1), 91–106. <https://doi.org/10.1016/J.JMB.2005.08.036>
- Nolfi-Donagan, D., Braganza, A., & Shiva, S. (2020). Mitochondrial electron transport chain: Oxidative phosphorylation, oxidant production, and methods of measurement. *Redox Biology*, 37, 101674. <https://doi.org/10.1016/J.REDOX.2020.101674>
- Nolte, H., MacVicar, T. D., Tellkamp, F., & Krüger, M. (2018). Instant Clue: A Software Suite for Interactive Data Visualization and Analysis. *Scientific Reports* 2018 8:1, 8(1), 1–8. <https://doi.org/10.1038/s41598-018-31154-6>
- Nordlie, R. C., & Lardy, H. A. (1963). Mammalian Liver Phosphoenolpyruvate Carboxykinase Activities. *Journal of Biological Chemistry*, 238(7), 2259–2263. [https://doi.org/10.1016/S0021-9258\(19\)67962-7](https://doi.org/10.1016/S0021-9258(19)67962-7)
- Nussinov, R., Zhang, M., Maloney, R., Liu, Y., Tsai, C.-J., & Jang, H. (2022). Allostery: Allosteric Cancer Drivers and Innovative Allosteric Drugs. *Journal of Molecular Biology*, 167569. <https://doi.org/10.1016/J.JMB.2022.167569>
- Nye, C. K., Hanson, R. W., & Kalhan, S. C. (2008). *Glyceroneogenesis Is the Dominant Pathway for Triglyceride Glycerol Synthesis in Vivo in the Rat **. <https://doi.org/10.1074/jbc.M804393200>
- Olivares, O., Mayers, J. R., Gouirand, V., Torrence, M. E., Gicquel, T., Borge, L., Lac, S., Roques, J., Lavaut, M. N., Berthezène, P., Rubis, M., Secq, V., Garcia, S., Moutardier, V., Lombardo, D., Iovanna, J. L., Tomasini, R., Guillaumond, F., vander Heiden, M. G., & Vasseur, S. (2017). Collagen-derived proline promotes pancreatic ductal adenocarcinoma cell survival under nutrient limited conditions. *Nature Communications* 2017 8:1, 8(1), 1–14. <https://doi.org/10.1038/ncomms16031>
- Olswang, Y., Cohen, H., Papo, O., Cassuto, H., Croniger, C. M., Hakimi, P., Tilghman, S. M., Hanson, R. W., & Reshef, L. (2002). A mutation in the peroxisome proliferator-activated receptor γ -binding site in the gene for the cytosolic form of phosphoenolpyruvate carboxykinase reduces adipose tissue size and fat content in mice. *Proceedings of the National Academy of Sciences*, 99(2), 625–630. <https://doi.org/10.1073/PNAS.022616299>
- O'Malley, D. M., Blair, C. K., Greenbaum, A., Wiggins, C. L., Rajput, A., Chiu, V. K., & Kinney, A. Y. (2022). Colorectal Cancer Survivors' Receptivity toward Genomic Testing and Targeted Use of Non-Steroidal

- Anti-Inflammatory Drugs to Prevent Cancer Recurrence. *Journal of Community Genetics* 2022, 1, 1–14. <https://doi.org/10.1007/S12687-021-00574-9>
- Osthus, R. C., Shim, H., Kim, S., Li, Q., Reddy, R., Mukherjee, M., Xu, Y., Wonsey, D., Lee, L. A., & Dang, C. v. (2000). Deregulation of Glucose Transporter 1 and Glycolytic Gene Expression by c-Myc *. *Journal of Biological Chemistry*, 275(29), 21797–21800. <https://doi.org/10.1074/JBC.C000023200>
- Ou, R., Zhang, X., Cai, J., Shao, X., Lv, M., Qiu, W., Xuan, X., Liu, J., Li, Z., & Xu, Y. (2016). Downregulation of pyrroline-5-carboxylate reductase-2 induces the autophagy of melanoma cells via AMPK/mTOR pathway. *Tumor Biology*, 37(5), 6485–6491. <https://doi.org/10.1007/S13277-015-3927-8/FIGURES/5>
- Ou, Y., Wang, S. J., Jiang, L., Zheng, B., & Gu, W. (2015). p53 Protein-mediated Regulation of Phosphoglycerate Dehydrogenase (PHGDH) Is Crucial for the Apoptotic Response upon Serine Starvation *. *Journal of Biological Chemistry*, 290(1), 457–466. <https://doi.org/10.1074/JBC.M114.616359>
- Overholtzer, M., Maillieux, A. A., Mouneimne, G., Normand, G., Schnitt, S. J., King, R. W., Cibas, E. S., & Brugge, J. S. (2007). A Nonapoptotic Cell Death Process, Entosis, that Occurs by Cell-in-Cell Invasion. *Cell*, 131(5), 966–979. <https://doi.org/10.1016/J.CELL.2007.10.040/ATTACHMENT/3921C7C2-3F58-4C7A-BC45-D6FEE3DD3AF6/MMC14.MOV>
- Pacold, M. E., Brimacombe, K. R., Chan, S. H., Rohde, J. M., Lewis, C. A., Swier, L. J. Y. M., Possemato, R., Chen, W. W., Sullivan, L. B., Fiske, B. P., Cho, S., Freinkman, E., Birsoy, K., Abu-Remaih, M., Shaul, Y. D., Liu, C. M., Zhou, M., Koh, M. J., Chung, H., ... Sabatini, D. M. (2016). A PHGDH inhibitor reveals coordination of serine synthesis and one-carbon unit fate. *Nature Chemical Biology* 2016 12:6, 12(6), 452–458. <https://doi.org/10.1038/NCHEMBIO.2070>
- Palm, W., Park, Y., Wright, K., Pavlova, N. N., Tuveson, D. A., & Thompson, C. B. (2015). The Utilization of Extracellular Proteins as Nutrients Is Suppressed by mTORC1. *Cell*, 162(2), 259–270. <https://doi.org/10.1016/J.CELL.2015.06.017/ATTACHMENT/A2515018-B254-48B8-BD00-70753D20D5F9/MMC1.PDF>
- Pandhare, J., Donald, S. P., Cooper, S. K., & Phang, J. M. (2009). Regulation and function of proline oxidase under nutrient stress. *Journal of Cellular Biochemistry*, 107(4), 759–768. <https://doi.org/10.1002/jcb.22174>
- Pankova, D., Jiang, Y., Chatzifrangkeskou, M., Vendrell, I., Buzzelli, J., Ryan, A., Brown, C., & O'Neill, E. (2019). RASSF1A controls tissue stiffness and cancer stem-like cells in lung adenocarcinoma. *The EMBO Journal*, 38(13), e100532. <https://doi.org/10.15252/EMBJ.2018100532>
- Park, J. W., Kim, S. C., Kim, W. K., Hong, J. P., Kim, K. H., Yeo, H. Y., Lee, J. Y., Kim, M. S., Kim, J. H., Yang, S. Y., Kim, D. Y., Oh, J. H., Cho, J. Y., & Yoo, B. C. (2014). Expression of phosphoenolpyruvate carboxykinase linked to chemoradiation susceptibility of human colon cancer cells. *BMC Cancer*, 14(1), 1–12. <https://doi.org/10.1186/1471-2407-14-160/FIGURES/6>
- Parsa, N. (2012). Environmental Factors Inducing Human Cancers. *Iranian Journal of Public Health*, 41(11), 1. </pmc/articles/PMC3521879/>
- Pascual, G., Avgustinova, A., Mejetta, S., Martín, M., Castellanos, A., Attolini, C. S. O., Berenguer, A., Prats, N., Toll, A., Hueto, J. A., Bescós, C., di Croce, L., & Benitah, S. A. (2016). Targeting metastasis-initiating cells through the fatty acid receptor CD36. *Nature* 2016 541:7635, 541(7635), 41–45. <https://doi.org/10.1038/NATURE20791>
- Patel, A. P., Tirosh, I., Trombetta, J. J., Shalek, A. K., Gillespie, S. M., Wakimoto, H., Cahill, D. P., Nahed, B. v., Curry, W. T., Martuza, R. L., Louis, D. N., Rozenblatt-Rosen, O., Suvà, M. L., Regev, A., & Bernstein, B. E.

- (2014). Single-cell RNA-seq highlights intratumoral heterogeneity in primary glioblastoma. *Science (New York, N.Y.)*, 344(6190), 1396–1401. <https://doi.org/10.1126/SCIENCE.1254257>
- Pathak, R. K., Marrache, S., Harn, D. A., & Dhar, S. (2014). Mito-DCA: A Mitochondria Targeted Molecular Scaffold for Efficacious Delivery of Metabolic Modulator Dichloroacetate. *ACS Chemical Biology*, 9(5), 1178. <https://doi.org/10.1021/CB400944Y>
- Patra, K. C., & Hay, N. (2014). The pentose phosphate pathway and cancer. *Trends in Biochemical Sciences*, 39(8), 347–354. <https://doi.org/10.1016/J.TIBS.2014.06.005>
- Pavlidis, S., Whitaker-Menezes, D., Castello-Cros, R., Flomenberg, N., Witkiewicz, A. K., Frank, P. G., Casimiro, M. C., Wang, C., Fortina, P., Addya, S., Pestell, R. G., Martinez-Outschoorn, U. E., Sotgia, F., & Lisanti, M. P. (2009). The reverse Warburg effect: Aerobic glycolysis in cancer associated fibroblasts and the tumor stroma. *Http://Dx.Doi.Org.Sire.Ub.Edu/10.4161/Cc.8.23.10238*, 8(23), 3984–4001. <https://doi.org/10.4161/CC.8.23.10238>
- Pavlova, N. N., & Thompson, C. B. (2016). The Emerging Hallmarks of Cancer Metabolism. *Cell Metabolism*, 23(1), 27–47. <https://doi.org/10.1016/J.CMET.2015.12.006>
- Perozzo, R., Folkers, G., & Scapozza, L. (2004). Thermodynamics of protein-ligand interactions: history, presence, and future aspects. *Journal of Receptor and Signal Transduction Research*, 24(1–2), 1–52. <https://doi.org/10.1081/RRS-120037896>
- Phang, J. M. (1985). The regulatory functions of proline and pyrroline-5-carboxylic acid. *Current Topics in Cellular Regulation*, 25(C), 91–132. <https://doi.org/10.1016/B978-0-12-152825-6.50008-4>
- Phang, J. M. (2019). Proline metabolism in cell regulation and cancer biology: Recent advances and hypotheses. In *Antioxidants and Redox Signaling* (Vol. 30, Issue 4, pp. 635–649). Mary Ann Liebert Inc. <https://doi.org/10.1089/ars.2017.7350>
- Phang, J. M., Liu, W., & Zabirnyk, O. (2010). Proline Metabolism and Microenvironmental Stress. *Annual Review of Nutrition*, 30, 441. <https://doi.org/10.1146/ANNUREV.NUTR.012809.104638>
- Phang, J. M., Yeh, G. C., & Hagedorn, C. H. (1981). The intercellular proline cycle. *Life Sciences*, 28(1), 53–58. [https://doi.org/10.1016/0024-3205\(81\)90365-9](https://doi.org/10.1016/0024-3205(81)90365-9)
- Pi, J., Leung, L., Xue, P., Wang, W., Hou, Y., Liu, D., Yehuda-Shnaidman, E., Lee, C., Lau, J., Kurtz, T. W., & Chan, J. Y. (2010). Deficiency in the Nuclear Factor E2-related Factor-2 Transcription Factor Results in Impaired Adipogenesis and Protects against Diet-induced Obesity. *The Journal of Biological Chemistry*, 285(12), 9292. <https://doi.org/10.1074/JBC.M109.093955>
- Pietranico, S. L., Foley, L. H., Huby, N., Yun, W., Dunten, P., Vermeulen, J., Wang, P., Toth, K., Ramsey, G., Gubler, M. lou, & Wertheimer, S. J. (2007). C-8 Modifications of 3-alkyl-1,8-dibenzylxanthines as inhibitors of human cytosolic phosphoenolpyruvate carboxykinase. *Bioorganic & Medicinal Chemistry Letters*, 17(14), 3835–3839. <https://doi.org/10.1016/J.BMCL.2007.05.013>
- Pinzi, L., & Rastelli, G. (2019). Molecular Docking: Shifting Paradigms in Drug Discovery. *International Journal of Molecular Sciences*, 20(18). <https://doi.org/10.3390/IJMS20184331>
- Poitout, V., & Robertson, R. P. (2008). Glucolipototoxicity: Fuel Excess and β -Cell Dysfunction. *Endocrine Reviews*, 29(3), 351–366. <https://doi.org/10.1210/ER.2007-0023>
- Pons-Tostivint, E., Thibault, B., & Guillermet-Guibert, J. (2017). Targeting PI3K Signaling in Combination Cancer Therapy. *Trends in Cancer*, 3(6), 454–469. <https://doi.org/10.1016/J.TRECAN.2017.04.002>

- Possemato, R., Marks, K. M., Shaul, Y. D., Pacold, M. E., Kim, D., Birsoy, K., Sethumadhavan, S., Woo, H. K., Jang, H. G., Jha, A. K., Chen, W. W., Barrett, F. G., Stransky, N., Tsun, Z. Y., Cowley, G. S., Barretina, J., Kalaany, N. Y., Hsu, P. P., Ottina, K., ... Sabatini, D. M. (2011). Functional genomics reveal that the serine synthesis pathway is essential in breast cancer. *Nature* 2011 476:7360, 476(7360), 346–350. <https://doi.org/10.1038/nature10350>
- Ravez, S., Corbet, C., Spillier, Q., Dutu, A., Robin, A. D., Mullarky, E., Cantley, L. C., Feron, O., & Frédérick, R. (2017). α -Ketothioamide Derivatives: A Promising Tool to Interrogate Phosphoglycerate Dehydrogenase (PHGDH). *Journal of Medicinal Chemistry*, 60(4), 1591–1597. https://doi.org/10.1021/ACS.JMEDCHEM.6B01166/SUPPL_FILE/JM6B01166_SI_002.CSV
- Ravez, S., Spillier, Q., Marteau, R., Feron, O., & Frédérick, R. (2017). Challenges and Opportunities in the Development of Serine Synthetic Pathway Inhibitors for Cancer Therapy. *Journal of Medicinal Chemistry*, 60(4), 1227–1237. https://doi.org/10.1021/ACS.JMEDCHEM.6B01167/SUPPL_FILE/JM6B01167_SI_001.PDF
- Reimand, J., Isserlin, R., Voisin, V., Kucera, M., Tannus-Lopes, C., Rostamianfar, A., Wadi, L., Meyer, M., Wong, J., Xu, C., Merico, D., & Bader, G. D. (2019). Pathway enrichment analysis and visualization of omics data using g:Profiler, GSEA, Cytoscape and EnrichmentMap. *Nature Protocols* 2019 14:2, 14(2), 482–517. <https://doi.org/10.1038/s41596-018-0103-9>
- Ren, Z., Wang, Y., Ren, Y., Zhang, Z., Gu, W., Wu, Z., Chen, L., Mou, L., Li, R., Yang, H., & Dai, Y. (2017). Enhancement of porcine intramuscular fat content by overexpression of the cytosolic form of phosphoenolpyruvate carboxykinase in skeletal muscle. *Scientific Reports* 2017 7:1, 7(1), 1–7. <https://doi.org/10.1038/srep43746>
- Revathidevi, S., & Munirajan, A. K. (2019). Akt in cancer: Mediator and more. *Seminars in Cancer Biology*, 59, 80–91. <https://doi.org/10.1016/J.SEMCANCER.2019.06.002>
- Roberti, A., Fernández, A. F., & Fraga, M. F. (2021). Nicotinamide N-methyltransferase: At the crossroads between cellular metabolism and epigenetic regulation. *Molecular Metabolism*, 45, 101165. <https://doi.org/10.1016/J.MOLMET.2021.101165>
- Robinson, B. H., & Oei, J. (1975). 3-Mercaptopicolinic acid, a preferential inhibitor of the cytosolic phosphoenolpyruvate carboxykinase. *FEBS Letters*, 58(1–2), 12–15. [https://doi.org/10.1016/0014-5793\(75\)80214-6](https://doi.org/10.1016/0014-5793(75)80214-6)
- Rosella, G., Zajac, J. D., Baker, L., Kaczmarczyk, S. J., Andrikopoulos, S., Adams, T. E., & Proietto, J. (1995). Impaired glucose tolerance and increased weight gain in transgenic rats overexpressing a non-insulin-responsive phosphoenolpyruvate carboxykinase gene. *Molecular Endocrinology (Baltimore, Md.)*, 9(10), 1396–1404. <https://doi.org/10.1210/MEND.9.10.8544847>
- Rossmann, M. G., Moras, D., & Olsen, K. W. (1974). Chemical and biological evolution of a nucleotide-binding protein. *Nature* 1974 250:5463, 250(5463), 194–199. <https://doi.org/10.1038/250194A0>
- Rothberg, J. M., Bailey, K. M., Wojtkowiak, J. W., Ben-Nun, Y., Bogyo, M., Weber, E., Moin, K., Blum, G., Mattingly, R. R., Gillies, R. J., & Sloane, B. F. (2013). Acid-Mediated Tumor Proteolysis: Contribution of Cysteine Cathepsins. *Neoplasia (New York, N.Y.)*, 15(10), 1125. <https://doi.org/10.1593/NEO.13946>
- Rotondo, F., Ho-Palma, A. C., Remesar, X., Fernández-López, J. A., Romero, M. D. M., & Alemany, M. (2017). Glycerol is synthesized and secreted by adipocytes to dispose of excess glucose, via glycerogenesis and increased acyl-glycerol turnover. *Scientific Reports* 2017 7:1, 7(1), 1–14. <https://doi.org/10.1038/s41598-017-09450-4>

- Rudy, B. C., & Senkowski, B. Z. (2022). Fluorouracil. *Analytical Profiles of Drug Substances and Excipients*, 2(C), 221–244. [https://doi.org/10.1016/S0099-5428\(08\)60041-6](https://doi.org/10.1016/S0099-5428(08)60041-6)
- Ruiz-Carmona, S., Alvarez-Garcia, D., Foloppe, N., Garmendia-Doval, A. B., Juhos, S., Schmidtke, P., Barril, X., Hubbard, R. E., & Morley, S. D. (2014). rDock: A Fast, Versatile and Open Source Program for Docking Ligands to Proteins and Nucleic Acids. *PLOS Computational Biology*, 10(4), e1003571. <https://doi.org/10.1371/JOURNAL.PCBI.1003571>
- Ruszkowski, M., Nocek, B., Forlani, G., & Dauter, Z. (2015). The structure of Medicago truncatula $\delta(1)$ -pyrroline-5-carboxylate reductase provides new insights into regulation of proline biosynthesis in plants. *Frontiers in Plant Science*, 6(October). <https://doi.org/10.3389/FPLS.2015.00869>
- Ryan, E. A., Imes, S., & Wallace, C. (2004). Short-Term Intensive Insulin Therapy in Newly Diagnosed Type 2 Diabetes. *Diabetes Care*, 27(5), 1028–1032. <https://doi.org/10.2337/DIACARE.27.5.1028>
- Rysman, E., Brusselmans, K., Scheys, K., Timmermans, L., Derua, R., Munck, S., van Veldhoven, P. P., Waltregny, D., Daniëls, V. W., Machiels, J., Vanderhoydonc, F., Smans, K., Waelkens, E., Verhoeven, G., & Swinnen, J. v. (2010). De novo Lipogenesis Protects Cancer Cells from Free Radicals and Chemotherapeutics by Promoting Membrane Lipid Saturation. *Cancer Research*, 70(20), 8117–8126. <https://doi.org/10.1158/0008-5472.CAN-09-3871>
- Sahu, N., Cruz, D. dela, Gao, M., Classon, M., Hatzivassiliou, G., Settleman, J., Sandoval, W., Haverty, P. M., Liu, J., Stephan, J.-P., & Haley, B. (2016). Proline Starvation Induces Unresolved ER Stress and Hinders mTORC1-Dependent Tumorigenesis Cell Metabolism Proline Starvation Induces Unresolved ER Stress and Hinders mTORC1-Dependent Tumorigenesis. *Cell Metabolism*, 24, 753–761. <https://doi.org/10.1016/j.cmet.2016.08.008>
- Salsbury, F. R., & Jr. (2010). Molecular Dynamics Simulations of Protein Dynamics and their relevance to drug discovery. *Current Opinion in Pharmacology*, 10(6), 738. <https://doi.org/10.1016/J.COPH.2010.09.016>
- Samanta, D., Park, Y., Andrabi, S. A., Shelton, L. M., Gilkes, D. M., & Semenza, G. L. (2016). PHGDH Expression Is Required for Mitochondrial Redox Homeostasis, Breast Cancer Stem Cell Maintenance, and Lung Metastasis. *Cancer Research*, 76(15), 4430–4442. <https://doi.org/10.1158/0008-5472.CAN-16-0530>
- Sang, S., Zhang, C., & Shan, J. (2019). Pyrroline-5-Carboxylate Reductase 1 Accelerates the Migration and Invasion of Non-small Cell Lung Cancer In Vitro. *Cancer Biotherapy and Radiopharmaceuticals*, 34(6), 380–387. <https://doi.org/10.1089/CBR.2019.2782/ASSET/IMAGES/LARGE/FIGURE5.JPEG>
- Sattar Alaqbi, S., Burke, L., Guterman, I., Green, C., West, K., Palacios-Gallego, R., Cai, H., Alexandrou, C., Ni Moe Myint, N., Parrott, E., Howells, L. M., Higgins, J. A., L JonesID, D. J., Singh, R., Britton, R. G., TufarelliID, C., Thomas, A., & RufiniID, A. (2022). Increased mitochondrial proline metabolism sustains proliferation and survival of colorectal cancer cells. *PLOS ONE*, 17(2), e0262364. <https://doi.org/10.1371/JOURNAL.PONE.0262364>
- Scalise, M., Pochini, L., Galluccio, M., Console, L., & Indiveri, C. (2017). Glutamine transport and mitochondrial metabolism in cancer cell growth. *Frontiers in Oncology*, 7(DEC), 306. <https://doi.org/10.3389/FONC.2017.00306/BIBTEX>
- Schoolwerth, A. C., Smith, B. C., & Culpepper, R. M. (1988). Renal gluconeogenesis. *Mineral and Electrolyte Metabolism*, 14(6), 347–361. <https://pubmed.ncbi.nlm.nih.gov/3068502/>
- Schwörer, S., Berisa, M., Violante, S., Qin, W., Zhu, J., Hendrickson, R. C., Cross, J. R., & Thompson, C. B. (2020). Proline biosynthesis is a vent for TGF β -induced mitochondrial redox stress. *The EMBO Journal*, 39(8), e103334. <https://doi.org/10.15252/EMBJ.2019103334>

- Sehn, L. H., & Gascoyne, R. D. (2015). Diffuse large B-cell lymphoma: optimizing outcome in the context of clinical and biologic heterogeneity. *Blood*, *125*(1), 22–32. <https://doi.org/10.1182/BLOOD-2014-05-577189>
- Sellers, K., Fox, M. P., Li, M. B., Slone, S. P., Higashi, R. M., Miller, D. M., Wang, Y., Yan, J., Yuneva, M. O., Deshpande, R., Lane, A. N., & Fan, T. W. M. (2015). Pyruvate carboxylase is critical for non-small-cell lung cancer proliferation. *The Journal of Clinical Investigation*, *125*(2), 687–698. <https://doi.org/10.1172/JCI72873>
- Semakova, J., Hyroššová, P., Méndez-Lucas, A., Cutz, E., Bermudez, J., Burgess, S., Alcántara, S., & Perales, J. C. (2017). PEPCK-C reexpression in the liver counters neonatal hypoglycemia in Pck1 del/del mice, unmasking role in non-gluconeogenic tissues. *Journal of Physiology and Biochemistry*, *73*(1), 89–98. <https://doi.org/10.1007/S13105-016-0528-Y/FIGURES/6>
- Semenza, G. L., Roth, P. H., Fang, H. M., & Wang, G. L. (1994). Transcriptional regulation of genes encoding glycolytic enzymes by hypoxia-inducible factor 1. *Journal of Biological Chemistry*, *269*(38), 23757–23763. [https://doi.org/10.1016/S0021-9258\(17\)31580-6](https://doi.org/10.1016/S0021-9258(17)31580-6)
- Shay, J. W., & Wright, W. E. (2005). Senescence and immortalization: role of telomeres and telomerase. *Carcinogenesis*, *26*(5), 867–874. <https://doi.org/10.1093/CARCIN/BGH296>
- She, P., Burgess, S. C., Shiota, M., Flakoll, P., Donahue, E. P., Malloy, C. R., Sherry, A. D., & Magnuson, M. A. (2003). Mechanisms by which liver-specific PEPCK knockout mice preserve euglycemia during starvation. *Diabetes*, *52*(7), 1649–1654. <https://doi.org/10.2337/DIABETES.52.7.1649>
- She, P., Shiota, M., Shelton, K. D., Chalkley, R., Postic, C., & Magnuson, M. A. (2000). Phosphoenolpyruvate Carboxykinase Is Necessary for the Integration of Hepatic Energy Metabolism. *Molecular and Cellular Biology*, *20*(17), 6508–6517. <https://doi.org/10.1128/MCB.20.17.6508-6517.2000/ASSET/C74C0624-29C3-41EF-A444-D602B99AF8/ASSETS/GRAPHIC/MB1700549006.JPEG>
- Shenoy, A., Belugali Nataraj, N., Perry, G., Loayza Puch, F., Nagel, R., Marin, I., Balint, N., Bossel, N., Pavlovsky, A., Barshack, I., Kaufman, B., Agami, R., Yarden, Y., Dadiani, M., & Geiger, T. (2020). Proteomic patterns associated with response to breast cancer neoadjuvant treatment. *Molecular Systems Biology*, *16*(9), e9443. <https://doi.org/10.15252/msb.20209443>
- Shi, H., Fang, R., Li, Y., Li, L., Zhang, W., Wang, H., Chen, F., Zhang, S., Zhang, X., & Ye, L. (2016). The oncoprotein HBXIP suppresses gluconeogenesis through modulating PCK1 to enhance the growth of hepatoma cells. *Cancer Letters*, *382*(2), 147–156. <https://doi.org/10.1016/J.CANLET.2016.08.025>
- Shi, Y., Felley-Bosco, E., Marti, T. M., Orłowski, K., Pruschy, M., & Stahel, R. A. (2012). Starvation-induced activation of ATM/Chk2/p53 signaling sensitizes cancer cells to cisplatin. *BMC Cancer*, *12*(1), 1–10. <https://doi.org/10.1186/1471-2407-12-571/FIGURES/6>
- Shim, H., Dolde, C., Lewis, B. C., Wu, C. S., Dang, G., Jungmann, R. A., Dalla-Favera, R., & Dang, C. v. (1997). c-Myc transactivation of LDH-A: Implications for tumor metabolism and growth. *Proceedings of the National Academy of Sciences*, *94*(13), 6658–6663. <https://doi.org/10.1073/PNAS.94.13.6658>
- Singh, A., Faccenda, D., & Campanella, M. (2021). Pharmacological advances in mitochondrial therapy. *EBioMedicine*, *65*. <https://doi.org/10.1016/J.EBIOM.2021.103244>
- Singh, N., Baby, D., Rajguru, J., Patil, P., Thakkannavar, S., & Pujari, V. (2019). Inflammation and Cancer. *Annals of African Medicine*, *18*(3), 121. https://doi.org/10.4103/AAM.AAM_56_18

- Śledź, P., & Caflisch, A. (2018). Protein structure-based drug design: from docking to molecular dynamics. *Current Opinion in Structural Biology*, *48*, 93–102. <https://doi.org/10.1016/J.SBI.2017.10.010>
- Smith, R. A. J., Porteous, C. M., Gane, A. M., & Murphy, M. P. (2003). Delivery of bioactive molecules to mitochondria in vivo. *Proceedings of the National Academy of Sciences of the United States of America*, *100*(9), 5407. <https://doi.org/10.1073/PNAS.0931245100>
- Smolle, E., Leko, P., Stacher-Priehse, E., Brcic, L., El-Heliebi, A., Hofmann, L., Quehenberger, F., Hrzenjak, A., Popper, H. H., Olschewski, H., & Leithner, K. (2020). Distribution and prognostic significance of gluconeogenesis and glycolysis in lung cancer. *Molecular Oncology*. <https://doi.org/10.1002/1878-0261.12780>
- Smolle, E., Leko, P., Stacher-Priehse, E., Brcic, L., El-Heliebi, A., Hofmann, L., Quehenberger, F., Hrzenjak, A., Popper, H. H., Olschewski, H., & Leithner, K. (2020). Distribution and prognostic significance of gluconeogenesis and glycolysis in lung cancer. *Molecular Oncology*, *14*(11), 2853–2867. <https://doi.org/10.1002/1878-0261.12780>
- Sodhi, A., Montaner, S., Miyazaki, H., & Gutkind, J. S. (2001). MAPK and Akt Act Cooperatively but Independently on Hypoxia Inducible Factor-1 α in rasV12 Upregulation of VEGF. *Biochemical and Biophysical Research Communications*, *287*(1), 292–300. <https://doi.org/10.1006/BBRC.2001.5532>
- Sok, M., Šentjerc, M., Schara, M., Stare, J., & Rott, T. (2002). Cell membrane fluidity and prognosis of lung cancer. *The Annals of Thoracic Surgery*, *73*(5), 1567–1571. [https://doi.org/10.1016/S0003-4975\(02\)03458-6](https://doi.org/10.1016/S0003-4975(02)03458-6)
- Söling, H. -D, Kleineke, J., Janson, G., Kuhn, A., & Willms, B. (1973). Relationship between intracellular distribution of phosphoenolpyruvate carboxykinase, regulation of gluconeogenesis, and energy cost of glucose formation. *European Journal of Biochemistry*, *37*(2), 233–243. <https://doi.org/10.1111/J.1432-1033.1973.TB02980.X>
- Sonveaux, P., Copetti, T., de Saedeleer, C. J., Végran, F., Verrax, J., Kennedy, K. M., Moon, E. J., Dhup, S., Danhier, P., Frérart, F., Gallez, B., Ribeiro, A., Michiels, C., Dewhirst, M. W., & Feron, O. (2012). Targeting the Lactate Transporter MCT1 in Endothelial Cells Inhibits Lactate-Induced HIF-1 Activation and Tumor Angiogenesis. *PLOS ONE*, *7*(3), e33418. <https://doi.org/10.1371/JOURNAL.PONE.0033418>
- Sonveaux, P., Végran, F., Schroeder, T., Wergin, M. C., Verrax, J., Rabbani, Z. N., de Saedeleer, C. J., Kennedy, K. M., Diepart, C., Jordan, B. F., Kelley, M. J., Gallez, B., Wahl, M. L., Feron, O., & Dewhirst, M. W. (2008). Targeting lactate-fueled respiration selectively kills hypoxic tumor cells in mice. *The Journal of Clinical Investigation*, *118*(12), 3930. <https://doi.org/10.1172/JCI36843>
- Soucek, L., Whitfield, J., Martins, C. P., Finch, A. J., Murphy, D. J., Sodik, N. M., Karnezis, A. N., Swigart, L. B., Nasi, S., & Evan, G. I. (2008). Modelling Myc inhibition as a cancer therapy. *Nature* *2008* *455*:7213, 455(7213), 679–683. <https://doi.org/10.1038/NATURE07260>
- Stark, R., Guebre-Egziabher, F., Zhao, X., Feriod, C., Dong, J., Alves, T. C., Ioja, S., Pongratz, R. L., Bhanot, S., Roden, M., Cline, G. W., Shulman, G. I., & Kibbey, R. G. (2014). A role for mitochondrial phosphoenolpyruvate carboxykinase (PEPCK-M) in the regulation of hepatic gluconeogenesis. *The Journal of Biological Chemistry*, *289*(11), 7257–7263. <https://doi.org/10.1074/JBC.C113.544759>
- Stark, R., & Kibbey, R. G. (2014). The mitochondrial isoform of phosphoenolpyruvate carboxykinase (PEPCK-M) and glucose homeostasis: has it been overlooked? *Biochimica et Biophysica Acta*, *1840*(4), 1313. <https://doi.org/10.1016/J.BBAGEN.2013.10.033>

- Stark, R., Pasquel, F., Turcu, A., Pongratz, R. L., Roden, M., Cline, G. W., Shulman, G. I., & Kibbey, R. G. (2009). Phosphoenolpyruvate cycling via mitochondrial phosphoenolpyruvate carboxykinase links anaplerosis and mitochondrial GTP with insulin secretion. *The Journal of Biological Chemistry*, *284*(39), 26578–26590. <https://doi.org/10.1074/JBC.M109.011775>
- Stern, R., Shuster, S., Neudecker, B. A., & Formby, B. (2002). Lactate Stimulates Fibroblast Expression of Hyaluronan and CD44: The Warburg Effect Revisited. *Experimental Cell Research*, *276*(1), 24–31. <https://doi.org/10.1006/EXCR.2002.5508>
- Stiffin, R. M., Sullivan, S. M., Carlson, G. M., & Holyoak, T. (2008). Differential Inhibition of Cytosolic PEPCK by Substrate Analogues. Kinetic and Structural Characterization of Inhibitor Recognition. *Biochemistry*, *47*(7), 2099–2109. <https://doi.org/10.1021/BI7020662>
- Still, E. R., & Yuneva, M. O. (2017). Hopefully devoted to Q: targeting glutamine addiction in cancer. *British Journal of Cancer* *2017 116:11*, *116*(11), 1375–1381. <https://doi.org/10.1038/bjc.2017.113>
- Stolzing, A., & Grune, T. (2004). Neuronal apoptotic bodies: phagocytosis and degradation by primary microglial cells. *The FASEB Journal*, *18*(6), 743–745. <https://doi.org/10.1096/FJ.03-0374FJE>
- Sullivan, L. B., Gui, D. Y., Hosios, A. M., Bush, L. N., Freinkman, E., Heiden, M. G. vander, & vander Heiden, M. G. (2015). Supporting Aspartate Biosynthesis Is an Essential Function of Respiration in Proliferating Cells Article Supporting Aspartate Biosynthesis Is an Essential Function of Respiration in Proliferating Cells. *Cell*, *162*, 552–563. <https://doi.org/10.1016/j.cell.2015.07.017>
- Sullivan, M. R., Mattaini, K. R., Dennstedt, E. A., Bosenberg, M. W., Lewis, C. A., Vander, M. G., & Correspondence, H. (2019). Increased Serine Synthesis Provides an Advantage for Tumors Arising in Tissues Where Serine Levels Are Limiting. *Cell Metabolism*, *30*. <https://doi.org/10.1016/j.cmet.2019.02.015>
- Sullivan, M. R., Mattaini, K. R., Dennstedt, E. A., Nguyen, A. A., Sivanand, S., Reilly, M. F., Meeth, K., Muir, A., Darnell, A. M., Bosenberg, M. W., Lewis, C. A., & vander Heiden, M. G. (2019). Increased Serine Synthesis Provides an Advantage for Tumors Arising in Tissues Where Serine Levels Are Limiting. *Cell Metabolism*, *29*(6), 1410–1421.e4. <https://doi.org/10.1016/J.CMET.2019.02.015>
- Sullivan, M. R., & vander Heiden, M. G. (2019). Determinants of nutrient limitation in cancer. *Critical Reviews in Biochemistry and Molecular Biology*, *54*(3), 193. <https://doi.org/10.1080/10409238.2019.1611733>
- Sun, Q., Luo, T., Ren, Y., Florey, O., Shirasawa, S., Sasazuki, T., Robinson, D. N., & Overholtzer, M. (2014). Competition between human cells by entosis. *Cell Research* *2014 24:11*, *24*(11), 1299–1310. <https://doi.org/10.1038/cr.2014.138>
- Swisa, A., Glaser, B., & Dor, Y. (2017). Metabolic stress and compromised identity of pancreatic beta cells. *Frontiers in Genetics*, *8*(FEB), 21. <https://doi.org/10.3389/FGENE.2017.00021/BIBTEX>
- Sylvia Grünewald, Michael Steckel, Manfred Husemann, Hanna Meyer, Weiping Han, & Zhaobing Ding. (2019). *US20190031773A1 - Inhibitors and antagonists of human pycr1 - Google Patents*. <https://patents.google.com/patent/US20190031773A1/en>
- Tajan, M., Hennequart, M., Cheung, E. C., Zani, F., Hock, A. K., Legrave, N., Maddocks, O. D. K., Ridgway, R. A., Athineos, D., Suárez-Bonnet, A., Ludwig, R. L., Novellasdemunt, L., Angelis, N., Li, V. S. W., Vlachogiannis, G., Valeri, N., Mainolfi, N., Suri, V., Friedman, A., ... Vousden, K. H. (2021). Serine synthesis pathway inhibition cooperates with dietary serine and glycine limitation for cancer therapy. *Nature Communications* *2021 12:1*, *12*(1), 1–16. <https://doi.org/10.1038/s41467-020-20223-y>

- Tang, Y., Zhang, Y., Wang, C., Sun, Z., Li, L., Cheng, S., & Zhou, W. (2018). Overexpression of PCK1 Gene Antagonizes Hepatocellular Carcinoma Through the Activation of Gluconeogenesis and Suppression of Glycolysis Pathways. *Cellular Physiology and Biochemistry: International Journal of Experimental Cellular Physiology, Biochemistry, and Pharmacology*, 47(1), 344–355. <https://doi.org/10.1159/000489811>
- Tanner, J. J. (2019). Structural Biology of Proline Catabolic Enzymes. *Antioxidants & Redox Signaling*, 30(4), 650. <https://doi.org/10.1089/ARS.2017.7374>
- Tanner, J. J., Fendt, S. M., & Becker, D. F. (2018). The Proline Cycle As a Potential Cancer Therapy Target. *Biochemistry*, 57(25), 3433–3444. <https://doi.org/10.1021/acs.biochem.8b00215>
- Tarrado-Castellarnau, M., Atauri, P. de, Cascante, M., Tarrado-Castellarnau, M., Atauri, P. de, & Cascante, M. (2016). Oncogenic regulation of tumor metabolic reprogramming. *Oncotarget*, 7(38), 62726–62753. <https://doi.org/10.18632/ONCOTARGET.10911>
- Teague, J., Gyte, A., Peel, J. E., Young, K. C., Loxham, S. J. G., Mayers, R. M., & Poucher, S. M. (2011). Reversibility of hyperglycaemia and islet abnormalities in the high fat-fed female ZDF rat model of type 2 diabetes. *Journal of Pharmacological and Toxicological Methods*, 63(1), 15–23. <https://doi.org/10.1016/J.VASCN.2010.04.001>
- Teperino, R., Schoonjans, K., & Auwerx, J. (2010). Histone Methyl Transferases and Demethylases; Can They Link Metabolism and Transcription? *Cell Metabolism*, 12(4), 321–327. <https://doi.org/10.1016/J.CMET.2010.09.004>
- Tibbetts, A. S., & Appling, D. R. (2010). Compartmentalization of Mammalian Folate-Mediated One-Carbon Metabolism. *Http://Dx.Doi.Org.Sire.Ub.Edu/10.1146/Annurev.Nutr.012809.104810*, 30, 57–81. <https://doi.org/10.1146/ANNUREV.NUTR.012809.104810>
- Tilghman, S. M., Hanson, R. W., Reshef, L., Hopgood, M. F., & Ballard, F. J. (1974). Rapid Loss of Translatable Messenger RNA of Phosphoenolpyruvate Carboxykinase During Glucose Repression in Liver. *Proceedings of the National Academy of Sciences of the United States of America*, 71(4), 1304. <https://doi.org/10.1073/PNAS.71.4.1304>
- Tonelli, C., Chio, I. I. C., & Tuveson, D. A. (2018). Transcriptional Regulation by Nrf2. In *Antioxidants and Redox Signaling* (Vol. 29, Issue 17, pp. 1727–1745). Mary Ann Liebert Inc. <https://doi.org/10.1089/ars.2017.7342>
- US National Library of Medicine. (2022). *CB-839 clinical trials - ClinicalTrials.gov*. <https://clinicaltrials.gov/ct2/results?recrs=&cond=&term=cb-839&cntry=&state=&city=&dist=>
- Utter, M. F., & Kurahashi, K. (1953). Mechanism of action of oxalacetic carboxylase from liver. *Journal of the American Chemical Society*, 75(3), 758. <https://doi.org/10.1021/JA01099A522>
- Valastyan, S., & Weinberg, R. A. (2011). Tumor Metastasis: Molecular Insights and Evolving Paradigms. *Cell*, 147(2), 275–292. <https://doi.org/10.1016/J.CELL.2011.09.024>
- Valera, A., Pujol, A., Pelegrin, M., & Bosch, F. (1994). Transgenic mice overexpressing phosphoenolpyruvate carboxykinase develop non-insulin-dependent diabetes mellitus. *Proceedings of the National Academy of Sciences*, 91(19), 9151–9154. <https://doi.org/10.1073/PNAS.91.19.9151>
- vander Heiden, M. G., & DeBerardinis, R. J. (2017). Understanding the Intersections between Metabolism and Cancer Biology. *Cell*, 168(4), 657–669. <https://doi.org/10.1016/J.CELL.2016.12.039>

- Vanhaesebroeck, B., Guillermet-Guibert, J., Graupera, M., & Bilanges, B. (2010). The emerging mechanisms of isoform-specific PI3K signalling. *Nature Reviews Molecular Cell Biology* 2010 11:5, 11(5), 329–341. <https://doi.org/10.1038/NRM2882>
- Vettore, L. A., Westbrook, R. L., & Tennant, D. A. (2021). Proline metabolism and redox; maintaining a balance in health and disease. *Amino Acids* 2021, 1, 1–10. <https://doi.org/10.1007/S00726-021-03051-2>
- Vincent, E. E., Sergushichev, A., Griss, T., Gingras, M. C., Samborska, B., Ntimbane, T., Coelho, P. P., Blagih, J., Raissi, T. C., Choinière, L., Bridon, G., Loginicheva, E., Flynn, B. R., Thomas, E. C., Tavaré, J. M., Avizonis, D., Pause, A., Elder, D. J. E., Artyomov, M. N., & Jones, R. G. (2015). Mitochondrial Phosphoenolpyruvate Carboxykinase Regulates Metabolic Adaptation and Enables Glucose-Independent Tumor Growth. *Molecular Cell*, 60(2), 195–207. <https://doi.org/10.1016/J.MOLCEL.2015.08.013>
- Wagner, A. D., Grothe, W., Haerting, J., Kleber, G., Grothey, A., & Fleig, W. E. (2006). Chemotherapy in advanced gastric cancer: A systematic review and meta-analysis based on aggregate data. *Journal of Clinical Oncology*, 24(18), 2903–2909. <https://doi.org/10.1200/JCO.2005.05.0245>
- Waldrop, G. L. (2009). A qualitative approach to enzyme inhibition. *Biochemistry and Molecular Biology Education*, 37(1), 11–15. <https://doi.org/10.1002/BMB.20243>
- Walling, J. (2006). From methotrexate to pemetrexed and beyond. A review of the pharmacodynamic and clinical properties of antifolates. *Investigational New Drugs* 2006 24:1, 24(1), 37–77. <https://doi.org/10.1007/S10637-005-4541-1>
- Wan, B., Lanoue, K. F., Cheung, J. Y., & Scaduto, R. C. \$. (1989). Regulation of Citric Acid Cycle by Calcium*. *Journal of Biological Chemistry*, 264(23), 13430–13439. [https://doi.org/10.1016/S0021-9258\(18\)80015-1](https://doi.org/10.1016/S0021-9258(18)80015-1)
- Wang, D., & Dubois, R. N. (2010). Eicosanoids and cancer. *Nature Reviews Cancer* 2010 10:3, 10(3), 181–193. <https://doi.org/10.1038/NRC2809>
- Wang, D., Wang, L., Zhang, Y., Yan, Z., Liu, L., & Chen, G. (2019). PYCR1 promotes the progression of non-small-cell lung cancer under the negative regulation of miR-488. *Biomedicine & Pharmacotherapy*, 111, 588–595. <https://doi.org/10.1016/J.BIOPHA.2018.12.089>
- Wang, X., Decker, C. C., Zechner, L., Krstin, S., & Wink, M. (2019). In vitro wound healing of tumor cells: Inhibition of cell migration by selected cytotoxic alkaloids. *BMC Pharmacology and Toxicology*, 20(1), 1–12. <https://doi.org/10.1186/S40360-018-0284-4/FIGURES/4>
- Wang, Z., & Dong, C. (2019). Gluconeogenesis in Cancer: Function and Regulation of PEPCK, FBPase, and G6Pase. In *Trends in Cancer* (Vol. 5, Issue 1, pp. 30–45). Cell Press. <https://doi.org/10.1016/j.trecan.2018.11.003>
- Warburg, O. (1956). On the origin of cancer cells. *Science*, 123(3191), 309–314. <https://doi.org/10.1126/SCIENCE.123.3191.309/ASSET/A8D38B53-799F-4009-AAD3-E77CEF33D301/ASSETS/SCIENCE.123.3191.309.FP.PNG>
- Warburg, O., Wind, F., & Negelein, E. (1927). THE METABOLISM OF TUMORS IN THE BODY. *The Journal of General Physiology*, 8(6), 519–530. <https://doi.org/10.1085/JGP.8.6.519>
- Watt, M. J., Clark, A. K., Selth, L. A., Haynes, V. R., Lister, N., Rebello, R., Porter, L. H., Niranjana, B., Whitby, S. T., Lo, J., Huang, C., Schittenhelm, R. B., Anderson, K. E., Furic, L., Wijayarathne, P. R., Matzaris, M., Montgomery, M. K., Papargiris, M., Norden, S., ... Taylor, R. A. (2019). Suppressing fatty acid uptake has

- therapeutic effects in preclinical models of prostate cancer. *Science Translational Medicine*, 11(478). https://doi.org/10.1126/SCITRANSLMED.AAU5758/SUPPL_FILE/AAU5758_TABLE_S2.XLSX
- Weber, M. M., Fottner, C., Liu, S. bin, Jung, M. C., Engelhardt, D., & Baretton, G. B. (2002). Overexpression of the insulin-like growth factor I receptor in human colon carcinomas. *Cancer*, 95(10), 2086–2095. <https://doi.org/10.1002/CNCR.10945>
- Weijin, F., Zhibin, X., Shengfeng, Z., Xiaoli, Y., Qijian, D., Jiayi, L., Qiumei, L., Yilong, C., Hua, M., Deyun, L., & Jiwen, C. (2019). The clinical significance of PYCR1 expression in renal cell carcinoma. *Medicine (United States)*, 98(28). <https://doi.org/10.1097/MD.00000000000016384>
- Weinberg, F., Hamanaka, R., Wheaton, W. W., Weinberg, S., Joseph, J., Lopez, M., Kalyanaraman, B., Mutlu, G. M., Budinger, G. R. S., & Chandel, N. S. (2010). Mitochondrial metabolism and ROS generation are essential for Kras-mediated tumorigenicity. *Proceedings of the National Academy of Sciences of the United States of America*, 107(19), 8788–8793. <https://doi.org/10.1073/PNAS.1003428107/-/DCSUPPLEMENTAL>
- Weinhouse, S. (1976). The Warburg hypothesis fifty years later. *Zeitschrift Für Krebsforschung Und Klinische Onkologie 1976 87:2*, 87(2), 115–126. <https://doi.org/10.1007/BF00284370>
- Wheaton, W. W., Weinberg, S. E., Hamanaka, R. B., Soberanes, S., Sullivan, L. B., Anso, E., Glasauer, A., Dufour, E., Mutlu, G. M., Scott Budigner, G. R., & Chandel, N. S. (2014). Metformin inhibits mitochondrial complex I of cancer cells to reduce tumorigenesis. *ELife*, 2014(3). <https://doi.org/10.7554/ELIFE.02242>
- Wise, D. R., Deberardinis, R. J., Mancuso, A., Sayed, N., Zhang, X. Y., Pfeiffer, H. K., Nissim, I., Daikhin, E., Yudkoff, M., McMahon, S. B., & Thompson, C. B. (2008). Myc regulates a transcriptional program that stimulates mitochondrial glutaminolysis and leads to glutamine addiction. *Proceedings of the National Academy of Sciences*, 105(48), 18782–18787. <https://doi.org/10.1073/PNAS.0810199105>
- Witsch, E., Sela, M., & Yarden, Y. (2010). Roles for Growth Factors in Cancer Progression. *Physiology*, 25(2), 85–101. <https://doi.org/10.1152/PHYSIOL.00045.2009/ASSET/IMAGES/LARGE/PHY0021000080004.JPEG>
- Wondrak, G. T., Jacobson, M. K., & Jacobson, E. L. (2005). Identification of Quenchers of Photoexcited States as Novel Agents for Skin Photoprotection. *Journal of Pharmacology and Experimental Therapeutics*, 312(2), 482–491. <https://doi.org/10.1124/JPET.104.075101>
- Wong, C. F. (2015). Flexible receptor docking for drug discovery. <Http://Dx.Doi.Org.Sire.Ub.Edu/10.1517/17460441.2015.1078308>, 10(11), 1189–1200. <https://doi.org/10.1517/17460441.2015.1078308>
- Wong, C. H., Siah, K. W., & Lo, A. W. (2019). Estimation of clinical trial success rates and related parameters. *Biostatistics*, 20(2), 273–286. <https://doi.org/10.1093/BIOSTATISTICS/KXX069>
- Wu, C. I., Wang, H. Y., Ling, S., & Lu, X. (2016). The Ecology and Evolution of Cancer: The Ultra-Microevolutionary Process. *Annual Review of Genetics*, 50, 347–369. <https://doi.org/10.1146/ANNUREV-GENET-112414-054842>
- Wu, C. R., Chen, L. X., Jin, S., & Li, H. (2018). Glutaminase inhibitors: a patent review. <Https://Doi-Org.Sire.Ub.Edu/10.1080/13543776.2018.1530759>, 28(11), 823–835. <https://doi.org/10.1080/13543776.2018.1530759>
- Xiao, B., Sanders, M. J., Underwood, E., Heath, R., Mayer, F. v., Carmena, D., Jing, C., Walker, P. A., Eccleston, J. F., Haire, L. F., Saiu, P., Howell, S. A., Aasland, R., Martin, S. R., Carling, D., & Gamblin, S. J. (2011).

- Structure of mammalian AMPK and its regulation by ADP. *Nature* 2011 472:7342, 472(7342), 230–233. <https://doi.org/10.1038/NATURE09932>
- Xiao, M., Yang, H., Xu, W., Ma, S., Lin, H., Zhu, H., Liu, L., Liu, Y., Yang, C., Xu, Y., Zhao, S., Ye, D., Xiong, Y., & Guan, K. L. (2012). Inhibition of α -KG-dependent histone and DNA demethylases by fumarate and succinate that are accumulated in mutations of FH and SDH tumor suppressors. *Genes & Development*, 26(12), 1326–1338. <https://doi.org/10.1101/GAD.191056.112>
- Xiao, S., Li, S., Yuan, Z., & Zhou, L. (2020). Pyrroline-5-carboxylate reductase 1 (PYCR1) upregulation contributes to gastric cancer progression and indicates poor survival outcome. *Annals of Translational Medicine*, 8(15), 937–937. <https://doi.org/10.21037/ATM-19-4402>
- Xiong, G., Deng, L., Zhu, J., Rychahou, P. G., & Xu, R. (2014). Prolyl-4-hydroxylase α subunit 2 promotes breast cancer progression and metastasis by regulating collagen deposition. *BMC Cancer*, 14(1), 1–12. <https://doi.org/10.1186/1471-2407-14-1/FIGURES/6>
- Xiong, Y., Lei, Q. Y., Zhao, S., & Guan, K. L. (2011). Regulation of Glycolysis and Gluconeogenesis by Acetylation of PKM and PEPCK. *Cold Spring Harbor Symposia on Quantitative Biology*, 76, 285–289. <https://doi.org/10.1101/SQB.2011.76.010942>
- Xu, D., Wang, Z., Xia, Y., Shao, F., Xia, W., Wei, Y., Li, X., Qian, X., Lee, J. H., Du, L., Zheng, Y., Lv, G., Leu, J. shiun, Wang, H., Xing, D., Liang, T., Hung, M. C., & Lu, Z. (2020). The gluconeogenic enzyme PCK1 phosphorylates INSIG1/2 for lipogenesis. *Nature* 2020 580:7804, 580(7804), 530–535. <https://doi.org/10.1038/S41586-020-2183-2>
- Xu, S., Xu, H., Wang, W., Li, S., Li, H., Li, T., Zhang, W., Yu, X., & Liu, L. (2019). The role of collagen in cancer: from bench to bedside. *Journal of Translational Medicine* 2019 17:1, 17(1), 1–22. <https://doi.org/10.1186/S12967-019-2058-1>
- Xu, X., Lai, Y., & Hua, Z. C. (2019). Apoptosis and apoptotic body: Disease message and therapeutic target potentials. *Bioscience Reports*, 39(1), 20180992. <https://doi.org/10.1042/BSR20180992/191>
- Yan, K., Xu, X., Wu, T., Li, J., Cao, G., Li, Y., & Ji, Z. (2019). Knockdown of PYCR1 inhibits proliferation, drug resistance and EMT in colorectal cancer cells by regulating STAT3-Mediated p38 MAPK and NF- κ B signalling pathway. *Biochemical and Biophysical Research Communications*, 520(2), 486–491. <https://doi.org/10.1016/J.BBRC.2019.10.059>
- Yang, G., Murashige, D. S., Humphrey, S. J., & James, D. E. (2015). A Positive Feedback Loop between Akt and mTORC2 via SIN1 Phosphorylation. *Cell Reports*, 12(6), 937–943. <https://doi.org/10.1016/J.CELREP.2015.07.016/ATTACHMENT/7D541480-9410-419F-86B0-22EFAC2DC091/MMC1.PDF>
- Yang, J., Kalhan, S. C., & Hanson, R. W. (2009). What Is the Metabolic Role of Phosphoenolpyruvate Carboxykinase? *Journal of Biological Chemistry*, 284(40), 27025–27029. <https://doi.org/10.1074/JBC.R109.040543>
- Ye, D., Guan, K. L., & Xiong, Y. (2018). Metabolism, Activity, and Targeting of D- and L-2-Hydroxyglutarates. *Trends in Cancer*, 4(2), 151–165. <https://doi.org/10.1016/J.TRECAN.2017.12.005>
- Ye, J., Mancuso, A., Tong, X., Ward, P. S., Fan, J., Rabinowitz, J. D., & Thompson, C. B. (2012). Pyruvate kinase M2 promotes de novo serine synthesis to sustain mTORC1 activity and cell proliferation. *Proceedings of the National Academy of Sciences of the United States of America*, 109(18), 6904–6909. <https://doi.org/10.1073/PNAS.1204176109/-/DCSUPPLEMENTAL>

- Yi, K. H., & Lauring, J. (2016). Recurrent AKT mutations in human cancers: functional consequences and effects on drug sensitivity. *Oncotarget*, *7*(4), 4241–4251. <https://doi.org/10.18632/ONCOTARGET.6648>
- Yu, S., Meng, S., Xiang, M., & Ma, H. (2021). Phosphoenolpyruvate carboxykinase in cell metabolism: Roles and mechanisms beyond gluconeogenesis. *Molecular Metabolism*, *53*, 101257. <https://doi.org/10.1016/J.MOLMET.2021.101257>
- Yuneva, M., Zamboni, N., Oefner, P., Sachidanandam, R., & Lazebnik, Y. (2007). Deficiency in glutamine but not glucose induces MYC-dependent apoptosis in human cells. *The Journal of Cell Biology*, *178*(1), 93–105. <https://doi.org/10.1083/JCB.200703099>
- Zeng, T., Zhu, L., Liao, M., Zhuo, W., Yang, S., Wu, W., & Wang, D. (2017). Knockdown of PYCR1 inhibits cell proliferation and colony formation via cell cycle arrest and apoptosis in prostate cancer. *Medical Oncology*, *34*(2), 1–9. <https://doi.org/10.1007/S12032-016-0870-5/FIGURES/6>
- Zhang, J., Mao, S., Guo, Y., Wu, Y., Yao, X., & Huang, Y. (2019). Inhibition of GLS suppresses proliferation and promotes apoptosis in prostate cancer. *Bioscience Reports*, *39*(6). <https://doi.org/10.1042/BSR20181826>
- Zhang, Z., Chen, F., & Shang, L. (2018). Advances in antitumor effects of NSAIDs. *Cancer Management and Research*, *10*, 4631–4640. <https://doi.org/10.2147/CMAR.S175212>
- Zhao, J., Li, J., Fan, T. W. M., & Hou, S. X. (2017a). Glycolytic reprogramming through PCK2 regulates tumor initiation of prostate cancer cells. *Oncotarget*, *8*(48), 83602–83618. <https://doi.org/10.18632/ONCOTARGET.18787>
- Zhao, J., Li, J., Fan, T. W. M., & Hou, S. X. (2017b). Glycolytic reprogramming through PCK2 regulates tumor initiation of prostate cancer cells. *Oncotarget*, *8*(48), 83602. <https://doi.org/10.18632/ONCOTARGET.18787>
- Zhao, W., Prijic, S., Urban, B. C., Tisza, M. J., Zuo, Y., Li, L., Tan, Z., Chen, X., Mani, S. A., & Chang, J. T. (2016). Candidate Antimetastasis Drugs Suppress the Metastatic Capacity of Breast Cancer Cells by Reducing Membrane Fluidity. *Cancer Research*, *76*(7), 2037. <https://doi.org/10.1158/0008-5472.CAN-15-1970>
- Zhao, Y., Feng, X., Chen, Y., Eva Selfridge, J., Gorityala, S., Du, Z., Wang, J. M., Hao, Y., Cioffi, G., Conlon, R. A., Barnholtz-Sloan, J. S., Saltzman, J., Krishnamurthi, S. S., Vinayak, S., Veigl, M., Xu, Y., Bajor, D. L., Markowitz, S. D., Meropol, N. J., ... Wang, Z. (2020). 5-Fluorouracil Enhances the Antitumor Activity of the Glutaminase Inhibitor CB-839 against PIK3CA-Mutant Colorectal Cancers. *Cancer Research*, *80*(21), 4815–4827. <https://doi.org/10.1158/0008-5472.CAN-20-0600>
- Zhou, D., Jiang, L., Jin, L., Yao, Y., Wang, P., & Zhu, X. (2020). Glucose Transporter-1 Cooperating with AKT Signaling Promote Gastric Cancer Progression. *Cancer Management and Research*, *12*, 4151. <https://doi.org/10.2147/CMAR.S251596>
- Zhu, W., Gincherman, Y., Docherty, P., Spilling, C. D., & Becker, D. F. (2002). Effects of proline analog binding on the spectroscopic and redox properties of PutA. *Archives of Biochemistry and Biophysics*, *408*(1), 131–136. [https://doi.org/10.1016/S0003-9861\(02\)00535-0](https://doi.org/10.1016/S0003-9861(02)00535-0)
- Zhuang, J., Song, Y., Ye, Y., He, S., Ma, X., Zhang, M., Ni, J., Wang, J., & Xia, W. (2019). PYCR1 interference inhibits cell growth and survival via c-Jun N-terminal kinase/insulin receptor substrate 1 (JNK/IRS1) pathway in hepatocellular cancer. *Journal of Translational Medicine*, *17*(1), 1–10. <https://doi.org/10.1186/S12967-019-2091-0/FIGURES/5>

- Zhuo, B., Li, Y., Li, Z., Qin, H., Sun, Q., Zhang, F., Shen, Y., Shi, Y., & Wang, R. (2015). PI3K/Akt signaling mediated Hexokinase-2 expression inhibits cell apoptosis and promotes tumor growth in pediatric osteosarcoma. *Biochemical and Biophysical Research Communications*, *464*(2), 401–406. <https://doi.org/10.1016/J.BBRC.2015.06.092>
- Zielonka, J., Joseph, J., Sikora, A., Hardy, M., Ouari, O., Vasquez-Vivar, J., Cheng, G., Lopez, M., & Kalyanaraman, B. (2017). Mitochondria-Targeted Triphenylphosphonium-Based Compounds: Syntheses, Mechanisms of Action, and Therapeutic and Diagnostic Applications. *Chemical Reviews*, *117*(15), 10043. <https://doi.org/10.1021/ACS.CHEMREV.7B00042>
- Zong, W. X., Rabinowitz, J. D., & White, E. (2016). Mitochondria and Cancer. *Molecular Cell*, *61*(5), 667. <https://doi.org/10.1016/J.MOLCEL.2016.02.011>
- Zu, X. L., & Guppy, M. (2004). Cancer metabolism: facts, fantasy, and fiction. *Biochemical and Biophysical Research Communications*, *313*(3), 459–465. <https://doi.org/10.1016/J.BBRC.2003.11.136>